

Ministry of Education and Science of the Russian Federation
Saint Petersburg National Research University of Information
Technologies, Mechanics, and Optics

NANOSYSTEMS:
PHYSICS, CHEMISTRY, MATHEMATICS

2017, volume 8(2)

Наносистемы: физика, химия, математика

2017, том 8, № 2



NANOSYSTEMS:

PHYSICS, CHEMISTRY, MATHEMATICS

ADVISORY BOARD MEMBERS

Chairman: V.N. Vasiliev (*St. Petersburg, Russia*),
V.M. Buznik (*Moscow, Russia*); V.M. Ievlev (*Voronezh, Russia*), P.S. Kop'ev (*St. Petersburg, Russia*), N.F. Morozov (*St. Petersburg, Russia*), V.N. Parmon (*Novosibirsk, Russia*),
A.I. Rusanov (*St. Petersburg, Russia*),

EDITORIAL BOARD

Editor-in-Chief: I.Yu. Popov (*St. Petersburg, Russia*)

Section Co-Editors:

Physics – V.M. Uzdin (*St. Petersburg, Russia*),
Chemistry, material science – V.V. Gusarov (*St. Petersburg, Russia*),
Mathematics – I.Yu. Popov (*St. Petersburg, Russia*).

Editorial Board Members:

V.M. Adamyan (*Odessa, Ukraine*); O.V. Al'myasheva (*St. Petersburg, Russia*);
A.P. Alodjants (*Vladimir, Russia*); S. Bechta (*Stockholm, Sweden*); J. Behrndt (*Graz, Austria*);
M.B. Belonenko (*Volgograd, Russia*); V.G. Bepalov (*St. Petersburg, Russia*); J. Brasche (*Clausthal, Germany*);
A. Chatterjee (*Hyderabad, India*); S.A. Chivilikhin (*St. Petersburg, Russia*); A.V. Chizhov (*Dubna, Russia*);
A.N. Enyashin (*Ekaterinburg, Russia*), P.P. Fedorov (*Moscow, Russia*); E.A. Gudilin (*Moscow, Russia*);
V.K. Ivanov (*Moscow, Russia*), H. Jónsson (*Reykjavik, Iceland*); A.A. Kiselev (*Madison, USA*); Yu.S. Kivshar (*Canberra, Australia*);
S.A. Kozlov (*St. Petersburg, Russia*); P.A. Kurasov (*Stockholm, Sweden*); A.V. Lukashin (*Moscow, Russia*);
V.A. Margulis (*Saransk, Russia*); I.V. Melikhov (*Moscow, Russia*); G.P. Miroschnichenko (*St. Petersburg, Russia*);
I.Ya. Mittova (*Voronezh, Russia*); H. Neidhardt (*Berlin, Germany*); V.V. Pankov (*Minsk, Belarus*); K. Pankrashkin (*Orsay, France*);
A.V. Ragulya (*Kiev, Ukraine*); V. Rajendran (*Tamil Nadu, India*); A.A. Rempel (*Ekaterinburg, Russia*);
V.Ya. Rudyak (*Novosibirsk, Russia*); D. Shoikhet (*Karmiel, Israel*); P. Stovicek (*Prague, Czech Republic*);
V.M. Talanov (*Novocherkassk, Russia*); A.Ya. Vul' (*St. Petersburg, Russia*); A.V. Yakimansky (*St. Petersburg, Russia*), V.A. Zagrebnev (*Marseille, France*).

Editors:

I.V. Blinova; A.I. Popov; A.I. Trifanov; E.S. Trifanova (*St. Petersburg, Russia*),
R. Simoneaux (*Philadelphia, Pennsylvania, USA*).

Address: University ITMO, Kronverkskiy pr., 49, St. Petersburg 197101, Russia.

Phone: +7(812)232-67-65, **Journal site:** <http://nanojournal.ifmo.ru/>,

E-mail: popov1955@gmail.com

AIM AND SCOPE

The scope of the journal includes all areas of nano-sciences. Papers devoted to basic problems of physics, chemistry, material science and mathematics inspired by nanosystems investigations are welcomed. Both theoretical and experimental works concerning the properties and behavior of nanosystems, problems of its creation and application, mathematical methods of nanosystem studies are considered.

The journal publishes scientific reviews (up to 30 journal pages), research papers (up to 15 pages) and letters (up to 5 pages). All manuscripts are peer-reviewed. Authors are informed about the referee opinion and the Editorial decision.

CONTENT

MATHEMATICS

- S. Albeverio, S. Fassari, F. Rinaldi
The behaviour of the three-dimensional Hamiltonian $-\Delta + \lambda[\delta(x + x_0) + \delta(x - x_0)]$ as the distance between the two centres vanishes 153
- G. Cardone
Waveguides with fast oscillating boundary 160
- V. Derkach, C. Trunk
Coupling of definitizable operators in Kreĭn spaces 166
- L. Grubišić, J. Tambača
Quasi-semidefinite eigenvalue problem and applications 180
- A.S. Melikhova
Zigzag chain model and its spectrum 188
- D.L. Meynster, I.Y. Popov, A.I. Popov
Model of tunneling through double quantum layer in a magnetic field 194
- H. Neidhardt, A. Stephan, V.A. Zagrebnov
On convergence rate estimates for approximations of solution operators for linear non-autonomous evolution equations 202
- N. Peyerimhoff, M. Täufer, I. Veselić
Unique continuation principles and their absence for Schrödinger eigenfunctions on combinatorial and quantum graphs and in continuum space 216

PHYSICS

- S.A. Botman, S.B. Leble
Electrical conductivity model for quasi-one-dimensional structures 231
- S.I. Ezhenkova
Mathematical modeling of sedimentation of nanoparticles in the vessel of finite depth 236
- A.E. Ivanova, S.A. Chivilikhin, A.V. Gleim
Quantum random number generator based on homodyne detection 239

K.V. Gubaidullina, S.A. Chivilikhin Stability of Grover's algorithm in respect to perturbations in quantum circuit	243
S.B. Leble Kolmogorov equation for Bloch electrons and electrical resistivity models for nanowires	247
I.F. Melikhov Asymptotic solution of ultrasonic near-field levitation problem	260
M.N. Nikolaeva, T.D. Anan'eva, A.N. Bugrov, A.T. Dideikin, E.M. Ivankova Correlation between structure and resistance of composites based on polystyrene and multilayered graphene oxide	266
E.O. Samsonov Error analysis in circuits building at the quantum computing platform IBM Quantum Experience	272
A.S. Starkov, K.V. Korzenkov, K.A. Starkov Two eccentric cylinders in a uniform electric field	277
<u>CHEMISTRY AND MATERIAL SCIENCE</u>	
N.R. Popova, A.L. Popov, A.B. Shcherbakov, V.K. Ivanov Layer-by-layer capsules as smart delivery systems of CeS₂ nanoparticles-based theranostic agents	282
I.V. Zagaynov, A.K. Buryak A surface and catalytic investigation of ceria by laser desorption ionization mass spectrometry	290
Information for authors	296

The behaviour of the three-dimensional Hamiltonian $-\Delta + \lambda [\delta(x + x_0) + \delta(x - x_0)]$ as the distance between the two centres vanishes

S. Albeverio^{1,2}, S. Fassari^{2,3,4} and F. Rinaldi^{2,3}

¹Institut für Angewandte Mathematik, HCM, IZKS, BiBoS, Universität Bonn,
Endenicherallee 60, D-53115 Bonn, Germany

²CERFIM, PO Box 1132, CH-6601 Locarno, Switzerland

³Università degli Studi Guglielmo Marconi, Via Plinio 44, I-00193 Rome, Italy

⁴Departamento de Física Teórica, Atómica y Óptica, Universidad de Valladolid, E-47011 Valladolid, Spain
sifassari@gmail.com

PACS 02.30.Gp, 02.30.Hq, 02.30.Hq, 02.30.Lt, 02.30.Sa, 02.30.Tb, 03.65.Db, 03.65.Ge, 68.65.Hb

DOI 10.17586/2220-8054-2017-8-2-153-159

In this note, we continue our analysis of the behavior of self-adjoint Hamiltonians with symmetric double wells given by twin point interactions perturbing various types of “free Hamiltonians” as the distance between the two centers shrinks to zero. In particular, by making the coupling constant to be renormalized and also dependent on the separation distance between the two impurities, we prove that it is possible to rigorously define the unique self-adjoint Hamiltonian that, differently from the one studied in detail by Albeverio and collaborators, behaves smoothly as the separation distance between the impurities shrinks to zero. In fact, we rigorously prove that the Hamiltonian introduced in this note converges in the norm resolvent sense to that of the negative three-dimensional Laplacian perturbed by a single attractive point interaction situated at the origin having double strength, thus making this three-dimensional model more similar to its one-dimensional analog (not requiring the renormalization procedure) as well as to the three-dimensional model involving impurities given by potentials whose range may even be physically very short but non-zero.

Keywords: point interactions, renormalisation, Schrödinger operators, quantum dots.

Received: 3 February 2017

Revised: 12 February 2017

1. Introduction

In this brief presentation, we wish to further investigate the phenomenon that had been first observed in [1] for the one-dimensional Salpeter Hamiltonian perturbed by a pair of identical Dirac distributions symmetrically situated around the origin and later in [2, 3] for the Hamiltonian of the three-dimensional isotropic harmonic oscillator with the same perturbation: as the distance between the two centers shrinks to zero, the Hamiltonian does not approach the Hamiltonian with a single δ -perturbation centered at the origin and having twice the strength. Here, we consider the model that can be regarded as the most pedagogical one, that is to say the three-dimensional Hamiltonian $-\Delta + \lambda[\delta(x + x_0) + \delta(x - x_0)]$.

As stated in those papers, such a problematic behavior does not occur in the case of one-dimensional Schrödinger Hamiltonians with the same singular double well, as attested by the findings of [4, 5]. The absence of the aforementioned phenomenon in this case is due to the fact that the δ -perturbation need not be defined by means of the coupling constant renormalization, since it is an infinitesimally small perturbation of the one-dimensional negative Laplacian due to the KLMN theorem.

2. The rigorous definition of the three-dimensional Hamiltonian $-\Delta + \lambda[\delta(x + x_0) + \delta(x - x_0)]$

As is well known (see, e.g., the references in [6]), the Dirac measure in three dimensions was seen to be far more singular as a perturbation of the negative Laplacian than its one-dimensional counterpart even in the early days of Quantum Mechanics. In fact, one has that the matrix element:

$$(f, \delta)(\delta, f) = (\hat{f}, \hat{\delta}) (\hat{\delta}, \hat{f}) = \frac{1}{(2\pi)^3} (\hat{f}, 1) (1, \hat{f}) = \frac{1}{(2\pi)^3} \left((|p|^2 + 1)^{1/2} \hat{f}, (|p|^2 + 1)^{-1/2} \right) \left((|p|^2 + 1)^{-1/2}, (|p|^2 + 1)^{1/2} \hat{f} \right),$$

diverges since the function $(|p|^2 + 1)^{-1}$ is not in $L^1(\mathbb{R}^3)$ because the integral

$$4\pi \int_0^{+\infty} p^2 (p^2 + 1)^{-1} dp,$$

is clearly divergent.

As a consequence, the coupling constant renormalization will have to be exploited. In view of the detailed study of the important phenomenon mentioned earlier, the case of a singular double well consisting of two Dirac distributions symmetrically centered around the origin will be considered, precisely at the points:

$$\pm \vec{x}_0 = (\pm x_0, 0, 0), \quad x_0 > 0.$$

Therefore, after introducing the ultraviolet cut-off given by $k > 0$, i.e.:

$$|\vec{p}| = \sqrt{p_x^2 + p_y^2 + p_z^2} \leq k, \quad (2.1)$$

the resolvent limit, as $k \rightarrow +\infty$, of the Hamiltonian describing in momentum space the negative Laplacian plus a sum of symmetric δ -potentials at $\pm \vec{x}_0$, with cut-off k and coupling constant $\lambda(k) \neq 0$ depending on it:

$$h(k, x_0) = |\vec{p}|^2 + \frac{\lambda(k)}{(2\pi)^3} \left[|\chi_{|\vec{p}| \leq k} e^{-i\vec{x}_0 \cdot \vec{p}} \langle \chi_{|\vec{p}| \leq k} e^{-i\vec{x}_0 \cdot \vec{p}} | + |\chi_{|\vec{p}| \leq k} e^{i\vec{x}_0 \cdot \vec{p}} \langle \chi_{|\vec{p}| \leq k} e^{i\vec{x}_0 \cdot \vec{p}} | \right], \quad (2.2)$$

is to be studied ($\chi(\cdot)$ denoting the indicator function of the set (\cdot)). As the intermediate steps are essentially along the same lines of those in the three aforementioned papers [1–3], it is quite straightforward to obtain the expression for the resolvent of $H(k, x_0)$ for any $E < 0$:

$$\begin{aligned} [h(k, x_0) + |E|]^{-1} &= [|\vec{p}|^2 + |E|]^{-1} - \\ &\frac{2}{(2\pi)^3} \frac{|\chi_{|\vec{p}| \leq k} \cos(\vec{x}_0 \cdot \vec{p}) \cdot (|\vec{p}|^2 + |E|)^{-1} \rangle \langle \chi_{|\vec{p}| \leq k} \cos(\vec{x}_0 \cdot \vec{p}) \cdot (|\vec{p}|^2 + |E|)^{-1} |}{\frac{1}{\lambda(k)} + \frac{2}{(2\pi)^3} \left\| \chi_{|\vec{p}| \leq k} \cos(\vec{x}_0 \cdot \vec{p}) \cdot (|\vec{p}|^2 + |E|)^{-1/2} \right\|_2^2} \\ &\frac{2}{(2\pi)^3} \frac{|\chi_{|\vec{p}| \leq k} \sin(\vec{x}_0 \cdot \vec{p}) \cdot (|\vec{p}|^2 + |E|)^{-1} \rangle \langle \chi_{|\vec{p}| \leq k} \sin(\vec{x}_0 \cdot \vec{p}) \cdot (|\vec{p}|^2 + |E|)^{-1} |}{\frac{1}{\lambda(k)} + \frac{2}{(2\pi)^3} \left\| \chi_{|\vec{p}| \leq k} \sin(\vec{x}_0 \cdot \vec{p}) \cdot (|\vec{p}|^2 + |E|)^{-1/2} \right\|_2^2}. \end{aligned} \quad (2.3)$$

Furthermore,

$$\begin{aligned} \frac{2}{(2\pi)^3} \left\| \chi_{|\vec{p}| \leq k} \cos(\vec{x}_0 \cdot \vec{p}) \cdot (|\vec{p}|^2 + |E|)^{-1/2} \right\|_2^2 &= \frac{2}{(2\pi)^3} \int_{|\vec{p}| \leq k} \cos^2(\vec{x}_0 \cdot \vec{p}) \cdot (|\vec{p}|^2 + |E|)^{-1} d^3 p = \\ &\frac{1}{(2\pi)^3} \int_{|\vec{p}| \leq k} \frac{1 + \cos(2\vec{x}_0 \cdot \vec{p})}{|\vec{p}|^2 + |E|} d^3 p = \frac{1}{(2\pi)^3} \left[4\pi \int_{|\vec{p}| \leq k} \frac{|\vec{p}|^2}{|\vec{p}|^2 + |E|} d|\vec{p}| + \int_{|\vec{p}| \leq k} \frac{\cos(2\vec{x}_0 \cdot \vec{p})}{|\vec{p}|^2 + |E|} d^3 p \right] = \\ &\frac{1}{(2\pi)^3} \left[4\pi k - 4\pi |E| \int_0^k \frac{1}{|\vec{p}|^2 + |E|} d|\vec{p}| + \int_{|\vec{p}| \leq k} \frac{\cos(2\vec{x}_0 \cdot \vec{p})}{|\vec{p}|^2 + |E|} d^3 p \right] = \\ &\frac{4\pi}{(2\pi)^3} \left[k - |E|^{1/2} \tan^{-1} \left(\frac{k}{|E|^{1/2}} \right) \right] + \frac{1}{(2\pi)^3} \int_{|\vec{p}| \leq k} \frac{\cos(2\vec{x}_0 \cdot \vec{p})}{|\vec{p}|^2 + |E|} d^3 p. \end{aligned} \quad (2.4)$$

Similarly,

$$\begin{aligned} \frac{2}{(2\pi)^3} \left\| \chi_{|\vec{p}| \leq k} \sin(\vec{x}_0 \cdot \vec{p}) \cdot (|\vec{p}|^2 + |E|)^{-1/2} \right\|_2^2 &= \\ &\frac{4\pi}{(2\pi)^3} \left[k - |E|^{1/2} \tan^{-1} \left(\frac{k}{|E|^{1/2}} \right) \right] - \frac{1}{(2\pi)^3} \int_{|\vec{p}| \leq k} \frac{\cos(2\vec{x}_0 \cdot \vec{p})}{|\vec{p}|^2 + |E|} d^3 p. \end{aligned} \quad (2.5)$$

The removal of the cut-off, that is to say the limit $k \rightarrow +\infty$, does not constitute a problem for the two rank one operators in the last two terms of (2.3) since:

$$\left\| \cos(\vec{x}_0 \cdot \vec{p}) \cdot (|\vec{p}|^2 + |E|)^{-1} \right\|_2 < \infty, \quad \left\| \sin(\vec{x}_0 \cdot \vec{p}) \cdot (|\vec{p}|^2 + |E|)^{-1} \right\|_2 < \infty.$$

Then, it is clear that the reciprocal of $\lambda(k)$ is to be chosen in such a way as to get the cancellation of the divergent quantity proportional to k . In fact, by setting:

$$\frac{1}{\lambda(k, \beta)} = -\frac{1}{(2\pi)^3} \int_{|\vec{p}| \leq k} \frac{1}{|\vec{p}|^2} d^3 p - \frac{1}{\beta} = -\frac{k}{2\pi^2} - \frac{1}{\beta},$$

or equivalently:

$$\lambda(k, \beta) = -\frac{\beta}{1 + \frac{1}{(2\pi)^3} \int_{|\vec{p}| \leq k} \frac{1}{|\vec{p}|^2} d^3 p},$$

for any real β , the limit of the right hand side of (2.3), as $k \rightarrow +\infty$, is given by:

$$\begin{aligned} R(|E|; \beta, x_0) &= \left[|\vec{p}|^2 + |E| \right]^{-1} + \\ &\frac{2}{(2\pi)^3} \frac{|\cos(\vec{x}_0 \cdot \vec{p}) \rangle \langle \cos(\vec{x}_0 \cdot \vec{p})|}{|\vec{p}|^2 + |E|} + \frac{2}{(2\pi)^3} \frac{|\sin(\vec{x}_0 \cdot \vec{p}) \rangle \langle \sin(\vec{x}_0 \cdot \vec{p})|}{|\vec{p}|^2 + |E|} = \\ &\frac{\frac{1}{\beta} + \frac{|E|^{1/2}}{4\pi} - \frac{1}{(2\pi)^3} \lim_{k \rightarrow +\infty} \int_{|\vec{p}| \leq k} \frac{\cos(2\vec{x}_0 \cdot \vec{p})}{|\vec{p}|^2 + |E|} d^3 p}{\frac{1}{\beta} + \frac{|E|^{1/2}}{4\pi} + \frac{1}{(2\pi)^3} \lim_{k \rightarrow +\infty} \int_{|\vec{p}| \leq k} \frac{\cos(2\vec{x}_0 \cdot \vec{p})}{|\vec{p}|^2 + |E|} d^3 p} = \\ &\left[|\vec{p}|^2 + |E| \right]^{-1} + \frac{\frac{2}{(2\pi)^3} \frac{|\cos(\vec{x}_0 \cdot \vec{p}) \rangle \langle \cos(\vec{x}_0 \cdot \vec{p})|}{|\vec{p}|^2 + |E|}}{\frac{1}{\beta} + \frac{|E|^{1/2}}{4\pi} - \frac{1}{4\pi} \frac{e^{-2|E|^{1/2}x_0}}{2x_0}} + \frac{\frac{2}{(2\pi)^3} \frac{|\sin(\vec{x}_0 \cdot \vec{p}) \rangle \langle \sin(\vec{x}_0 \cdot \vec{p})|}{|\vec{p}|^2 + |E|}}{\frac{1}{\beta} + \frac{|E|^{1/2}}{4\pi} + \frac{1}{4\pi} \frac{e^{-2|E|^{1/2}x_0}}{2x_0}}. \quad (2.6) \end{aligned}$$

At this stage, one should prove that $R(|E|, \beta, x_0)$ is the resolvent of a self-adjoint operator $h(\beta, x_0)$. However, such a proof will be omitted here given that it would be almost identical to the one provided in [6] in the case of a single point perturbation centred at the origin, the only difference represented by the possibility of having a second point to be excluded along the negative energy semiaxis, namely the possible zero of the denominator of the last term in (2.6).

The above findings can be summarized in the following theorem:

Theorem 2.1. *The Hamiltonian of the three-dimensional negative Laplacian perturbed by two identical attractive point interactions situated symmetrically with respect to the origin at the points $\pm \vec{x}_0 = (\pm x_0, 0, 0)$, $x_0 = |\pm \vec{x}_0| > 0$, making sense of the merely formal expression:*

$$h_{\{\lambda(\beta), \vec{x}_0\}} = -\Delta + \lambda(\beta) [\delta(\vec{x} - \vec{x}_0) + \delta(\vec{x} + \vec{x}_0)],$$

with:

$$\lambda(\beta) = -\frac{\beta}{1 + \frac{1}{(2\pi)^3} \int_{\mathbb{R}^3} \frac{1}{|\vec{p}|^2} d^3 p},$$

being the self-adjoint operator $h(\beta, x_0)$ whose resolvent is given by the bounded operator (2.6). The latter is the limit of the resolvents (2.3) of the Hamiltonians (2.2) (with the energy cut-off k defined by (2.1)) in the norm topology of bounded operators on $L^2(\mathbb{R}^3)$ once the energy cut-off is removed, i.e. for $k \rightarrow +\infty$. Furthermore, $h(\beta, x_0)$ regarded as a function of β is an analytic family in the sense of Kato.

Hence, the equation leading to the calculation of the ground state energy is:

$$\alpha + \frac{|E|^{1/2}}{4\pi} - \frac{1}{4\pi} \frac{e^{-2|E|^{1/2}x_0}}{2x_0} = 0, \quad \alpha = \frac{1}{\beta}, \quad (2.7)$$

while the one leading to the calculation of the energy of the other bound state is:

$$\alpha + \frac{|E|^{1/2}}{4\pi} + \frac{1}{4\pi} \frac{e^{-2|E|^{1/2}x_0}}{2x_0} = 0. \quad (2.8)$$

These two equations are exactly those thoroughly studied at the end of section II.1 in [6]: as shown graphically in Fig. 1 below for $x_0 = 1/2$,

- i) both eigenvalues are absent if $4\pi\alpha \geq (2x_0)^{-1}$;
- ii) the ground state is the only bound state if $-(2x_0)^{-1} \leq \pi\alpha < (2x_0)^{-1}$;
- iii) there are two bound states if $4\pi\alpha < -(2x_0)^{-1}$.

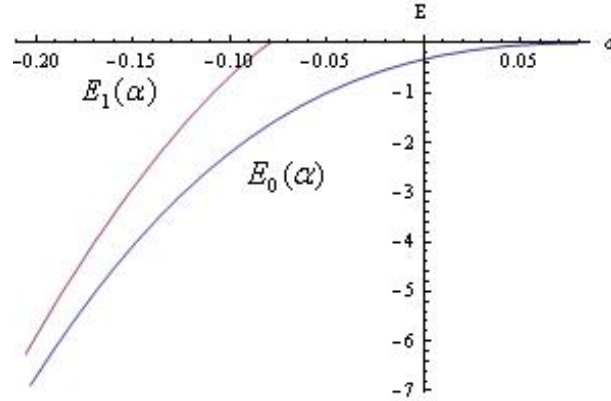


FIG. 1. The spectral curves of the two eigenvalues of $h(1/\alpha, x_0)$ as functions of the extension parameter α for $x_0 = 1/2$

As can be seen in the above plot, whilst the excited state energy gets absorbed into the absolutely continuous spectrum at the point $\alpha = -(4\pi)^{-1}$, the ground state energy gets absorbed into the absolutely continuous spectrum at the opposite value $\alpha = (4\pi)^{-1}$. This is entirely consistent, of course, with the fact that, for any fixed value of x_0 , as $\alpha \rightarrow +\infty$, $h(1/\alpha, x_0)$ approaches the free Hamiltonian in the norm resolvent sense.

The interesting phenomenon previously anticipated is that, as $x_0 \rightarrow 0_+$, the two eigenvalues exhibit different behaviors: whilst the second eigenvalue gets absorbed into the absolutely continuous spectrum, the magnitude of the ground state energy diverges, clearly implying that the Hamiltonian does not converge to the one in which the perturbation is represented by a single point interaction having double the strength. As mentioned earlier, the same phenomenon was observed in [1] dealing with the one-dimensional Salpeter Hamiltonian perturbed by a pair of twin Dirac distributions symmetrically situated with respect to the origin, the spectrum of which also consists of two eigenvalues below the absolutely continuous spectrum, as well as in [2, 3] dealing instead with an operator having only infinitely many eigenvalues, namely the Hamiltonian of the three-dimensional harmonic oscillator perturbed by a pair of twin Dirac distributions symmetrically situated with respect to the origin. Such a singular behavior is in contrast with the smooth one of one-dimensional Schrödinger Hamiltonians with or without the harmonic confinement under the same perturbation (see [4, 5]), as well as with that exhibited by three-dimensional Hamiltonians with perturbations whose range might be even very short but non-zero.

The strategy needed to regularize this singular behavior, thus making three-dimensional zero range perturbations behave like positive range ones, is the one adopted in the aforementioned papers, that is to say the coupling constant to be renormalized must also suitably depend on x_0 . It is quite instructive to see how this works in the case of the model analyzed in this note.

By setting:

$$\frac{1}{\lambda(k, \beta, x_0)} = -\frac{k}{(2\pi)^2} - \frac{1}{\beta} - \frac{1}{(2\pi)^3} \int_{|\vec{p}| \leq k} \frac{\cos(2\vec{x}_0 \cdot \vec{p})}{|\vec{p}|^2} d^3 p, \quad (2.9)$$

and

$$H(k, x_0) = |\vec{p}|^2 + \frac{\lambda(k, \beta, x_0)}{(2\pi)^3} \left[|\chi_{|\vec{p}| \leq k} e^{-i\vec{x}_0 \cdot \vec{p}} \langle \chi_{|\vec{p}| \leq k} e^{-i\vec{x}_0 \cdot \vec{p}} | + |\chi_{|\vec{p}| \leq k} e^{i\vec{x}_0 \cdot \vec{p}} \langle \chi_{|\vec{p}| \leq k} e^{i\vec{x}_0 \cdot \vec{p}} | \right], \quad (2.10)$$

it is rather straightforward to obtain the new limit of the resolvent of (2.10) once the ultraviolet cut-off gets removed, namely:

$$\begin{aligned} \tilde{R}(|E|; \beta, x_0) &= \left[|\vec{p}|^2 + |E| \right]^{-1} + \\ &\frac{\frac{2}{(2\pi)^3} \left| \frac{\cos(\vec{x}_0 \cdot \vec{p})}{|\vec{p}|^2 + |E|} \right\rangle \left\langle \frac{\cos(\vec{x}_0 \cdot \vec{p})}{|\vec{p}|^2 + |E|} \right|}{\frac{1}{\beta} + \frac{|E|^{1/2}}{4\pi} + \frac{1}{(2\pi)^3} \lim_{k \rightarrow +\infty} \int_{|\vec{p}| \leq k} \cos(2\vec{x}_0 \cdot \vec{p}) \left[\frac{1}{|\vec{p}|^2} - \frac{1}{|\vec{p}|^2 + |E|} \right] d^3 p} + \\ &\frac{\frac{2}{(2\pi)^3} \left| \frac{\sin(\vec{x}_0 \cdot \vec{p})}{|\vec{p}|^2 + |E|} \right\rangle \left\langle \frac{\sin(\vec{x}_0 \cdot \vec{p})}{|\vec{p}|^2 + |E|} \right|}{\frac{1}{\beta} + \frac{|E|^{1/2}}{4\pi} + \frac{1}{(2\pi)^3} \lim_{k \rightarrow +\infty} \int_{|\vec{p}| \leq k} \cos(2\vec{x}_0 \cdot \vec{p}) \left[\frac{1}{|\vec{p}|^2} + \frac{1}{|\vec{p}|^2 + |E|} \right] d^3 p} = \\ &\left[|\vec{p}|^2 + |E| \right]^{-1} + \frac{\frac{2}{(2\pi)^3} \left| \frac{\cos(\vec{x}_0 \cdot \vec{p})}{|\vec{p}|^2 + |E|} \right\rangle \left\langle \frac{\cos(\vec{x}_0 \cdot \vec{p})}{|\vec{p}|^2 + |E|} \right|}{\frac{1}{\beta} + \frac{|E|^{1/2}}{4\pi} + \frac{1}{4\pi} \frac{1 - e^{-2|E|^{1/2}x_0}}{2x_0}} + \frac{\frac{2}{(2\pi)^3} \left| \frac{\sin(\vec{x}_0 \cdot \vec{p})}{|\vec{p}|^2 + |E|} \right\rangle \left\langle \frac{\sin(\vec{x}_0 \cdot \vec{p})}{|\vec{p}|^2 + |E|} \right|}{\frac{1}{\beta} + \frac{|E|^{1/2}}{4\pi} + \frac{1}{4\pi} \frac{1 + e^{-2|E|^{1/2}x_0}}{2x_0}}. \quad (2.11) \end{aligned}$$

This operator can be rigorously shown to be the resolvent of another self-adjoint operator $H(\beta, x_0) = H(1/\alpha, x_0)$ by means of a proof again patterned after the aforementioned one in [6]. Therefore, also in this case our findings can be summarized in the following theorem:

Theorem 2.2. *The Hamiltonian of the three-dimensional negative Laplacian perturbed by two identical attractive point interactions situated symmetrically with respect to the origin at the points $\pm \vec{x}_0 = (\pm x_0, 0, 0)$, $x_0 = |\pm \vec{x}_0| > 0$, making sense of the merely formal expression:*

$$H_{\{\lambda(\beta, x_0), \vec{x}_0\}} = -\Delta + \lambda(\beta, x_0) [\delta(\vec{x} - \vec{x}_0) + \delta(\vec{x} + \vec{x}_0)],$$

with:

$$\lambda(\beta, x_0) = -\frac{\beta}{1 + \frac{1}{(2\pi)^3} \int_{\mathbb{R}^3} \frac{1 + \cos(2\vec{x}_0 \cdot \vec{p})}{|\vec{p}|^2} d^3 p},$$

is the self-adjoint operator $H(\beta, x_0)$ whose resolvent is given by the bounded operator (2.11). The latter is the limit of the resolvents of the Hamiltonians (2.10) (with the energy cut-off k defined by (2.1)) in the norm topology of bounded operators on $L^2(\mathbb{R}^3)$ once the energy cut-off is removed, i.e. for $k \rightarrow +\infty$. Furthermore, $H(\beta, x_0)$ regarded as a function of β is an analytic family in the sense of Kato.

The discrete spectrum of $H(\beta, x_0) = H(1/\alpha, x_0)$ may also have up to two eigenvalues, namely the solutions of:

$$\alpha + \frac{|E|^{1/2}}{4\pi} + \frac{1}{4\pi} \frac{1 - e^{-2|E|^{1/2}x_0}}{2x_0} = 0, \quad \alpha = \frac{1}{\beta} \quad (\text{ground state energy equation}), \quad (2.12)$$

$$\alpha + \frac{|E|^{1/2}}{4\pi} + \frac{1}{4\pi} \frac{1 + e^{-2|E|^{1/2}x_0}}{2x_0} = 0, \quad \alpha = \frac{1}{\beta} \quad (\text{excited state energy equation}). \quad (2.13)$$

The solutions of both equations are plotted below in Fig. 2 as functions of $\alpha = 1/\beta$, for $x_0 = 1/2$, for the sake of comparison with those of $h(1/\alpha, x_0)$ shown earlier in Fig. 1.

The above plot shows that the ground state energy gets absorbed into the absolutely continuous spectrum exactly at $\alpha = 0$, thus implying $e_0(0) = 0$. This is entirely consistent with the expectation that this operator should approach, as $x_0 \rightarrow 0_+$, the negative Laplacian perturbed by a single point interaction centred at the origin which is known to have a *zero energy resonance* at $\alpha = 0$, characterised by the fact that the corresponding x -space wave function is only *locally* square integrable (see [6]).

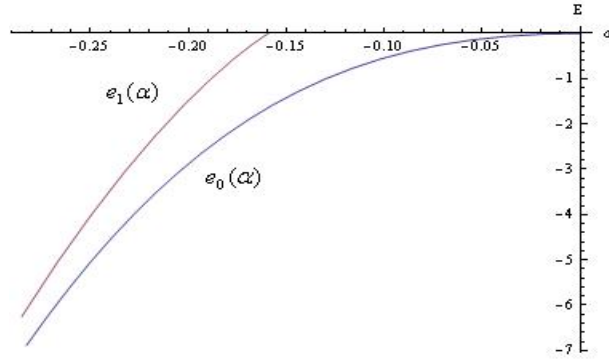


FIG. 2. The spectral curves of the two eigenvalues of $H(1/\alpha, x_0)$ as functions of the extension parameter α for $x_0 = 1/2$

The norm resolvent limit of $H(\beta, x_0)$, as $x_0 \rightarrow 0_+$, is clearly given by:

$$\left[|\vec{p}|^2 + |E| \right]^{-1} + \frac{1}{(2\pi)^3} \left| \frac{1}{|\vec{p}|^2 + |E|} \right\rangle \left\langle \frac{1}{|\vec{p}|^2 + |E|} \right| \frac{1}{\frac{1}{2\beta} + \frac{|E|^{1/2}}{4\pi}}. \quad (2.14)$$

The latter is nothing else but the resolvent in momentum space of the negative Laplacian perturbed by a single point interaction centered at the origin having double strength, as can be understood by looking at either (1.1.21), its x -space counterpart, in Section I.1 of [6] or (1.1.24) in Section II.1 of the same monograph for $N = 1$ with the origin being the location of the single point perturbation, taking into account that the extension parameter α used therein is the reciprocal of the strength. Apart from the absolutely continuous spectrum $[0, +\infty)$, if $\beta < 0$, there is an isolated eigenvalue below the absolutely continuous spectrum, namely:

$$E_0(2\beta) = - \left(\frac{2\pi}{\beta} \right)^2.$$

3. Final remarks

In this brief note, we have considered the most pedagogical three-dimensional model involving a symmetric double well consisting of two identical Dirac distributions, whose Hamiltonian is heuristically given by $-\Delta + \lambda[\delta(x + x_0) + \delta(x - x_0)]$. We have first reviewed the coupling constant renormalization procedure leading to the rigorous definition of the self-adjoint operator fully investigated in [6] as well as the two ensuing equations determining the two possible eigenvalues generated by the perturbation. Since the ground state eigenenergy does not converge to the single eigenvalue of the self-adjoint Hamiltonian $-\Delta_{1/2\beta,0}$, defined in [6] (with $\beta < 0$) as the distance between the two centres shrinks to zero, an alternative renormalization procedure has been adopted in order to regularise this problematic behavior. By making the coupling constant suitably dependent also on $x_0 = |\pm \vec{x}_0| > 0$, in addition to the usual momentum cut-off, it has been possible to define a new self-adjoint Hamiltonian whose resolvent converges in norm to that of $-\Delta_{1/2\beta,0}$ as $x_0 \rightarrow 0_+$. The crucial difference between the discrete spectra of the two operators is that, whilst the ground state eigenenergy of the former Hamiltonian gets absorbed into the absolutely continuous spectrum at $\alpha = (8\pi x_0)^{-1}$ ($\alpha = 1/\beta$ being the extension parameter), the ground state eigenenergy of the latter gets absorbed into the absolutely continuous spectrum at $\alpha = 0$ independently of x_0 . As pointed out earlier, this is entirely consistent with the fact that the limiting operator, that is to say the negative Laplacian perturbed by a single point interaction centered at the origin, is known to have a zero energy resonance at $\alpha = 0$, so that the corresponding x -space wave function is only locally square integrable (see [6]).

This might have some relevant implications in the study of quantum three-body models consisting of two heavy particles and a light one interacting with each other via two-body zero range interactions, at least in the adiabatic approximation, as might be implied by the findings of [7].

We also intend to extend the analysis of the singular phenomenon carried out in this note and in the aforementioned papers [1–3] to another type of quantum oscillator with a different confinement, namely the one whose Hamiltonian is given by:

$$H_0 = \frac{1}{2} (-\Delta + |\vec{x}|),$$

even though the resolvent of this three-dimensional operator will have to be determined first since, differently from its one-dimensional counterpart (see [10, 11]), it is not yet explicitly known.

Acknowledgements

Fabio Rinaldi wishes to express his heartfelt gratitude to Prof. I. Popov for his kind invitation to present the main contents of this note during one of the sessions of the conference “Mathematical Challenge of Quantum Transport in Nanosystems – Pierre Duclos Workshop”, held at ITMO University, St. Petersburg, Russian Federation (14–15 November 2016).

S. Fassari gratefully acknowledges financial support from the “Grants for Visiting Researchers at the Campus of International Excellence Triangular-E3”, as part of the “Attraction of Excellent Researchers and Stays for Visiting Researchers Program”, carried out under the subvention of the Ministry of Education, Culture and Sports to the Campus of International Excellence Triangular-E3. Partial financial support is acknowledged to the Spanish Junta de Castilla y Leon (VA057U16) and MINECO (Project MTM2014-57129-C2-1-P). S. Fassari also wishes to thank the entire staff at Departamento de Física Teórica, Atómica y Óptica, Universidad de Valladolid, for their warm hospitality throughout his stay.

References

- [1] Albeverio S., Fassari S., Rinaldi F. The discrete spectrum of the spinless Salpeter Hamiltonian perturbed by δ -interactions. *Journal of Physics A: Mathematical and Theoretical*, 2015, **48** (18), P. 185301.
- [2] Albeverio S., Fassari S., Rinaldi F. Spectral properties of a symmetric three-dimensional quantum dot with a pair of identical attractive δ -impurities symmetrically situated around the origin. *Nanosystems: Physics, Chemistry, Mathematics*, 2016, **7** (2), P. 268–289.
- [3] Albeverio S., Fassari S., Rinaldi F. Spectral properties of a symmetric three-dimensional quantum dot with a pair of identical attractive δ -impurities symmetrically situated around the origin II. *Nanosystems: Physics, Chemistry, Mathematics*, 2016, **7** (5), P. 803–815.
- [4] Fassari S., Rinaldi F. On the spectrum of the Schrödinger Hamiltonian with a particular configuration of three point interactions. *Reports on Mathematical Physics*, 2009, **64** (3), P. 367–393.
- [5] Fassari S., Rinaldi F. On the spectrum of the Schrödinger Hamiltonian of the one-dimensional harmonic oscillator perturbed by two identical attractive point interactions. *Reports on Mathematical Physics*, 2012, **69** (3), P. 353–370.
- [6] Albeverio S., Gesztesy F., Høegh-Krohn R., Holden H. *Solvable models in Quantum Mechanics* AMS (Chelsea Series) second ed., 2004.
- [7] Kato T. *Perturbation Theory for Linear Operators*. Springer Verlag, Heidelberg-NY, 1995.
- [8] Reed M., Simon B. *Analysis of Operators – Methods of Modern Mathematical Physics IV*. Academic Press NY, 1978.
- [9] Bhaduri R.K., Chatterjee A., Van Zyl B.P. An elementary exposition of the Efimov effect. *American Journal of Physics*, 2011, **79** (3), P. 274–281.
- [10] Glasser M.L., Nieto L.M. The energy level structure of a variety of one-dimensional confining potentials and the effects of a local singular perturbation. *Canadian Journal of Physics*, 2015, **93** (12), P. 1588.
- [11] Lörinczi J., Malecki J. Spectral properties of the massless relativistic harmonic oscillator. *Journal of Differential Equations*, 2012, **253** (10), P. 2846–2871.

Waveguides with fast oscillating boundary

G. Cardone

University of Sannio, Department of Engineering,
Corso Garibaldi, 107, 82100 Benevento, Italy
gcardone@unisannio.it

DOI 10.17586/2220-8054-2017-8-2-160-165

We consider an elliptic operator in a planar waveguide with a fast oscillating boundary where we impose Dirichlet, Neumann or Robin boundary conditions assuming that both the period and the amplitude of the oscillations are small. We describe the homogenized operator, establish the norm resolvent convergence of the perturbed resolvent to the homogenized one, and prove the estimates for the rate of convergence. It is shown that under the homogenization, the type of the boundary condition can change.

Keywords: elliptic operator, unbounded domain, norm resolvent convergence.

Received: 4 January 2017

Revised: 29 January 2017

1. Introduction

We study the problem of homogenization of boundary value problems in domains with a fast oscillating boundary when such boundary is given by the graph of the function $x_2 = \eta(\varepsilon)b(x_1\varepsilon^{-1})$, where ε is a small positive parameter, $\eta(\varepsilon)$ is a positive function tending to zero as $\varepsilon \rightarrow +0$, and b is a smooth periodic function. The parameter ε describes the period of the boundary oscillations while $\eta(\varepsilon)$ is their amplitude.

In previous results, the weak or strong resolvent convergence of the solutions was proved and the resolvents were also treated in various possible norms. In some cases, the estimates for the convergence rate were proven. It was also shown that when constructing the next terms of the asymptotics for the perturbed solutions, one can get estimates for the convergence rate or improve it [1–8]. In some cases, complete asymptotic expansions were constructed [9–12].

One more type of established results is the uniform resolvent convergence for the problems. Such convergence was established just for few models, see [13, Ch. III, Sec. 4], [8]. The estimates for the rates of convergence were also established. In both papers, the amplitude and the period of oscillations were of the same order. At the same time, the uniform resolvent convergence for the models considered in the homogenization theory provided quite strong results. Moreover, recently a series of papers by M. Sh. Birman, T. A. Suslina, V. V. Zhikov and S. E. Pastukhova have stimulated interest in this aspect (see [14–27] and references therein and further papers by these authors). The uniform resolvent convergence was shown to hold true for the elliptic operators with fast oscillating coefficients and the estimates for the rates of convergence were obtained. There are also similar results for some problems in bounded domains, see [26]. Similar results but for the boundary homogenization were established in [28–32]. Here, the Laplacian in a planar straight infinite strip with frequently alternating boundary conditions was considered. Such boundary conditions were imposed by partitioning the boundary into small segments where Dirichlet and Robin conditions were imposed in turn. The homogenized problem involves one of the classical boundary conditions instead of the alternating ones. For all possible homogenized problems, the uniform resolvent and the estimates for the rates of convergence were proven and the asymptotics for the spectra were constructed.

In the present paper, we also consider the boundary homogenization for the elliptic operators in unbounded domains but the perturbation is a fast oscillating boundary. As the domain, we choose a planar straight infinite strip with a periodic fast oscillating boundary; the operator is a general self-adjoint second order elliptic operator. The operator is regarded as an unbounded one in an appropriate L_2 space. On the oscillating boundary, we impose Dirichlet, Neumann, or Robin conditions. Apart from a mathematical interest in this problem, as a physical motivation, we can mention a model of a planar quantum or acoustic waveguide with a fast oscillating boundary.

Our main result is the form of the homogenized operator and the uniform resolvent convergence of the perturbed operator to the homogenized one. This convergence is established in the sense of the norm of the operator acting from L_2 into W_2^1 . The estimates for the rate of convergence are provided. Most of the estimates are sharp. In the case of the Dirichlet or Neumann conditions on the oscillating boundary, the homogenized problem involves the same condition on the mollified boundary no matter how the period and amplitude of the oscillations

behave. Provided the amplitude is not greater than the period (in order), the Robin conditions on the oscillating boundary leads us to a similar condition but with an additional term in the coefficient. If the amplitude is greater than the period, the homogenization transforms the Robin conditions into those of Dirichlet. The last result is in a good accordance with a similar case, treated in [33]. The difference is that in [33], the strong resolvent convergence was proven provided the coefficient in the Robin conditions was positive, while we succeeded to prove the uniform resolvent convergence provided the coefficient is either positive or non-negative and vanishing on the set of zero measure. All the results stated in this paper are proved in [34].

2. Problem and main results

Let $x = (x_1, x_2)$ be the Cartesian coordinates in \mathbb{R}^2 , ε be a small positive parameter, $\eta = \eta(\varepsilon)$ be a non-negative function uniformly bounded for sufficiently small ε , $b = b(t)$ be a non-negative 1-periodic function belonging to $C^2(\mathbb{R})$. We define two domains, cf. Fig. 1:

$$\Omega_0 := \{x : 0 < x_2 < d\}, \quad \Omega_\varepsilon := \{x : \eta(\varepsilon)b(x_1\varepsilon^{-1}) < x_2 < d\},$$

where $d > 0$ is a constant, and its boundaries are indicated as:

$$\Gamma := \{x : x_2 = d\}, \quad \Gamma_0 := \{x : x_2 = 0\}, \quad \Gamma_\varepsilon := \{x : x_2 = \eta(\varepsilon)b(x_1\varepsilon^{-1})\}.$$

By $A_{ij} = A_{ij}(x)$, $A_j = A_j(x)$, $A_0 = A_0(x)$, $i, j = 1, 2$, we denote the functions defined on Ω_0 and satisfying the belongings $A_{ij} \in W_\infty^2(\Omega_0)$, $A_j \in W_\infty^1(\Omega_0)$, $A_0 \in L_\infty(\Omega_0)$. Functions A_{ij} , A_j are assumed to be complex-valued, while A_0 is real-valued. In addition, functions A_{ij} satisfy the ellipticity condition:

$$A_{ij} = \overline{A_{ji}}, \quad \sum_{i,j=1}^2 A_{ij} z_i \overline{z_j} \geq c_0(|z_1|^2 + |z_2|^2), \quad x \in \Omega_0, \quad z_j \in \mathbb{C}. \quad (2.1)$$

By $a = a(x)$ we denote a real function defined on $\{x : 0 < x_2 < \delta\}$ for some small fixed δ , and it is supposed that $a \in W_\infty^1(\{x : 0 < x_2 < d\})$.

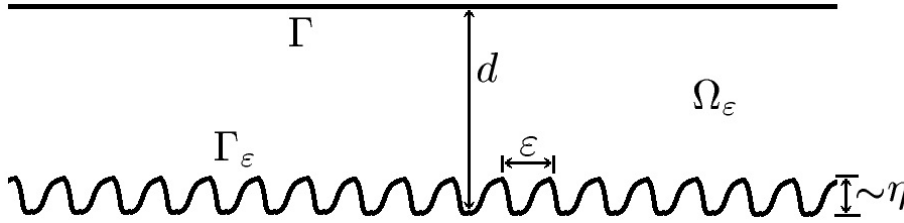


FIG. 1. Domain with oscillating boundary

The main object of our study is the operator:

$$-\sum_{i,j=1}^2 \frac{\partial}{\partial x_j} A_{ij} \frac{\partial}{\partial x_i} + \sum_{j=1}^2 A_j \frac{\partial}{\partial x_j} - \frac{\partial}{\partial x_j} \overline{A_j} + A_0 \quad \text{in } L_2(\Omega_\varepsilon), \quad (2.2)$$

subject to Dirichlet conditions on Γ . On the other boundary, we choose either Dirichlet conditions:

$$u = 0 \quad \text{on } \Gamma_\varepsilon,$$

or Robin conditions:

$$\left(\frac{\partial}{\partial \nu^\varepsilon} + a \right) u = 0 \quad \text{on } \Gamma_\varepsilon, \quad \frac{\partial}{\partial \nu^\varepsilon} = - \sum_{i,j=1}^2 A_{ij} \nu_j^\varepsilon \frac{\partial}{\partial x_i} - \sum_{j=1}^2 \overline{A_j} \nu_j^\varepsilon,$$

where $\nu^\varepsilon = (\nu_1^\varepsilon, \nu_2^\varepsilon)$ is the outward normal to Γ_ε . In the case of Dirichlet conditions on Γ_ε we denote this operator as $\mathcal{H}_{\varepsilon,\eta}^D$, while for Robin conditions it is $\mathcal{H}_{\varepsilon,\eta}^R$. The former also includes the case of Neumann conditions since the function a can be identically zero.

Rigorously, we introduce $\mathcal{H}_{\varepsilon,\eta}^D$ as the lower-semibounded self-adjoint operator in $L_2(\Omega_\varepsilon)$ associated with the closed symmetric lower-semibounded sesquilinear form:

$$\lambda \mathfrak{h}_{\varepsilon,\eta}^D(u, v) := \sum_{i,j=1}^2 \left(A_{ij} \frac{\partial u}{\partial x_j}, \frac{\partial v}{\partial x_i} \right)_{L_2(\Omega_\varepsilon)} + \sum_{j=1}^2 \left(A_j \frac{\partial u}{\partial x_j}, v \right)_{L_2(\Omega_\varepsilon)} + \sum_{j=1}^2 \left(u, \overline{A_j} \frac{\partial v}{\partial x_j} \right)_{L_2(\Omega_\varepsilon)} + (A_0 u, v)_{L_2(\Omega_\varepsilon)},$$

in $L_2(\Omega_\varepsilon)$ with the domain $\mathfrak{D}(\mathfrak{h}_{\varepsilon,\eta}^D) := W_{2,0}^1(\Omega_\varepsilon, \partial\Omega_\varepsilon)$. Hereinafter $\mathfrak{D}(\cdot)$ is the domain of a form or an operator, and $W_{2,0}^j(\Omega, S)$ denotes the Sobolev space consisting of the functions in $W_2^j(\Omega)$ with zero trace on a curve S lying in a domain $\Omega \subset \mathbb{R}^2$. The operator $\mathcal{H}_{\varepsilon,\eta}^R$ is introduced in the same way via the sesquilinear form:

$$\begin{aligned} \mathfrak{h}_{\varepsilon,\eta}^R(u, v) &:= \sum_{i,j=1}^2 \left(A_{ij} \frac{\partial u}{\partial x_j}, \frac{\partial v}{\partial x_i} \right)_{L_2(\Omega_\varepsilon)} + \sum_{j=1}^2 \left(A_j \frac{\partial u}{\partial x_j}, v \right)_{L_2(\Omega_\varepsilon)} \\ &+ \sum_{j=1}^2 \left(u, A_j \frac{\partial v}{\partial x_j} \right)_{L_2(\Omega_\varepsilon)} + (A_0 u, v)_{L_2(\Omega_\varepsilon)} + (a u, v)_{L_2(\Gamma_\varepsilon)}, \end{aligned}$$

with the domain $\mathfrak{D}(\mathfrak{h}_{\varepsilon,\eta}^R) := W_{2,0}^1(\Omega_\varepsilon, \Gamma)$.

The main aim of the paper is to study the asymptotic behavior of the resolvents of $\mathcal{H}_{\varepsilon,\eta}^D$ and $\mathcal{H}_{\varepsilon,\eta}^R$ as $\varepsilon \rightarrow +0$. To formulate the main results we first introduce some additional operators.

By \mathcal{H}_0^D we denote operator (2.2) in $L_2(\Omega_0)$ subject to Dirichlet conditions. We introduce it by analogy with $\mathcal{H}_{\varepsilon,\eta}^D$ as associated with the form:

$$\begin{aligned} \mathfrak{h}_0^D(u, v) &:= \sum_{i,j=1}^2 \left(A_{ij} \frac{\partial u}{\partial x_j}, \frac{\partial v}{\partial x_i} \right)_{L_2(\Omega_0)} + \sum_{j=1}^2 \left(A_j \frac{\partial u}{\partial x_j}, v \right)_{L_2(\Omega_0)} \\ &+ \sum_{j=1}^2 \left(u, A_j \frac{\partial v}{\partial x_j} \right)_{L_2(\Omega_0)} + (A_0 u, v)_{L_2(\Omega_0)}, \end{aligned} \quad (2.3)$$

in $L_2(\Omega_0)$ with the domain $\mathfrak{D}(\mathfrak{h}_0^D) := W_{2,0}^1(\Omega_0, \partial\Omega_0)$. The domain of operator \mathcal{H}_0^D is $W_{2,0}^2(\Omega_0, \partial\Omega_0)$ that can be shown by analogy with [35, Ch. III, Sec. 7,8], [36, Lm. 2.2].

Our first main result (proved in section 2 in [34]) describes the uniform resolvent convergence for $\mathcal{H}_{\varepsilon,\eta}^D$.

Theorem 2.1. *Let $f \in L_2(\Omega_0)$. For sufficiently small ε , the estimate:*

$$\|(\mathcal{H}_{\varepsilon,\eta}^D - i)^{-1} f - (\mathcal{H}_0^D - i)^{-1} f\|_{W_2^1(\Omega_\varepsilon)} \leq C \eta^{1/2} \|f\|_{L_2(\Omega_0)},$$

holds true, where C is a constant independent of ε and f .

The next four theorems describe the resolvent convergence for operator $\mathcal{H}_{\varepsilon,\eta}^R$. Given $a_0 \in W_\infty^1(\Gamma_0)$, let \mathcal{H}_0^R be the self-adjoint operator in $L_2(\Omega_0)$ associated with the lower-semibounded sesquilinear symmetric form:

$$\begin{aligned} \mathfrak{h}_0^R(u, v) &:= \sum_{i,j=1}^2 \left(A_{ij} \frac{\partial u}{\partial x_j}, \frac{\partial v}{\partial x_i} \right)_{L_2(\Omega_0)} + \sum_{j=1}^2 \left(A_j \frac{\partial u}{\partial x_j}, v \right)_{L_2(\Omega_0)} \\ &+ \sum_{j=1}^2 \left(u, A_j \frac{\partial v}{\partial x_j} \right)_{L_2(\Omega_0)} + (A_0 u, v)_{L_2(\Omega_0)} + (a_0 u, v)_{L_2(\Gamma_0)}, \end{aligned}$$

with the domain $\mathfrak{D}(\mathfrak{h}_0^R) := W_{2,0}^1(\Omega_0, \Gamma)$. It can be shown by analogy with [35, Ch. III, Sec. 7,8], [36, Lm. 2.2] that the domain of \mathcal{H}_0^R consists of the functions $u \in W_{2,0}^2(\Omega_0, \Gamma)$ satisfying Robin conditions:

$$\left(\frac{\partial}{\partial \nu^0} + a_0 \right) u = 0 \quad \text{on } \Gamma_0, \quad \frac{\partial}{\partial \nu^0} := - \sum_{i=1}^2 A_{i2} \frac{\partial}{\partial x_i} - \bar{A}_2. \quad (2.4)$$

First, we consider the particular case of Neumann conditions on Γ_ε , i.e., $a = 0$. Operator $\mathcal{H}_{\varepsilon,\eta}^R$ and associated quadratic form $\mathfrak{h}_{\varepsilon,\eta}^R$ are re-denoted in this case by $\mathcal{H}_{\varepsilon,\eta}^N$ and $\mathfrak{h}_{\varepsilon,\eta}^N$. By \mathcal{H}_0^N , we denote the self-adjoint lower-semibounded operator in $L_2(\Omega_0)$ associated with the sesquilinear form \mathfrak{h}_0^N which is \mathfrak{h}_0^R taken for $a_0 \equiv 0$. Its domain is the set of the functions in $W_{2,0}^2(\Omega_0, \Gamma)$ satisfying boundary conditions (2.4) with $a_0 = 0$. The resolvent convergence in this case is given in following theorem (for the proof see section 3 in [34]).

Theorem 2.2. *Let $f \in L_2(\Omega_\varepsilon)$. Then for sufficiently small ε the estimate*

$$\|(\mathcal{H}_{\varepsilon,\eta}^N - i)^{-1} f - (\mathcal{H}_0^N - i)^{-1} f\|_{W_2^1(\Omega_\varepsilon)} \leq C \eta^{1/2} \|f\|_{L_2(\Omega_0)}$$

holds true, where C is a constant independent of ε and f .

Assume now $a \not\equiv 0$. Here we consider separately two cases:

$$\varepsilon^{-1}\eta(\varepsilon) \rightarrow \alpha = \text{const} \geq 0, \quad \varepsilon \rightarrow +0, \quad (2.5)$$

$$\varepsilon^{-1}\eta(\varepsilon) \rightarrow +\infty, \quad \varepsilon \rightarrow +0. \quad (2.6)$$

The first assumption means that the amplitude of the oscillation of curve Γ_ε is of the same order (or smaller) as the period. The other assumption corresponds to the case when the amplitude is much greater than the period. In what follows, the first case is referred to as a relatively slow oscillating boundary Γ_ε while the other describes relatively high oscillating boundary Γ_ε .

We begin with the slowly oscillating boundary. We denote:

$$a_0(x_1) := a(x_1, 0) \int_0^1 \sqrt{1 + \alpha^2 (b'(t))^2} dt. \quad (2.7)$$

The proof of the following theorem is given in section 3 in [34].

Theorem 2.3. *Suppose (2.5) and let $f \in L_2(\Omega_\varepsilon)$. Then, for sufficiently small ε , the estimate*

$$\|(\mathcal{H}_{\varepsilon, \eta}^R - i)^{-1}f - (\mathcal{H}_0^R - i)^{-1}f\|_{W_2^1(\Omega_\varepsilon)} \leq C(\eta^{1/2}(\varepsilon) + |\varepsilon^{-2}\eta^2(\varepsilon) - \alpha^2|)\|f\|_{L_2(\Omega_0)}$$

holds true, where function a_0 in (2.4) is defined in (2.7), and C is a constant independent of ε and f .

We proceed to the case of the highly oscillating boundary Γ_ε . Here, the homogenized operator happens to be quite sensitive to the sign of a and zero level set of this function. In the paper, we describe the resolvent convergence as a is non-negative. We first suppose that a is bounded from below by a positive constant. Surprisingly, but here the homogenized operator has the Dirichlet condition on Γ_0 as in Theorem 2.1. The proof of the following Theorem is given in section 4 in [34].

Theorem 2.4. *Suppose (2.6),*

$$a(x) \geq c_1 > 0, \quad c_1 = \text{const}, \quad (2.8)$$

and that the function b is not identically constant. Let $f \in L_2(\Omega_0)$. Then, for sufficiently small ε , the estimate:

$$\|(\mathcal{H}_{\varepsilon, \eta}^R - i)^{-1}f - (\mathcal{H}_0^D - i)^{-1}f\|_{W_2^1(\Omega_\varepsilon)} \leq C(\eta^{1/2} + \varepsilon^{1/2}\eta^{-1/2})\|f\|_{L_2(\Omega_0)} \quad (2.9)$$

holds true, where C is a constant independent of ε and f .

In the next theorem, that is proved in section 4 in [34], we still suppose that a is non-negative but can have zeroes. An essential assumption is that zero level set of a is of zero measure. We let $b_* := \max_{[0,1]} b$.

Theorem 2.5. *Suppose (2.6),*

$$a \geq 0, \quad (2.10)$$

and that the function b is not identically constant. Assume also that for all sufficiently small δ , the set $\{x : a(x) \leq \delta, 0 < x_2 < (b_* + 1)\eta\}$ is contained in an at most countable union of the rectangles $\{x : |x_1 - X_n| < \mu(\delta), 0 < x_2 < (b_* + 1)\eta\}$, where $\mu(\delta)$ is a some nonnegative function such that $\mu(\delta) \rightarrow +0$ as $\delta \rightarrow +0$, and numbers X_n , $n \in \mathbb{Z}$, are independent of δ , are taken in the ascending order, and satisfy uniform in n and m estimate:

$$|X_n - X_m| \geq c > 0, \quad n \neq m. \quad (2.11)$$

Let $f \in L_2(\Omega_0)$. Then, for sufficiently small ε , the estimate:

$$\begin{aligned} & \|(\mathcal{H}_{\varepsilon, \eta}^R - i)^{-1}f - (\mathcal{H}_0^D - i)^{-1}f\|_{W_2^1(\Omega_\varepsilon)} \\ & \leq C(\eta^{1/2} + \varepsilon^{1/2}\eta^{-1/2}\delta^{-1/2} + \mu^{1/2}(\delta)|\ln \mu(\delta)|^{1/2})\|f\|_{L_2(\Omega_0)} \end{aligned} \quad (2.12)$$

holds true, where C is a constant independent of ε and f , and $\delta = \delta(\varepsilon)$ is any function tending to zero as $\varepsilon \rightarrow +0$.

Let us discuss the main results. We first observe that under the hypotheses of all theorems we have the corresponding spectral convergence, namely, the convergence of the spectrum and the associated spectral projectors – see, for instance, [37, Thms. VIII.23, VIII.24]. We also stress that in all Theorems 2.1–2.5 the resolvent convergence is established in the sense of the uniform norm of bounded operator acting from $L_2(\Omega_0)$ into $W_2^1(\Omega_\varepsilon)$.

In the case of the Dirichlet conditions on Γ_ε , the homogenized operator has the same condition on Γ_0 no matter how the boundary Γ_ε oscillates, slowly or highly. The estimate for the rate of convergence is also universal being $\mathcal{O}(\eta^{1/2})$. Despite here we consider a periodically oscillating boundary, in the proof of Theorem 2.1 this fact

is not used. This is why its statement is also valid for a periodically oscillating boundary described by the equation $x_2 = \eta b(x_1, \varepsilon)$, where b is an arbitrary function bounded uniformly in ε and such that $b(\cdot, \varepsilon) \in C(\mathbb{R})$. The estimate in Theorem 2.1 is sharp, see the discussion in the end of Sec. 2 in [34].

A similar situation occurs if we have Neumann conditions on Γ_ε . Here, Theorem 2.2 says that the homogenized operator is subject to Neumann conditions on Γ_0 and the rate of the uniform resolvent convergence is the same as in Theorem 2.1, namely, $\mathcal{O}(\varepsilon^{1/2})$. This estimate is again sharp, as the example in the end of Sec. 3 in [34] shows.

Once we have Robin conditions on Γ_ε , the situation is completely different. If the boundary oscillates slowly, the homogenized operator still has Robin conditions on Γ_0 , but the coefficient depends on the geometry of the original oscillations, cf. (2.7). The estimate for the rate of the resolvent convergence in this case involves an additional term in comparison with the Dirichlet or Neumann cases, cf. Theorem 2.3. The estimate in this theorem is again sharp, see the example in the end of Sec. 3 in [34].

As boundary Γ_ε oscillates relatively highly, the resolvent convergence changes dramatically. If coefficient a is strictly positive, the homogenized operator has Dirichlet conditions on Γ_0 . A new term, $\varepsilon^{1/2}\eta^{-1/2}$, appears in the estimate for the rate of the uniform resolvent convergence, cf. Theorem 2.4. We are able to prove that this term is sharp, see the discussion in the end of Sec. 4 in [34].

Provided function a is non-negative and vanishes only on a set of zero measure, the homogenized operator still has Dirichlet conditions on Γ_0 , but the estimate for the rate of the uniform resolvent convergence becomes worse. Namely, the behavior of a in a vicinity of its zeroes becomes important. This is reflected by functions $\mu(\delta)$ and δ in (2.12). The latter should be chosen so that $\delta \rightarrow +0$, $\varepsilon^{1/2}\eta^{-1/2}\delta^{-1/2} \rightarrow +0$, $\varepsilon \rightarrow +0$, that is always possible. The optimal choice of δ is so that:

$$\begin{aligned} \mu^{1/2}(\delta) |\ln \mu(\delta)|^{1/2} &\sim \varepsilon^{1/2} \eta^{-1/2} \delta^{-1/2}, \\ \delta \mu(\delta) |\ln \mu(\delta)| &\sim \varepsilon \eta^{-1}. \end{aligned} \quad (2.13)$$

As we see, the choice of δ depends on a particular structure of $\mu(\delta)$. The most typical case is $\mu(\delta) \sim \delta^{1/2}$, i.e., the function a vanishes by the quadratic law in a vicinity of its zeroes. In this case, condition (2.13) becomes:

$$\delta^{3/2} |\ln \delta| \sim \varepsilon \eta^{-1},$$

which implies:

$$\delta \sim \varepsilon^{2/3} \eta^{-2/3} |\ln \varepsilon \eta^{-1}|^{-2/3}.$$

Then, the estimate for the resolvent convergence in Theorem 2.5 is of order $\mathcal{O}((\eta^{1/2} + \varepsilon^{1/6} \eta^{-1/6} |\ln \varepsilon \eta^{-1}|^{1/3}))$.

We are not able to prove the sharpness of estimate (2.12), but in the end of Sec. 4 in [34] we provide some arguments showing that estimate (2.12) is rather close to being optimal.

In conclusion, we discuss the case of Robin conditions on highly oscillating Γ_ε when the coefficient a does not satisfy the hypotheses of Theorems 2.4, 2.5. If it is still non-negative but vanishes for a set of non-zero values, and at the end-points of this set the vanishing happens with certain rate like in Theorem 2.5, we conjecture that the homogenized operator involves mixed Dirichlet and Neumann conditions on Γ_0 . Namely, if $a(x_1, 0) \equiv 0$ on Γ_0^N and $a(x_1, 0) > 0$ on Γ_0^D , $\Gamma_0 = \Gamma_0^N \cup \Gamma_0^D$, it is natural to expect that the homogenized operator has Neumann conditions on Γ_0^N and Dirichlet one on Γ_0^D . This conjecture can be regarded as the mixture of the statements of Theorems 2.2 and 2.5. The main difficulty of proving this conjecture is that the domain of such homogenized operator is no longer a subset of $W_2^2(\Omega_0)$ because of the mixed boundary conditions. At the same time, this fact was essentially used in all our proofs. An even more complicated situation occurs once a is negative or sign-indefinite. If a is negative on a set of non-zero measure, it can be shown that the bottom of the spectrum of the perturbed operator goes to $-\infty$ as $\varepsilon \rightarrow +0$. In such cases, one should study the resolvent convergence near this bottom, i.e., for the spectral parameter tending to $-\infty$. This makes the issue quite troublesome. We stress that under the hypotheses of all Theorems 2.1–2.5, the bottom of the spectrum is lower-semibounded uniformly in ε .

References

- [1] Friedman A., Hu B., Liu Y. A boundary value problem for the poisson equation with multi-scale oscillating Boundary. *J. Diff. Eq.*, 1997, **137**, P. 54–93.
- [2] Friedman A., Hu B. A Non-stationary Multi-scale Oscillating Free Boundary for the Laplace and Heat Equations. *J. Diff. Eq.*, 1997, **137**, P. 119–165.
- [3] Belyaev A.G., Pyatnitskii A.L., Chechkin G.A. Asymptotic behavior of a solution to a boundary value problem in a perforated domain with oscillating boundary. *Siberian Math. J.*, 1998, **39**, P. 621–644.
- [4] Kozlov V.A., Nazarov S.A. Asymptotics of the spectrum of the Dirichlet problem for the biharmonic operator in a domain with a deeply indented boundary. *St. Petersburg Math. J.*, 2011, **22**, P. 941–983.
- [5] Chechkin G.A., Chechkina T.P. On homogenization of problems in domains of the “Infusorium” type. *J. Math. Sci., New York*, 2004, **120**, P. 1470–1482.

- [6] Mikielić A. *Rough boundaries and wall laws. Qualitative properties of solutions to partial differential equations, Lecture notes of Necas Center for mathematical modeling*, ed. by E. Feireisl, P. Kaplicky and J. Malek, Vol. 5, Matfyzpress, Publishing House of the Faculty of Mathematics and Physics Charles University in Prague, Prague, 2009, P. 103–134.
- [7] Nazarov S.A. The two terms asymptotics of the solutions of spectral problems with singular perturbations. *Math. USSR-Sb.*, 1991, **69**, P. 307–340.
- [8] Nazarov S.A. Dirichlet problem in an angular domain with rapidly oscillating boundary: Modeling of the problem and asymptotics of the solution. *St. Petersburg Math. J.*, 2008, **19**, P. 297–326.
- [9] Amirat Y., Chechkin G.A., Gadyl'shin R.R. Asymptotics for eigenelements of Laplacian in domain with oscillating boundary: multiple eigenvalues. *Appl. Anal.*, 2007, **86**, P. 873–897.
- [10] Amirat Y., Chechkin G.A., Gadyl'shin R.R. Asymptotics of simple eigenvalues and eigenfunctions for the Laplace operator in a domain with oscillating boundary. *Computational Mathematics and Mathematical Physics*, 2006, **46**, P. 97–110.
- [11] Nazarov S.A. Asymptotics of solutions and modeling the problems of elasticity theory in domains with rapidly oscillating boundaries. *Izv. Math.*, 2008, **72**.
- [12] Gobbert M.K., Ringhofer C.A. An Asymptotic Analysis for a Model of Chemical Vapor Deposition on a Microstructured Surface. *SIAM Jour. Appl. Math.*, 1998, **58**, P. 737–752.
- [13] Olejnik O.A., Shamaev A.S., Yosifyan G.A. *Mathematical problems in elasticity and homogenization*. Studies in Mathematics and its Applications. **26**, North-Holland, Amsterdam etc., 1992.
- [14] Bunoiu R., Cardone G., Suslina T. Spectral approach to homogenization of an elliptic operator periodic in some directions. *Math. Meth. Appl. Sci.*, 2011, **34**, P. 1075–1096.
- [15] Cardone G., Pastukhova S.E., Zhikov V.V. Some estimates for nonlinear homogenization. *Rend. Accad. Naz. Sci. XL Mem. Mat. Appl.*, 2005, **29**, P. 101–110.
- [16] Cardone G., Pastukhova S.E., Perugia C. Estimates in homogenization of degenerate elliptic equations by spectral method. *Asympt. Anal.*, 2013, **81**, P. 189–209.
- [17] Pastukhova S.E., Tikhomirov R.N. Operator Estimates in Reiterated and Locally Periodic Homogenization. *Dokl. Math.*, 2006, **76**, P. 548–553.
- [18] Pastukhova S.E. Some Estimates from Homogenized Elasticity Problems. *Dokl. Math.*, 2006, **73**, P. 102–106.
- [19] Birman M.S. On homogenization procedure for periodic operators near the edge of an internal gap. *St. Petersburg Math. J.*, 2004, **15**, P. 507–513.
- [20] Birman M.S., Suslina T.A. Homogenization of a multidimensional periodic elliptic operator in a neighbourhood of the edge of the internal gap. *J. Math. Sciences*, 2006, **136**, P. 3682–3690.
- [21] Birman M.S., Suslina T.A. Homogenization with corrector term for periodic elliptic differential operators. *St. Petersburg Math. J.*, 2006, **17**, P. 897–973.
- [22] Birman M.S., Suslina T.A. Homogenization with corrector for periodic differential operators. Approximation of solutions in the Sobolev class $H^1(\mathbb{R}^d)$. *St. Petersburg Math. J.*, 2007, **18**, P. 857–955.
- [23] Vasilevskaya E.S., Suslina T.A. Threshold approximations for a factorized selfadjoint operator family with the first and second correctors taken into account. *St. Petersburg Math. J.*, 2012, **23**, P. 275–308.
- [24] Zhikov V.V. On operator estimates in homogenization theory. *Dokl. Math.*, 2005, **72**, P. 534–538.
- [25] Zhikov V.V. Spectral method in homogenization theory. *Proc. Steklov Inst. Math.*, 2005, **250**, P. 85–94.
- [26] Zhikov V.V. Some estimates from homogenization theory. *Dokl. Math.*, 2006, **73**, P. 96–99.
- [27] Zhikov V.V., Pastukhova S.E., Tikhomirova S.V. On the homogenization of degenerate elliptic equations. *Dokl. Math.*, 2006, **74**, P. 716–720.
- [28] Borisov D., Bunoiu R., Cardone G. On a waveguide with frequently alternating boundary conditions: homogenized Neumann condition. *Ann. H. Poincaré*, 2010, **11**, P. 1591–1627.
- [29] Borisov D., Bunoiu R., Cardone G. On a waveguide with an infinite number of small windows. *C.R. Mathématique*, 2011, **349**, P. 53–56.
- [30] Borisov D., Bunoiu R., Cardone G. Homogenization and asymptotics for a waveguide with an infinite number of closely located small windows. *J. of Math. Sci.*, 2009, **176**, P. 774–785.
- [31] Borisov D., Bunoiu R., Cardone G. Waveguide with non-periodically alternating Dirichlet and Robin conditions: homogenization and asymptotics. *Z. Ang. Math. Phys.*, 2013, **64** (3), P. 439–472.
- [32] Borisov D., Cardone G. Homogenization of the planar waveguide with frequently alternating boundary conditions. *J. of Phys. A: Mathematics and General*, 2009, **42**, P. 365205 (21 pp.).
- [33] Chechkin G.A., Friedman A., Piatnitski A.L. The Boundary-value Problem in Domains with Very Rapidly Oscillating Boundary. *J. Math. Anal. Appl.*, 1999, **231**, P. 213–234.
- [34] Borisov D., Cardone G., Faella L., Perugia C. Uniform resolvent convergence for a strip with fast oscillating boundary. *J. Diff. Eq.*, 2013, **255**, P. 4378–4402.
- [35] Ladyzhenskaya O.A., Ural'tseva N.N. *Linear and quasilinear elliptic equations*. Academic Press, New York, 1968.
- [36] Borisov D. Asymptotics for the solutions of elliptic systems with fast oscillating coefficients. *St. Petersburg Math. J.*, 2009, **20**, P. 175–191.
- [37] Reed M., Simon B. *Methods of mathematical physics. Functional analysis*, Academic Press, 1980.

Coupling of definitizable operators in Kreĭn spaces

V. Derkach^{1,2}, C. Trunk³

¹Department of Mathematics, Dragomanov National Pedagogical University, Pirogova 9, Kiev, 01601, Ukraine

²Department of Mathematics, Vasyl Stus Donetsk National University, 600-Richchya Str 21, Vinnytsya, 21021, Ukraine

³Institut für Mathematik, Technische Universität Ilmenau, Postfach 100565, D-98684 Ilmenau, Germany

derkach.v@gmail.com, carsten.trunk@tu-ilmenau.de

DOI 10.17586/2220-8054-2017-8-2-166-179

Indefinite Sturm–Liouville operators defined on \mathbb{R} are often considered as a coupling of two semibounded symmetric operators defined on \mathbb{R}^+ and \mathbb{R}^- , respectively. In many situations, those two semibounded symmetric operators have in a special sense good properties like a Hilbert space self-adjoint extension.

In this paper, we present an abstract approach to the coupling of two (definitizable) self-adjoint operators. We obtain a characterization for the definitizability and the regularity of the critical points. Finally we study a typical class of indefinite Sturm–Liouville problems on \mathbb{R} .

Keywords: self-adjoint extension, symmetric operator, Kreĭn space, locally definitizable operator, coupling of operators, boundary triple, Weyl function, regular critical point.

Received: 18 January 2017

Revised: 1 February 2017

1. Introduction

Let \mathcal{K} be a Hilbert space with the inner product (\cdot, \cdot) and let J be a linear operator in \mathcal{K} , such that $J = J^* = J^{-1}$. The space \mathcal{K} endowed with Hermitian sesquilinear form $[\cdot, \cdot]_{\mathcal{K}} = (J\cdot, \cdot)$ is called a *Kreĭn space* and is denoted by $(\mathcal{K}, [\cdot, \cdot]_{\mathcal{K}})$, for details see [1, 2] or Section 2.1 below.

The Hermitian sesquilinear form $[\cdot, \cdot]_{\mathcal{K}}$ induces in an obvious way a sign type spectrum for linear operators. In the last two decades, this notion was frequently used in theoretical physics in connection with \mathcal{PT} -symmetric problems; here, we mention only [3–7] and in the study of \mathcal{PT} -symmetric operators, we refer to [8–11].

A self-adjoint operator A in a Kreĭn space $(\mathcal{K}, [\cdot, \cdot]_{\mathcal{K}})$ is said to be *definitizable* [12], if its resolvent set $\rho(A)$ is nonempty and there exists a real polynomial p such that $p(A)$ is nonnegative in $(\mathcal{K}, [\cdot, \cdot]_{\mathcal{K}})$. If $\alpha_1 < \alpha_2 < \dots < \alpha_N$ is the set of all real zeros of p , then there exists a spectral function $E(\Delta)$ of A , which is defined on all intervals Δ , such that the endpoints of Δ do not belong to the set $\{\alpha_j\}_{j=1}^N$, $E(\Delta)$ takes values in the set of orthogonal projections, commuting with A and $E(\Delta)$ is monotone on each interval (α_j, α_{j+1}) . These intervals are classified in [12] as intervals of positive and negative type and the points α_j which are spectral points of neither positive type nor negative type are called *critical*, see exact denitions in Section 2.2. A critical point α is called *regular*, if the operators $E(\Delta)$ are uniformly bounded for all small Δ containing α , otherwise it is called *singular*. The set of critical points of A is denoted by $c(A)$, the set of regular (singular) critical points of A is denoted by $c_r(A)$ ($c_s(A)$, respectively). The notion of local definitizability of a self-adjoint operator A in a Kreĭn space $(\mathcal{K}, [\cdot, \cdot]_{\mathcal{K}})$ was introduced in [13, 14], see Section 3 below.

In the present paper, the following problem is studied: the problem of the definitizability of the coupling A of two symmetric operators A_+ and A_- and the regularity of their critical points. Note the definition of the coupling from [15] adapted to the case of Kreĭn spaces. Let a Kreĭn space $(\mathcal{K}, [\cdot, \cdot]_{\mathcal{K}})$ be the orthogonal sum $\mathcal{K} = \mathcal{K}_+ \dot{+} \mathcal{K}_-$ of $(\mathcal{K}, [\cdot, \cdot]_{\mathcal{K}})$ of two Kreĭn spaces $(\mathcal{K}_+, [\cdot, \cdot]_{\mathcal{K}_+})$ and $(\mathcal{K}_-, [\cdot, \cdot]_{\mathcal{K}_-})$, such that the subspaces:

$$\mathcal{D}_+ = \{f \in \mathcal{K}_+ \cap (\text{dom } A) : Af \in \mathcal{K}_+\} \quad \text{and} \quad \mathcal{D}_- = \{f \in \mathcal{K}_- \cap (\text{dom } A) : Af \in \mathcal{K}_-\}$$

are dense in \mathcal{K}_+ and \mathcal{K}_- and the restrictions:

$$A_+ = A|_{\mathcal{D}_+} \quad \text{and} \quad A_- = A|_{\mathcal{D}_-}$$

are symmetric operators with defect numbers $(1, 1)$ in the Kreĭn spaces $(\mathcal{K}_+, [\cdot, \cdot]_{\mathcal{K}_+})$ and $(\mathcal{K}_-, [\cdot, \cdot]_{\mathcal{K}_-})$, respectively. The operator A is called a *coupling* of two symmetric operators A_+ and A_- . The coupling A of two symmetric operators A_+ and A_- is not uniquely defined by the above definition. We will make this definition more precise in Theorem 4.4 by using the boundary triple approach developed in [16–19]. For differential operators with indefinite weights, the coupling method was used in [20], and also in [21–23] to study the similarity problem and in [24] to study definitizability.

The main result of the paper is Theorem 4.6, where conditions for regularity of the critical point $\infty \in c(A)$ are found under the assumptions that the symmetric operators A_+ and A_- admit definitizable and semibounded extensions $A_{+,0}$ and $A_{-,0}$. The proof is based on the K. Veselić criterion of regularity [25,26] adapted to the case of definitizable operators in [27]. In the case when A_+ and A_- are Hilbert space symmetric operators, similar results were obtained in [23] and [28].

Typically, such problems arise in the study of indefinite Sturm–Liouville operators:

$$\ell(f)(t) := \frac{\operatorname{sgn} t}{w(t)} \left(-\frac{d}{dt} \left(\frac{df}{r(t)dt} \right) + q(t)f(t) \right) \quad \text{for a.a. } t \in \mathbb{R}, \quad (1.1)$$

where the coefficients r , q and w are real functions on \mathbb{R} satisfying the conditions:

- (C1) $r, q, w \in L^1_{\text{loc}}(\mathbb{R})$ and $r, w > 0$ a.e. on \mathbb{R} ,
- (C2) the expression ℓ is in the limit point case at $-\infty$ and at $+\infty$,
- (C3) minimal differential operators B_{\pm} generated by $\pm\ell$ in $L^2_w(\mathbb{R}_{\pm})$ are semibounded from below.

The operator A generated by the differential expression (1.1) in the Kreĩn space is the coupling of two semibounded symmetric operators $A_{\pm} := \pm B_{\pm}$. In Proposition 5.1, it is shown that the operator A is definitizable over a vicinity of ∞ and conditions (4.18) for $\infty \notin c_s(A)$ are formulated in terms of the m -coefficients for the operators B_{\pm} . In the case $w \equiv 1$, the conditions (4.18) are fulfilled automatically [28]. This fact was proved earlier by another method in [29].

1.1. Notations and preliminaries

By \mathbb{C}_+ , we denote the set of all $z \in \mathbb{C}$ with positive imaginary part and we set $\overline{\mathbb{C}} := \mathbb{C} \cup \{\infty\}$ and $\overline{\mathbb{R}} := \mathbb{R} \cup \{\infty\}$.

A complex function m is called a *Nevanlinna function* if m is holomorphic at least on $\mathbb{C} \setminus \mathbb{R}$ and satisfies the following two conditions:

$$m(\bar{z}) = \overline{m(z)} \quad \text{and} \quad \operatorname{Im} m(z) \geq 0, \quad \text{for all } z \in \mathbb{C}_+. \quad (1.2)$$

For information on Nevanlinna functions, we refer readers to [30] and [31, Chapter II].

All operators in this paper are closed densely defined linear operators. For such an operator T , we use the common notation $\rho(T)$, $\operatorname{dom}(T)$, $\operatorname{ran}(T)$ and $\ker(T)$ for the resolvent set, the domain, the range and the null-space, respectively, of T . We define the extended spectrum $\tilde{\sigma}(A)$ of A by $\tilde{\sigma}(A) := \sigma(A)$ if A is bounded and $\tilde{\sigma}(A) := \sigma(A) \cup \{\infty\}$ if A is unbounded and we set $\tilde{\rho}(A) := \overline{\mathbb{C}} \setminus \tilde{\sigma}(A)$.

2. Definitizable operators in Kreĩn spaces

2.1. Kreĩn spaces

We recall standard notation and some basic results on Kreĩn spaces. For a complete exposition on the subject (and the proofs of the results below) see the books by Azizov and Iokhvidov [1] and Bognár [2]. A vector space \mathcal{K} with a Hermitian sesquilinear form $[\cdot, \cdot]_{\mathcal{K}}$ is called a *Kreĩn space* if there exists a so-called *fundamental decomposition*

$$\mathcal{K} = \mathcal{K}_+ \dot{+} \mathcal{K}_-,$$

such that $(\mathcal{K}_+, [\cdot, \cdot]_{\mathcal{K}})$ and $(\mathcal{K}_-, -[\cdot, \cdot]_{\mathcal{K}})$ are Hilbert spaces which are orthogonal to each other with respect to $[\cdot, \cdot]_{\mathcal{K}}$. Those two Hilbert spaces induce in a natural way a Hilbert space inner product (\cdot, \cdot) and, hence, a Hilbert space topology on the Kreĩn space \mathcal{K} . Observe that the indefinite metric $[\cdot, \cdot]_{\mathcal{K}}$ and the Hilbert space inner product (\cdot, \cdot) of \mathcal{K} are related by means of a *fundamental symmetry*, i.e. a unitary self-adjoint operator J which satisfies

$$(x, y) = [Jx, y]_{\mathcal{K}} \quad \text{for } x, y \in \mathcal{K}. \quad (2.1)$$

If \mathcal{H} and \mathcal{K} are Kreĩn spaces and $T : \mathcal{H} \rightarrow \mathcal{K}$ a bounded operator, the adjoint operator T^+ of T with respect to the Kreĩn spaces \mathcal{H} and \mathcal{K} is defined by:

$$T^+ := J_{\mathcal{H}} T^* J_{\mathcal{K}},$$

where $J_{\mathcal{H}}$ and $J_{\mathcal{K}}$ are the fundamental symmetries associated with \mathcal{H} and \mathcal{K} , respectively; the operator T^+ satisfies $[Tx, y]_{\mathcal{K}} = [x, T^+y]_{\mathcal{K}}$ for all $x \in \mathcal{H}$, $y \in \mathcal{K}$. If A is a densely defined operator in \mathcal{K} then the *adjoint* A^+ of A with respect to $[\cdot, \cdot]_{\mathcal{K}}$ is defined analogously. In fact, if J is a fundamental symmetry on $(\mathcal{K}, [\cdot, \cdot]_{\mathcal{K}})$ and (\cdot, \cdot) is the corresponding Hilbert space inner product (2.1), then $A^+ = JA^*J$. The operator A^+ satisfies the following:

$$[Ax, y]_{\mathcal{K}} = [x, A^+y]_{\mathcal{K}} \quad \text{for all } x \in \operatorname{dom}(A), y \in \operatorname{dom}(A^+).$$

By analogy with the definitions in Hilbert spaces, A is *symmetric in* $(\mathcal{K}, [\cdot, \cdot]_{\mathcal{K}})$ if A^+ is an extension of A and A is *self-adjoint in* $(\mathcal{K}, [\cdot, \cdot]_{\mathcal{K}})$ if $A = A^+$.

A densely defined operator A is called *nonnegative in* $(\mathcal{K}, [\cdot, \cdot]_{\mathcal{K}})$ if $[Af, f]_{\mathcal{K}} \geq 0$ for all $f \in \text{dom}(A)$. A nonnegative self-adjoint operator in a Kreĭn space can have an empty resolvent set; a specific example is given in [12, Section 1.2] and [2, Example VII.1.5]. But if a nonnegative self-adjoint operator in a Kreĭn space also has a nonempty resolvent set, then it has real spectrum only.

An operator A is called *semibounded from below* in the Kreĭn spaces $(\mathcal{K}, [\cdot, \cdot]_{\mathcal{K}})$, if there exists $\alpha \in \mathbb{R}$ such that:

$$[Af, f]_{\mathcal{K}} \geq \alpha[f, f]_{\mathcal{K}}, \quad f \in \text{dom}(A).$$

2.2. Definitizable operators

In this section, we recall some facts on definitizable operators in Kreĭn spaces. For an overview, we refer to [32], see also [33]. For this purpose, it is convenient to introduce in Definition 2.1 below the notion of sign-type spectra, cf. [34–37].

Let A be a closed operator in a Kreĭn space $(\mathcal{K}, [\cdot, \cdot]_{\mathcal{K}})$. A point $\lambda_0 \in \mathbb{C}$ is said to belong to the *approximative point spectrum* $\sigma_{ap}(A)$ of A if there exists a sequence (x_n) in $\text{dom}(A)$ with $\|x_n\| = 1$, $n = 1, 2, \dots$, and $\|(A - \lambda_0)x_n\| \rightarrow 0$ if $n \rightarrow \infty$. For a self-adjoint operator A in $(\mathcal{K}, [\cdot, \cdot]_{\mathcal{K}})$, all real spectral points of A belong to $\sigma_{ap}(A)$ (see e.g. [2, Corollary VI.6.2]).

Definition 2.1. For a self-adjoint operator A in $(\mathcal{K}, [\cdot, \cdot]_{\mathcal{K}})$ a point $\lambda_0 \in \sigma(A)$ is called a spectral point of *positive (negative) type* of A if $\lambda_0 \in \sigma_{ap}(A)$ and for every sequence (x_n) in $\text{dom}(A)$ with $\|x_n\| = 1$, $n = 1, 2, \dots$, and $\|(A - \lambda_0)x_n\| \rightarrow 0$ for $n \rightarrow \infty$, we have:

$$\liminf_{n \rightarrow \infty} [x_n, x_n]_{\mathcal{K}} > 0 \quad (\text{resp. } \limsup_{n \rightarrow \infty} [x_n, x_n]_{\mathcal{K}} < 0).$$

The point ∞ is said to be a point of *positive (negative) type* of the extended spectrum of A if A is unbounded and for every sequence (x_n) in $\text{dom}(A)$ with $\lim_{n \rightarrow \infty} \|x_n\| = 0$ and $\|Ax_n\| = 1$, $n = 1, 2, \dots$, we have:

$$\liminf_{n \rightarrow \infty} [Ax_n, Ax_n]_{\mathcal{K}} > 0 \quad (\text{resp. } \limsup_{n \rightarrow \infty} [Ax_n, Ax_n]_{\mathcal{K}} < 0).$$

We denote the set of all points of $\tilde{\sigma}(A)$ of positive (negative) type by $\sigma_{++}(A)$ (resp. $\sigma_{--}(A)$). Points from $\tilde{\sigma}(A)$ of neither positive nor negative type are called *critical*. In the following proposition, we collect some properties. For a proof, we refer to [34].

Proposition 2.2. (i) The sets $\sigma_{++}(A)$ and $\sigma_{--}(A)$ are contained in $\overline{\mathbb{R}}$.
(ii) The non-real spectrum of A cannot accumulate to $\sigma_{++}(A) \cup \sigma_{--}(A)$.
(iii) The sets $\sigma_{++}(A)$ and $\sigma_{--}(A)$ are relatively open in $\tilde{\sigma}(A)$.
(iv) Let λ_0 be a point of $\sigma_{++}(A)$ ($\sigma_{--}(A)$, respectively). Then there exists an open vicinity \mathcal{U} in $\overline{\mathbb{C}}$ of λ_0 and a number $M > 0$ such that:

$$\|(A - \lambda)^{-1}\| \leq \frac{M}{|\text{Im } \lambda|} \quad \text{for all } \lambda \in \mathcal{U} \setminus \overline{\mathbb{R}}.$$

We shall say that an open subset Δ of $\overline{\mathbb{R}}$ is of *positive type (negative type)* with respect to A if:

$$\Delta \cap \tilde{\sigma}(A) \subset \sigma_{++}(A) \quad (\text{resp. } \Delta \cap \tilde{\sigma}(A) \subset \sigma_{--}(A)).$$

An open set Δ of $\overline{\mathbb{R}}$ is called of *definite type* if Δ is of positive or of negative type with respect to A . If we relate Definition 2.1 to nonnegative operators in Kreĭn spaces (cf. Section 2.1), we obtain from the properties of the spectral function of a nonnegative operator in a Kreĭn space, see, e.g., [1, 32, 38], and [34, Proposition 25] the following.

Proposition 2.3. Let A be a nonnegative operator with $\rho(A) \neq \emptyset$ in a Kreĭn space $(\mathcal{K}, [\cdot, \cdot]_{\mathcal{K}})$. Then $c(A) \subset \{0, \infty\}$ and

$$\sigma(A) \cap (0, \infty) \subset \sigma_{++}(A) \subset \overline{\mathbb{R}} \setminus (-\infty, 0), \quad \sigma(A) \cap (-\infty, 0) \subset \sigma_{--}(A) \subset \overline{\mathbb{R}} \setminus (0, \infty).$$

In particular, we have:

$$c(A) = \tilde{\sigma}(A) \setminus (\sigma_{++}(A) \cup \sigma_{--}(A)). \quad (2.2)$$

A generalization of the class of nonnegative operators in Kreĭn spaces is given by the class of definitizable operators. Recall, that a self-adjoint operator A in a Kreĭn space $(\mathcal{K}, [\cdot, \cdot]_{\mathcal{K}})$ is called *definitizable* if $\rho(A) \neq \emptyset$ and if there exists a rational function $p \neq 0$ having poles only in $\rho(A)$ such that $[p(A)x, x]_{\mathcal{K}} \geq 0$ for all $x \in \mathcal{K}$. Such a function p is called *definitizing function* for A . Then the spectrum of A is real or its non-real part consists

of a finite number of points. Inspired by Proposition 2.3 we introduce the set of *critical points* of a definitizable operator A via:

$$c(A) := \tilde{\sigma}(A) \setminus (\sigma_{++}(A) \cup \sigma_{--}(A)). \quad (2.3)$$

It is known (cf. [32]) that $c(A)$ is contained in $\{t \in \mathbb{R} : p(t) = 0\} \cup \{\infty\}$.

For the definitizable operator A , the spectral function $E(\Delta)$ can be introduced for every interval Δ such that the endpoints of Δ belong to intervals of definite type, see [32], [14]. We mention only that $E(\Delta)$ is defined and is a self-adjoint projection in $(\mathcal{K}, [\cdot, \cdot]_{\mathcal{K}})$ for every such interval. Moreover,

$$(E(\Delta)\mathcal{K}, [\cdot, \cdot]_{\mathcal{K}}) \text{ is a Hilbert space whenever } \Delta \subset \{t \in \mathbb{R} : p(t) > 0\}. \quad (2.4)$$

If a critical point α is the endpoint of two intervals (λ_1, α) and (α, λ_2) of the definite type, then the sequences $E([\lambda_1, t])$ and $E([t, \lambda_2])$ are monotone in (λ_1, α) and (α, λ_2) , resp. The point α is called a *regular critical point* of A , if the limits

$$\lim_{t \uparrow \alpha} E([\lambda_1, t]) \quad \text{and} \quad \lim_{t \downarrow \alpha} E([t, \lambda_2]) \quad (2.5)$$

exist in the strong operator topology. A critical point of A which is not regular is called *singular critical point* of A . The set of all singular critical points of A is denoted by $c_s(A)$.

In Subsection 4.2, we essentially use the following resolvent criterion of K. Veselić [25, 26] for $\infty \notin c_s(A)$. We state a special case of this criterion as it has appeared in [27, Corollary 1.6].

Theorem 2.4. *Let A be a definitizable self-adjoint operator in a Kreĭn space $(\mathcal{K}, [\cdot, \cdot]_{\mathcal{K}})$. Then:*

- (a) $\infty \notin c_s(A)$ if and only if there is $\eta_0 > 0$, such that the set of numbers:

$$\int_{\eta_0}^{\eta} \operatorname{Re} [(A - iy)^{-1}f, f]_{\mathcal{K}} dy \quad (\eta \in (\eta_0, \infty))$$

is bounded for every $f \in \mathcal{K}$.

- (b) Let $\xi_0 \in \mathbb{R}$. Then $\xi_0 \notin c_s(A)$ and $\ker(A - \xi_0) = \ker(A - \xi_0)^2$ if and only if there is $\eta_0 > 0$, such that the set of numbers:

$$\int_{\eta}^{\eta_0} \operatorname{Re} [(A - \xi_0 - iy)^{-1}f, f]_{\mathcal{K}} dy \quad (\eta \in (0, \eta_0))$$

is bounded for every $f \in \mathcal{K}$.

A characterization of definitizable operators via their sign-type spectrum together with some growth conditions for the resolvent is provided by the following theorem. Its proof follows from [35, Definition 4.4 and Theorem 4.7].

Theorem 2.5. *Let A be a self-adjoint operator in the Kreĭn space $(\mathcal{K}, [\cdot, \cdot]_{\mathcal{K}})$. Then A is definitizable if and only if the following holds.*

- (i) *The non-real spectrum $\sigma(A) \setminus \mathbb{R}$ consists of isolated points which are poles of the resolvent of A , and no point of $\overline{\mathbb{R}}$ is an accumulation point of the non-real spectrum $\sigma(A) \setminus \mathbb{R}$ of A .*
(ii) *There is an open vicinity \mathcal{U} of $\overline{\mathbb{R}}$ in $\overline{\mathbb{C}}$ and numbers $m \geq 1$, $M > 0$ with*

$$\|(A - \lambda)^{-1}\| \leq M(|\lambda| + 1)^{2m-2} |\operatorname{Im} \lambda|^{-m} \quad \text{for all } \lambda \in \mathcal{U} \setminus \overline{\mathbb{R}}.$$

- (iii) *Every point $\lambda \in \overline{\mathbb{R}}$ has an open connected vicinity I_{λ} in $\overline{\mathbb{R}}$ such that both components of $I_{\lambda} \setminus \{\lambda\}$ are of definite type with respect to A .*

3. Locally definitizable operators and their direct sum

3.1. Locally definitizable operators in Kreĭn spaces

In view of Theorem 2.5, it is natural to introduce a local version of definitizability which will play an important role in the following. The next notion is due to P. Jonas, see [13, 14], we mention also the overview in [39].

Definition 3.1. Let Ω be a domain in $\overline{\mathbb{C}}$ which is symmetric with respect to \mathbb{R} such that $\Omega \cap \overline{\mathbb{R}} \neq \emptyset$ and the intersections with the open upper and lower half-plane are simply connected. Let A be a self-adjoint operator in the Kreĭn space $(\mathcal{K}, [\cdot, \cdot]_{\mathcal{K}})$. The operator A is called *definitizable over Ω* if the following holds:

- (i) *The non-real spectrum in Ω , i.e. $\sigma(A) \cap (\Omega \setminus \overline{\mathbb{R}})$, consists of isolated points which are poles of the resolvent of A , and no point of $\Omega \cap \overline{\mathbb{R}}$ is an accumulation point of the non-real spectrum $\sigma(A) \setminus \mathbb{R}$ of A .*

- (ii) For every closed subset Δ of $\Omega \cap \overline{\mathbb{R}}$ there exist an open vicinity \mathcal{U} of Δ in $\overline{\mathbb{C}}$ and numbers $m \geq 1$, $M > 0$ such that

$$\|(A - \lambda)^{-1}\| \leq M(|\lambda| + 1)^{2m-2} |\operatorname{Im} \lambda|^{-m} \quad \text{for all } \lambda \in \mathcal{U} \setminus \overline{\mathbb{R}}.$$

- (iii) Every point $\lambda \in \Omega \cap \overline{\mathbb{R}}$ has an open connected vicinity I_λ in $\overline{\mathbb{R}}$ such that both components of $I_\lambda \setminus \{\lambda\}$ are of definite type with respect to A .

Let A be definitizable over Ω . Similar as in (2.3) we call a point $t \in \Omega \cap \overline{\mathbb{R}}$ a *critical point* of the operator A if there is no open subset Δ of definite type with $t \in \Delta$. The set of critical points of A is denoted by $c(A)$. As in Section 2.1, critical points admit a classification into singular and regular critical points: If for some $\lambda \in c(A) \setminus \{\infty\}$ the limits analogous to (2.5) exist, then λ is called a *regular critical point* of A . If ∞ is a critical point of A and the limits (2.5) exist in the strong operator topology for some $\lambda_1, \lambda_2 \in \mathbb{R} \setminus \{0\}$, then ∞ is called *regular critical point* of A . A critical point of A which is not regular is called *singular critical point* of A . The set of all singular critical points of A is denoted by $c_s(A)$.

Theorem 2.4 has a counterpart for locally definitizable operators: Let A be definitizable over a vicinity Ω of ∞ . Then, A admits an orthogonal decomposition into two operators: a definitizable one with spectrum in $\overline{\Delta}$ and a self-adjoint one with spectrum outside Δ , where $\Delta (\subset \Omega)$ is a vicinity of ∞ , for details we refer to [35, Theorem 4.8]. Then, the following theorem follows easily from this decomposition and Theorem 2.4:

Theorem 3.2. *Let a self-adjoint operator A in a Kreĭn space $(\mathcal{K}, [\cdot, \cdot])$ be locally definitizable over a neighborhood Ω of ∞ . Then $\infty \notin c_s(A)$ if and only if there is $\eta_0 > 0$, such that the set of numbers:*

$$\int_{\eta_0}^{\eta} \operatorname{Re} [(A - iy)^{-1} f, f]_{\mathcal{K}} dy \quad (\eta \in (\eta_0, \infty)),$$

is bounded for every $f \in \mathcal{K}$.

Similarly, if $\xi_0 \in \mathbb{R}$ and A is locally definitizable over a vicinity Ω of ξ_0 , then $\xi_0 \notin c_s(A)$ and $\ker(A - \xi_0) = \ker(A - \xi_0)^2$ if and only if there is $\eta_0 > 0$, such that the set of numbers:

$$\int_{\eta}^{\eta_0} \operatorname{Re} [(A - \xi_0 - iy)^{-1} f, f]_{\mathcal{K}} dy \quad (\eta \in (0, \eta_0))$$

is bounded for every $f \in \mathcal{K}$.

Roughly speaking, the property of an operator to be definitizable or to be locally definitizable is stable under finite rank perturbations. This is made more precise in the following theorem which is taken from J. Behrndt [40, Theorem 2.2]:

Theorem 3.3. *Let A_0 and A_1 be self-adjoint operators in a Kreĭn space $(\mathcal{K}, [\cdot, \cdot]_{\mathcal{K}})$ with $\rho(A_0) \cap \rho(A_1) \neq \emptyset$ and assume that for some $\lambda_0 \in \rho(A_0) \cap \rho(A_1)$ the difference:*

$$(A_0 - \lambda_0)^{-1} - (A_1 - \lambda_0)^{-1}$$

is a finite rank operator. Then, A_0 is definitizable over Ω if and only if A_1 is definitizable over Ω .

Moreover, if A_0 is definitizable over Ω and $\delta \subset \Omega \cap \overline{\mathbb{R}}$ is an open interval with endpoint $\mu \in \Omega \cap \overline{\mathbb{R}}$ and the spectral points of A_0 in δ are only of positive type (negative type), then there exists an open interval δ' , $\delta' \subset \delta$, with endpoint μ such that the spectral points of A_1 in δ' are only of positive type (negative type, respectively).

Theorem 3.3 also holds for definitizable operators as the class of definitizable operators over $\overline{\mathbb{C}}$ coincides with the class of definitizable operators ([35, Theorem 4.7]). For definitizable operators, this fact is already contained in [41].

3.2. Local definitizability of the direct sum of two operators

In this section, we characterize the definitizability of an operator which is the direct sum of two definitizable operators. For this, we provide the following definition:

Definition 3.4. We shall say that the sets S_1 and S_2 , $S_1, S_2 \subset \overline{\mathbb{R}}$, are separated by a finite number of points if there exists a finite ordered set $\{\alpha_j\}_{j=1}^N$, $N \in \mathbb{N}$:

$$-\infty = \alpha_0 < \alpha_1 \leq \dots \leq \alpha_N < \alpha_{N+1} = +\infty,$$

such that one of the sets S_j , $j = 1, 2$, is a subset of $\bigcup_{k \text{ is even}} [\alpha_k, \alpha_{k+1}]$ and the other one is a subset of $\bigcup_{k \text{ is odd}} [\alpha_k, \alpha_{k+1}]$. Here, we agree that 0 is even, $[\alpha_0, \alpha_1]$ stands for $(-\infty, \alpha_1] \cup \{\infty\}$ and $[\alpha_N, \alpha_{N+1}]$ for $[\alpha_N, \infty) \cup \{\infty\}$.

The following theorem can be considered as a refinement of [42, Theorem 3.6]:

Theorem 3.5. *Consider two operators A and B where A is self-adjoint in the Kreĭn space $(\mathcal{K}_+, [\cdot, \cdot]_{\mathcal{K}_+})$ and B in $(\mathcal{K}_-, [\cdot, \cdot]_{\mathcal{K}_-})$. Let the direct sum of the two Kreĭn spaces:*

$$\mathcal{K} = \mathcal{K}_+ [+] \mathcal{K}_-,$$

be endowed with the natural inner product:

$$[f, g]_{\mathcal{K}} := [P_+ f, P_+ g]_{\mathcal{K}_+} + [P_- f, P_- g]_{\mathcal{K}_-} \quad (f, g \in \mathcal{K}), \quad (3.1)$$

where P_{\pm} are the orthogonal projections onto \mathcal{K}_{\pm} . Then, the sum of the operators $A [+] B$ is self-adjoint in the direct sum of the Kreĭn spaces \mathcal{K} with the natural inner product from (3.1). We set the following:

$$S_+ := \sigma_{++}(A) \cup \sigma_{++}(B) \quad \text{and} \quad S_- := \sigma_{--}(A) \cup \sigma_{--}(B).$$

Then, $A [+] B$ is definitizable if and only if the operators A and B are definitizable and S_+ and S_- are separated by a finite number of points.

Proof. The non-real-spectrum of $A [+] B$ coincides with the union of the non-real spectra of A and of B . Therefore, if $A [+] B$ is definitizable, then item (i) of Theorem 2.5 holds for A and for B . Conversely, if A and B are both definitizable, then (i) of Theorem 2.5 holds for $A [+] B$. Therefore, it is no restriction to assume that $A [+] B$, A , and B have real spectrum only.

If $A [+] B$ is definitizable, then by the definition of the inner product in $\mathcal{K} = \mathcal{K}_+ [+] \mathcal{K}_-$ a definitizing function p for $A [+] B$ is also a definitizing function for A and for B . From (2.4), we deduce:

$$\begin{aligned} \{t \in \mathbb{R} : p(t) > 0\} &\subset \sigma_{++}(A) \cup \rho(A), & \{t \in \mathbb{R} : p(t) < 0\} &\subset \sigma_{--}(A) \cup \rho(A), \\ \{t \in \mathbb{R} : p(t) > 0\} &\subset \sigma_{++}(B) \cup \rho(B), & \{t \in \mathbb{R} : p(t) < 0\} &\subset \sigma_{--}(B) \cup \rho(B), \end{aligned}$$

and, hence, the zeros of p are the points separating S_+ and S_- , cf. Definition 3.4.

It remains to prove the converse. We assume that S_+ and S_- are separated by the points $\{\alpha_0, \dots, \alpha_{N+1}\}$, cf. Definition 3.4, then we have:

$$S_+ \cap S_- \subset \{\alpha_0, \dots, \alpha_{N+1}\}.$$

Note that S_+ and $c(A)$ may have a non-empty intersection (and the same applies to $S_+ \cap c(B)$, $S_- \cap c(A)$, and $S_- \cap c(B)$). Indeed, let $\lambda \in \sigma_{++}(B)$ (and, hence, $\lambda \in S_+$) such that λ is an isolated spectral point of A which belongs to $c(A)$. Then, $\lambda \in S_+ \cap c(A)$ and, moreover as $\lambda \notin S_-$, we have in addition $\lambda \notin \{\alpha_0, \dots, \alpha_{N+1}\}$.

We define:

$$\Lambda := \{\alpha_0, \dots, \alpha_{N+1}\} \cup c(A) \cup c(B),$$

and for $\lambda \in S_+ \setminus \Lambda$, the following statements are true:

- (i) $\lambda \in \sigma_{++}(A) \cup \sigma_{++}(B)$ (as $\lambda \in S_+$),
- (ii) $\lambda \notin \sigma_{--}(A) \cup \sigma_{--}(B)$ (as $\lambda \notin S_-$),
- (iii) $\lambda \notin c(A) \cup c(B)$ (as $\lambda \notin \Lambda$).

Thus, by (2.2) applied to both A and B , we obtain:

$$\lambda \in \sigma_{++}(A) \cup \tilde{\rho}(A) \quad \text{and} \quad \lambda \in \sigma_{++}(B) \cup \tilde{\rho}(B).$$

This implies:

$$\lambda \in \sigma_{++}(A [+] B),$$

and we obtain:

$$S_+ \setminus \Lambda \subset \sigma_{++}(A [+] B), \quad (3.2)$$

and with similar arguments:

$$S_- \setminus \Lambda \subset \sigma_{--}(A [+] B). \quad (3.3)$$

From (2.2), we conclude:

$$\begin{aligned}\tilde{\sigma}(A[+]B) &= \tilde{\sigma}(A) \cup \tilde{\sigma}(B) \\ &= \sigma_{++}(A) \cup c(A) \cup \sigma_{--}(A) \cup \sigma_{++}(B) \cup c(B) \cup \sigma_{--}(B) \\ &= S_+ \cup c(A) \cup c(B) \cup S_- \subset S_+ \cup S_- \cup \Lambda.\end{aligned}\quad (3.4)$$

Obviously, for the operator $A[+]B$ the statements (i) and (ii) from Theorem 2.5 are satisfied as A and B are definitizable operators. It remains to show (iii). Clearly, for $\lambda \in \overline{\mathbb{C}} \setminus \tilde{\sigma}(A[+]B)$ (iii) in Theorem 2.5 is satisfied. Let $\lambda \in \tilde{\sigma}(A[+]B)$. If $\lambda \in (S_+ \cup S_-) \setminus \Lambda$ we deduce from (3.2) and (3.3) that either $\lambda \in \sigma_{++}(A[+]B)$ or $\lambda \in \sigma_{--}(A[+]B)$. As the sets $\sigma_{++}(A[+]B)$ and $\sigma_{--}(A[+]B)$ are relatively open in $\tilde{\sigma}(A[+]B)$ (cf. Proposition 2.2), (iii) follows. By (3.4), it remains to consider $\lambda \in \Lambda$. For $\lambda \in \{\alpha_0, \dots, \alpha_{N+1}\}$ (iii) follows from (3.2) and (3.3). Therefore, consider $\lambda \in c(A) \cup c(B)$. It is sufficient to consider $\lambda \in c(A) \setminus \{\alpha_0, \dots, \alpha_{N+1}\}$. It follows from the definition of the points $\{\alpha_0, \dots, \alpha_{N+1}\}$ and the fact that $\lambda \notin \{\alpha_0, \dots, \alpha_{N+1}\}$ that there exists open connected vicinities I_λ, J_λ in $\overline{\mathbb{R}}$ of λ with:

$$(I_\lambda \setminus \{\lambda\}) \cap \tilde{\sigma}(A) \subset \sigma_{++}(A) \quad \text{and} \quad (J_\lambda \setminus \{\lambda\}) \cap \tilde{\sigma}(B) \subset \sigma_{++}(B)$$

or

$$(I_\lambda \setminus \{\lambda\}) \cap \tilde{\sigma}(A) \subset \sigma_{--}(A) \quad \text{and} \quad (J_\lambda \setminus \{\lambda\}) \cap \tilde{\sigma}(B) \subset \sigma_{--}(B).$$

This shows $(I_\lambda \cap J_\lambda \setminus \{\lambda\}) \cap \tilde{\sigma}(A[+]B)$ is a subset of $\sigma_{++}(A[+]B)$ or of $\sigma_{--}(A[+]B)$ and (iii) follows. \square

Corollary 3.6. *Let A_+ and A_- be self-adjoint and semibounded from below in the Kreĩn spaces $(\mathcal{K}_+, [\cdot, \cdot]_{\mathcal{K}_+})$ and $(\mathcal{K}_-, [\cdot, \cdot]_{\mathcal{K}_-})$, respectively:*

$$[A_\pm f_\pm, f_\pm]_{\mathcal{K}_\pm} \geq \alpha_\pm [f_\pm, f_\pm]_{\mathcal{K}_\pm}, \quad f_\pm \in \text{dom}(A_\pm), \quad (3.5)$$

for some $\alpha_\pm \in \mathbb{R}$. Let $\rho(A_+) \neq \emptyset$, $\rho(A_-) \neq \emptyset$. Then, their direct sum $A_+[+]A_-$ is definitizable over:

$$\Omega := \overline{\mathbb{C}} \setminus [\min\{\alpha_+, \alpha_-\}, \max\{\alpha_+, \alpha_-\}], \quad (3.6)$$

in the direct sum of the Kreĩn spaces $\mathcal{K} = \mathcal{K}_+[+] \mathcal{K}_-$. In particular, $A_+[+]A_-$ is definitizable if and only if the sets S_+ and S_- from Theorem 3.5 are separated by a finite number of points.

This is fulfilled in the following special cases:

- (I) $\alpha_- = \alpha_+$.
- (II) $\alpha_- < \alpha_+$ and either $\sigma(A_+) \cap (\alpha_-, \alpha_+)$ is finite or $\sigma(A_-) \cap (\alpha_-, \alpha_+)$ is finite.
- (III) $\alpha_+ < \alpha_-$ and either $\sigma(A_+) \cap (\alpha_+, \alpha_-)$ is finite or $\sigma(A_-) \cap (\alpha_+, \alpha_-)$ is finite.

Proof. The assumptions on A_\pm imply that $A_+ - \alpha_+$ and $A_- - \alpha_-$ are nonnegative operators and, hence, A_\pm are definitizable operators. Then, with Proposition 2.3, we see that:

$$(\alpha_\pm, \infty) \cap \sigma(A_\pm) \subset \sigma_{++}(A_\pm) \quad \text{and} \quad (-\infty, \alpha_\pm) \cap \sigma(A_\pm) \subset \sigma_{--}(A_\pm) \quad (3.7)$$

and properties (i)–(iii) from Definition 3.1 for the operator $A_+[+]A_-$ and Ω as in (3.6) are easily shown, cf. Proposition 2.2. Therefore, $A_+[+]A_-$ is definitizable over Ω .

The statements on the definitizability of the operator $A_+[+]A_-$ now follow directly from (3.7) and Theorem 3.5. \square

4. Coupling of definitizable operators in Kreĩn spaces

4.1. Boundary triples and Weyl functions of symmetric operators

Starting from this section, we will denote by A a closed densely defined symmetric operator in a Kreĩn space $(\mathcal{K}, [\cdot, \cdot]_{\mathcal{K}})$. Let $\widehat{\rho}(A)$ denote the set of points of regular type of A , see [43], and let \mathfrak{N}_z denote the defect subspace of the operator A :

$$\mathfrak{N}_z := \mathcal{H} \ominus \text{ran}(A - \bar{z}) = \ker(A^+ - z), \quad z \in \widehat{\rho}(A).$$

In what follows, we assume that the operator A admits a self-adjoint extension \widetilde{A} in $(\mathcal{K}, [\cdot, \cdot]_{\mathcal{K}})$ with a nonempty resolvent set $\rho(\widetilde{A})$. Then, for all $z \in \rho(\widetilde{A})$, we have:

$$\text{dom}(A^+) = \text{dom}(\widetilde{A}) \dot{+} \mathfrak{N}_z \quad \text{direct sum in } \mathcal{H}. \quad (4.1)$$

This implies, in particular, that the dimension $\dim(\mathfrak{N}_z)$ is constant for all $z \in \rho(\widetilde{A})$.

Definition 4.1. Let Γ_0 and Γ_1 be linear mappings from $\text{dom}(A^+)$ to \mathbb{C}^d such that:

- (i) the mapping $\Gamma : f \rightarrow \{\Gamma_0 f, \Gamma_1 f\}$ from $\text{dom}(A^+)$ to \mathbb{C}^{2d} is surjective;
(ii) the abstract Green's identity:

$$[A^+ f, g]_{\mathcal{K}} - [f, A^+ g]_{\mathcal{K}} = (\Gamma_0 g)^*(\Gamma_1 f) - (\Gamma_1 g)^*(\Gamma_0 f) \quad (4.2)$$

holds for all $f, g \in \text{dom}(A^+)$.

Then, the triplet $\Pi = \{\mathbb{C}^d, \Gamma_0, \Gamma_1\}$ is said to be a *boundary triple* for A^+ , see [19, 44, 45, Sect.3.1.4] for a much more general setting.

It follows from (4.2) that the extensions A_0, A_1 of A defined as restrictions of A^+ to the domains:

$$\text{dom}(A_0) := \ker(\Gamma_0) \quad \text{and} \quad \text{dom}(A_1) := \ker(\Gamma_1) \quad (4.3)$$

are self-adjoint extensions of A .

If A has a self-adjoint extension \tilde{A} , with $\rho(\tilde{A}) \neq \emptyset$, then the operator A^+ admits a boundary triple $\{\mathbb{C}^d, \Gamma_0, \Gamma_1\}$, such that $A_0 = \tilde{A}$ and $d = \dim \mathfrak{N}_z$ ($z \in \rho(A_0)$). In this case, for every $z \in \rho(A_0)$, the decomposition (4.1) holds with $\tilde{A} = A_0$ and the mapping $\Gamma_0|_{\mathfrak{N}_z}$ is invertible for every $z \in \rho(A_0)$. Therefore, the operator-function:

$$\gamma(z) := (\Gamma_0|_{\mathfrak{N}_z})^{-1}, \quad (4.4)$$

is well defined and takes values in the set of bounded operators from \mathbb{C}^d to \mathfrak{N}_z . The operator-function $\gamma(z)$ is called the γ -field of A , associated with the boundary triple Π . Notice, that $\gamma(z)$ satisfies the equality:

$$\gamma(z) = (A_0 - z_0)(A_0 - z)^{-1}\gamma(z_0) \quad (z, z_0 \in \rho(A_0)).$$

Definition 4.2. The matrix valued function $M : \rho(A_0) \rightarrow \mathbb{C}^{d \times d}$ is defined by the equality:

$$M(z)\Gamma_0 f_z = \Gamma_1 f_z, \quad f_z \in \mathfrak{N}_z, z \in \rho(A_0). \quad (4.5)$$

The matrix valued function M is called the *Weyl function* of A corresponding to the boundary triple $\Pi = \{\mathbb{C}^d, \Gamma_0, \Gamma_1\}$.

Clearly,

$$M(z) = \Gamma_1 \gamma(z), \quad z \in \rho(A_0), \quad (4.6)$$

and hence $M(z)$ is well defined and takes values in $\mathbb{C}^{d \times d}$. It follows from the identity that the Weyl function $M(\lambda)$ satisfies the identities:

$$M(z) - M(w)^* = (z - \bar{w})\gamma(w)^+\gamma(z), \quad z, w \in \rho(A_0). \quad (4.7)$$

With $w = \bar{z}$ the identity (4.7) yields that the Weyl function M satisfies the symmetry condition:

$$M(\bar{z})^* = M(z) \quad \text{for all } z \in \rho(A_0). \quad (4.8)$$

The identity (4.7) was used in [46] as a definition of the Q -function. In the case when $(\mathcal{K}, [\cdot, \cdot]_{\mathcal{K}})$ is a Hilbert space, it follows from (4.7) and (4.8) that M is a Nevanlinna matrix valued function cf. (1.2).

In what follows, the function:

$$\hat{f}(z) := [f, \gamma(\bar{z})]_{\mathcal{K}} \quad (f \in \mathcal{K}, z \in \rho(A_0))$$

is called the generalized Fourier transform of f associated with the boundary triple $\{\mathbb{C}, \Gamma_0, \Gamma_1\}$. A motivation for this name is hidden in the fact, that the mapping $f \mapsto \hat{f}$ is a unitary mapping from \mathcal{K} to a reproducing kernel Kreĭn space with the kernel $\frac{M(z) - M(\bar{w})}{z - \bar{w}}$ (see [28] for the Hilbert space case).

Proposition 4.3. [44–46] *Let A_1 be the self-adjoint extension of A with the domain defined in (4.3) and let $d = 1$. For every $z \in \rho(A_0)$, the following equivalence holds:*

$$z \in \rho(A_1) \iff M(z) \neq 0,$$

and the resolvent of A_1 can be found by the formula:

$$(A_1 - z)^{-1}f = (A_0 - z)^{-1}f - \frac{\hat{f}(z)}{M(z)}\gamma(z),$$

for all $f \in \mathcal{H}$ and all $z \in \rho(A_0) \cap \rho(A_1)$.

4.2. Construction of the coupling of two self-adjoint operators in a Kreĭn space

In this section, we consider two Kreĭn spaces $(\mathcal{K}_+, [\cdot, \cdot]_{\mathcal{K}_+})$ and $(\mathcal{K}_-, [\cdot, \cdot]_{\mathcal{K}_-})$. Let their direct sum:

$$\mathcal{K} = \mathcal{K}_+ [+] \mathcal{K}_-,$$

be endowed with the natural inner product (3.1). Consider two closed symmetric densely defined operators A_+ and A_- with defect numbers $(1, 1)$ acting in the Kreĭn spaces $(\mathcal{K}_+, [\cdot, \cdot]_{\mathcal{K}_+})$ and $(\mathcal{K}_-, [\cdot, \cdot]_{\mathcal{K}_-})$. Let $\{\mathbb{C}, \Gamma_0^\pm, \Gamma_1^\pm\}$ be a boundary triple for A_\pm^\pm . Let M_\pm be the corresponding Weyl function and γ_{A_\pm} the γ -field. By $A_{\pm,0}$, we denote the self-adjoint extension of A_\pm which is defined on:

$$\text{dom}(A_{\pm,0}) = \ker(\Gamma_0^\pm) \quad \text{by} \quad A_{\pm,0} = A_\pm^\pm|_{\ker(\Gamma_0^\pm)},$$

and assume that $\rho(A_{+,0}) \cap \rho(A_{-,0}) \neq \emptyset$. Then, the functions M_\pm are defined and holomorphic on $\rho(A_{\pm,0})$.

The following theorem is the indefinite version of a result from [47] (see also [28]).

Theorem 4.4. *Under the general assumptions of this subsection we have:*

(a) *The linear operator A defined as the restriction of $A_+^\pm [+] A_-^\pm$ to the domain:*

$$\text{dom}(A) = \left\{ \begin{pmatrix} f_+ \\ f_- \end{pmatrix} : \begin{array}{l} \Gamma_0^+(f_+) = \Gamma_0^-(f_-) = 0, \\ \Gamma_1^+(f_+) + \Gamma_1^-(f_-) = 0, \end{array} f_\pm \in \text{dom}(A_\pm^\pm) \right\}, \quad (4.9)$$

is closed, densely defined and symmetric with defect numbers $(1, 1)$ in the Kreĭn space \mathcal{K} .

(b) *The adjoint A^+ of A is the restriction of $A_+^\pm [+] A_-^\pm$ to the domain:*

$$\text{dom}(A^+) = \left\{ \begin{pmatrix} f_+ \\ f_- \end{pmatrix} : \Gamma_0^+(f_+) - \Gamma_0^-(f_-) = 0, f_\pm \in \text{dom}(A_\pm^\pm) \right\}. \quad (4.10)$$

(c) *A boundary triple $\{\mathbb{C}, \Gamma_0, \Gamma_1\}$ for A^+ is given by:*

$$\Gamma_0 f = \Gamma_0^+ f_+, \quad \Gamma_1 f = \Gamma_1^+ f_+ + \Gamma_1^- f_-, \quad f = \begin{pmatrix} f_+ \\ f_- \end{pmatrix} \in \text{dom}(A^+). \quad (4.11)$$

(d) *The Weyl function $M(z)$ and the γ -field of A relative to the boundary triple $\{\mathbb{C}, \Gamma_0, \Gamma_1\}$ are given by:*

$$M(z) = M_+(z) + M_-(z), \quad \gamma(z) = \begin{pmatrix} \gamma_{A_+}(z) \\ \gamma_{A_-}(z) \end{pmatrix} \quad z \in \mathbb{C} \setminus \mathbb{R}. \quad (4.12)$$

(e) *The self-adjoint extension A_1 of A such that $\text{dom}(A_1) = \ker(\Gamma_1)$ coincides with the restriction of $A_+^\pm [+] A_-^\pm$ to the domain:*

$$\text{dom}(A_1) = \left\{ \begin{pmatrix} f_+ \\ f_- \end{pmatrix} : \begin{array}{l} \Gamma_0^+(f_+) - \Gamma_0^-(f_-) = 0, \\ \Gamma_1^+(f_+) + \Gamma_1^-(f_-) = 0, \end{array} f_\pm \in \text{dom}(A_\pm^\pm) \right\}, \quad (4.13)$$

and is called a coupling of A_+ and A_- relative to the boundary triples $\{\mathbb{C}, \Gamma_0^+, \Gamma_1^+\}$ and $\{\mathbb{C}, \Gamma_0^-, \Gamma_1^-\}$.

(f) *The self-adjoint extension A_0 of A coincides with the direct sum $A_{+,0} [+] A_{-,0}$ and $\rho(A_0) = \rho(A_{+,0}) \cap \rho(A_{-,0}) \neq \emptyset$.*

(g) *The resolvent set $\rho(A_1)$ is nonempty if and only if*

$$M_+ + M_- \neq 0.$$

For every $z \in \rho(A_1) \cap \rho(A_0)$ and $f = \begin{pmatrix} f_+ \\ f_- \end{pmatrix} \in \mathcal{K} = \mathcal{K}_+ [+] \mathcal{K}_-$, the resolvent of A_1 is given by:

$$(A_1 - z)^{-1} f = (A_0 - z)^{-1} f - \frac{\widehat{f}_{A_+}(z) + \widehat{f}_{A_-}(z)}{M_+(z) + M_-(z)} \gamma(z), \quad (4.14)$$

where:

$$\widehat{f}_{A_+}(z) := [f_+, \gamma_{A_+}(\bar{z})]_{\mathcal{K}_+}, \quad \widehat{f}_{A_-}(z) := [f_-, \gamma_{A_-}(\bar{z})]_{\mathcal{K}_-}. \quad (4.15)$$

Proof. (a)–(c) Since $\{\mathbb{C}, \Gamma_0^\pm, \Gamma_1^\pm\}$ is a boundary triple for A_\pm^\pm , it follows from (4.2) that for all $f_\pm \in \text{dom}(A_\pm^\pm)$:

$$\begin{aligned} [A_+^+ f_+, g_+]_{\mathcal{K}_+} - [f_+, A_+^+ g_+]_{\mathcal{K}_+} + [A_-^+ f_-, g_-]_{\mathcal{K}_-} - [f_-, A_-^+ g_-]_{\mathcal{K}_-} \\ = \overline{(\Gamma_0^+ g_+)(\Gamma_1^+ f_+)} - \overline{(\Gamma_1^+ g_+)(\Gamma_0^+ f_+)} + \overline{(\Gamma_0^- g_-)(\Gamma_1^- f_-)} - \overline{(\Gamma_1^- g_-)(\Gamma_0^- f_-)}. \end{aligned} \quad (4.16)$$

We denote by T the restriction of $A_+^+ [+] A_-^+$ to the set of the right hand side of (4.10).

If

$$f = \begin{pmatrix} f_+ \\ f_- \end{pmatrix}, \quad g = \begin{pmatrix} g_+ \\ g_- \end{pmatrix} \in \text{dom}(T) \quad \text{then} \quad \Gamma_0^+ f_+ = \Gamma_0^- f_- \quad \text{and} \quad \Gamma_0^+ g_+ = \Gamma_0^- g_-,$$

and hence, one obtains from (4.16):

$$[Tf, g]_{\mathcal{K}} - [f, Tg]_{\mathcal{K}} = \overline{\Gamma_0^+ g_+ (\Gamma_1^+ f_+ + \Gamma_1^- f_-)} - \overline{(\Gamma_1^+ g_+ + \Gamma_1^- g_-) \Gamma_0^+ f_+}. \quad (4.17)$$

Now, it follows from (4.17) that A is a closed, densely defined and symmetric operator in the Kreĭn space \mathcal{K} , $T = A^+$ and a boundary triple for A^+ can be chosen in the form (4.11).

(d) The formulas for M and γ are implied by (4.11), (4.4) and (4.5).

(e) & (f) As $\{\mathbb{C}, \Gamma_0, \Gamma_1\}$ is a boundary triple for A^+ , the extension A_1 with $\text{dom}(A_1) = \ker(\Gamma_1)$ being a restriction of $A_+^+ [+] A_-^+$. The formula (4.13) for the domain follows from $A_1 \subset A^+$ (see (4.10)) and $\text{dom}(A_1) = \ker(\Gamma_1)$. The statement (f) is immediate from (4.10) and (4.11).

(g) The statement (g) is implied by (4.12) and Proposition 4.3. \square

Remark 4.5. The construction in Theorem 4.4 shows that the coupling of two self-adjoint operators $A_{+,0}$ and $A_{-,0}$ is not uniquely defined. Namely, let the boundary triples $\Pi^- = \{\mathbb{C}, \Gamma_0^-, \Gamma_1^-\}$ and $\tilde{\Pi}^- = \{\mathbb{C}, \tilde{\Gamma}_0^-, \tilde{\Gamma}_1^-\}$ be related by

$$\tilde{\Gamma}_0^- = c\Gamma_0^-, \quad \tilde{\Gamma}_1^- = \bar{c}^{-1}\Gamma_1^-,$$

for some non-zero $c \in \mathbb{C}$, $c \neq 1$. Then, the extension \tilde{A}_1 defined as the restriction of $A_+^+ [+] A_-^+$ to the domain:

$$\text{dom}(\tilde{A}_1) = \left\{ \begin{pmatrix} f_+ \\ f_- \end{pmatrix} : \begin{aligned} \Gamma_0^+(f_+) - c\Gamma_0^-(f_-) &= 0, \\ \Gamma_1^+(f_+) + \bar{c}^{-1}\Gamma_1^-(f_-) &= 0, \end{aligned} \quad f_\pm \in \text{dom}(A_\pm^\pm) \right\},$$

is also a coupling of A_- and A_+ with $\tilde{A}_1 \neq A_1$.

However, when the boundary triples $\{\mathbb{C}, \Gamma_0^\pm, \Gamma_1^\pm\}$ are fixed, then the coupling A_1 of the operators A_\pm is uniquely defined by the formula (4.13) and is called the *coupling* of the operators $A_{\pm,0}$ relative to the boundary triples $\{\mathbb{C}, \Gamma_0^\pm, \Gamma_1^\pm\}$.

Let us suppose that the operators $A_{\pm,0}$ are semibounded from below, that is there exists $\alpha_\pm \in \mathbb{R}$ such that (3.5) holds. Then, the results of Section 3.2 allow us to show that the coupling A_1 of the operators $A_{+,0}$ and $A_{-,0}$ is at least locally definitizable in a vicinity of ∞ . In the next theorem, sufficient conditions for regularity of the critical point ∞ are given.

Theorem 4.6. *Under the general assumptions of this subsection, we assume that the operators $A_{\pm,0}$, the γ -fields γ_\pm and the Weyl functions M_\pm satisfy the following assumptions:*

(A1) *The operators $A_{\pm,0}$ are semibounded from below, $\rho(A_{\pm,0}) \neq \emptyset$, and*

$$\infty \notin c_s(A_{\pm,0}).$$

(A2) *($w(z) := |M_+(z) + M_-(z)| \neq 0$ on $\rho(A_{+,0}) \cap \rho(A_{-,0})$).*

(A3) *There is $y_1 > 0$, such that for all $f_{A_\pm} \in \mathcal{K}_\pm$:*

$$\int_{y_1}^{\infty} \frac{|\hat{f}_{A_\pm}(iy)|^2}{w(iy)} dy < \infty, \quad \int_{y_1}^{\infty} \frac{|\hat{f}_{A_\pm}(-iy)|^2}{w(iy)} dy < \infty, \quad (4.18)$$

where the generalized Fourier transforms \hat{f}_{A_+} and \hat{f}_{A_-} are defined by (4.15).

Then, the coupling A_1 of the operators $A_{+,0}$ and $A_{-,0}$ is definitizable over Ω , where Ω is as in (3.6). Moreover, we have:

$$\infty \notin c_s(A_1).$$

Proof. By Corollary 3.6, the operator $A_0 = A_{+,0}[+]A_{-,0}$ is definitizable over Ω . In view of Theorem 4.4, the assumption (A2) yields $\rho(A_1) \neq \emptyset$. Since the operator A_1 is a two-dimensional perturbation of A_0 , by Theorem 3.3, the operator A_1 is also definitizable over Ω .

Clearly, $\infty \notin c_s(A_0)$ and it follows from Theorem 3.2 that there is $y_2 > y_1 > 0$, such that:

$$\int_{y_2}^{\infty} |\operatorname{Re} [(A_0 - iy)^{-1}f, f]_{\mathcal{K}}| dy < \infty \quad \text{for all } f \in \mathcal{K}.$$

Let us set:

$$\mathcal{A}(f, iy) := \frac{(\widehat{f}_{A_+}(iy) + \widehat{f}_{A_-}(iy))(\overline{\widehat{f}_{A_+}(-iy) + \widehat{f}_{A_-}(-iy)})}{M_+(iy) + M_-(iy)}. \quad (4.19)$$

We show:

$$\int_{y_2}^{\infty} |\mathcal{A}(f, iy)| dy < \infty \quad \text{for all } f \in \mathcal{K}.$$

It follows from (A3) that for every $f_{A_{\pm}} \in \mathcal{K}_{\pm}$

$$\int_{y_2}^{\infty} \left| \widehat{f}_{A_{\pm}}(iy) \widehat{f}_{A_{\pm}}(-iy) \right| \frac{dy}{w(iy)} \leq \left(\int_{y_2}^{\infty} \left| \widehat{f}_{A_{\pm}}(iy) \right|^2 \frac{dy}{w(iy)} \right)^{1/2} \left(\int_{y_2}^{\infty} \left| \widehat{f}_{A_{\pm}}(-iy) \right|^2 \frac{dy}{w(iy)} \right)^{1/2} < \infty. \quad (4.20)$$

Similarly, one obtains for all $f_{A_{\pm}} \in \mathcal{K}_{\pm}$:

$$\int_{y_2}^{\infty} \left| \widehat{f}_{A_+}(iy) \widehat{f}_{A_-}(-iy) \right| \frac{dy}{w(iy)} < \infty. \quad (4.21)$$

Combining (4.20) and (4.21), one obtains from (4.19) for all $f \in \mathcal{K}$

$$\int_{y_2}^{\infty} |\mathcal{A}(f, iy)| dy = \int_{y_2}^{\infty} \left| \frac{(\widehat{f}_{A_+}(iy) + \widehat{f}_{A_-}(iy))(\overline{\widehat{f}_{A_+}(-iy) + \widehat{f}_{A_-}(-iy)})}{M_+(iy) + M_-(iy)} \right| dy < \infty.$$

Now the statement $\infty \notin c_s(A_1)$ is implied by Theorem 2.4 and (4.14). \square

Theorem 4.7. *Under the assumptions of this subsection we assume that the operators $A_{\pm,0}$, the γ -fields γ_{\pm} and the Weyl functions M_{\pm} satisfy the following conditions:*

(A1') *The operators $A_{\pm,0}$ are semibounded from below, $\rho(A_{\pm,0}) \neq \emptyset$, one of the conditions (i), (ii) or (iii) of Corollary 3.6 holds, and $\alpha := \min\{\alpha_-, \alpha_+\}$ satisfies:*

$$\alpha \notin c_s(A_{\pm,0}).$$

(A2') *($w(z) := |M_+(z) + M_-(z)| \neq 0$ on $\rho(A_{+,0}) \cap \rho(A_{-,0})$).*

(A3') *There is $y_1 > 0$, such that for all $f_{A_{\pm}} \in \mathcal{K}_{\pm}$:*

$$\int_0^{y_1} \frac{|\widehat{f}_{A_{\pm}}(\alpha + iy)|^2}{w(\alpha + iy)} dy < \infty, \quad \int_0^{y_1} \frac{|\widehat{f}_{A_{\pm}}(\alpha - iy)|^2}{w(\alpha + iy)} dy < \infty.$$

Then, the coupling A_1 of the operators $A_{+,0}$ and $A_{-,0}$ is a definitizable operator and

$$\alpha \notin c_s(A).$$

Proof. In view of Corollary 3.6, the operator $A_0 := A_{+,0}[+]A_{-,0}$ is definitizable. By Theorem 4.4, the assumption (A2') implies $\rho(A_1) \neq \emptyset$. Then by [41] the operator A_1 is also definitizable.

By the assumption (A1') $\alpha \notin c_s(A_{\pm,0})$, then $\alpha \notin c_s(A_0)$. Since by Theorem 2.4 there is $y_2 \in (0, y_1)$, such that:

$$\int_0^{y_2} |\operatorname{Re} [(A_0 - \alpha - iy)^{-1}f, f]_{\mathcal{K}}| dy < \infty \quad \text{for all } f \in \mathcal{K},$$

it remains to show that:

$$\int_0^{y_2} |\mathcal{A}(f, \alpha + iy)| dy < \infty \quad \text{for all } f \in \mathcal{K},$$

where \mathcal{A} is defined as in (4.19). The proof of this inequality is similar to that in Theorem 4.6 and is based on the assumption (A3'). \square

5. Application to Sturm–Liouville operators with indefinite weights

Consider the differential expression:

$$\ell(f)(t) := \frac{\operatorname{sgn} t}{w(t)} \left(-\frac{d}{dt} \left(\frac{df}{r(t)dt} \right) + q(t)f(t) \right) \quad \text{for a.a. } t \in \mathbb{R}, \quad (5.1)$$

where the coefficients r , q and w are real functions on \mathbb{R} satisfying the conditions:

(C1) $r, q, w \in L^1_{\text{loc}}(\mathbb{R})$ and $r, w > 0$ a.e. on \mathbb{R} ,

(C2) the expression ℓ is in the limit point case at $-\infty$ and at $+\infty$.

Let $\mathcal{H}_{\pm} = L^2_w(\mathbb{R}_{\pm})$ be the standard weighted L^2 -space with the positive definite inner product:

$$(f, g)_{\pm} = \int_{\mathbb{R}_{\pm}} f(t)\overline{g(t)}w(t)dt \quad (f, g \in L^2_w(\mathbb{R}_{\pm})).$$

Consider minimal differential operators B_{\pm} generated by $\pm\ell$ in $L^2_{w_{\pm}}(\mathbb{R}_{\pm})$, here w_{\pm} denotes the restriction of w to \mathbb{R}_{\pm} . Since we assume that ℓ is in the limit point case at $\pm\infty$, the operator B_{\pm} is a densely defined symmetric operator with defect numbers $(1, 1)$ in the Hilbert space $L^2_{w_{\pm}}(\mathbb{R}_{\pm})$ and:

$$\begin{aligned} \operatorname{dom}(B_{\pm}^*) &= \{f \in L^2_{w_{\pm}}(\mathbb{R}_{\pm}) : f, (r^{-1}f)' \in AC_{\text{loc}}[0, \pm\infty), \ell(f) \in L^2_{w_{\pm}}(\mathbb{R}_{\pm})\}, \\ \operatorname{dom}(B_{\pm}) &= \{f \in \operatorname{dom}(B_{\pm}^*) : f(0) = f'(0) = 0\}, \\ B_{\pm}f &:= \pm\ell(f), \quad f \in \operatorname{dom}(B_{\pm}). \end{aligned} \quad (5.2)$$

In addition to (C1), (C2), we assume that:

(C3) B_+ and B_- are semibounded from below in $L^2_{w_+}(\mathbb{R}_+)$ and $L^2_{w_-}(\mathbb{R}_-)$, respectively.

Let $z \in \mathbb{C} \setminus \mathbb{R}$ and denote by $\vartheta(\cdot, z)$ and $\varphi(\cdot, z)$ the unique solutions of the equation:

$$-(r^{-1}f')' + qf = zwf$$

satisfying the boundary conditions:

$$\varphi(0, z) = 1, \quad (r^{-1}\varphi')(0, z) = 0 \quad \text{and} \quad \vartheta(0, z) = 0, \quad (r^{-1}\vartheta')(0, z) = 1, \quad \text{respectively.}$$

Since we assume that $\pm\ell$ are in the limit point case at $\pm\infty$, for each $z \in \mathbb{C} \setminus \mathbb{R}$ there is a unique solution:

$$\psi_{\pm}(t, z) = \varphi(t, z) \pm m_{\pm}(z)\vartheta(t, z), \quad t \in \mathbb{R}_{\pm}, \quad (5.3)$$

of the restriction of $\pm\ell(f) = zf$ to \mathbb{R}_{\pm} which belongs to $L^2_{w_{\pm}}(\mathbb{R}_{\pm})$. Relation (5.3) defines the function $m_{\pm} : \mathbb{C} \setminus \mathbb{R} \rightarrow \mathbb{C}$ uniquely. The function m_{\pm} is called the *Dirichlet m -coefficient* of the restriction of the expression $\pm\ell$ to \mathbb{R}_{\pm} .

A boundary triple for B_{\pm}^* is $\{\mathbb{C}, \Gamma_0^{\pm}, \Gamma_1^{\pm}\}$, where:

$$\Gamma_0^{\pm}f := f(0_{\pm}), \quad \Gamma_1^{\pm}(f) = \pm(r^{-1}f')(0_{\pm}), \quad f \in \operatorname{dom}(B_{\pm}^*). \quad (5.4)$$

It follows from (4.6) and (5.4) that the Dirichlet m -coefficient m_{\pm} defined by (5.3) coincides with the Weyl function of the operator B_{\pm} in (5.2) relative to the boundary triple in (5.4).

It is natural to consider the expression ℓ in the Kreĭn space $(\mathcal{K}, [\cdot, \cdot]_{\mathcal{K}})$, where $\mathcal{K} = L^2_w(\mathbb{R})$ is the standard weighted L^2 -space endowed with the indefinite inner product:

$$[f, g]_{\mathcal{K}} = (Jf, g)_{L^2_w(\mathbb{R})} = \int_{\mathbb{R}} \operatorname{sgn} t f(t)\overline{g(t)}dt, \quad f, g \in L^2_w(\mathbb{R}),$$

and the operator:

$$(Jf)(t) = (\operatorname{sgn} t)f(t), \quad f \in L^2_w(\mathbb{R}),$$

is a fundamental symmetry on $(\mathcal{K}, [\cdot, \cdot]_{\mathcal{K}})$. We set:

$$\mathcal{K}_{\pm} = \{f \in L^2_w(\mathbb{R}) : f = 0 \text{ a.e. on } \mathbb{R}_{\mp}\}.$$

Then $\mathcal{K} = \mathcal{K}_+[\dot{+}]\mathcal{K}_-$ is the fundamental decomposition corresponding to J .

Let the operators $A_{\pm} := \pm B_{\pm}$ be considered as semibounded symmetric operators in the Kreĭn spaces $(L^2_{w_{\pm}}(\mathbb{R}_{\pm}), \pm(\cdot, \cdot)_{L^2_{w_{\pm}}(\mathbb{R}_{\pm})})$. Then, the triples (5.4) are boundary triples for A_{\pm}^{\pm} . The corresponding Weyl functions of the operators A_+ and A_- take the form:

$$M_+(z) = m_+(z), \quad M_-(z) = m_-(-z).$$

Consider a symmetric operator A in the Kreĭn space $(\mathcal{K}, [\cdot, \cdot]_{\mathcal{K}})$ determined by the conditions (4.9). Then the domain of the adjoint operator A^+ is characterized by the boundary condition (4.10), which in view of (5.4), takes the form:

$$f(0+) = f(0-).$$

Consider the coupling A_1 of A_+ and A_- relative to the boundary triples (5.4). A_1 is characterized by the boundary conditions (4.13), which now can be rewritten as:

$$f(0+) = f(0-), \quad (r^{-1}f')(0+) = (r^{-1}f')(0-).$$

Therefore, the operator A_1 is associated with the expression in (5.1) in the Hilbert space $L^2_w(\mathbb{R})$; that is $A_1 f = \ell(f)$ for all:

$$f \in \text{dom}(A_1) = \{f \in L^2_w(\mathbb{R}) : f, r^{-1}f' \in AC_{\text{loc}}(\mathbb{R}), \ell(f) \in L^2_w(\mathbb{R})\}.$$

Notice, that the assumption (A1) of Theorem 4.6 is satisfied in view of (C3) and the assumption (A2) is satisfied since if $m_+(z) + m_-(-z) \equiv 0$ then $m_+(z) = -m_-(-z)$ is holomorphic on the half-line $(-\beta_-, \infty)$, what is impossible for the m -coefficient of the Sturm-Liouville operator. These considerations and Theorem 4.6 justify the following:

Proposition 5.1. *Let the differential operation ℓ satisfy (C1), (C2) and let the minimal differential operators B_{\pm} generated by $\pm \ell$ in $L^2_w(\mathbb{R}_{\pm})$ satisfy (C3) and let m_{\pm} be the Dirichlet m -functions of B_{\pm} . Then, the coupling A_1 of A_+ and A_- is locally definitizable in the Kreĭn space $(\mathcal{K}, [\cdot, \cdot]_{\mathcal{K}})$. If, in addition, m_+ and m_- satisfy the condition (4.18), then $\infty \notin c_s(A_1)$.*

Acknowledgements

The research of the first author was supported by the Deutsche Forschungsgemeinschaft (DFG) under grant no. TR 903/16-1 and Ministry of Education and Science of Ukraine (projects # 0115U000136, 0115U000556).

References

- [1] Azizov T.Ya., Iokhvidov I.S. *Linear operators in spaces with an indefinite metric*, John Wiley & Sons, 1990.
- [2] Bogner J. *Indefinite inner product spaces*, Springer, 1974.
- [3] Bender C.M., Brody D.C., Jones H.F. Complex extension of quantum mechanics. *Phys. Rev. Lett.*, 2002, **89**, P. 270401.
- [4] Bender C.M., Brody D.C., Jones H.F. Must a Hamiltonian be Hermitian? *Am. J. Phys.*, 2003, **71**, P. 1095–1102.
- [5] Caliceti E., Graffi S., Sjöstrand J. Spectra of \mathcal{PT} -symmetric operators and perturbation theory. *J. Phys. A: Math. Gen.*, 2005, **38**, P. 185–193.
- [6] Günther U., Stefani F., Znojil M. MHD α^2 -dynamo, squire equation and \mathcal{PT} -symmetric interpolation between square well and harmonic oscillator. *J. Math. Phys.*, 2005, **46**, P. 063504.
- [7] Langer H., Tretter C. A Kreĭn space approach to \mathcal{PT} -symmetry. *Czech. J. Phys.*, 2004, **54**, P. 1113–1120.
- [8] Albeverio S., Günther U., Kuzhel S. J -self-adjoint operators with C -symmetries: extension theory approach. *J. Phys. A: Math. Theor.*, 2009, **42**, P. 105205.
- [9] Caliceti E., Graffi S., Hitrik M., Sjöstrand J. Quadratic \mathcal{PT} -symmetric operators with real spectrum and similarity to self-adjoint operators. *J. Phys. A: Math. Theor.*, 2012, **45**, P. 444007.
- [10] Tanaka T. PT -symmetric quantum theory defined in a Kreĭn space. *J. Phys. A: Math. Gen.*, 2006, **39**, P. L369–L376.
- [11] Tanaka T. General aspects of PT -symmetric and P -self-adjoint quantum theory in a Kreĭn space. *J. Phys. A: Math. Gen.*, 2006, **39**, P. 14175–14203.
- [12] Langer H. Verallgemeinerte Resolventen eines J -nichtnegativen Operators mit endlichem Defekt. *J. Functional Analysis*, 1971, **8**, P. 287–320.
- [13] Jonas P. On a class of unitary operators in Kreĭn space. *Oper. Theory Adv. Appl.*, 1986, **17**, P. 151–172.
- [14] Jonas P. On a class of self-adjoint operators in Kreĭn space and their compact perturbations. *Integral Equations Operator Theory*, 1988, **11**, P. 351–384.
- [15] Štraus A.V. Extensions and generalized resolvents of a symmetric operator which is not densely defined. *Math. USSR-Izvestija*, 1970, **4**, P. 179–208.
- [16] Calkin J.W. Abstract symmetric boundary conditions. *Trans. Am. Math. Soc.*, 1939, **45**, P. 369–442.
- [17] Kochubei A.N. On extensions of symmetric operators and symmetric binary relations. *Matem. Zametki*, 1975, **17**, P. 41–48.
- [18] Bruk V.M. On a class of problems with the spectral parameter in the boundary conditions. *Mat. Sb.*, 1976, **100**, P. 210–216.
- [19] Gorbachuk V.I., Gorbachuk M.L. *Boundary value problems for operator differential equations*, Kluwer Academic Publishers Group, 1991.
- [20] Karabash I.M. J -self-adjoint ordinary differential operators similar to self-adjoint operators. *Methods Funct. Anal. Topology*, 2000, **6**, P. 22–49.

- [21] Karabash I.M., Malamud M.M. Indefinite Sturm-Liouville operators with finite zone potentials. *Operators and Matrices*, 2007, **1**, P. 301–368.
- [22] Karabash I.M., Kostenko A., Malamud M.M. The similarity problem for J -nonnegative Sturm-Liouville operators. *J. Differential Equations*, 2009, **246**, P. 964–997.
- [23] Kostenko A. The similarity problem for indefinite Sturm-Liouville operators and the HELP inequality. *Adv. Math.*, 2013, **246**, P. 368–413.
- [24] Behrndt J. On the spectral theory of singular indefinite Sturm-Liouville operators. *J. Math. Anal. Appl.*, 2007, **334**, P. 1439–1449.
- [25] Veselić K. On spectral properties of a class of J -self-adjoint operators I. *Glasnik Mat. Ser.*, 1972, **7**, P. 229–248.
- [26] Veselić K. On spectral properties of a class of J -self-adjoint operators II. *Glasnik Mat. Ser.*, 1972, **7**, P. 249–254.
- [27] Jonas P. Regularity criteria for critical points of definitizable operators. *Operator Theory: Advances and Applications*, 1984, **14**, P. 179–195.
- [28] Čurgus B., Derkach V. Partially fundamentally reducible operators in Kreĭn spaces. *Integral Equations Operator Theory*, 2015, **82**, P. 469–518.
- [29] Čurgus B., Langer H. A Kreĭn space approach to symmetric ordinary differential operators with an indefinite weight function. *J. Differential Equations*, 1989, **79**, P. 31–61.
- [30] Kac I.S., Kreĭn M.G. R -functions–analytic functions mapping the upper halfplane into itself. *Amer. Math. Soc. Transl. Ser.*, 1974, **103**, P. 1–18.
- [31] Donoghue W.F. *Monotone matrix functions and analytic continuation*. Die Grundlehren der mathematischen Wissenschaften, Band 207, Springer-Verlag, 1974.
- [32] Langer H. Spectral functions of definitizable operators in Kreĭn spaces. In *Functional analysis: Lecture Notes in Math.*, Springer, 1982, **948**, P. 1–46.
- [33] Langer H. *Spektraltheorie linearer Operatoren in J -Räumen und einige Anwendungen auf die Schar $L(\lambda) = \lambda^2 I + \lambda B + C$* . Habilitationsschrift, Technische Universität Dresden, 1965.
- [34] Azizov T. Ya., Jonas P., Trunk C. Spectral points of type π_+ and π_- of selfadjoint operators in Kreĭn spaces. *J. Funct. Anal.*, 2005, **226**, P. 114–137.
- [35] Jonas P. On Locally Definite Operators in Kreĭn Spaces. In *Spectral Theory and its Applications*, Ion Colojoară Anniversary Volume, Theta, Bucharest, 2003, P. 95–127.
- [36] Lancaster P., Markus A.S., Matsaev V.I. Definitizable operators and quasihyperbolic operator polynomials. *J. Funct. Anal.*, 1995, **131**, P. 1–28.
- [37] Langer H., Markus A.S., Matsaev V.I. Locally definite operators in indefinite inner product spaces. *Math. Ann.*, 1997, **308**, P. 405–424.
- [38] Ando T. *Linear Operators in Krein Spaces*, Lecture Notes, Hokkaido University, Sapporo, 1979.
- [39] Trunk C. Locally definitizable operators: The local structure of the spectrum. In: *Operator Theory*, D. Alpay (Ed.), Springer, 2015, P. 241–259.
- [40] Behrndt J. Finite rank perturbations of locally definitizable self-adjoint operators in Krein spaces. *J. Operator Theory*, 2007, **58**, P. 415–440.
- [41] Jonas P., Langer H. Compact perturbations of definitizable operators. *J. Operator Theory*, 1979, **2**, P. 63–77.
- [42] Karabash I., Trunk C. Spectral properties of singular Sturm-Liouville operators. *Proc. R. Soc. Edinb. Sect. A*, 2009, **139**, P. 483–503.
- [43] Akhiezer N.I., Glazman I.M. *Theory of Linear Operators in Hilbert Space*, Dover Publications, 1993.
- [44] Derkach V.A., Malamud M.M. Generalized resolvents and the boundary value problems for hermitian operators with gaps. *J. Funct. Anal.*, 1991, **95**, P. 1–95.
- [45] Derkach V.A. On Weyl function and generalized resolvents of a Hermitian operator in a Kreĭn space. *Integral Equations Operator Theory*, 1995, **23**, P. 387–415.
- [46] Kreĭn M.G., Langer H. Über einige Fortsetzungsprobleme, die eng mit der Theorie hermitescher Operatoren in Räume Π_κ zusammenhängen, Teil I: Einige Funktionenklassen und ihre Darstellungen. *Math. Nachr.*, 1977, **77**, P. 187–236.
- [47] Derkach V.A., Hassi S., Malamud M.M., de Snoo H.S.V. Generalized resolvents of symmetric operators and admissibility. *Methods Funct. Anal. Topol.*, 2000, **6**, P. 24–55.

Quasi-semidefinite eigenvalue problem and applications

L. Grubišić and J. Tambača

Department of Mathematics, Faculty of Science, University of Zagreb,
Bijenička 30, 10000 Zagreb, Croatia

luka.grubisic@math.hr, josip.tambaca@math.hr

PACS 02.30.Tb, 02.70.-c, 02.10.Ud

DOI 10.17586/2220-8054-2017-8-2-180-187

In this note, we study the eigenvalue problem for a class of block operator matrix pairs. Our study is motivated by an analysis of abstract differential algebraic equations. Such problems frequently appear in the study of complex systems, e.g. differential equations posed on metric graphs, in mixed variational formulation.

Keywords: block operator matrices, metric graphs, spectral theory and eigenvalue problems.

Received: 15 January 2017

Revised: 2 February 2017

1. Introduction

In this note, we will consider mixed variational formulations of evolution problems as abstract differential algebraic equations. More generally, abstract differential algebraic equations can be seen as a good tool to study the evolution of any system with constraints. Their theory and numerical analysis is fairly well known in the finite dimensional case, see eg. [1], but the corresponding results for infinite dimensional abstract differential algebraic equations are at an early stage of development, see [2, 3].

Let us note that simulations of complex systems, where one considers several physical regimes simultaneously can be described by a state vector in an appropriate product space called the state space. Experience indicates that mixed variational formulations are easier to combine in a state space formulation. In the mixed approach, the “agreement” between models/regimes is enforced a constraint in the state space.

Our approach to mixed variational problems is through the theory of 2×2 block operator matrices [4] and the representation theorems for quasi-definite quadratic forms by such operators from [5, 6].

Formally, we start from the problem of finding $u \in L^2(0, T, X)$ and $p \in L^2(0, T, Y)$, $T > 0$ so that:

$$\begin{bmatrix} M & 0 \\ 0 & 0 \end{bmatrix} \frac{d}{dt} \begin{bmatrix} u \\ p \end{bmatrix} + \begin{bmatrix} K & B \\ D^* & C \end{bmatrix} \begin{bmatrix} u \\ p \end{bmatrix} = \begin{bmatrix} f_1 \\ f_2 \end{bmatrix}, \quad (1)$$

holds in the state space $X \otimes Y$. As in [2, 3, 7], the time derivative is to be interpreted in the distributional sense and X and Y are assumed to be Hilbert spaces. We will call $X \otimes Y$ the state space. It is a Hilbert space with usual product space structure and we will write:

$$\psi = x \oplus y = \begin{bmatrix} x \\ y \end{bmatrix} \in X \otimes Y$$

for its elements, the state vectors.

An important class of model problems which can formally be posed in the form (1) originates from problems in fluid mechanics modeled by Stokes, Oseen or Navier-Stokes equations linearized about nonzero velocity, see [3] for some details. In this note, we will be interested in the homogeneous problem associated to the problem (1):

$$\begin{bmatrix} M & 0 \\ 0 & 0 \end{bmatrix} \frac{d}{dt} \begin{bmatrix} u \\ p \end{bmatrix} + \begin{bmatrix} K & B \\ D^* & C \end{bmatrix} \begin{bmatrix} u \\ p \end{bmatrix} = 0 \quad (2)$$

and its fundamental solutions $\psi(t) = \exp(\lambda t)\psi_0$. From the Floquet theorem, we know that $\lambda \in \mathbb{C}$ and $\psi_0 \in X \otimes Y$ must satisfy the algebraic problem:

$$\lambda \begin{bmatrix} M & 0 \\ 0 & 0 \end{bmatrix} \psi_0 + \begin{bmatrix} K & B \\ D^* & C \end{bmatrix} \psi_0 = 0. \quad (3)$$

Note that eigenvalue problem (3) also covers the case of some special second order systems. For instance, in the absence of damping we have:

$$\begin{bmatrix} M & 0 \\ 0 & 0 \end{bmatrix} \frac{d^2}{dt^2} \begin{bmatrix} u \\ p \end{bmatrix} + \begin{bmatrix} K & B \\ D^* & C \end{bmatrix} \begin{bmatrix} u \\ p \end{bmatrix} = 0 . \quad (4)$$

Equation (4) leads to the consideration of a quadratic eigenvalue problem. It is a special type of the quadratic eigenvalue problem which can be transformed into a linear eigenvalue problem by a simple change of spectral variable.

We will restrict our analysis to considering equations (4) where operator M is a bounded positive semi-definite operator and the block operator matrix is quasi-semidefinite. For the purposes of this note, a block operator matrix is called positive quasi semi-definite if it defines a boundedly invertible self-adjoint operator and has the structure:

$$\mathcal{K} = \begin{bmatrix} K & B \\ B^* & 0 \end{bmatrix},$$

where B is the closed range operator and K is positive semidefinite operator in the sense of Kato, [8]. To tackle both problems in a unified manner, we will analyze the generalized resolvents:

$$\mathcal{R}_1 : z \mapsto \begin{bmatrix} K - zM & B \\ B^* & 0 \end{bmatrix}^{-1}, \quad \mathcal{R}_2 : z \mapsto \begin{bmatrix} K - z^2M & B \\ B^* & 0 \end{bmatrix}^{-1} \quad (5)$$

as 2×2 block operator matrices. The only assumption which we will make is that there are complex numbers $z_1, z_2 \in \mathbb{C}$ such that $\mathcal{R}_1(z_1)$ and $\mathcal{R}_2(z_2)$ are bounded and that in addition, K^{-1} is compact. The terminology for quasi-definite block operator matrices comes from [9] and the references therein.

2. Matrix analysis of the generalized resolvent

In this section, we will present matrix analysis of the generalized resolvents (5) under the additional assumption that X and Y are finite dimensional. The computations are motivated by the considerations from [10, 11]. We will restrict our analysis to the following setting. Without reducing the level of generality, we consider a general Hermitian (self-adjoint) block 2×2 matrix of the form:

$$\mathcal{K} = \begin{bmatrix} K & B \\ B^* & 0 \end{bmatrix},$$

where matrix B is such that $\|(B^*B)^{-1}\| < \infty$. Such block matrices were called quasi-semidefinite in [9]. In this case, there exists a unitary matrix $Q = [Q_1 \ Q_2]$ and a lower triangular matrix R which is invertible and:

$$B = \begin{bmatrix} Q_1 & Q_2 \end{bmatrix} \begin{bmatrix} R^* \\ 0 \end{bmatrix} .$$

This directly implies the following for the range space of the operator B and the null space (kernel) of the operator B^* :

$$\begin{aligned} \text{Im}(B) &= \text{Im}(Q_1), \\ \text{Null}(B^*) &= \text{Im}(Q_2) . \end{aligned}$$

We define the unitary block matrix:

$$\mathbb{Q} = \begin{bmatrix} Q & 0 \\ 0 & I \end{bmatrix} = Q \oplus I .$$

In the state space formulation, we will henceforth use the notation $A \oplus B$ to denote the block diagonal matrix with diagonal blocks A and B . With these definitions, we compute:

$$\mathbb{Q}^* \mathcal{K} \mathbb{Q} = \left(\begin{bmatrix} Q_1 & Q_2 \end{bmatrix} \oplus I \right)^* \mathcal{K} \left(\begin{bmatrix} Q_1 & Q_2 \end{bmatrix} \oplus I \right) = \begin{bmatrix} K_{11} & K_{12} & R^* \\ K_{21} & K_{22} & 0 \\ R & 0 & 0 \end{bmatrix} . \quad (6)$$

The analysis of [12] implies the following technical lemma.

Lemma 1. Assume that B is such that $\|(B^*B)^{-1}\| < \infty$ and Q_1, Q_2 and R are as in (6). Then,

$$\mathcal{K} = \begin{bmatrix} K & B \\ B^* & 0 \end{bmatrix}$$

is invertible if and only if $Q_2^*KQ_2 = K_{22}$ is invertible. In that case u and p which satisfy:

$$\begin{bmatrix} K & B \\ B^* & 0 \end{bmatrix} \begin{bmatrix} u \\ p \end{bmatrix} = \begin{bmatrix} f \\ g \end{bmatrix}$$

are given by:

$$u = \begin{bmatrix} Q_1 R^{-1} g \\ Q_2 K_{22}^{-1} (Q_2^* f - K_{21} R^{-1} g) \end{bmatrix},$$

$$p = Q_1^* f - K_{11} R^{-1} g - K_{12} K_{22}^{-1} (Q_2^* f - K_{21} R^{-1} g).$$

Proof. According to [9], we have:

$$\text{Null}(\mathcal{K}) = (\text{Null}(K) \cap \text{Null}(B^*)) \otimes \text{Null}(B)$$

for the null space of \mathcal{K} . The assumptions on the matrix B imply that $\text{Null}(B) = \{0\}$ and $\text{Null}(B^*) = \text{Im}(Q_2)$, and so, if $K_{22} = Q_2^*KQ_2$ is invertible, so is $(\text{Null}(K) \cap \text{Null}(B^*))$ trivial. This proves the first claim. To finish the proof of the theorem, note that (6) implies:

$$\begin{bmatrix} K_{11} & K_{12} & R \\ K_{21} & K_{22} & 0 \\ R^* & 0 & 0 \end{bmatrix} \begin{bmatrix} Q_1^* u \\ Q_2^* u \\ p \end{bmatrix} = \begin{bmatrix} Q_1^* f \\ Q_2^* f \\ g \end{bmatrix},$$

and the claim follows by equating the matrix identity block element by block element. \square

Lemma 1 directly allows for the block matrix analysis of the resolvents and was used in [12] to analyze the eigenvalue problem associated to the resolvent \mathcal{R}_1 . In particular it holds:

$$\mathbb{Q}^* \mathcal{R}_i(z) \mathbb{Q} \begin{bmatrix} f_1 \\ f_2 \\ g \end{bmatrix} = \begin{bmatrix} R^{-1} g \\ \mathcal{R}_{22,i}(z)(f_2 - (K_{21} - z^i M_{21})R^{-1} g) \\ -(K_{12} - z^i M_{12})\mathcal{R}_{22,i}(z)(f_2 - (K_{21} - z^i M_{21})R^{-1} g) + f_1 - (K_{11} - z^i M_{11})R^{-1} g \end{bmatrix},$$

where

$$\mathcal{R}_{22,i}(z) := (K_{22} - z^i M_{22})^{-1}.$$

Here, we see that the singularities of the functions $z \mapsto \mathcal{R}_i(z)$ and $z \mapsto \mathcal{R}_{22,i}(z)$ coincide. Let $\rho_i(K_{22}, M_{22}) = \{z \in \mathbb{C} : \|(K_{22} - z^i M_{22})^{-1}\| < \infty\}$ be the resolvent set of $\mathcal{R}_{22,i}$. Its complement $\text{Spec}_i(K_{22}, M_{22}) = \mathbb{C} \setminus \rho_i(K_{22}, M_{22})$ is called the spectrum of \mathcal{R}_i . In particular, when K_{22} is a positive definite Hermitian (self-adjoint) matrix, then for each $\lambda \in \text{Spec}_i(K_{22}, M_{22})$ there is a vicinity $\mathcal{U} \subset \rho_i(K_{22}, M_{22})$ such that the expansion:

$$\mathcal{R}_i(z) = \frac{1}{z - \lambda} P_i + \mathcal{H}_i(z), \quad z \in \mathcal{U},$$

holds. Here, \mathcal{H}_i is a holomorphic operator valued function and $\text{Im}(P) = \text{Null}(K_{22} - \lambda^i M_{22})$. This result follows from the celebrated Keldysh' theorem, see [13, 14]. Let us note that in the case in which we assume that K_{22} is positive definite, as will be prototypical for the applications which we have in mind, then we will study the resolvents associated with the operator $K_{22}^{-1} M_{22}$ and so obtain the results for the resolvents \mathcal{R}_i , $i = 1, 2$, see [15] and the references therein. Note that [15] is obtained in the Hilbert space setting and this will allow a direct generalization in the next section.

3. The main results

In this section, we concentrate on the operator equivalent of the matrix results. Let us assume that X and Y are Hilbert spaces. Then, we assume we have operators $K : X \rightarrow X$ and $B : Y \rightarrow X$ such that:

- (A1): K is self-adjoint and positive semi-definite;
- (A2): B is closed;
- (A3): $\|B^*(I + K)^{-1/2}\| < \infty$;
- (A4): $Y = \text{Im}(B^*(I + K)^{1/2})$;
- (A5): The restriction of the operator K on the space $\text{Im}(B^*)$ is positive definite (in the sense of quadratic forms, see below).

The restriction of the operator K on the space $\text{Null}(B^*) \subset X$, denoted by K_{22} , is defined as the operator representation, in the sense of Kato [8], of the quadratic form:

$$k_{22}(u, v) := (K^{1/2}u, K^{1/2}v), \quad u, v \in \text{Null}(B^*) \cap \text{Dom}(K^{1/2}).$$

Here, $K^{1/2}$ is a self-adjoint operator defined by spectral calculus and satisfies the requirements of the Kato's second representation theorem and $V := \text{Dom}(K^{1/2}) \subset X$ denotes the operator domain of $K^{1/2}$. The operator K_{22} is now a self adjoint and positive definite operator from $\text{Null}(B^*)$ to $\text{Null}(B^*)$ such that:

$$(K_{22}^{1/2}u, K_{22}^{1/2}v) = k_{22}(u, v), \quad u, v \in \text{Null}(B^*) \cap \text{Dom}((I + K)^{1/2})$$

and $\text{Dom}(K_{22}^{1/2}) = \text{Null}(B^*) \cap \text{Dom}((I + K)^{1/2})$.

The null space of the closed operator is closed and the assumptions (A1) and (A2) together with the closed range theorem imply:

$$X = \text{Im}(B) \oplus \text{Null}(B^*).$$

Based on this decomposition, which is an abstract version of the Hodge–Helmholtz decomposition for the Stokes operator, we will seek a block 3×3 representation of the resolvents \mathcal{R}_1 and \mathcal{R}_2 in the state space:

$$X \otimes Y = (\text{Im}(B) \oplus \text{Null}(B^*)) \otimes Y = \text{Im}(B) \otimes Y \oplus \text{Null}(B^*) \otimes Y,$$

where we have tacitly identified isomorphic Hilbert spaces. Let us now consider the following forms:

$$\begin{aligned} k_{11}(u, v) &= (K^{1/2}u, K^{1/2}v), \quad u, v \in \text{Im}(B) \cap (\text{Dom}(I + K)^{1/2}), \\ k_{21}(u, v) &= (K^{1/2}u, K^{1/2}v), \quad u \in \text{Im}(B) \cap (\text{Dom}(I + K)^{1/2}), \quad v \in \text{Null}(B^*) \cap (\text{Dom}(I + K)^{1/2}), \\ b(u, v) &= (u, B^*v), \quad u \in Y, \quad v \in V \subset X. \end{aligned} \quad (7)$$

Further, let K_{11} be the operator representation of k_{11} in the sense of Kato, and let R be the maximal operator such that:

$$(u, Rv) = b(u, v), \quad u \in Y, \quad v \in \text{Im}(B) \cap \text{Dom}((I + K)^{1/2}). \quad (8)$$

Then, by the assumptions (A3) and (A4), the operator $R : \text{Im}(B) \rightarrow Y$ is closed and has a bounded inverse.

Note that the forms k_{12} and k_{21} need not have operator representations. Also, they are conjugate to each other as forms since K is self-adjoint. However, the operator K_R defined by:

$$(K_R u, v) = k_{21}(R^{-1}u, K_{22}^{-1/2}v), \quad u \in Y, \quad v \in \text{Null}(B^*), \quad (9)$$

is a bounded operator. Assumptions (A1) and (A3) also imply that $R^{-*}K_{11}R$ is a bounded self-adjoint operator.

We now present the main theorem on the block operator representation of the resolvents \mathcal{R}_i , $i = 1, 2$.

Theorem 1. *Let M be a bounded and self-adjoint semi-definite operator on $\text{Im}(B) \otimes \text{Null}(B^*)$ and let K and B be operators which satisfy (A1)–(A5). Let further K_{11} and K_{22} be the operators as defined in (7)–(9) and let K^{-1} be compact. Then for $z \in \mathbb{C}$ the operator $\mathcal{R}_i(z)$ is bounded if and only if $\mathcal{R}_{22,i}(z) = (K_{22} - z^i M_{22})^{-1}$ is bounded. Here we assumed the obvious notation for the block 2×2 representation of a bounded operator M on $\text{Im}(B) \otimes \text{Null}(B^*)$.*

Proof. Recall from [5, 6, 9] that the operator:

$$\mathcal{K} = \begin{bmatrix} K & B \\ B^* & 0 \end{bmatrix}$$

is semibounded from below and so due to its quasi semi-definitnes we can justify the following computation in the product space $(\text{Im}(B) \times \text{Null}(B^*)) \otimes Y$:

$$\mathcal{R}_i(z) = (R^{-*} \oplus K_{22}^{-1/2} \oplus I) \begin{bmatrix} R^{-*}K_{11}R^{-1} - z^i R^{-*}M_{11}R^{-1} & K_R - z^i R^{-*}M_{12}K_{22}^{-1/2} & I \\ K_R^* - z^i K_{22}^{-1/2}M_{21}R^{-1} & I - z^i K_{22}^{-1/2}M_{22}K_{22}^{-1/2} & 0 \\ I & 0 & 0 \end{bmatrix}^{-1} (R^{-1} \oplus K_{22}^{-1/2} \oplus I).$$

The 3×3 block operator matrix in the middle has only bounded entries and it is, using the same technique as in Lemma 1, boundedly invertible if and only if:

$$\|(I - z^i K_{22}^{-1/2} M_{22} K_{22}^{-1/2})^{-1}\| < \infty .$$

Since K_{22} has a compact inverse and M_{22} is bounded this is equivalent, see [15], to $\|(K_{22} - z^i M_{22})^{-1}\| < \infty$ which was the claim of the theorem. \square

Recall that under the assumption that K_{22}^{-1} is compact and K_{22} is positive definite and self-adjoint operator we can again apply Keldysch's theorem on the operator function $z \mapsto (K_{22} - z^i M_{22})^{-1}$. For any $i = 1, 2$ and $\lambda_i \in \rho_i(K_{22}, M_{22})$ there exists a vicinity $\mathcal{U}_i \subset \rho_i(K_{22}, M_{22})$ and an operator P_i and a holomorphic operator valued function \mathcal{H}_i such that:

$$\mathcal{R}_{22,i}(z) = (K_{22} - z^i M_{22})^{-1} = \frac{1}{z - \lambda_i} P_i + \mathcal{H}_i(z), \quad z \in \mathcal{U}_i.$$

Let us assume (A1)–(A5) and in addition let K^{-1} be compact then

$$\mathcal{K} = \begin{bmatrix} K & B \\ B^* & 0 \end{bmatrix}$$

is invertible. Based on the analysis in the state space $\text{Im}(B) \otimes \text{Null}(B^*) \otimes Y$ and following the steps from [11, 12], we can construct 2×2 block matrix representation of $\mathcal{K}^{-1}\mathcal{M}$ in the product space $\text{Null}(B^*) \otimes (\text{Im}(B) \otimes Y)$ which has the form:

$$\mathcal{K}^{-1}\mathcal{M} = L_1 \begin{bmatrix} A & \\ & N \end{bmatrix} L_1^{-1}, \quad (10)$$

where A is a self-adjoint compact operator and N is a nilpotent operator such that $N^2 = 0$ and L_1 and L_1^{-1} are bounded operators. We see that the eigenvalues of the operator $\mathcal{K}^{-1}\mathcal{M}$ are directly mapped by to the eigenvalues of \mathcal{R}_i by either inverting them or by inverting their squares. Note that A might have a zero as an eigenvalue. In this case, we say that this zero corresponds to the eigenvalue at infinity of the original eigenvalue problem associated with \mathcal{R}_i , $i = 1, 2$. The whole invariant space of $\mathcal{K}^{-1}\mathcal{M}$ associated with the operator N corresponds to the eigenvalue at infinity of \mathcal{R}_i , $i = 1, 2$. On the other hand, the eigenvalues of $\mathcal{K}^{-1}\mathcal{M}$ in the invariant subspace associated with the operator A are all semisimple.

4. A model problem

As a model problem, we consider the curved rod model from [16, 17]. A discussion of the model is beyond the scope of this article. In the weak formulation model is given for the unknowns y and θ being the displacement of the middle curve and the infinitesimal rotation of the cross-section. Having in mind the mixed formulation of the model, see [18] for more details, we set:

$$V := H_0^1(0, l; \mathbb{R}^3) \times H_0^1(0, l; \mathbb{R}^3) \subset L^2(0, l; \mathbb{R}^3) \times L^2(0, l; \mathbb{R}^3) =: X, \quad Y := L^2(0, l; \mathbb{R}^3),$$

and define the bilinear forms:

$$k : V \times V \rightarrow \mathbb{R}, \quad k((y, \theta), (\tilde{y}, \tilde{\theta})) = \int_0^l \mathbf{Q}\mathbf{H}\mathbf{Q}^* \partial_s \theta \cdot \partial_s \tilde{\theta} ds,$$

$$b : Y \times V \rightarrow \mathbb{R}, \quad b(n, (\tilde{y}, \tilde{\theta})) = \int_0^l n \cdot (\partial_s \tilde{y} + \mathbf{t} \times \tilde{\theta}) ds,$$

where $\mathbf{H} \in \mathbb{R}^{3 \times 3}$ is a symmetric positive definite matrix describing the elastic properties of the material the rod is made of and the geometry of the cross-sections, $\mathbf{Q} = [\mathbf{t} \ \mathbf{n} \ \mathbf{b}] \in \mathbb{R}^{3 \times 3}$ is the orthogonal matrix whose columns are the tangent, the normal and the binormal of the of the middle line of the curved rod, see Fig. 1. The elastic energy of the rod is given in the form k , while the form b defines the inextensibility and unshearability conditions of the rod ($\partial_s y + \mathbf{t} \times \theta = 0$). Thus the elements of the state space $X \otimes Y$ are given by $(y, \theta) \oplus n$ and also include the Lagrange multiplier (being the contact force) related to the inextensibility and unshearability conditions.

Since V is dense in X and the form k , defined on the domain V , is closed and positive semidefinite in X and so it defines the self-adjoint positive semi-definite operator K in X in the sense of Kato. Furthermore, this choice of V allows us to conclude that the operator $B^* : X \rightarrow Y$ such that:

$$(n, B^*(y, \theta))_Y = b(n, (y, \theta))$$

is a closed operator and $\|B^*(I + K)^{-1/2}\| < \infty$. Here it is central that $\text{Im}(I + K)^{-1/2} = V$. To prove the assertion (A4) we use the inf – sup estimates for B . The details can be found in [18]. The form m , which defines

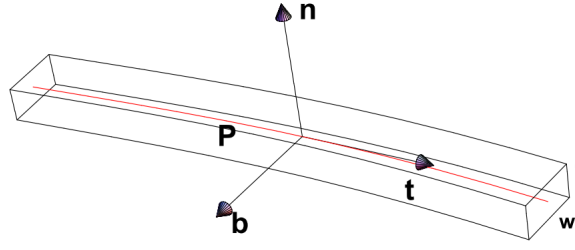


FIG. 1. A 3D elastic strut modeled by the curved rod model on the middle line of length l which is parametrized by $P : [0, l] \rightarrow \mathbb{R}^3$

the M , is given by the bounded form:

$$m : X \times X \rightarrow \mathbb{R}, \quad m((y, \theta), (\tilde{y}, \tilde{\theta})) = \int_0^l \rho A y \cdot \tilde{y} ds, \quad (11)$$

and ρ and A are the density and the area of the cross section of the rod.

4.1. Endovascular stents

Following the approach from [17] it is possible to consider the curved rod equations on the metric graph $\mathcal{N} = (\mathcal{V}, \mathcal{E})$, where \mathcal{V} are vertices and \mathcal{E} are edges which are assumed to be parametrized by $P^i : [0, l_i] \rightarrow \mathbb{R}^3$, $i = 1, \dots, \#\mathcal{E}$. Here $\#\mathcal{E} < \infty$ is the number of edges in \mathcal{N} . As before deformation of the i th edge is described by $u^i = (y^i, \theta^i)$, the displacement of the i th middle curve and the infinitesimal rotation of its cross-section. We further impose the restriction that between edges the displacements and the rotations of the cross-sections have to be continuous. Thus, for the domain of the form of the elastic energy, we have:

$$V = \{\mathbf{u} = (u^1, \dots, u^{\#\mathcal{E}}) \in \prod_{i=1}^{\#\mathcal{E}} H^1(0, l_i; \mathbb{R}^3) \times H^1(0, l_i; \mathbb{R}^3) : \\ u^i((P^i)^{-1}(v)) = u^j((P^j)^{-1}(v)), \forall v \in \mathcal{V}, v \in e^i \cap e^j, i, j = 1, \dots, \#\mathcal{E}\}.$$

For the spaces X and Y , we choose:

$$X = \prod_{i=1}^{\#\mathcal{E}} L^2(0, l_i; \mathbb{R}^3) \times L^2(0, l_i; \mathbb{R}^3), \\ Y = \prod_{i=1}^{\#\mathcal{E}} L^2(0, l_i; \mathbb{R}^3) \times \mathbb{R}^3 \times \mathbb{R}^3.$$

The forms that define the problem are now given by:

$$k : V \times V \rightarrow \mathbb{R}, \quad k(\mathbf{u}, \tilde{\mathbf{u}}) = \sum_{i=1}^{\#\mathcal{E}} \int_0^{l_i} \mathbf{Q}^i \mathbf{H}^i \mathbf{Q}^i * \partial_s \theta^i \cdot \partial_s \tilde{\theta}^i ds, \\ b : Y \times V \rightarrow \mathbb{R}, \quad b(\mathbf{n}, \tilde{\mathbf{u}}) = \sum_{i=1}^{\#\mathcal{E}} \int_0^{l_i} n^i \cdot (\partial_s \tilde{y}^i + \mathbf{t}^i \times \tilde{\theta}^i) ds + \alpha \cdot \sum_{i=1}^{\#\mathcal{E}} \int_0^{l_i} \tilde{y}^i ds + \beta \cdot \sum_{i=1}^{\#\mathcal{E}} \int_0^{l_i} \tilde{\theta}^i ds.$$

Here, we used the notation:

$$\mathbf{n} = (n^1, \dots, n^{\#\mathcal{E}}, \alpha, \beta) \in Y$$

for the Lagrange multipliers in the mixed formulations; n^i is the contact force associated to the i th edge while α and β are multipliers associated to fixing the overall center of mass and overall infinitesimal rotation.

With this, we again obtain the resolvent:

$$\mathcal{K} - z^2 \mathcal{M} = \begin{bmatrix} K - z^2 M & B \\ B^* & 0 \end{bmatrix},$$

where the operator K is the “stiffness” operator, the operator B implements the inextensibility of the middle curve of all edges and ushearability of cross-sections of all edges of the stent and fixing the overall center of mass and rotation of the whole stent and the “mass” operator M is defined by the bounded form:

$$m : X \times X \rightarrow \mathbb{R}, \quad m(\mathbf{u}, \tilde{\mathbf{u}}) = \sum_{i=1}^{\#\mathcal{E}} \int_0^{l_i} \rho^i A^i y^i \cdot \tilde{y}^i ds. \quad (12)$$

Since the boundary conditions for the stent problem are homogeneous Neumann type nonuniqueness of the solution of the problem is associated. Thus, by fixing the overall translation and rotation, we obtain uniqueness of the problem, i.e. the operator K is invertible on $\text{Null } B^*$. More details on the model and its properties can be found in [18].

This construction of the operator B and the space Y illustrates a use of the freedom in formulating the mixed problem so that (A1)–(A5) hold. The inf – sup analysis of B can be performed in the metric graph setting following a similar argument as in the single rod case to show that (A4) holds. For details see [18]. Also, as is known from the Stokes problem, the freedom in the choice of Y , which is there the pressure space, is directly used to satisfy condition (A4) possibly by restricting the size of Y . A description of the code which was used to generate Fig. 2, as well as discretization details, is based on [19].

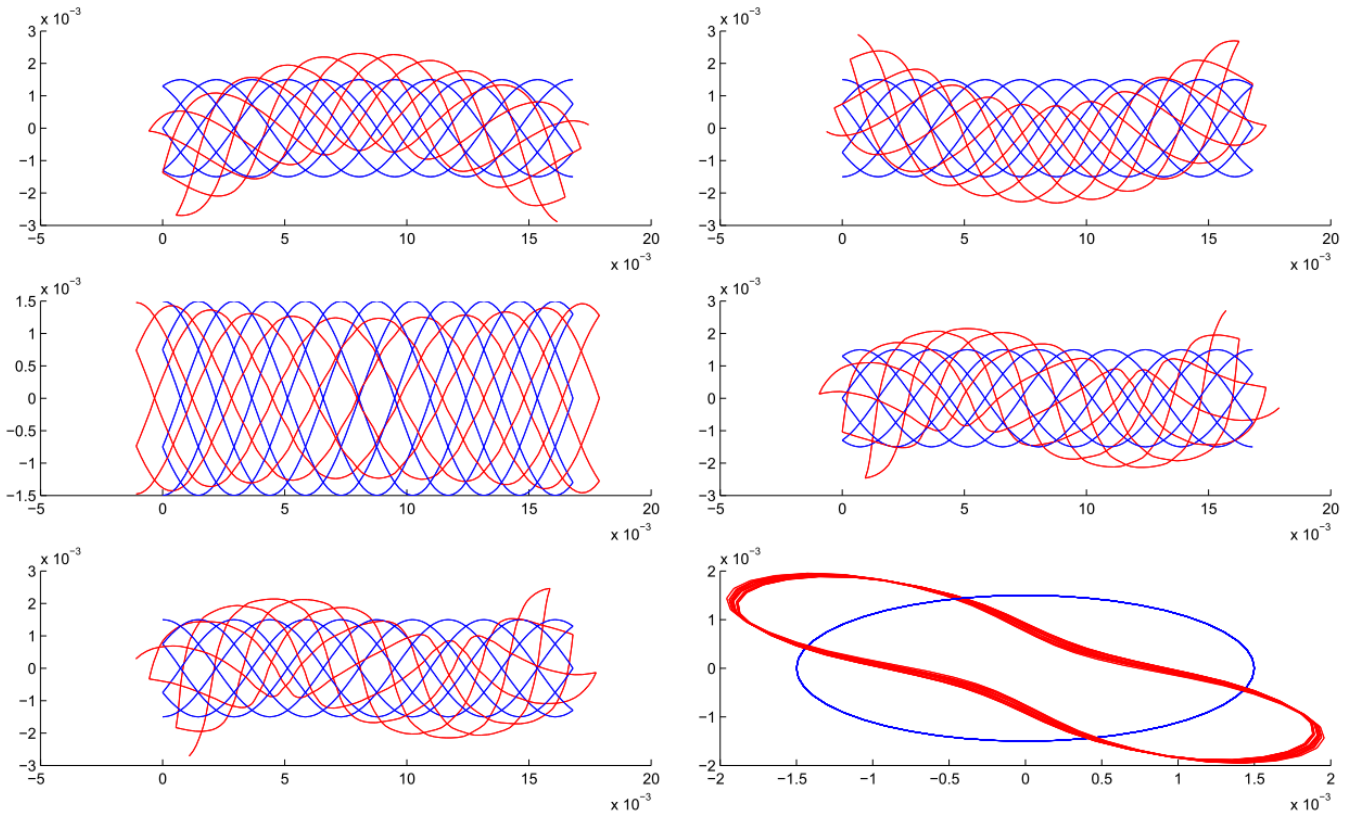


FIG. 2. A metric graph model of an endovascular stent. Six lowermost eigenmodes of the Palmaz stent computed with the MATLAB based on [19]

Acknowledgements

This research has been supported by the grant HRZZ-9345 of the Croatian Science Foundation. We gratefully acknowledge the support. We use the MATLAB [19].

References

- [1] Kunkel P., Mehrmann V. *Differential-algebraic equations*. EMS Textbooks in Mathematics. European Mathematical Society (EMS), Zürich, 2006.
- [2] Altmann R., Levajković T., Mena H. Operator differential-algebraic equations with noise arising in fluid dynamics. *Monatshefte für Mathematik*, 2016, P. 1–40.
- [3] Emmrich E., Mehrmann V. Operator differential-algebraic equations arising in fluid dynamics. *Comput. Methods Appl. Math.*, 2013, **13** (4), P. 443–470.
- [4] Tretter C. *Spectral theory of block operator matrices and applications*. Imperial College Press, London, 2008.
- [5] Grubišić L., Kostrykin V., Makarov K.A., Veselić K. Representation theorems for indefinite quadratic forms revisited. *Mathematika*, 2013, **59** (1), P. 169–189.
- [6] Grubišić L., Kostrykin V., Makarov K.A., Veselić K. The Tan 2Θ theorem for indefinite quadratic forms. *J. Spectr. Theory*, 2013, **3** (1), P. 83–100.
- [7] Tartar L. *An introduction to Navier-Stokes equation and oceanography*, **1** of *Lecture Notes of the Unione Matematica Italiana*. Springer-Verlag, Berlin; UMI, Bologna, 2006.
- [8] Kato T. *Perturbation Theory for Linear Operators*. Springer-Verlag, Berlin, 1980.
- [9] Veselić I., Veselić K. Spectral gap estimates for some block matrices. *Oper. Matrices*, 2015, **9** (2), P. 241–275.
- [10] Cliffe K.A., Garratt T.J., Spence A. Eigenvalues of the discretized Navier-Stokes equation with application to the detection of Hopf bifurcations. *Adv. Comput. Math.*, 1993, **1** (3–4), P. 337–356.
- [11] Stykel T. Low-rank iterative methods for projected generalized Lyapunov equations. *Electron. Trans. Numer. Anal.*, 2008, **30**, P. 187–202.
- [12] Cliffe K.A., Garratt T.J., Spence A. Eigenvalues of block matrices arising from problems in fluid mechanics. *SIAM J. Matrix Anal. Appl.*, 1994, **15** (4), P. 1310–1318.
- [13] Markus A.S., Macaev V.I. On the spectral theory of holomorphic operator-valued functions in Hilbert space. *Funkcional. Anal. i Priložen.*, 1975, **9** (1), P. 76–77.
- [14] Mennicken R., Möller M. Non-self-adjoint boundary eigenvalue problems. In *North-Holland Mathematics Studies*, **192**, North-Holland Publishing Co., Amsterdam, 2003.
- [15] Nakić I. On the correspondence between spectra of the operator pencil $A - \lambda B$ and of the operator $B^{-1}A$. *Glas. Mat. Ser. III*, 2016, **51** (71), P. 197–221.
- [16] Jurak M., Tambača J. Linear curved rod model. General curve. *Math. Models Methods Appl. Sci.*, 2001, **11** (7), P. 1237–1252.
- [17] Čanić S., Tambača J. Cardiovascular stents as PDE nets: 1D vs. 3D. *IMA J. Appl. Math.*, 2012, **77** (6), P. 748–770.
- [18] Grubišić L., Iveković J., Tambača J., Žugec B. Mixed formulation of the equilibrium problem for elastic stents. *Submitted to Rad HAZU*, 2017, URL: <http://arxiv.org/abs/1703.05074>.
- [19] Iveković J. Numerical method for the model of linearized stents. Diploma thesis, Department of Mathematics, Faculty of Science, University of Zagreb, 2015.

Zigzag chain model and its spectrum

A. S. Melikhova

ITMO University, Kronverkskiy, 49, St. Petersburg, 197101, Russia

alina.s.melikhova@gmail.com

PACS 02.30.Tb

DOI 10.17586/2220-8054-2017-8-2-188-193

This work describes the development of a model using a zigzag chain of weakly-coupled ball resonators with Neumann boundary conditions. The chain is assumed to be constructed of identical resonators connected through point-like apertures. The connecting points are described by their delta-coupling with a constant intensity. The model is based on the theory of self-adjoint extensions of symmetrical operators. Due to effectively one-dimensional joints, the 3D problem can be solved with assistance from the transfer matrix approach. This allows us to study the spectrum of the physical system. In particular, it is proven that the discrete spectrum of direct zigzag chain is empty while bending deformation leads to the appearance of non-empty discrete spectrum. In addition, the continuous spectrum has band structure. With the help of asymptotic study, we obtain the dependence of the spectrum structure on the geometrical and physical parameters of the system: zigzag angle, bend angle and coupling intensity.

Keywords: bending deformation, extension theory, transfer-matrix approach, discrete spectrum.

Received: 18 January 2017

Revised: 18 February 2017

1. Introduction

Various chain structures have been widely discussed recently. These structures can be constructed of elements of different dimensions. Regarding one-dimensional elements, spectral properties of an infinite chain-like quantum graph, which consists of identical rings, were studied in [1, 2]. In [3] authors deal with a similar chain made up of hexagons. Two-dimensional resonators are in the focus of the papers [4–6], which studies spectral problems of direct and zigzag-like chains of disks, and bent chain of nanospheres respectively. Finally, chains consisting of three-dimensional resonators are presented in [7–9].

Different chains structures with resonators as cells are used in optical systems (see, for example, so called SCISSOR device [10], optical waveguide system [11], optical delay line [12]), in nanoelectronics (see, for instance, nano peapod and similar systems [13–17]) and in molecular biology (for example, for creation of biosensors [18]).

The spectrum of stationary Schrödinger equation in the zigzag-like chain system will be examined in the present paper. The Hamiltonian for this model is constructed in the framework of extension's theory (see, for example, [19] and the extensive bibliography of [20]). We assume that resonators in our model are weakly coupled, i. e. we employ the approach known as model of zero-width slit [21–24]. We consider Neumann boundary conditions at resonator's border and δ -coupling condition at its contact points. In this paper, we analyze the dependence of spectral characteristics on the geometrical and physical parameters of the system.

2. Model and geometry

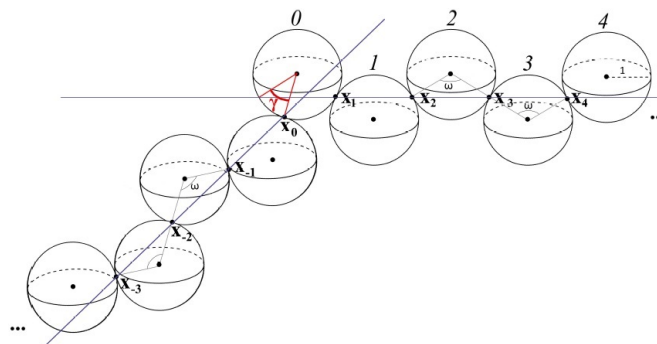


FIG. 1. Geometry of the system

The three-dimensional zigzag chain of weakly coupled ball resonators with a kink is considered (see Fig. 1). From geometrical point of view this system has the following properties:

- it is made up of infinite quantity of identical ball resonators (it is convenient to enumerate them: $j \in \mathbb{Z}_- \cup \{0\} \cup \mathbb{Z}_+$). Without loss of generality, we assume that all balls are of unit radius;
- any two neighboring resonators ($j-1$ and j) have only one common point (\mathbf{x}_j). Before applying "bending" deformation all such contact points lie on the same straight line;
- ω is the zigzag angle: $\omega \in (\pi/3; \pi]$;
- any two connected resonators can be taken as a basic cell;
- "bending" deformation (kink) occurs at a single point (\mathbf{x}_0) shifted by an angle γ : $\gamma \in [0; \omega - \pi/3)$.

When geometry of the system is comprehended, the Hamiltonian can be described. We employ the theory of self-adjoint extensions of symmetric operator to present states of non-relativistic spinless particles that are placed into the chain in the absence of external fields. For a better understanding of the restriction-extension scheme which is used for model construction, let one examine more scrupulously the simplest chain – two connected resonators. And then one just needs to extend this scheme for the infinite case.

Consider two coupled resonators (Ω_0, Ω_1) with one common point \mathbf{x}_1 at the border. Let $-\Delta$ be the orthogonal sum of the Laplace operators with Neumann boundary conditions in $L_2(\Omega_0) \oplus L_2(\Omega_1)$. Restrict this operator to the set of smooth functions vanishing at contact point \mathbf{x}_1 . This procedure gives us symmetric operator $-\Delta_0$ with deficiency indices $(2, 2)$, however, it is a non-self-adjoint operator. Its self-adjoint extension gives us the model of resonators coupled through point-like aperture. It is clear that the self-adjoint extension is a restriction of the adjoint operator. Therefore, one should first describe the adjoint operator. This can be done in several ways. For example, this can be done using the so-called boundary triplet approach (see, for example, [25, 26]) or the Von Neumann's formulas can be used (see, for instance, [27, 28]). In our case, the domain of the adjoint operator in our model (due to the positivity of the operator and, correspondingly, regularity of negative points at the real axis) can be written in such manner:

$$D(-\Delta_0^*) = D(-\Delta_0^F) \dot{+} N_{\lambda_0},$$

where $D(-\Delta_0^F)$ is the Friedrichs extension of our restricted operator and N_{λ_0} is a deficiency subspace that refers to negative real regular point λ_0 (see, for example, [29]). Correspondingly, elements $f \in D(-\Delta_0^*)$ have such form:

$$f = \begin{pmatrix} f_0 \\ f_1 \end{pmatrix} = \begin{pmatrix} f_0^0 + a_0^- G_0(\mathbf{x}, \mathbf{x}_1, \lambda_0) + b_0^- \\ f_1^0 + a_1^+ G_1(\mathbf{x}, \mathbf{x}_1, \lambda_0) + b_1^+ \end{pmatrix},$$

where $f_i^0 \in D(-\Delta_0)$, $i = 0, 1$ and a_0^- , a_1^+ , b_0^- , b_1^+ are some coefficients (by signs "+" and "-" nearby i -th coefficient we distinguish ones that refer to i -th resonator but to different contact points). By establishing the cross-linking between these coefficients the self-adjoint operator can be obtained.

These algorithm can be quite easily extended to the case of an infinite chain. In this case the initial (before including the interactions between resonators) operator is $-\Delta$: $-\Delta = \bigoplus_{j \in \mathbb{Z}} (-\Delta_j)$ in $\bigoplus_{j \in \mathbb{Z}} L_2(-\Delta_j)$. Moreover, this operator should be restricted on the set of all smooth functions from $D(-\Delta)$ that vanish at contact points \mathbf{x}_j . Such restriction is a symmetric operator with deficiency indices (∞, ∞) and Green's functions $G(\mathbf{x}, \mathbf{x}_j, \lambda_0)$ as deficiency elements.

An adjoint operator for an infinite chain is constructed similarly to the simple case of two resonators. Finally, the self-adjointness condition is satisfied with:

$$\begin{cases} a_j^+ = -a_{j-1}^-, \\ b_j^+ = b_{j-1}^-, \end{cases} \quad (1)$$

where coefficients b_j^\pm are defined by coefficients a_j^\pm :

$$b_j^+ = a_j^+ \lim_{\mathbf{x} \rightarrow \mathbf{x}_j} (G(\mathbf{x}, \mathbf{x}_j, \lambda) - G(\mathbf{x}, \mathbf{x}_j, \lambda_0)) + a_j^- G(\mathbf{x}_{j+1}, \mathbf{x}_j, \lambda), \quad (2)$$

$$b_{j-1}^- = a_{j-1}^+ G(\mathbf{x}_{j-1}, \mathbf{x}_j, \lambda) + a_{j-1}^- \lim_{\mathbf{x} \rightarrow \mathbf{x}_j} (G(\mathbf{x}, \mathbf{x}_j, \lambda) - G(\mathbf{x}, \mathbf{x}_j, \lambda_0)). \quad (3)$$

Moreover, when our model is supplemented by δ -coupling conditions at contact points \mathbf{x}_j (with coupling constant $\alpha \in \mathbb{R}$), system of equations (1) transforms to:

$$\begin{cases} a_j^+ = -a_{j-1}^-, \\ b_j^+ - b_{j-1}^- = -\alpha a_{j-1}^-. \end{cases} \quad (4)$$

3. Spectral analysis

The system being under investigation is periodic in part, and the transfer-matrix approach is a good tool for spectral analysis (see, e.g., [30]); in fact, that the asymptotic behavior of the $\left\| \begin{pmatrix} a_j^+ & a_j^- \end{pmatrix}^T \right\|$ is determined by the spectral properties of the transfer-matrix.

First, we consider a simple zigzag chain without kinks. By serial employment of the formulas (2)–(4), one can easily obtain the matrix relation between coefficients a_{j-1}^\pm and a_{j+1}^\pm as follows:

$$\begin{pmatrix} a_{j+1}^+ \\ a_{j+1}^- \end{pmatrix} = \mathbf{M} \begin{pmatrix} a_{j-1}^+ \\ a_{j-1}^- \end{pmatrix},$$

$$\mathbf{M} = \mathbf{M}_{j-1 \rightarrow j} \mathbf{M}_{j \rightarrow j+1} = \begin{pmatrix} -1 & -\frac{2g-\alpha}{G_\omega} \\ \frac{2g-\alpha}{G_\omega} & \left(\frac{2g-\alpha}{G_\omega}\right)^2 - 1 \end{pmatrix}, \quad (5)$$

where $g = \lim_{\mathbf{x} \rightarrow \mathbf{x}_j} (G(\mathbf{x}, \mathbf{x}_j, \lambda) - G(\mathbf{x}, \mathbf{x}_j, \lambda_0))$, $G_\omega = G(\mathbf{x}_j, \mathbf{x}_{j+1}, \lambda)$ ($j \neq 0$) and \mathbf{M} is a transfer-matrix that permits one to find proper conditions for spectral analysis. Namely, the value λ belongs to the continuous spectrum if the absolute value of the corresponding eigenvalue μ of matrix \mathbf{M} is equal to one. Whereas for belonging of the value λ to the discrete spectrum it is necessary for the corresponding eigenvalue μ of matrix \mathbf{M} in absolute value to be less than one.

From (5), one can find the explicit form of the transfer-matrix's eigenvalues and eigenvectors:

$$\mu_\pm = \frac{((2g-\alpha)/G_\omega)^2}{2} - 1 \pm \sqrt{\left(\frac{((2g-\alpha)/G_\omega)^2}{2} - 1\right)^2 - 1}, \quad (6)$$

$$\nu_\pm = \begin{pmatrix} -\frac{2g-\alpha}{2G_\omega} \pm \sqrt{\left(\frac{2g-\alpha}{2G_\omega}\right)^2 - 1} \\ 1 \end{pmatrix}. \quad (7)$$

Thus, keeping in mind the above-mentioned spectral properties of the transfer-matrix and (6), one can obtain the inequality that describes the band structure of the continuous spectrum of the model Hamiltonian:

$$\left| \frac{2g-\alpha}{G_\omega} \right| \leq 2. \quad (8)$$

It is clear that the presence of one kink in the chain (introduced as a shift of one contact point) does not affect the band structure. However, such bending deformation potentiates the appearance of bound states in the gaps.

Let us now examine the bending area more accurately. In order to find a decreasing at infinity solution, one should first merge two semi-infinite chains via a new transfer-matrix \mathbf{M}_γ :

$$\mathbf{M}_\gamma = \mathbf{M}_{-1 \rightarrow 0} \mathbf{M}_{0 \rightarrow -1} = \begin{pmatrix} -\frac{G_\gamma}{G_\omega} & -\frac{2g-\alpha}{G_\omega} \\ -\frac{2g-\alpha}{G_\omega} & \frac{(2g-\alpha)^2 - G_\omega^2}{G_\gamma G_\omega} \end{pmatrix}, \quad (9)$$

where $G_\gamma = G(\mathbf{x}_0, \mathbf{x}_1, \lambda)$. And then, one should satisfy the linear dependence condition:

$$\begin{vmatrix} a_1^+ & a_{-1}^+ \\ a_1^- & a_{-1}^- \end{vmatrix} = 0, \quad (10)$$

where $\begin{pmatrix} a_{-1}^+ & a_{-1}^- \end{pmatrix}^T = \zeta \nu_\pm$. By substituting expressions (5), (7) and (9) into condition (10), one can obtain the spectral equation in the most simple form as follows:

$$\frac{G_\gamma}{G_\omega} - \frac{G_\omega}{G_\gamma} + \left(\frac{2g-\alpha}{G_\omega}\right)^2 \left(\frac{G_\omega}{G_\gamma} - 1\right) = 0. \quad (11)$$

Finally, one should take into account that the solution λ^* of (11) must satisfy the corresponding condition on μ :

$$\left| \frac{2g-\alpha}{G_\omega} \right|_{\lambda^*} > 2. \quad (12)$$

Thus, the solutions of problem (11)–(12) draws up the discrete spectrum of the model Hamiltonian.

4. Results and discussions

Gathering all facts mentioned above, the Theorem representing spectrum of the model Hamiltonian is stated: **Theorem.** *Let the bend angle γ of the chain belong to $[0; \omega - \pi/3)$. The continuous spectrum has band structure and is given by Equation (8). There are eigenvalues of infinite multiplicity which are given by the eigenvalues of the Neumann Laplacian for the ball corresponding to the eigenfunctions vanishing at the both opposite points of the ball (\mathbf{x}_j and \mathbf{x}_{j-1}). If there is no bending deformation ($\gamma = 0$), the discrete spectrum is empty. There exist values of the model parameters α , γ , λ_0 and ω such that the model Hamiltonian has eigenvalues in the gaps in the case with $\gamma \neq 0$ and these eigenvalues are given by (11)–(12).*

Figures 2–5 depict the results of numerical modelling of the spectral problem. From these graphs, one can see how changing the parameters influence its spectral characteristics (gap widths, band’s splitting (Fig. 2–4) and eigenvalue’s appearance (Fig. 5)).

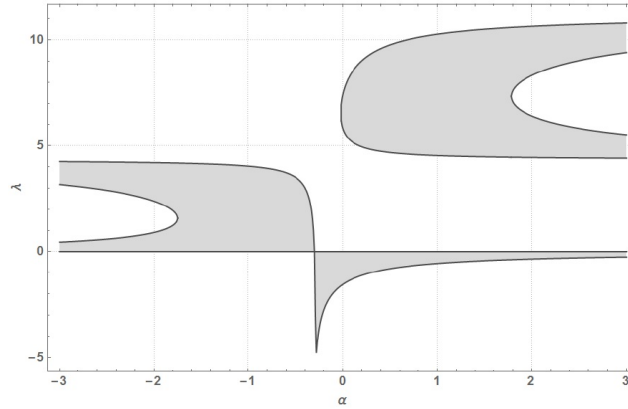


FIG. 2. Band structure of continuous spectrum depending on α (with $\omega = 5\pi/6$, $\gamma = 0$)

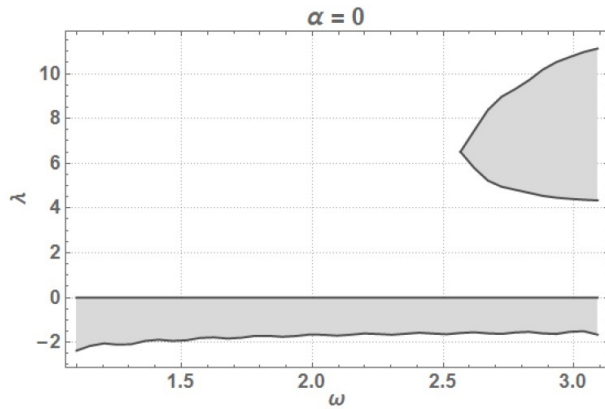


FIG. 3. Band structure of continuous spectrum depending on ω during “free particle motion” ($\alpha = 0$, $\gamma = 0$)

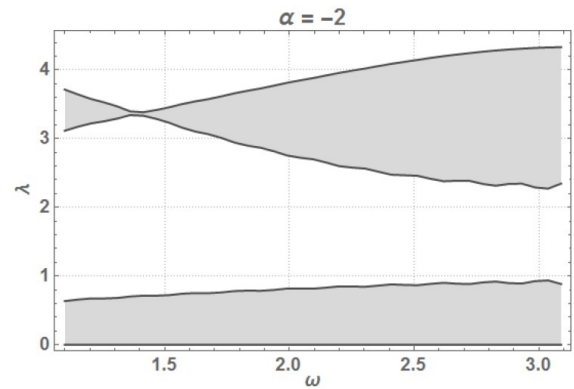


FIG. 4. Band structure of continuous spectrum depending on ω in the presence of δ -potentials at contact points \mathbf{x}_j ($\gamma = 0$)

Furthermore, analytical expressions for the lowest energy band can be obtained. Specifically, the asymptotic expressions for borders of the first energy band can be gained from (8) when λ tends to zero:

$$\lambda_1 = \frac{3}{2\pi} \left(\frac{3}{4\pi\lambda_0} - \frac{\alpha}{2} + \sum_{k=1, l=0}^{\infty} \frac{N_{l,k}}{x_{l,k}^2} \left(P_l(\cos \omega) - \frac{\lambda_0}{x_{l,k}^2 - \lambda_0} \right) \right)^{-1} + (\lambda_1^2),$$

$$\lambda_2 = \left[\frac{\alpha}{2} - \frac{3}{4\pi\lambda_0} + \sum_{k=1, l=0}^{\infty} \left(-\frac{N_{l,k}}{x_{l,k}^2} \left(\frac{\lambda_0}{x_{l,k}^2 - \lambda_0} + P_l(\cos \omega) \right) \right) \right] \left[\sum_{k=1, l=0}^{\infty} \frac{N_{l,k} (1 - P_l(\cos \omega))}{x_{l,k}^4} \right]^{-1} + O(\lambda_2^2),$$

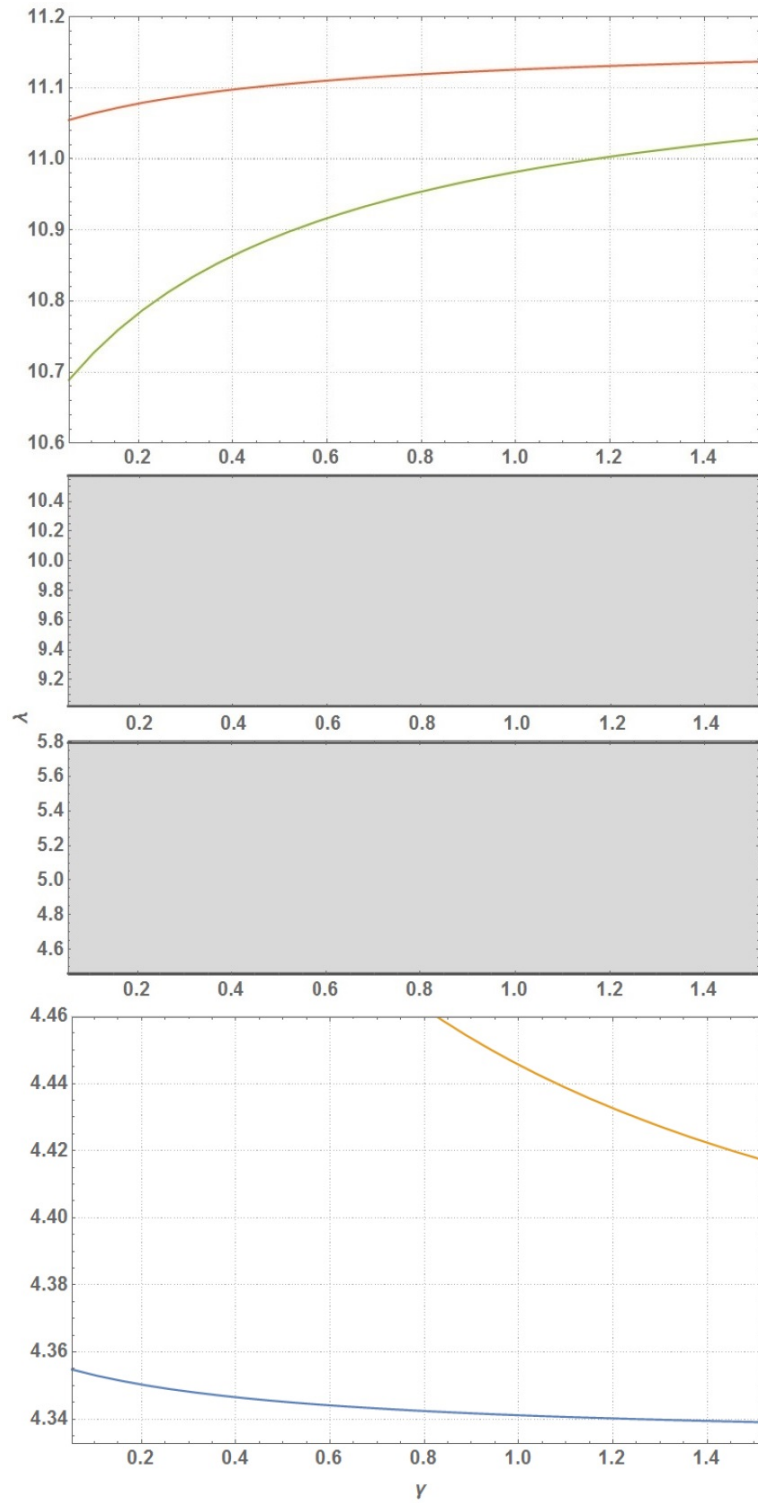


FIG. 5. Spectral structure depending on bending angle γ (with $\alpha = 2$ and $\omega = 5/6$): grey bands — the two neighboring bands of continuous spectrum (do not depend on γ), curves — values that belong to the discrete spectrum

where $x_{l,k}$ is a k -th root of the equation: $j'_l(x) = 0$ and $N_{l,k}$ is a normalization factor.

Thus, this model allows us to obtain both analytical and numerical results for a non-trivial three-dimensional system. Finally, the described model allows us to exert an influence on the spectrum of the zigzag-like chain of resonators. Variation of the model parameters is a tool which can be utilized to control and modify the spectrum structure.

Acknowledgements

This work was partially financially supported by the Government of the Russian Federation (grant 074-U01), by grant MK-5161.2016.1 of the President of the Russian Federation, by grant 16-11-10330 of Russian Science Foundation.

References

- [1] Duclos P., Exner P., Turek O. On the spectrum of a bent chain graph. *J. Phys. A: Math. Theor.*, 2008, **41**, P. 415206.
- [2] Popov I. Yu., Smirnov P. I. Spectral problem for branching chain quantum graph. *Phys. Lett. A*, 2013, **377**(6), P. 439–442.
- [3] Popov I. Yu., Skorynina A. N., Blinova I. V. On the existence of point spectrum for branching strips quantum graph. *J. Math. Phys.*, 2014, **55**, P. 033504.
- [4] Grishanov E. N., Eremin D. A., Ivanov D. A., Popov I. Yu. Periodic chain of disks in a magnetic field: bulk states and edge states. *Nanosystems: Phys. Chem. Math.*, 2015, **6**(5), P. 637–643.
- [5] Blinova I. V., Melikhova A. S., Popov I. Yu. Periodic chain of resonators: gap control and the system geometry. *Journal of Physics: Conference Series*, 2016, **735**, P. 012062.
- [6] Eremin D. A., Ivanov D. A., Popov I. Yu. Electron energy spectrum for a bent chain of nanospheres. *Eur. Phys. J. B*, 2014, **87**(8), P. 181.
- [7] Melikhova A. S., Popov I. Yu. Spectral problem for solvable model of bent nano peapod. *Applicable Analysis*, 2017, **96**(2), P. 215–224.
- [8] Melikhova A. S. Estimates for numbers of negative eigenvalues of Laplacian for Y-type weakly coupled chain of ball resonators. *Mathematical Results in Quantum Mechanics. Proceedings of the QMath12 Conference*, 2014, P. 325–330.
- [9] Melikhova A. S., Popov I. Yu. Bent and branched chains of nanoresonators. *Journal of Physics: Conference Series*, 2014, **541**, P. 012061.
- [10] Heebner J. E., Boyd R. W., and Park Q.-H. SCISSOR solitons and other novel propagation effects in microresonator-modified waveguides. *J. Opt. Soc. Am. B*, 2002, **19**, P. 722–731.
- [11] Popov I. Yu., Trifanov A. I. and Trifanova E. S. Coupled dielectric waveguides with photonic crystal properties. *Comput. Math. Math. Phys.*, 2010, **50**(11), P. 1830–1836.
- [12] Lenz G., Eggleton B. J., Madsen C. K., and Slusher L. E. Optical Delay Lines Based on Optical Filters. *IEEE J. Quantum Electron*, 2001, **37**(4), P. 525–532.
- [13] Wang Y., Zhang H. J., Lu L., Stubbs L. P., Wong C. C., Lin J. Designed Functional Systems from Peapod-like Co@Carbon to Co₃O₄@Carbon Nanocomposites. *ACS Nano*, 2010, **4**(8), P. 4753–4761.
- [14] Yang Y., Li L., Li W. Plasmon Absorption of Au-in-CoAl₂O₄ Linear Nanopeapod Chains. *J. Phys. Chem. C*, 2013, **117**(27), P. 14142–14148.
- [15] Enyashin A. N., Ivanovskii A. L. Nanotubular composites: modeling of capillary filling of nanotubes of disulfide of molybdenum by molecules of TiCl₄. *Nanosystems: Phys. Chem. Math.*, 2010, **1**(1), P. 63–71.
- [16] Krivanek O. L., Dellby N., Murfitt M. F., Chisholm M. F., Pennycook T. J., Suenaga K. and Nicolosi V. Gentle STEM: ADF imaging and EELS at low primary energies. *Ultramicroscopy*, 2010, **110**(8), P. 935–945.
- [17] Abou-Hamad E., Kim Yo., Talyzin A. V., Goze-Bac Ch., Luzzi D. E., Rubio A., Wagberg T. Hydrogenation of C60 in Peapods: Physical Chemistry in Nano Vessels. *J. Phys. Chem. C*, 2009, **113**, P. 8583–8587.
- [18] Boyd R. W. and Heebner J. E. Sensitive disk-resonator photonic biosensor. *Appl. Opt.*, 2001, **40**(31), P. 5742–5747.
- [19] Albeverio S., Gestesy F., Hoegh-Krohn R., et al. *Solvable models in quantum mechanics*. Springer-Verlag, Berlin, 1988.
- [20] Popov I. Y., Kurasov P. A., Naboko S. N., Kiselev A. A., Ryzhkov A. E., Yafyasov A. M., Miroshnichenko G. P., Kareshina E. Yu., Kruglov V. I., Pankratova T. F., Popov A. I. A distinguished mathematical physicist Boris S. Pavlov. *Nanosystems: Phys., Chem., Math.*, 2016, **7**(5), P. 782–788.
- [21] Popov I. Yu. The resonator with narrow slit and the model based on the operator extensions theory. *J. Math. Phys.*, 1992, **33**(11), P. 3794–3801.
- [22] Popov I. Yu. 2012 Operator extensions theory model for electromagnetic field-electron interaction. *J. Math. Phys.*, 2012, **53**(6), P. 063505.
- [23] Popov I. Yu. Extensions theory and localization of resonances for domains of trap type. *Mat. Sbornik*, 1990, **181**(10), P. 1366–1390.
- [24] Popov I. Yu. Model of point-like window for electromagnetic Helmholtz resonator. *Zeitschrift Anal. Anwend.*, 2013, **32**, P. 155–162.
- [25] Behrndt J., Langer M., Lotoreichik V. Boundary triples for Schrödinger operators with singular interactions on hypersurfaces. *Nanosystems: Phys., Chem., Math.*, 2016, **7**(2), P. 290–302.
- [26] Boitsev A. A., Neidhardt H., Popov I. Yu. Dirac operator coupled to bosons. *Nanosystems: Phys., Chem., Math.*, 2016, **7**(2), P. 332–339.
- [27] Geyler V. A., Pavlov B. S., Popov I. Yu. Spectral properties of a charged particle in antidot array: A limiting case of quantum billiard. *J. Math. Phys.*, 1996, **37**(10), P. 5171–5194.
- [28] Berndt J., Malamud M., Neidhardt H. Scattering matrices and Weyl functions. *Proc. London Math. Soc.*, 2008, **97**(3), P. 568–598.
- [29] Birman M. Sh., Solomjak M. Z. *Spectral Theory of Self-Adjoint Operators in Hilbert Space*. D. Reidel Publishing Company, Dordrecht, 1987, 301 pp.
- [30] Anikevich A. S. Negative eigenvalues of the Y-type chain of weakly coupled ball resonators. *Nanosystems: Phys. Chem. Math.*, 2013, **4**(4), P. 545–549.

Model of tunnelling through double quantum layer in a magnetic field

D. L. Meynster, I. Y. Popov, A. I. Popov

ITMO University, Kronverkskiy, 49, St. Petersburg, 197101, Russia
mldml@gmail.com, popov1955@gmail.com, popov239@gmail.com**PACS 73.21.Ac; 02.30.Tb****DOI 10.17586/2220-8054-2017-8-2-194-201**

Several explicitly solvable models are constructed for electron tunneling in a system of double two-dimensional periodic arrays of quantum dots with two laterally coupled leads in a homogeneous magnetic field are constructed. The theory of self-adjoint extensions of symmetric operators is used for modelling of electron transport. Dependencies of the transmission coefficient on the magnetic field, the energy of electron and the distance between layers are investigated. The results are compared with those of tunnelling through the corresponding single-layer periodic arrays.

Keywords: quantum dots array, magnetic field, scattering.*Received:* 16 February 2017*Revised:* 18 March 2017**1. Introduction**

Since the publication of famous Hofstadter paper [1], research interest in the spectral properties of two-dimensional periodic arrays in a magnetic field has greatly increased. The fractal structure of the spectrum has been a theoretical result for long time, but subsequently, experimental confirmation was obtained. Electron tunneling through periodic array of quantum dots in a homogeneous magnetic field has been intensively investigated over the last few years because it can be relevant for nanotechnology applications [2–4].

There are several different approaches for building models of quantum dot arrays. In this paper, the zero-range potential model [5,6] based on the theory of self-adjoint extensions of symmetric operators is used (see, e.g., [7–12] and references in [13]). One of its benefits is that the model is explicitly solvable.

In double-layer lattices, the layer number provides an additional degree of freedom, which leads to some interesting experimentally measurable physical effects [14]. We suggest several explicitly solvable models for double two-dimensional layer of quantum dots using the approach described in [15].

Because of high quality of nanostructure devices, large Fermi wave length (i.e. the de Broglie wavelength of electrons with energy close to the Fermi energy) (4×10^{-8} m) and long mean free path of electron (10^{-5} m) can be observed. Therefore, one deals with the ballistic regime of electron transport. In this case, the Landauer-Buttiker formalism can be used to derive the conductivity σ for the nanostructure with several leads from the transmission coefficient $T(E)|_{E=E_F}$ (here E_F is the Fermi energy).

In the simplest case (one incoming and one outgoing channel), the Landauer formula has the form $\sigma = \frac{e^2 T}{h(1-T)}$ [16]. Here, e is the electron charge, \hbar is the Planck's constant. The geometry of a nanostructure can influence transmission coefficient significantly [17].

In this article we, consider tunneling in the system consisting of double two-dimensional periodic array (with square or hexagonal (honeycomb) lattices in each layer) of quantum dots with two connected semi-infinite leads orthogonal to the plane of the array. We study the influence of the magnetic field and tunneling electron energy on the transmission coefficient and compare our results with the tunneling through the corresponding single-layer periodic arrays studied earlier [18, 19]. The main ideas of the present paper was described in an extended abstract [20].

We start from the Hamiltonian of a single particle in constant homogeneous magnetic field B . Let us assume that particle has mass m and electric charge e . Since the space is \mathbb{R}^3 , we choose a standard basis $\mathbf{i}, \mathbf{j}, \mathbf{k}$ such that \mathbf{B} is collinear to \mathbf{k} : $\mathbf{B} = B\mathbf{k}$, $B \neq 0$. Then, the particle can move freely along z axis, and the state space of the model is $L^2(\mathbb{R}^2)$, where \mathbb{R}^2 is the plane based on vectors \mathbf{i}, \mathbf{j} .

The Hamiltonian H_0 has the following form:

$$H_0 = \frac{1}{2m} \left(\hat{p} - \frac{e}{c} \mathbf{A}(\mathbf{r}) \right)^2, \quad (1)$$

where c is the speed of light, $\hat{p} = -i\hbar\nabla$ is the two-dimensional momentum operator, $\mathbf{A}(\mathbf{r})$ is a vector potential of the field \mathbf{B} ($\mathbf{B} = \text{rot } \mathbf{A}$). Vector potential is not unique, we will use the symmetric gauge ($\mathbf{A}(\mathbf{r}) = \frac{1}{2} \mathbf{B} \times \mathbf{r}$).

The following standard notations are used: $\omega = |eB|/cm$ is the cyclotron frequency; $\Phi_0 = 2\pi\hbar c/|e|$ is the quantum of the magnetic flux; $\xi = \pm B/\Phi_0$ – number of the flux quanta through the unit area in \mathbb{R}^2 . The sign of ξ is chosen in such a way that the condition $\xi eB > 0$ holds. We will also use the system of units in which $e = \hbar = m = c = 1$, to simplify the calculations. Then, H_0 can be rewritten in the following form:

$$H_0 = -\frac{1}{2} \left[\left(\frac{\partial}{\partial x} + \pi i \xi y \right)^2 + \left(\frac{\partial}{\partial y} - \pi i \xi x \right)^2 \right]. \quad (2)$$

We will also need the Green function of H_0 , which has the form ([6]):

$$G_0(\mathbf{r}, \mathbf{r}', E) = \frac{1}{2\pi} \Gamma \left(\frac{1}{2} - \frac{E}{\omega} \right) \exp \left(-\pi i \mathbf{r} \wedge \mathbf{r}' - \frac{1}{2} \pi \xi \|\mathbf{r} - \mathbf{r}'\|^2 \right) \times \Phi \left(\frac{1}{2} - \frac{E}{\omega}, 1, \pi \xi \|\mathbf{r} - \mathbf{r}'\|^2 \right). \quad (3)$$

Here, $\Gamma(x)$ is the Euler Gamma-function, $\Phi(a, c, x)$ is the confluent hypergeometric function of the second kind [21].

2. Tunnelling through double layer

Note that different explicitly solvable models can be built here, depending on how electron tunneling between layers is considered (see Fig. 1 and Fig. 2). Both model types will be built here for hexagonal and square lattices.

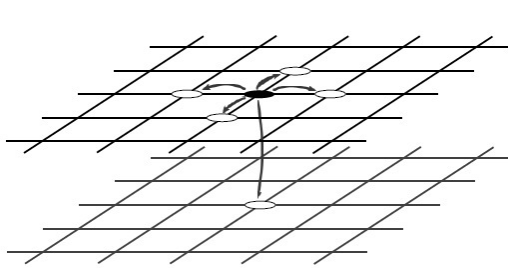


FIG. 1. Model with immediate tunnelling between layers

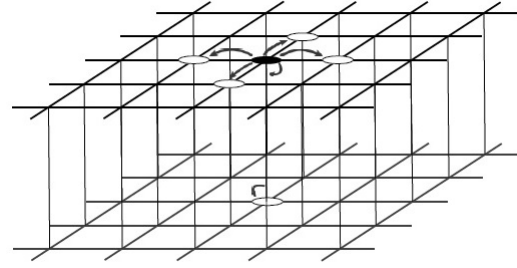


FIG. 2. Model with channel between layers represented by wire of finite length

2.1. Model with immediate tunneling between layers

First, we build the model for the square lattice. We assume that the state space of the model is a direct sum of two identical state spaces, one for each layer:

$$\mathcal{H} = L_2(\mathbb{R}^2) \oplus L_2(\mathbb{R}^2). \quad (4)$$

Then, the unperturbed Hamiltonian has the following form:

$$H_0 = H_L \oplus H_L, \quad (5)$$

where H_L is the Hamiltonian for the single layer with lattice Ξ (see, e.g., [20]).

To use the Krein's resolvent formula, we first restrict operator H_L onto the set of smooth functions vanishing at the points of the lattice, let the restricted operator be S_L . Then, the restriction of H_0 has the form:

$$S_0 = S_L \oplus S_L. \quad (6)$$

The deficiency space for S_0 is the direct sum:

$$\mathcal{G} = \mathcal{G}_L \oplus \mathcal{G}_L, \quad (7)$$

where $\mathcal{G}_L = l_2(\Xi)$ is the deficiency space for operator S_L .

In its turn, the Krein Q-function is the direct sum:

$$Q = Q_L \oplus Q_L, \quad (8)$$

where Q_L is the Krein Q-function for the corresponding single layer.

Let f be a function from $l_2(\Xi)$, then the Krein Γ -function of pair (H_L, S_L) for a single layer has the following form:

$$(\Gamma_L(\zeta)f)(\mathbf{r}) = \sum_{\gamma \in \Xi} G_0(\mathbf{r}, \gamma; \zeta) f(\gamma), \quad (9)$$

and the Krein Γ -function for the whole system can be defined as the direct sum:

$$\Gamma = \Gamma_L \oplus \Gamma_L. \quad (10)$$

Finally, using the Krein resolvent formula for infinite deficiency indices, we obtain an expression for the Green function of H :

$$G(\mathbf{r}, \mathbf{r}'; \zeta) = G_0(\mathbf{r}, \mathbf{r}'; \zeta) - \sum_{\gamma, \gamma' \in \Xi \oplus \Xi} [Q(z) + A]_{\gamma, \gamma'}^{-1} G_0(\mathbf{r}, \gamma; \zeta) G_0(\gamma', \mathbf{r}'; \zeta). \quad (11)$$

Now, we need a self-adjoint operator. It is related with the properties of A . We assume that the probability of tunneling between non-adjacent points of the lattice is negligible. Due to the periodicity of the system, the Hamiltonian of a single layer H_L should be invariant with respect to the magnetic translation group transformations (see, e.g., [25]), therefore, we have the following property for the terms of operator A_L of the single layer:

$$A_{L\lambda-\gamma, \mu-\gamma} = \exp(i\pi\xi(\gamma \wedge (\lambda - \mu))) A_{L\lambda, \mu}. \quad (12)$$

As a consequence, it is sufficient to define elements $A_{L\lambda, 0}$ (see [22] for more detailed explanation):

$$A_{L\lambda, 0} = \alpha \left(\delta(\lambda_1, 0)(\delta(1, \lambda_2) + \delta(-1, \lambda_2)) + \delta(0, \lambda_2)(\delta(\lambda_2, 1) + \delta(\lambda_2, -1)) \right). \quad (13)$$

Here α is some constant which characterizes the intensity of the interaction.

Now, we need to take into account tunneling between layers, hence, operator A takes the following form:

$$A = \begin{bmatrix} A_L & \alpha I \\ \alpha I & A_L \end{bmatrix}. \quad (14)$$

In the case of hexagonal lattice the main change is different magnetic translations group which lead to changes of the form of operator A_L [26]:

$$\begin{aligned} A_{L\lambda_i, \lambda_j} = \alpha & \left[\delta(\lambda_i - \mathbf{a}_1, \lambda_j - \mathbf{b}) + \delta(\lambda_i - \mathbf{a}_2, \lambda_j - \mathbf{b}) + \delta(\lambda_i - \mathbf{a}_1 - \mathbf{a}_2, \lambda_j - \mathbf{b}) \right. \\ & + \exp\left(\frac{2}{3}i\pi\xi(\delta(\lambda_i + \mathbf{a}_1 - \mathbf{b}, \lambda_j) - \delta(\lambda_i + \mathbf{a}_2 - \mathbf{b}, \lambda_j))\right) \\ & \left. \times \left(\delta(\lambda_i + \mathbf{a}_1 - \mathbf{b}, \lambda_j) + \delta(\lambda_i + \mathbf{a}_2 - \mathbf{b}, \lambda_j) + \delta(\lambda_i + \mathbf{a}_1 + \mathbf{a}_2 - \mathbf{b}, \lambda_j) \right) \right]. \quad (15) \end{aligned}$$

2.2. Model with channel between layers

First, we need to define the state space of this model. As in the previous case, the state space of a single layer is \mathcal{H}_L . We assume that the distance between layers is d . Let \mathcal{H}_v be the state space of a single vertical wire, $\mathcal{H}_v = L_2([0; d])$. Obviously, the state space of the whole set of wires is defined as a direct sum:

$$\mathcal{H}_V = \bigoplus_{\gamma \in \Xi} \mathcal{H}_v. \quad (16)$$

Then, the whole model has the following state space:

$$\mathcal{H} = \mathcal{H}_L \oplus \mathcal{H}_V \oplus \mathcal{H}_L. \quad (17)$$

Therefore, the Hamiltonian of the system (if the interaction is switched off) has the form:

$$H = H_L \oplus H_V \oplus H_L, \quad (18)$$

where $H_V = \bigoplus_{\gamma} H_{v\gamma}$, $H_v = -\frac{\partial}{\partial x^2}$ — operator under Neumann conditions at points 0 and d .

Restrict H_v onto $D = \{\varphi \mid \varphi(0) = \varphi(d) = 0\}$, if S_v is the restricted (symmetric) operator and $S_V = \bigoplus_{\gamma} S_{v\gamma}$, then, the Hamiltonian $S = S_L \oplus S_V \oplus S_L$ is the restriction of H .

The deficiency space for operator S_v is $\mathcal{G}_v = \mathbb{C}^2$, for G_V : $\mathcal{G}_V = \bigoplus_{\gamma} \mathcal{G}_{v\gamma}$. Then, for S , one has:

$$\mathcal{G} = \mathcal{G}_L \oplus \mathcal{G}_V \oplus \mathcal{G}_L. \quad (19)$$

The Green function for H_v is well-known:

$$G_v(x, x'; \zeta) = -\frac{1}{2k \sin(kd)} \left(\cos(k(d - |x' - x|)) + \cos(k(d - (x' + x))) \right). \quad (20)$$

The Krein Γ -function for a single wire has the following form:

$$\left(\Gamma_v(\zeta) \begin{pmatrix} \xi_1 \\ \xi_2 \end{pmatrix} \right) (x) = \begin{pmatrix} G_v(x, 0; \zeta) \xi_1 \\ G_v(x, d; \zeta) \xi_2 \end{pmatrix}. \quad (21)$$

Then, $\Gamma_V = \bigoplus_{\gamma} \Gamma_v$ and $\Gamma = \Gamma_L \oplus \Gamma_V \oplus \Gamma_L$. The Krein Q -function for a single wire has the form of 2×2 -matrix:

$$Q_v(\zeta) = \begin{bmatrix} G_v(0, 0; \zeta) & G_v(0, d; \zeta) \\ G_v(d, 0; \zeta) & G_v(d, d; \zeta) \end{bmatrix}. \quad (22)$$

Hence, the Krein Q -function for the set of wires is $Q_V(\zeta) = \bigoplus_{\gamma \in \Xi} Q_v(\zeta)$, and for the whole system, we have:

$$Q(\zeta) = Q_L(\zeta) \oplus Q_V(\zeta) \oplus Q_L(\zeta). \quad (23)$$

To obtain the matrix of interactions A , let us first define matrices A_{1V} and A_{2V} , which characterize the tunneling from the first or the second layer, correspondingly, to the layer of vertical wires. For the single wire, we have

$A_{1v} = \begin{bmatrix} \alpha & 0 \end{bmatrix}$. Then, one has $A_{1V} = \bigoplus_{\gamma \in \Xi} A_{1v\gamma}$. Similarly, $A_{v2} = \begin{bmatrix} \alpha \\ 0 \end{bmatrix}$ and $A_{V2} = \bigoplus_{\gamma \in \Xi} A_{v2\gamma}$. Consider also

$A_{V1} = A_{1V}^T$, $A_{2V} = A_{V2}^T$. Finally, we get the following matrix A :

$$A = \begin{bmatrix} A_L & A_{1V} & 0 \\ A_{V1} & 0 & A_{V2} \\ 0 & A_{2V} & A_L \end{bmatrix}. \quad (24)$$

3. Model of tunnelling

Now, we would like to construct the general model of tunneling through the quantum layer (single or double, it doesn't matter). To do that, we use the idea from [27, 28]: let D be any device that is connected to a pair of semi-infinite leads at points C_- and C_+ (Fig. 3) We assume that the Green function G_D for D is already known. Let \mathcal{H}_D be the state space for the device, \mathcal{H}_{\pm} be the state spaces for leads, then, the state space for the whole system is given as follows:

$$\mathcal{H}_0 = \mathcal{H}_- \oplus \mathcal{H}_D \oplus \mathcal{H}_+. \quad (25)$$

The Hamiltonian of the system without interaction between the device and the channels is just the orthogonal sum of the corresponding operators:

$$H_0 = H_- \oplus H_D \oplus H_+, \quad (26)$$

where H_D is the Hamiltonian of a charged particle in D , H_{\pm} is the Hamiltonian of the charged particle in space $L^2(R_{\pm})$ under Neumann conditions at the edge (it has the form $-\frac{\partial}{\partial x^2}$). It is easy to find the Green functions for H_{\pm} :

$$G_{\pm}(x, x'; \zeta) = \frac{i}{2k} \left[\exp(ik|x - x'|) + \exp(\pm ik(x + x')) \right], \quad (27)$$

where $k^2 = \zeta$.

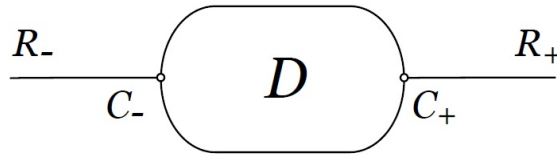


FIG. 3. Model of the device with connected leads

Using the theory of self-adjoint extensions again, we can obtain the model Hamiltonian \mathcal{H} . To do that, we, first, restrict H_0 onto the set of smooth functions vanishing at the points C_{\pm} , then, build its extension H .

After solving the scattering problem for H , we obtain the following formula for the transmission coefficient $T(E)$:

$$T(E) = \frac{|(\alpha_- \alpha_+ Q_{21}^D)^2|}{E |\det[Q(E) + A]|^2}. \quad (28)$$

Here A is the matrix of the self-adjoint operator that characterizes the extension,

$$A = \begin{bmatrix} 0 & \alpha_- & 0 & 0 \\ \alpha_- & 0 & 0 & 0 \\ 0 & 0 & 0 & \alpha_+ \\ 0 & 0 & \alpha_+ & 0 \end{bmatrix}, \quad (29)$$

$Q(E)$ is the Krein Q-function:

$$Q(E) = \begin{bmatrix} Q_-(E) & 0 & 0 & 0 \\ 0 & Q_D^{11}(E) & Q_D^{12}(E) & 0 \\ 0 & Q_D^{21}(E) & Q_D^{22}(E) & 0 \\ 0 & 0 & 0 & Q_+(E) \end{bmatrix}, \quad (30)$$

$Q_{\pm}(E) = G_{\pm}(0, 0; E)$ and Q_D is 2×2 Krein Q-function for the extension, where $Q_D^{12}(E) = \overline{Q_D^{21}(E)} = G_D(\mathbf{r}_1, \mathbf{r}_2; E)$ and $Q_D^{11}(E), Q_D^{22}(E)$ are the regular parts of $G_D(r_1, r_1; E), G_D(r_2, r_2; E)$, correspondingly. Values α_{\pm} describe the quality of contacts C_{\pm} . This technique was used in [18] to construct a model of tunneling through single quantum electron layer.

4. Results and comparison with single-layer arrays

For numerical experiments in this section, constants $\alpha, \alpha_-, \alpha_+$ were all selected to be equal to 1. Only a finite fragment of an infinite lattice is used for calculations since points which are far enough from contacts don't have much influence on transmission coefficient value. For the square lattice, the basic vectors $a_1 = (1, 0), a_2 = (0, 1)$ were used; the hexagonal (honeycomb) lattice is presented as a sum of two square lattices.

The transmission coefficient T is calculated as a function of electron energy E for different values of the magnetic field B . The resulting function of two values is represented as a contour plot. We assume that both contacts are in the same lattice cell, calculations show that putting them in different cells of the lattice leads to decreasing of T but doesn't add or remove any other significant effects.

During the investigation of tunneling through single-layer lattices, wide zones in the resulting contour plot with very low value of T were discovered [18, 19]. The widths of these zones are greater than the product of the Boltzmann constant and the temperature value and, thus, this phenomenon is physically measurable. Our calculations show that these zones are preserved both in the square and the hexagonal lattice cases (see Figs. 4, 5, 6 and 7). Plots were built for the model with direct tunneling between the layers. The model with channels between the layers gives one qualitatively analogous result – such zones exist too.

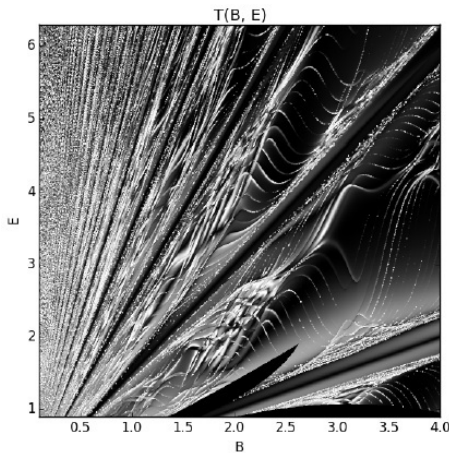


FIG. 4. Dependence of transmission coefficient value T on electron energy E and magnetic field B : case of single-layer square lattice. B and E are in dimensionless units

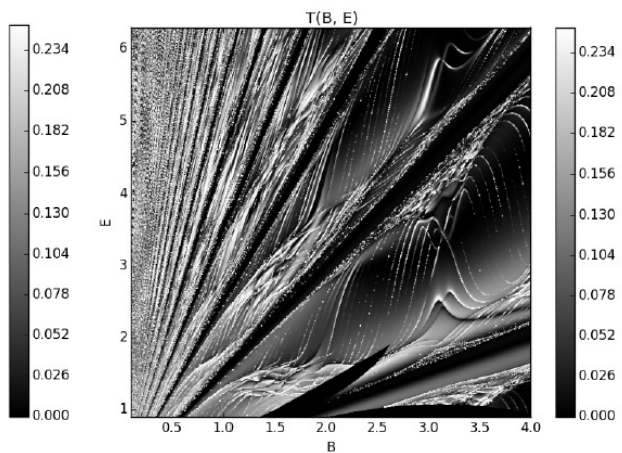


FIG. 5. Dependence of transmission coefficient value T on electron energy E and magnetic field B : case of double-layer square lattice. B and E are in dimensionless units

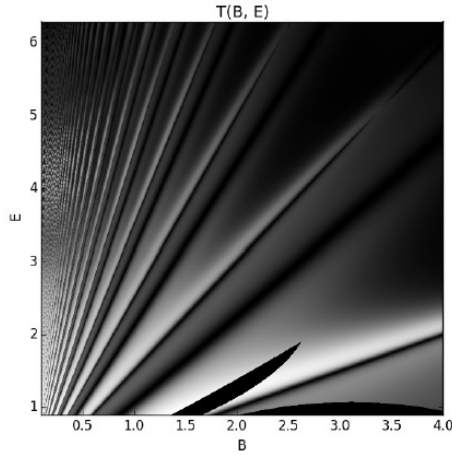


FIG. 6. Dependence of transmission coefficient value T on electron energy E and magnetic field B : case of single-layer hexagonal lattice. B and E are in dimensionless units

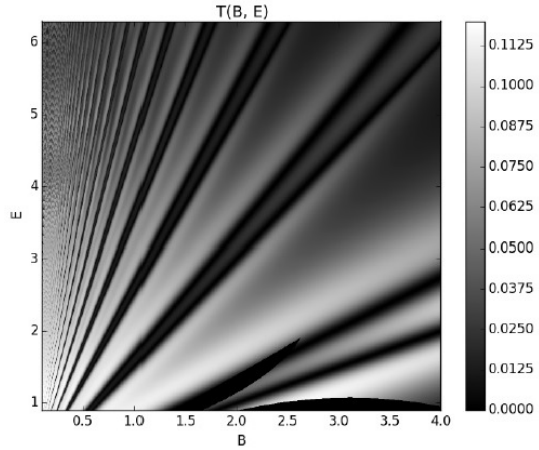


FIG. 7. Dependence of transmission coefficient value T on electron energy E and magnetic field B : case of double-layer hexagonal lattice. B and E are in dimensionless units

It can be observed that the middle of each dark stripe in Fig. 4 and Fig. 5 coincides with some singularity of $\Gamma\left(\frac{1}{2} - \frac{E}{\omega}\right)$ (which is one of multipliers in (3)). The dependence of T on B and E shown in the figures is very complicated. For the hexagonal (honeycomb) lattice, it is also complicated but local oscillations of T have less amplitude, that is why in Figs. 6, 7 looks more monotone. Such effect is related to the complex structure of the spectrum of the Hamiltonian for periodic array of quantum dots. Particularly, it is known that if the number of the magnetic flux quanta through the basic cell of the lattice is rational irreducible fraction N/M , then each Landau level (energy level for single center in a magnetic field) splits into M sublevels. For the case of irrational flux, the spectrum has fractal structure. Correspondingly, one has so-called Hofstadter-type “energy-flux” diagram. It was proved theoretically for different cases (see, e.g., [29,30,32]) and was observed experimentally (see, e.g., [34,35]). As for the comparison of tunneling for single-layer and double-layer cases, one observes that in the model with double layer, dark stripes are wider and inside zones between these stripes, T value is, generally, greater. In the case of the hexagonal lattice, when considering double-layer model, dark stripes pairs are closer to each other and value of T in zones between them is less than in the single-layer case. The behavior of T in a neighborhoods of “zero transmission stripes” is shown in details in Figs. 8, 9 for a particular value of the magnetic field.

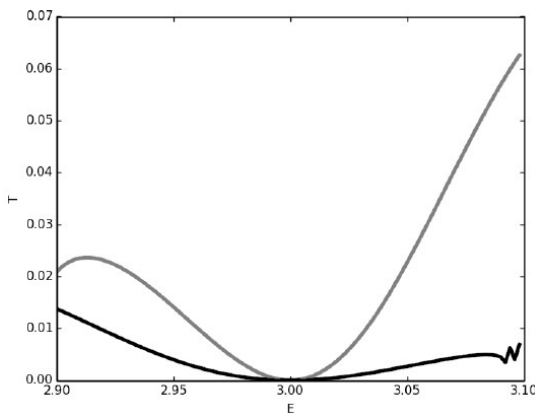


FIG. 8. Comparison of $T(E)$ for $B = 2.0$ (square lattice). Black line is for double layer model, grey one is for single layer model. B and E are in dimensionless units

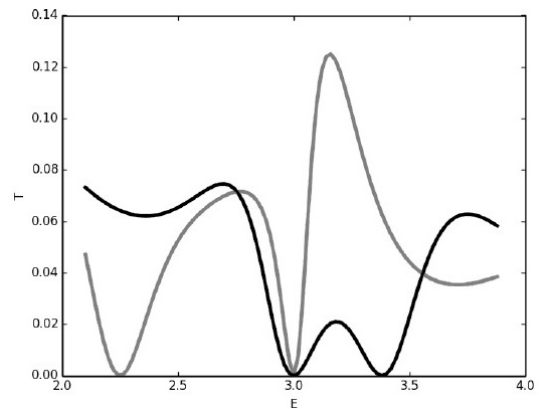


FIG. 9. Comparison of $T(E)$ for $B = 2.0$ (hexagonal lattice). Black line is for double layer model, grey one is for single layer model. B and E are in dimensionless units

It is also interesting to look for the dependence of transmission coefficient value T on the distance d between the layers in the models with channels between the quantum layers. The function $T(d)$ is oscillating. It can be explained by some resonance effects in the quantum structure due to the additional operator for the connecting segments (see Figs. 10 and 11).

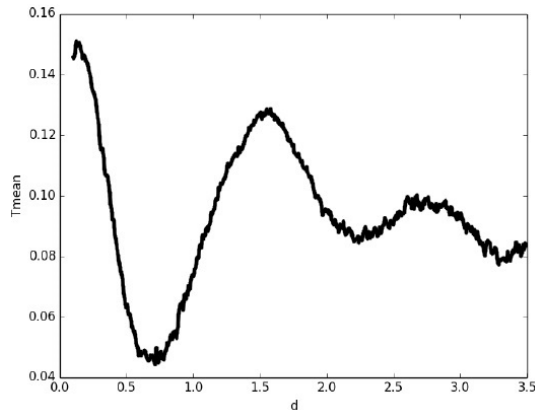


FIG. 10. Dependence of transmission coefficient T on distance between layers d (square lattice). d is in dimensionless units

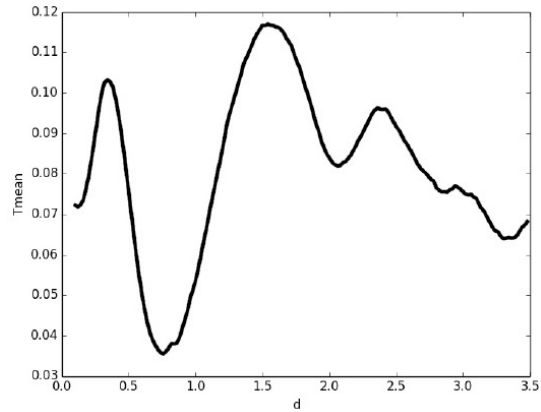


FIG. 11. Dependence of transmission coefficient T on distance between layers d (hexagonal lattice). d is in dimensionless units

Acknowledgements

This work was partially financially supported by the Government of the Russian Federation (grant 074-U01), by grant MK-5161.2016.1 of the President of the Russian Federation, DFG Grant NE 1439/3-1, by grant 16-11-10330 of Russian Science Foundation.

References

- [1] Hofstadter D.R. Energy levels and wavefunctions of Bloch electrons in rational and irrational magnetic fields. *Phys. Rev.*, 1976, **B14**, P. 2239–2249.
- [2] Gonzalez A., Capote R. Vertical magneto-tunneling through a quantum dot and the density of states of small electronic systems. *Physica E*, 2001, **10**(4), P. 528–534.
- [3] Brunner R., Meisels R., et al. Magneto-transport in open quantum dot arrays at the transition from low to high magnetic fields: regularity and chaos. *Int. J. Mod. Phys.*, 2007, **B21**, P. 1288–1296.
- [4] Roco M.C., Mirkin C.A., Hersam M.C. *Nanotechnology Research Directions for Societal Needs in 2020. Retrospective and Outlook*. Berlin, Springer, 2010.
- [5] Bloch I., Dalibard J., Zwerger W. Many-body physics with ultracold gases. *Rev. Mod. Phys.*, 2008, **80**, P. 885–964. DOI: 10.1103/RevModPhys.80.885.
- [6] Geyler V.A. The two-dimensional Schrödinger operator with a homogeneous magnetic field and its perturbations by periodic zero-range potentials. *St. Petersburg Mathematical Journal*, 1992, **3**(3), P. 489–532.
- [7] Mantile A. A linearized model of quantum transport in the asymptotic regime of quantum wells. *Nanosystems: Phys. Chem. Math.*, 2015, **6**, P. 100–112.
- [8] Dabrowski L., Grosse H. On nonlocal point interactions in one, two, and three dimensions. *J. Math. Phys.*, 1985, **26**, P. 2777–2780.
- [9] Albeverio S., Kurasov P. *Singular perturbations of differential operators. Solvable Schrödinger type operators*. London Mathematical Society Lecture Notes, 2005, 271 pp.
- [10] Geyler V.A., Pavlov B.S., Popov I.Yu. One-particle spectral problem for superlattice with a constant magnetic field. *Atti Sem. Mat. Fis. Univ. Modena.*, 1998, **46**, P. 79–124.
- [11] Pavlov B.S. Extensions theory and explicitly-solvable models. *Uspekhi Mat. Nauk*, 1987, **42**(6), P. 99–131.
- [12] Geyler V.A., Pavlov B.S., Popov I.Yu. Spectral properties of a charged particle in antidot array: A limiting case of quantum billiard. *J. Math. Phys.*, 1996, **37**(10), P. 5171–5194.
- [13] Popov I.Y., Kurasov P.A., et al. A distinguished mathematical physicist Boris S. Pavlov. *Nanosystems: Phys. Chem. Math.*, 2016, **7**(5), P. 782–788.
- [14] Eisenstein J.P., et al. New fractional quantum Hall state in double-layer two-dimensional electron systems. *Phys. Rev. Lett.*, 1992, **68**(9), P. 1383–1386.
- [15] Geyler V.A., Popov I.Yu. Solvable model of a double quantum electron layer in a magnetic field. *Proc. Royal Soc. London*, 1998, **A. 454**, P. 697–705. doi: 10.1098/rspa.1998.0181.
- [16] Landauer R. Spatial variation of currents and fields due to localized scatterers in metallic conduction. *IBM J. Res. Dev.*, 1957, **49**(24), P. 17177–17184.

- [17] Pavlov B.S., Yafyasov A.M. Resonance scattering across the superlattice barrier and the dimensional quantization. *Nanosystems: Phys. Chem. Math.*, 2016, **7**(5), P. 816–834.
- [18] Popov I.Yu., Osipov S.A. Model of tunnelling through periodic array of quantum dots in a magnetic field. *Chinese Phys.*, 2012, **B21**, P. 117306.
- [19] Eremin D.A., Grishanov E.N., et al. An explicitly solvable model for tunneling through a quantum dots array in a magnetic field. *Chinese J. Phys.*, 2014, **52**(24), P. 1100–1109.
- [20] Meynster D., Popov A., Popov I. Model of tunnelling through periodic array of quantum dots. *ITM Web of Conferences*, 2017, **9**, P. 01008/1-5.
- [21] Bateman H., Erdelyi A. *Higher Transcendental Functions* (vol. 1). McGraw-Hill, New York, 1953.
- [22] Geyley V.A., Popov I.Yu. The spectrum of a magneto-Bloch electron in a periodic array of quantum dots: explicitly solvable model. *Z. Phys. B*, 1994, **93**, P. 437–439.
- [23] Geerinckx F., Peeters F.M., Devreese J.T. Effect of the confining potential on the magneto optical spectrum of a quantum dot. *J. Appl. Phys.*, 1990, **68**(7), P. 3435–3438.
- [24] Albeverio S., Gesztesy F., Hoegh-Krohn R., Holden H. *Solvable Models in Quantum Mechanics: Second Edition*. AMS Chelsea Publishing, Providence, R.I., 2005.
- [25] Geyley V.A., Popov I.Yu. Group-theoretical analysis of lattice Hamiltonian with a magnetic field. *Phys. Lett.*, 1995, **A, 201**, P. 359–364.
- [26] Geyley V.A., Popov I.Yu. Periodic array of quantum dots in a magnetic field: irrational flux, honeycomb lattice. *Z. Phys.*, 1995, **B98**, P. 473–477.
- [27] Geyley V.A., Popov I.Yu. Ballistic transport in nanostructures: explicitly solvable model. *Theor. Math. Phys.*, 1996, **107**, P. 427–434.
- [28] Geyley V.A., Popov I.Yu. Resonant tunnelling in zero-dimensional systems: Explicitly solvable model. *Phys. Lett. A*, 1994, **187**, P. 410–412.
- [29] Geyley V.A., Popov I.Yu., Popov A.V., Ovechkina A.A. Fractal spectrum of periodic quantum system in a magnetic field. *Chaos, Solitons, and Fractals*, 2000, **11**(1-3), P. 281–288.
- [30] Nemeč N., Cuniberti G. Hofstadter butterflies of bilayer graphene. *Phys. Rev. B Rapid Comm.*, 2007, **75**, 201404/1-4 (R).
- [31] Popov I.Yu., Grishanov E.N. Spectral properties of multi-layered graphene in a magnetic field. *Superlatt. Microstruct.*, 2015, **86**, P. 68–72.
- [32] Popov I.Yu., Grishanov E.N. Electron spectrum for aligned SWNT array in a magnetic field. *Superlatt. Microstruct.*, 2016, **100**, P. 1276–1282.
- [33] Grishanov E.N., Popov I.Y. Computer simulation of periodic nanostructures. *Nanosystems: Phys. Chem. Math.*, 2016, **7**(5), P. 865–868.
- [34] Albrecht C., Smet J.H., et al. Evidence of Hofstadter’s fractal energy spectrum in the quantized Hall conductance. *Phys. Rev. Lett.*, 2001, **86**, P. 147–150.
- [35] Wang Z.F., Liu F., Chou M.Y. Fractal Landau-level spectra in twisted bilayer graphene. *Nano Lett.*, 2012, **12**, P. 3833–3838.

On convergence rate estimates for approximations of solution operators for linear non-autonomous evolution equations

H. Neidhardt¹, A. Stephan², V. A. Zagrebnov³

¹WIAS Berlin, Mohrenstr. 39, D-10117 Berlin, Germany

²Humboldt Universität zu Berlin, Institut für Mathematik
Unter den Linden 6, D-10099 Berlin, Germany

³Université d’Aix-Marseille and Institut de Mathématiques de Marseille (I2M)
UMR 7373, CMI – Technopôle Château-Gombert, 13453 Marseille, France

hagen.neidhardt@wias-berlin.de, stephan@math.hu-berlin.de, valentin.zagrebnov@univ-amu.fr

PACS 02.30.Sa,02.30.Tb,02.60.Cb

DOI 10.17586/2220-8054-2017-8-2-202-215

We improve some recent estimates of the rate of convergence for product approximations of solution operators for linear non-autonomous Cauchy problem. The Trotter product formula approximation is proved to converge to the solution operator in the operator-norm. We estimate the rate of convergence of this approximation. The result is applied to diffusion equation perturbed by a time-dependent potential.

Keywords: Evolution equations, non-autonomous Cauchy problem, solution operators (propagators), Trotter product approximation, operator-norm convergence, convergence rate, operator splitting.

Received: 19 January 2017

Revised: 29 January 2017

1. Introduction

The theory of equations of evolution plays an important role in various areas of pure and applied mathematics, physics and other natural sciences [1–3]. We focus on a non-autonomous linear Cauchy problem of the form:

$$\dot{u}(t) = -(A + B(t))u(t), \quad u(s) = u_s \in X, \quad 0 < s \leq t \leq T, \quad (1.1)$$

where $\{A+B(t), \text{dom}(A) \cap \text{dom}(B(t))\}_{t \in \mathcal{I}}$ is a family of closed linear operators on the separable Banach space X , $\mathcal{I} = [0, T] \subset \mathbb{R}$. Let $\mathcal{I}_0 = (0, T]$. The solution operator $\{U(t, s)\}_{(t,s) \in \Delta}$, i.e. $u(t) = U(t, s)u_s$ solves (1.1) in some sense, can be obtained using the Howland–Evans approach. The main idea of this approach is to reformulate the *non-autonomous* problem (1.1) on X in such a way that it becomes equivalent to an *autonomous* Cauchy problem on the Banach space $L^p(\mathcal{I}, X)$ of p -summable functions on \mathcal{I} with values in X . Then solutions of the autonomous and the non-autonomous Cauchy problem are in one-to-one correspondence, and therefore, it is equivalent which of them one has to solve. Once, the solution is obtained, the problem of a good approximation arises. The Trotter product formula [4] or [5, Theorem 3.5.8] provides approximation in the strong topology. In practice, a convergence in the operator-norm topology is more useful, especially, if the error bound for approximation can be estimated. Then, for example, independent of the initial condition, the smallness of the iteration steps and their number can be calculated in such a way that the error bound of the approximation will be smaller than a given accuracy.

We are going to analyze a linear non-autonomous Cauchy problem of the form (1.1) where the aim is to find for the problem (1.1) a so-called *solution operator* or *propagator*: $\{U(t, s)\}_{(t,s) \in \Delta}$, $\Delta = \{(t, s) \in \mathcal{I}_0 \times \mathcal{I}_0 : 0 < s \leq t \leq T\}$, $\mathcal{I}_0 = (0, T]$. It has the property that $u(t) = U(t, s)u_s$ for $(t, s) \in \Delta$ is a “solution” of the Cauchy problem (1.1) for an appropriate set of initial data u_s . By definition, the propagator $\{U(t, s)\}_{(t,s) \in \Delta}$ is a *strongly continuous* operator-valued function $U(\cdot, \cdot) : \Delta \rightarrow \mathcal{B}(X)$ satisfying:

$$U(t, t) = I \quad \text{for } t \in \mathcal{I}_0, \quad U(t, r)U(r, s) = U(t, s) \quad \text{for } t, r, s \in \mathcal{I}_0 \quad \text{with } s \leq r \leq t, \\ \|U\|_{\mathcal{B}(X)} := \sup_{(t,s) \in \Delta} \|U(t, s)\|_{\mathcal{B}(X)} < \infty.$$

Our goal is to find an approximation operator $\{U_n(t, s)\}_{(t,s) \in \Delta}$, $n \in \mathbb{N}$, for the solution operator $\{U(t, s)\}_{(t,s) \in \Delta}$, which approximates the solution operator in the operator-norm topology, and to estimate of its convergence rate. Such convergence rate estimates have been already found by Ichinose and Tamura for positive self-adjoint operators [6] in the Hilbert space setting. Recently (see [7]) the operator norm convergence and an error estimate were proved when the underlying space is a Banach space. In our paper [7], the main technical tool to construct such approximation is the Trotter product formula. We proved that under the assumptions formulated in this paper,

the Trotter product formula converges not only in the strong but in the operator-norm topology. To lift the strong topology to the operator-norm, we used the Trotter product formula and the relation between solution operator and evolution semigroup.

Following the ideas of [7], we improve in the present paper the convergence rate estimate $O(1/n^{\beta-\alpha})$, $0 < \alpha < \beta < 1$, which was obtained there. We assume in [7] that the involved operators A and $B(t)$ verify conditions inspired by [6] in a Hilbert space, although we do not suppose that for each t the operator $B(t)$ generates a bounded holomorphic semigroup. This gives us an extension of results [6] for the rate $O(\ln(n)/n)$ in a Hilbert space to a Banach space. On the other hand, it is not surprising that the error bound estimate in [7] is weaker than $O(\ln(n)/n^{1-\alpha})$ obtained for the first time in a Banach space by [8] under the same conditions as in [7], but for the autonomous Cauchy problem. Note that below (Section 2.2) our conditions (A2) and (A3) are a bit stronger conditions than in [7] or in [8]. Despite that, we were unable to reproduce the strikingly fast convergence rate of [6] for the case of Banach spaces. Although these stronger conditions allow us to push β up to $\beta = 1$. So the obtained in the present paper rate $O(1/n^{1-\alpha})$ is improved compared to [7] and also to [8] by elimination of the $\ln(n)$.

2. Preliminaries and assumptions

2.1. Preliminaries

Throughout the paper, we are dealing with a separable Banach space $(X, \|\cdot\|_X)$. For a linear operator $A : \text{dom}(A) \subset X \rightarrow X$, we define the resolvent by $R(\lambda, A) := (A - \lambda)^{-1} : X \rightarrow \text{dom}(A)$. A family $\{T(t)\}_{t \geq 0}$ of bounded linear operators on a Banach space X is called a strongly continuous (one-parameter) semigroup if it satisfies the functional equation:

$$T(0) = I, \quad T(t + s) = T(t)T(s), \quad t, s \geq 0,$$

and the orbit maps $[0, \infty) \ni t \mapsto T(t)x$ are continuous for every $x \in X$. In the following we simply call them semigroups. For a given semigroup we define its generator by:

$$Ax := \lim_{h \searrow 0} \frac{1}{h} (x - T(h)x),$$

with domain:

$$\text{dom}(A) := \left\{ x \in X : \lim_{h \searrow 0} \frac{1}{h} (x - T(h)x) \text{ exists} \right\}.$$

Note that the definition differs from the standard one by the minus sign. It is well-known that the generator of a semigroup is a closed and densely defined linear operator which uniquely determines the semigroup (see e.g. [5, Theorem I.1.4]). For a given generator A we will write $T(\tau) = e^{-\tau A}$, $\tau \geq 0$.

For any semigroup $\{T(t)\}_{t \geq 0}$ there are constants M_A, γ_A , such that it holds $\|T(t)\| \leq M_A e^{\gamma_A t}$ for all $t \geq 0$. Such semigroups are called of class $\mathcal{G}(M_A, \gamma_A)$ and we write $A \in \mathcal{G}(M_A, \gamma_A)$. If $\gamma_A \leq 0$, $\{T(t)\}_{t \geq 0}$ is called a bounded semigroup. If $\|T(t)\| \leq 1$, the semigroup is called contractive.

For any semigroup we can construct a bounded semigroup by adding some constant $\nu \geq \gamma_A$ to its generator: the operator $\tilde{A} := A + \nu$ generates a semigroup $\{\tilde{T}(t)\}_{t \geq 0}$ with $\|\tilde{T}(t)\| \leq M_A$. It is known that for a generator $A \in \mathcal{G}(M_A, \gamma_A)$, the open half plane $\{z \in \mathbb{C} : \text{Re}(z) < \gamma_A\}$ is contained in the resolvent set $\rho(A)$ of A and the estimate $\|R(\lambda, A)\| \leq M_A / (\text{Re}(\lambda) - \gamma_A)$ holds. If $\tilde{A} = A + \nu$, then the open half-plane $\{z \in \mathbb{C} : \text{Re}(z) < \gamma_A - \nu\}$ is contained in the resolvent set of \tilde{A} .

The semigroup $\{T(t)\}_{t \geq 0}$ on X is called a bounded holomorphic semigroup if its generator A satisfies $\text{ran}(T(t)) \subset \text{dom}(A)$ for all $t > 0$ and $\sup_{t > 0} \|tAT(t)\| < \infty$. It is well-known, that in this case the semigroup $\{T(t)\}_{t \geq 0}$ can be extended holomorphically to a sector $\{z \in \mathbb{C} : |\arg(z)| < \delta\} \cup \{0\} \subset \mathbb{C}$ of angle $\delta > 0$. For generators A of bounded holomorphic semigroups with $0 \in \rho(A)$ one can define fractional powers A^α . Then, for $\alpha \in (0, 1)$, it holds $\text{dom}(A) \subset \text{dom}(A^\alpha) \subset \text{dom}(A^0) = X$. In the following we need the well-known estimate for generators of a bounded holomorphic semigroup:

$$\sup_{t > 0} \|t^\alpha A^\alpha T(t)\| = M_\alpha^A < \infty. \tag{2.1}$$

2.2. Assumptions

Below we made the following assumptions with respect to the operator A and the family $\{B(t)\}_{t \in \Delta}$.

Assumption 2.1.

(A1) The operator A is a generator of a bounded holomorphic semigroup of class $\mathcal{G}(M_A, 0)$ and $0 \in \varrho(A)$. Let $\{B(t)\}_{t \in \mathcal{I}}$ be a family of generators on X belonging to the same class $\mathcal{G}(M_B, \beta)$. The function $\mathcal{I} \ni t \mapsto (B(t) + \xi)^{-1}x \in X$ is strongly measurable for any $x \in X$ and any $\xi > \beta$.

(A2) There is an $\alpha \in (1/2, 1)$ such that for a.e. $t \in \mathcal{I}$ it holds that $\text{dom}(A^\alpha) \subset \text{dom}(B(t))$ and $\text{dom}((A^\alpha)^*) \subset \text{dom}(B(t)^*)$. Moreover, it holds:

$$C_\alpha := \text{ess sup}_{t \in \mathcal{I}} \|B(t)A^{-\alpha}\|_{\mathcal{B}(X)} < \infty \quad \text{and} \quad C_\alpha^* := \text{ess sup}_{t \in \mathcal{I}} \|B(t)^*(A^{-\alpha})^*\|_{\mathcal{B}(X^*)} < \infty, \quad (2.2)$$

where A^* and $B(t)^*$ denote the adjoint operators of A and $B(t)$, respectively.

(A3) There is a constant $L > 0$ such that estimate:

$$\|A^{-\alpha}(B(t) - B(s))A^{-\alpha}\|_{\mathcal{B}(X)} \leq L|t - s|,$$

holds for a.e. $t, s \in \mathcal{I}$.

Remark 2.2.

(a) In [7], the assumptions are slightly weaker. It is assumed that the domains satisfy $\text{dom}(A^*) \subset \text{dom}(B(t)^*)$.

(b) The assumption $0 \in \varrho(A)$ is just for simplicity. Otherwise, the generator A can be shifted by a constant $\eta > 0$. One can prove that the domain of the fractional power of A does not change either.

(c) In [6] both operators A and $B(t)$ are assumed to be positive self-adjoint operators on a separable Hilbert space. The assumptions made in [6] yield that Assumption 2.1 is valid. We note that the first results in Banach spaces for *autonomous* Cauchy problem are due to [8]. The Trotter product approximation was proven there in the framework of Assumption 2.1: (A1), (A2).

(d) The assumptions above imply that for a.e. $t \in \mathcal{I}$ the operator $B(t)$ is infinitesimally small with respect to A . Indeed, fix $t \in \mathcal{I}$ and assuming (A1), (A2) we conclude:

$$\text{dom}(A + \eta) = \text{dom}(A) \subset \text{dom}(A^\alpha) \subset \text{dom}(B(t)),$$

for $\eta > 0$ and hence:

$$\|B(t)(A + \eta)^{-1}\|_{\mathcal{B}(X)} \leq \|B(t)A^{-\alpha}\|_{\mathcal{B}(X)} \cdot \|A^\alpha(A + \eta)^{-1}\|_{\mathcal{B}(X)} \leq \frac{C_\alpha C_0}{\eta^{1-\alpha}}.$$

Therefore for any $x \in \text{dom}(A) \subset \text{dom}(B(t))$, we get:

$$\|B(t)x\|_X \leq \frac{C_\alpha C_0}{\eta^{1-\alpha}} \cdot \|(A + \eta)x\|_X \leq C_\alpha C_0 \eta^\alpha \left(\frac{1}{\eta} \|Ax\|_X + \|x\|_X \right).$$

The relative bound can be chosen arbitrarily small by shifting $\eta > 0$. In particular, using standard perturbation results ([9, Corollary IX.2.5]), we conclude that $A + B(t)$ is the generator of a holomorphic semigroup, i.e. problem (1.1) is a parabolic evolution equation.

3. Construction of solution operators

We start by description of our strategy. Details can be found in [7]. Our approach to construct the solution operator $\{U(t, s)\}_{(t, s) \in \Delta}$ of (1.1) leads to a perturbation or extension problem for linear operators. It can be used in very general settings and it is quite flexible. The idea can be described as follows: The *non-autonomous* Cauchy problem in X can be reformulated as an *autonomous* Cauchy problem in a new Banach space $L^p(\mathcal{I}, X)$, $p \in [1, \infty)$, of p -summable functions on the interval \mathcal{I} with values in the Banach space X . An operator family $\{C(t)\}_{t \in \mathcal{I}}$ on X induces an multiplication operator \mathcal{C} on $L^p(\mathcal{I}, X)$ defined by:

$$(\mathcal{C}f)(t) := C(t)f(t),$$

$$\text{dom}(\mathcal{C}) := \left\{ f \in L^p(\mathcal{I}, X) : \begin{array}{l} f(t) \in \text{dom}(C(t)) \text{ for a.e. } t \in \mathcal{I} \\ \mathcal{I} \ni t \mapsto C(t)f(t) \in L^p(\mathcal{I}, X) \end{array} \right\}.$$

Theorem 3.1 ([7, Theorem 2.8]). *Let $\{C(t)\}_{t \in \mathcal{I}}$ be a family of generators on X such that for almost all $t \in \mathcal{I}$ it holds that $C(t) \in \mathcal{G}(M, \beta)$ for some $M \geq 1$ and $\beta \in \mathbb{R}$. If the function $\mathcal{I} \ni t \mapsto (C(t) + \xi)^{-1}x \in X$ is strongly measurable for $\xi > \beta$, $x \in X$, then the induced multiplication operator \mathcal{C} is a generator in $L^p(\mathcal{I}, X)$ and its semigroup is given by:*

$$(e^{-\tau \mathcal{C}} f)(t) = e^{-\tau C(t)} f(t), \quad f \in L^p(\mathcal{I}, X),$$

for a.e. $t \in \mathcal{I}$. In particular, for the operator-norms we get:

$$\|e^{-\tau \mathcal{C}}\|_{\mathcal{B}(L^p(\mathcal{I}, X))} = \operatorname{ess\,sup}_{t \in \mathcal{I}} \|e^{-\tau C(t)}\|_{\mathcal{B}(X)}.$$

So the generators $C(t)$ and \mathcal{C} belong to the same class.

In particular in our case, the operator family $\{B(t)\}_{t \in \mathcal{I}}$ induces the generator \mathcal{B} and A induces trivially the generator \mathcal{A} on $L^p(\mathcal{I}, X)$. Assuming (A1) and (A2) it turns out that the operators $\mathcal{B}\mathcal{A}^{-\alpha}$ and $\mathcal{A}^{-\alpha}\mathcal{B}$ are bounded on $L^p(\mathcal{I}, X)$ and it holds that $\|\mathcal{B}\mathcal{A}^{-\alpha}\|_{\mathcal{B}(L^p(\mathcal{I}, X))} \leq C_\alpha$ and $\|\mathcal{A}^{-\alpha}\mathcal{B}\|_{\mathcal{B}(L^p(\mathcal{I}, X))} \leq C_\alpha^*$.

Let us introduce the operator $D_0 := \partial_t$ on $L^p(\mathcal{I}, X)$ defined by:

$$D_0 f(t) := \partial_t f(t), \quad \operatorname{dom}(D_0) := \{f \in W^{1,p}([0, T], X) : f(0) = 0\}.$$

Then, D_0 is a generator of class $\mathcal{G}(1, 0)$ of the right-shift semigroup $\{S(\tau)\}_{\tau \geq 0}$ that has the form:

$$(e^{-\tau D_0} f)(t) = (S(\tau)f)(t) := f(t - \tau)\chi_{\mathcal{I}}(t - \tau), \quad f \in L^p(\mathcal{I}, X), \quad \text{a.e. } t \in \mathcal{I}.$$

We note that the generator D_0 has empty spectrum since the semigroup $\{S(\tau)\}_{\tau \geq 0}$ is nilpotent and therefore the integral $\int_0^\infty d\tau e^{-\tau \lambda} S(\tau)f$ exists for any $\lambda \in \mathbb{C}$ and for any $f \in L^p(\mathcal{I}, X)$.

Let us look at the operator sum D_0 and \mathcal{A} . Since A is time-independent, the operators \mathcal{A} and D_0 commute, and, hence, also their semigroups commute. So, the operator family $\{e^{-\tau \mathcal{A}} e^{-\tau D_0}\}_{\tau \geq 0}$ defines a semigroup on $L^p(\mathcal{I}, X)$. Its generator is denoted by \mathcal{K}_0 . It is closure of the operator sum $D_0 + \mathcal{A}$, i.e. $\mathcal{K}_0 = \overline{D_0 + \mathcal{A}}$. We note that all the generators \mathcal{K}_0 , \mathcal{A} , A belong to the same class.

Remark 3.2. By assumption (A1) the operator \mathcal{A} generates a holomorphic semigroup. Note that the operator \mathcal{K}_0 is not a generator of a holomorphic semigroup. Indeed, if we have:

$$(e^{-\tau \mathcal{K}_0} f)(t) = (e^{-\tau D_0} e^{-\tau \mathcal{A}} f)(t) = e^{-\tau \mathcal{A}} f(t - \tau)\chi_{\mathcal{I}}(t - \tau), \quad f \in L^p(\mathcal{I}, X).$$

Since the right-hand side is zero for $\tau \geq t$, the semigroup can not be extended holomorphically to the complex plane.

Now, look at the operator sum:

$$\tilde{\mathcal{K}} = D_0 + \mathcal{A} + \mathcal{B}, \quad \operatorname{dom}(\tilde{\mathcal{K}}) = \operatorname{dom}(D_0) \cap \operatorname{dom}(\mathcal{A}) \cap \operatorname{dom}(\mathcal{B}). \quad (3.1)$$

In [7], the following theorem is proved.

Theorem 3.3 ([7, Theorems 4.3 and 4.4]). *Assume (A1) and (A2). Then, the operator closure $\overline{\tilde{\mathcal{K}}} =: \mathcal{K}$ is a generator on $L^p(\mathcal{I}, X)$, and it holds:*

$$\mathcal{K} = \mathcal{K}_0 + \mathcal{B}, \quad \operatorname{dom}(\mathcal{K}) = \operatorname{dom}(\mathcal{K}_0) \cap \operatorname{dom}(\mathcal{B}). \quad (3.2)$$

Moreover, it is an evolution generator, i.e. there is a unique propagator or solution operator $\{U(t, s)\}_{(t,s) \in \Delta}$ such that the representation:

$$(e^{-\tau \mathcal{K}} f)(t) = (\mathcal{U}(\tau)f)(t) = U(t, t - \tau)\chi_{\mathcal{I}}(t - \tau)f(t - \tau), \quad \tau \geq 0, \quad t \in \mathcal{I}.$$

holds.

We note that for the proof it is not necessary that the operators $B(t)$ themselves are generators. After proving the existence of the unique solution operator the goal is to approximate the solution operator $\{U(t, s)\}_{(t,s) \in \Delta}$. This will be done by proving an operator-norm convergence for the Trotter product formula for $\mathcal{K} = \mathcal{K}_0 + \mathcal{B}$.

4. Stability

Proving the Trotter product formula, it is important to establish stability conditions. Notice that stability is satisfied if the contractivity of the involved semigroups is assumed which might be too strong in applications. There are many stability conditions known for evolution equations. In particular, the Kato-stability is of interest, cf. [10, Definition 4.1], which is equivalent to a renormalizability conditions of the underlying Banach space, cf. [10]. We note that our following stability condition is weaker than Kato-stability.

Definition 4.1. Let A be a generator and let $\{B(t)\}_{t \in \mathcal{I}}$ be a family of generators in X . The family $\{B(t)\}_{t \in \mathcal{I}}$ is called A -stable if there is a constant $M > 0$ such that:

$$\operatorname{ess\,sup}_{(t,s) \in \Delta} \left\| \prod_{j=1}^{n \leftarrow} G_j(t, s; n) \right\|_{\mathcal{B}(X)} \leq M,$$

holds for any $n \in \mathbb{N}$ where $G_j(t, s; n) := e^{-\frac{t-s}{n}B(s+j\frac{t-s}{n})}e^{-\frac{t-s}{n}A}$, $j = 0, 1, 2, \dots, n$, and the product is ordered increasingly in j from the right to the left.

Let us introduce the notion:

$$T(\tau) = e^{-\tau B}e^{-\tau K_0}, \quad \tau \geq 0.$$

Lemma 4.2 ([7, Lemma 5.8]). *If the operator family $\{B(t)\}_{t \in \mathcal{I}}$ is A -stable, then:*

$$\|T(\tau/n)^m\|_{\mathcal{B}(L^p(\mathcal{I}, X))} \leq M,$$

for any $m \in \mathbb{N}$, $n \in \mathbb{N}$ and $\tau \geq 0$. In particular, we have:

$$\|T(\tau)^m\|_{\mathcal{B}(L^p(\mathcal{I}, X))} \leq M,$$

for any $m \in \mathbb{N}$ and $\tau \geq 0$.

5. Convergence in the operator-norm topology

Theorem 3.3 leads to the problem, how the semigroup of \mathcal{K} can be approximated in terms of the semigroups generated by D_0 , \mathcal{A} and \mathcal{B} . The classical Trotter product formula gives an approximation in the strong topology. In this section, we establish an approximation in the operator-norm topology on $L^p(\mathcal{I}, X)$. This is done in several steps. This approximation in $L^p(\mathcal{I}, X)$ can be used to prove an convergence rate estimate in X for the propagators.

5.1. Technical lemmata

In this section, we state and prove all technical lemmas that we used to prove the convergence and estimate of the Trotter product formula in the operator-norm in $L^p(\mathcal{I}, X)$. As above we set $T(\tau) := e^{-\tau B}e^{-\tau K_0}$, $\tau \geq 0$. Note that $T(\tau) = 0$ for $\tau \geq T$. Similarly, $e^{-\tau K} = 0$ for $\tau \geq T$.

Lemma 5.1. *Let the assumptions (A1) and (A2) be satisfied.*

(i) *Then, $\operatorname{dom}(K_0) \subset \operatorname{dom}(\mathcal{A}^\alpha)$ and there is a constant $\Lambda_\alpha > 0$ such that:*

$$\|\mathcal{A}^\alpha e^{-\tau K}\|_{\mathcal{B}(L^p(\mathcal{I}, X))} \leq \frac{\Lambda_\alpha}{\tau^\alpha}, \tag{5.1}$$

holds for $\tau > 0$.

(ii) *If $\{B(t)\}_{t \in \mathcal{I}}$ is A -stable, then there is a constant $\Pi_\alpha > 0$ such that the estimates:*

$$\|(T(\tau) - e^{-\tau K})\mathcal{A}^{-\alpha}\|_{\mathcal{B}(L^p(\mathcal{I}, X))} \leq \Pi_\alpha \tau, \tag{5.2}$$

$$\|\mathcal{A}^{-\alpha}(T(\tau) - e^{-\tau K})\|_{\mathcal{B}(L^p(\mathcal{I}, X))} \leq \Pi_\alpha \tau, \tag{5.3}$$

are valid for $\tau > 0$.

(iii) *If $\{B(t)\}_{t \in \mathcal{I}}$ is A -stable, then there is a constant $Y_\alpha > 0$ such that the estimate:*

$$\|\overline{T(\tau)^k \mathcal{A}^\alpha}\|_{\mathcal{B}(L^p(\mathcal{I}, X))} \leq Y_\alpha \left(\tau^{1-2\alpha} + \frac{1}{(k\tau)^\alpha} \right), \quad \tau > 0, \quad k \in \mathbb{N}, \tag{5.4}$$

holds for $\tau > 0$.

Proof. (i)–(ii) The assertions $\text{dom}(\mathcal{K}_0) \subseteq \text{dom}(\mathcal{A}^\alpha)$ as well as (5.1) and (5.2) follow from Lemma 7.3, Lemma 7.4 and Lemma 7.6 of [7]. To prove (5.3) one has slightly to modify the second part of the proof of Lemma 7.6 of [7].

(iii) For $k\tau \geq T$ we have $T(\tau)^k = 0$. Hence, one has to prove the estimate (5.4) only for $k\tau \leq T$. In fact, using Lemma 4.2, we get $\|T(\tau)^k\| \leq M$, $\tau \in [0, \infty)$. Hence:

$$\begin{aligned} \|T(\tau)^k \mathcal{A}^\alpha f\| &\leq \|(T(\tau)^k - e^{-k\tau\mathcal{K}_0})\mathcal{A}^\alpha f\| + \|e^{-k\tau\mathcal{K}_0} \mathcal{A}^\alpha f\| \\ &\leq \left\| \sum_{j=0}^{k-1} T(\tau)^{k-1-j} (e^{-\tau\mathcal{B}} - I) e^{-(j+1)\tau\mathcal{K}_0} \mathcal{A}^\alpha f \right\| + \|e^{-k\tau\mathcal{K}_0} \mathcal{A}^\alpha f\| \\ &\leq M \sum_{j=0}^{k-1} \int_0^\tau d\sigma \|e^{-\sigma\mathcal{B}} \mathcal{B} \mathcal{A}^{-\alpha}\| \|\mathcal{A}^{2\alpha} e^{-(j+1)\tau\mathcal{K}_0} f\| + \|e^{-k\tau\mathcal{K}_0} \mathcal{A}^\alpha f\|, \end{aligned}$$

where we have used $I - e^{-\tau\mathcal{B}} = \int_0^\tau \mathcal{B} e^{-\sigma\mathcal{B}} d\sigma$. Moreover, from (2.1) we get:

$$\|\mathcal{A}^{2\alpha} e^{-(j+1)\tau\mathcal{K}_0} f\| \leq \frac{M_{2\alpha}^A}{((j+1)\tau)^{2\alpha}} \|f\| \quad \text{and} \quad \|\mathcal{A}^\alpha e^{-k\tau\mathcal{K}_0} f\| \leq \frac{M_\alpha^A}{(k\tau)^\alpha} \|f\|,$$

for $\tau > 0$. Hence, using $\alpha > \frac{1}{2}$, we get:

$$\begin{aligned} \|T(\tau)^k \mathcal{A}^\alpha f\| &\leq \frac{MM_{\mathcal{B}}^T M_{2\alpha}^A C_\alpha \tau}{\tau^{2\alpha}} \sum_{j=0}^{k-1} \frac{1}{(j+1)^{2\alpha}} \|f\| + \frac{M_\alpha^A}{(k\tau)^\alpha} \|f\| \\ &\leq \frac{MM_{\mathcal{B}}^T M_{2\alpha}^A C_\alpha \zeta(2\alpha)}{\tau^{2\alpha-1}} \|f\| + \frac{M_\alpha^A}{(k\tau)^\alpha} \|f\|, \end{aligned}$$

for $\tau \in \mathcal{I}$, where $\zeta(\beta) := \sum_{j=1}^{\infty} 1/j^\beta$, $\beta > 1$, is the Riemann ζ -function and we have set $M_{\mathcal{B}}^T := \sup_{\tau \in \mathcal{I}} \|e^{-\tau\mathcal{B}}\|$. Using that $T(\tau)^k = 0$ for $\tau k \geq T$ we find:

$$\|T(\tau)^k \mathcal{A}^\alpha f\| \leq \frac{MM_{\mathcal{B}}^T M_{2\alpha}^A C_\alpha \zeta(2\alpha)}{\tau^{2\alpha-1}} \|f\| + \frac{M_\alpha^A}{(k\tau)^\alpha} \|f\|, \quad f \in \text{dom}(\mathcal{A}),$$

for $\tau > 0$. Taking the supremum over the unit ball in $\text{dom}(\mathcal{A})$, we prove (5.4). \square

Lemma 5.2. *Let the assumptions (A1), (A2), and (A3) be satisfied. Then, there is a constant $Z_\alpha > 0$ such that:*

$$\|\mathcal{A}^{-\alpha}(T(\tau) - e^{-\tau\mathcal{K}})\mathcal{A}^{-\alpha}\|_{\mathcal{B}(L^p(\mathcal{I}, X))} \leq Z_\alpha \tau^{1+\alpha}, \quad \tau \geq 0. \quad (5.5)$$

Proof. Let $f \in \text{dom}(\mathcal{K}_0) = \text{dom}(\mathcal{K})$. We have:

$$\begin{aligned} \frac{d}{d\sigma} T(\sigma) e^{-(\tau-\sigma)\mathcal{K}} f &= \frac{d}{d\sigma} e^{-\sigma\mathcal{B}} e^{-\sigma\mathcal{K}_0} e^{-(\tau-\sigma)\mathcal{K}} f \\ &= -e^{-\sigma\mathcal{B}} \mathcal{B} e^{-\sigma\mathcal{K}_0} e^{-(\tau-\sigma)\mathcal{K}} f - e^{-\sigma\mathcal{B}} e^{-\sigma\mathcal{K}_0} \mathcal{K}_0 e^{-(\tau-\sigma)\mathcal{K}} f + e^{-\sigma\mathcal{B}} e^{-\sigma\mathcal{K}_0} \mathcal{K} e^{-(\tau-\sigma)\mathcal{K}} f \\ &= -e^{-\sigma\mathcal{B}} \mathcal{B} e^{-\sigma\mathcal{K}_0} e^{-(\tau-\sigma)\mathcal{K}} f + e^{-\sigma\mathcal{B}} e^{-\sigma\mathcal{K}_0} \mathcal{B} e^{-(\tau-\sigma)\mathcal{K}} f \\ &= e^{-\sigma\mathcal{B}} \{e^{-\sigma\mathcal{K}_0} \mathcal{B} f - \mathcal{B} e^{-\sigma\mathcal{K}_0}\} e^{-(\tau-\sigma)\mathcal{K}} f, \end{aligned}$$

which yields:

$$T(\tau)f - e^{-\tau\mathcal{K}} f = \int_0^\tau \frac{d}{d\sigma} T(\sigma) e^{-(\tau-\sigma)\mathcal{K}} f d\sigma = \int_0^\tau d\sigma e^{-\sigma\mathcal{B}} \{e^{-\sigma\mathcal{K}_0} \mathcal{B} - \mathcal{B} e^{-\sigma\mathcal{K}_0}\} e^{-(\tau-\sigma)\mathcal{K}} f. \quad (5.6)$$

Now, we have the following identity:

$$\begin{aligned} e^{-\sigma\mathcal{B}} (e^{-\sigma\mathcal{K}_0} \mathcal{B} - \mathcal{B} e^{-\sigma\mathcal{K}_0}) e^{-(\tau-\sigma)\mathcal{K}} f &= (e^{-\sigma\mathcal{B}} - I) \{e^{-\sigma\mathcal{K}_0} \mathcal{B} - \mathcal{B} e^{-\sigma\mathcal{K}_0}\} (e^{-(\tau-\sigma)\mathcal{K}} - e^{-(\tau-\sigma)\mathcal{K}_0}) f \\ &\quad + (e^{-\sigma\mathcal{B}} - I) \{e^{-\sigma\mathcal{K}_0} \mathcal{B} - \mathcal{B} e^{-\sigma\mathcal{K}_0}\} e^{-(\tau-\sigma)\mathcal{K}_0} f \\ &\quad + \{e^{-\sigma\mathcal{K}_0} \mathcal{B} - \mathcal{B} e^{-\sigma\mathcal{K}_0}\} (e^{-(\tau-\sigma)\mathcal{K}} - e^{-(\tau-\sigma)\mathcal{K}_0}) f + \{e^{-\sigma\mathcal{K}_0} \mathcal{B} - \mathcal{B} e^{-\sigma\mathcal{K}_0}\} e^{-(\tau-\sigma)\mathcal{K}_0} f, \end{aligned}$$

which yields for $f = \mathcal{A}^{-\alpha}g$:

$$\begin{aligned}
& \mathcal{A}^{-\alpha}e^{-\sigma\mathcal{B}}(e^{-\sigma\mathcal{K}_0}\mathcal{B} - \mathcal{B}e^{-\sigma\mathcal{K}_0})e^{-(\tau-\sigma)\mathcal{K}}\mathcal{A}^{-\alpha}g \\
&= \mathcal{A}^{-\alpha}(e^{-\sigma\mathcal{B}} - I)\{e^{-\sigma\mathcal{K}_0}\mathcal{B} - \mathcal{B}e^{-\sigma\mathcal{K}_0}\}(e^{-(\tau-\sigma)\mathcal{K}} - e^{-(\tau-\sigma)\mathcal{K}_0})\mathcal{A}^{-\alpha}g \\
&+ \mathcal{A}^{-\alpha}(e^{-\sigma\mathcal{B}} - I)\{e^{-\sigma\mathcal{K}_0}\mathcal{B} - \mathcal{B}e^{-\sigma\mathcal{K}_0}\}\mathcal{A}^{-\alpha}e^{-(\tau-\sigma)\mathcal{K}_0}g \\
&+ \mathcal{A}^{-\alpha}\{e^{-\sigma\mathcal{K}_0}\mathcal{B} - \mathcal{B}e^{-\sigma\mathcal{K}_0}\}(e^{-(\tau-\sigma)\mathcal{K}} - e^{-(\tau-\sigma)\mathcal{K}_0})\mathcal{A}^{-\alpha}g \\
&+ \mathcal{A}^{-\alpha}\{(e^{-\sigma\mathcal{K}_0} - e^{-\sigma D_0})\mathcal{B} - \mathcal{B}(e^{-\sigma\mathcal{K}_0} - e^{-\sigma D_0})\}e^{-(\tau-\sigma)\mathcal{K}_0}\mathcal{A}^{-\alpha}g \\
&+ \mathcal{A}^{-\alpha}(e^{-\sigma D_0}\mathcal{B} - \mathcal{B}e^{-\sigma D_0})\mathcal{A}^{-\alpha}e^{-(\tau-\sigma)\mathcal{K}_0}g.
\end{aligned} \tag{5.7}$$

In the following, we estimate the five terms separately.

Initially, we use the fact that \mathcal{A} and \mathcal{K}_0 commute and conclude that:

$$(e^{-(\tau-\sigma)\mathcal{K}} - e^{-(\tau-\sigma)\mathcal{K}_0})\mathcal{A}^{-\alpha}g = \int_0^{\tau-\sigma} dr e^{-(\tau-\sigma-r)\mathcal{K}}\mathcal{B}\mathcal{A}^{-\alpha}e^{-r\mathcal{K}_0}g.$$

Thus, for the first term we get:

$$\begin{aligned}
& \mathcal{A}^{-\alpha}(e^{-\sigma\mathcal{B}} - I)\{e^{-\sigma\mathcal{K}_0}\mathcal{B} - \mathcal{B}e^{-\sigma\mathcal{K}_0}\}(e^{-(\tau-\sigma)\mathcal{K}} - e^{-(\tau-\sigma)\mathcal{K}_0})\mathcal{A}^{-\alpha}g \\
&= - \int_0^{\sigma} d\tau \mathcal{A}^{-\alpha}\mathcal{B}e^{-r\mathcal{B}}[e^{-\sigma\mathcal{K}_0}, \mathcal{B}]\mathcal{A}^{-\alpha} \int_0^{\tau-\sigma} dr \mathcal{A}^{-\alpha}e^{-(\tau-\sigma-r)\mathcal{K}}\mathcal{B}\mathcal{A}^{-\alpha}e^{-r\mathcal{K}_0}g,
\end{aligned}$$

where:

$$[e^{-\sigma\mathcal{K}_0}, \mathcal{B}]f := \{e^{-\sigma\mathcal{K}_0}\mathcal{B} - \mathcal{B}e^{-\sigma\mathcal{K}_0}\}f, \quad f \in \text{dom}(\mathcal{K}_0), \quad \tau \geq 0.$$

Using Lemma 5.1, we obtain the estimate:

$$\begin{aligned}
& \|\mathcal{A}^{-\alpha}(e^{-\sigma\mathcal{B}} - I)\{e^{-\sigma\mathcal{K}_0}\mathcal{B} - \mathcal{B}e^{-\sigma\mathcal{K}_0}\}(e^{-(\tau-\sigma)\mathcal{K}} - e^{-(\tau-\sigma)\mathcal{K}_0})\mathcal{A}^{-\alpha}g\| \\
&\leq \sigma 2C_{\alpha}^*C_{\alpha}^2\Lambda_{\alpha}M_{\mathcal{B}}^T M_{\mathcal{A}}^2 \int_0^{\tau-\sigma} dr \frac{1}{(\tau-\sigma-r)^{\alpha}} \|g\| \leq \sigma(\tau-\sigma)^{1-\alpha} \frac{2C_{\alpha}^*C_{\alpha}^2\Lambda_{\alpha}M_{\mathcal{B}}^T M_{\mathcal{A}}^2}{1-\alpha} \|g\|,
\end{aligned} \tag{5.8}$$

for $\sigma \in [0, \tau]$ and $\tau \geq 0$. For the second term, we get the estimate:

$$\|\mathcal{A}^{-\alpha}(e^{-\sigma\mathcal{B}} - I)\{e^{-\sigma\mathcal{K}_0}\mathcal{B} - \mathcal{B}e^{-\sigma\mathcal{K}_0}\}\mathcal{A}^{-\alpha}e^{-(\tau-\sigma)\mathcal{K}_0}g\| \leq \sigma 2C_{\alpha}^*C_{\alpha}M_{\mathcal{B}}^T M_{\mathcal{A}}^2 \|g\|. \tag{5.9}$$

for $\sigma \in [0, \tau]$ and $\tau \geq 0$. Since we have:

$$e^{-(\tau-\sigma)\mathcal{K}} - e^{-(\tau-\sigma)\mathcal{K}_0}h = \int_0^{\tau-\sigma} dr e^{-(\tau-r-\sigma)\mathcal{K}}\mathcal{B}e^{-r\mathcal{K}_0}h, \quad h \in \text{dom}(\mathcal{K}_0),$$

one obtains for the third term the estimate:

$$\|\mathcal{A}^{-\alpha}\{e^{-\sigma\mathcal{K}_0}\mathcal{B} - \mathcal{B}e^{-\sigma\mathcal{K}_0}\}(e^{-(\tau-\sigma)\mathcal{K}} - e^{-(\tau-\sigma)\mathcal{K}_0})\mathcal{A}^{-\alpha}g\| \leq (\tau-\sigma) 2C_{\alpha}^*C_{\alpha}M_{\mathcal{A}}^2 M_{\mathcal{K}} \|g\|, \tag{5.10}$$

for $\sigma \in [0, \tau]$ and $\tau \geq 0$. Moreover, using:

$$e^{-\sigma\mathcal{K}_0} - e^{-\sigma D_0}h = - \int_0^{\sigma} dr e^{-r\mathcal{K}_0}\mathcal{A}e^{-(\sigma-r)D_0}h,$$

we get for the fourth term:

$$\begin{aligned}
& \mathcal{A}^{-\alpha}\{(e^{-\sigma\mathcal{K}_0} - e^{-\sigma D_0})\mathcal{B} - \mathcal{B}(e^{-\sigma\mathcal{K}_0} - e^{-\sigma D_0})\}e^{-(\tau-\sigma)\mathcal{K}_0}\mathcal{A}^{-\alpha}g \\
&= \left(- \int_0^{\sigma} dr \mathcal{A}^{1-\alpha}e^{-r\mathcal{K}_0}e^{-(\sigma-r)D_0}\mathcal{B}\mathcal{A}^{-\alpha} + \mathcal{A}^{-\alpha}\mathcal{B} \int_0^{\sigma} dr e^{-r\mathcal{K}_0}\mathcal{A}^{1-\alpha}e^{-(\sigma-r)D_0} \right) e^{-(\tau-\sigma)\mathcal{K}_0}g,
\end{aligned}$$

which yields the estimate:

$$\begin{aligned} & \|\mathcal{A}^{-\alpha} \left\{ (e^{-\sigma\mathcal{K}_0} - e^{-\sigma D_0})\mathcal{B} - \mathcal{B}(e^{-\sigma\mathcal{K}_0} - e^{-\sigma D_0}) \right\} e^{-(\tau-\sigma)\mathcal{K}_0} \mathcal{A}^{-\alpha} g\| \\ & \leq C_\alpha M_{\mathcal{A}} M_{1-\alpha}^A \int_0^\sigma dr \frac{1}{r^{1-\alpha}} \|g\| + C_\alpha^* M_{\mathcal{A}} M_{1-\alpha}^A \int_0^\sigma dr \frac{1}{r^{1-\alpha}} \|g\| = \frac{(C_\alpha + C_\alpha^*) M_{\mathcal{A}} M_{1-\alpha}^A}{\alpha} \sigma^\alpha \|g\| \end{aligned} \quad (5.11)$$

for $\sigma \in [0, \tau]$ and $\tau \geq 0$. To estimate the fifth term, we note that:

$$\begin{aligned} (e^{-\sigma D_0} \mathcal{B} - \mathcal{B} e^{-\sigma D_0}) f &= e^{-\sigma D_0} B(\cdot) f(\cdot) - \mathcal{B} \chi_{\mathcal{I}}(\cdot - \sigma) f(\cdot - \sigma) \\ &= \chi_{\mathcal{I}}(\cdot - \sigma) B(\cdot - \sigma) f(\cdot - \sigma) - B(\cdot) \chi_{\mathcal{I}}(\cdot - \sigma) f(\cdot - \sigma) \\ &= \chi_{\mathcal{I}}(\cdot - \sigma) \{B(\cdot - \sigma) - B(\cdot)\} f(\cdot - \sigma), \end{aligned}$$

and therefore:

$$\begin{aligned} \|\mathcal{A}^{-\alpha} (e^{-\sigma D_0} \mathcal{B} - \mathcal{B} e^{-\sigma D_0}) e^{-(\tau-\sigma)\mathcal{K}_0} \mathcal{A}^{-\alpha} g\| &\leq M_{\mathcal{A}} \|\mathcal{A}^{-\alpha} \{e^{-\sigma D_0} \mathcal{B} - \mathcal{B} e^{-\sigma D_0}\} \mathcal{A}^{-\alpha} g\| \\ &\leq \operatorname{ess\,sup}_{t \in \mathcal{I}} \|\mathcal{A}^{-\alpha} \{B(t - \sigma) - B(t)\} \mathcal{A}^{-\alpha}\|_{\mathcal{B}(X)} \|g\| \leq L \sigma \|g\|, \end{aligned} \quad (5.12)$$

for $\sigma \in [0, \tau]$ and $\tau \geq 0$. From (5.7) we find the estimate:

$$\begin{aligned} & \|\mathcal{A}^{-\alpha} e^{-\sigma \mathcal{B}} (e^{-\sigma \mathcal{K}_0} \mathcal{B} - \mathcal{B} e^{-\sigma \mathcal{K}_0}) e^{-(\tau-\sigma)\mathcal{K}} \mathcal{A}^{-\alpha} g\| \\ & \leq \|\mathcal{A}^{-\alpha} (e^{-\sigma \mathcal{B}} - I) \{e^{-\sigma \mathcal{K}_0} \mathcal{B} - \mathcal{B} e^{-\sigma \mathcal{K}_0}\} (e^{-(\tau-\sigma)\mathcal{K}} - e^{-(\tau-\sigma)\mathcal{K}_0}) \mathcal{A}^{-\alpha} g\| \\ & + \|\mathcal{A}^{-\alpha} (e^{-\sigma \mathcal{B}} - I) \{e^{-\sigma \mathcal{K}_0} \mathcal{B} - \mathcal{B} e^{-\sigma \mathcal{K}_0}\} \mathcal{A}^{-\alpha} e^{-(\tau-\sigma)\mathcal{K}_0} g\| \\ & + \|\mathcal{A}^{-\alpha} \{e^{-\sigma \mathcal{K}_0} \mathcal{B} - \mathcal{B} e^{-\sigma \mathcal{K}_0}\} (e^{-(\tau-\sigma)\mathcal{K}} - e^{-(\tau-\sigma)\mathcal{K}_0}) \mathcal{A}^{-\alpha} g\| \\ & + \|\mathcal{A}^{-\alpha} \left\{ (e^{-\sigma \mathcal{K}_0} - e^{-\sigma D_0}) \mathcal{B} - \mathcal{B} (e^{-\sigma \mathcal{K}_0} - e^{-\sigma D_0}) \right\} e^{-(\tau-\sigma)\mathcal{K}_0} \mathcal{A}^{-\alpha} g\| \\ & + \|\mathcal{A}^{-\alpha} (e^{-\sigma D_0} \mathcal{B} - \mathcal{B} e^{-\sigma D_0}) \mathcal{A}^{-\alpha} e^{-(\tau-\sigma)\mathcal{K}_0} g\|, \end{aligned}$$

for $\sigma \in [0, \tau]$ and $\tau \geq 0$. Taking into account (5.8), (5.9), (5.10), (5.11), and (5.12) we find:

$$\begin{aligned} & \|\mathcal{A}^{-\alpha} e^{-\sigma \mathcal{B}} (e^{-\sigma \mathcal{K}_0} \mathcal{B} - \mathcal{B} e^{-\sigma \mathcal{K}_0}) e^{-(\tau-\sigma)\mathcal{K}} \mathcal{A}^{-\alpha} g\| \\ & \leq \left\{ \sigma (\tau - \sigma)^{1-\alpha} \frac{2C_\alpha^* C_\alpha^2 \Lambda_\alpha M_{\mathcal{B}}^T M_{\mathcal{A}}^2}{1-\alpha} + \sigma 2C_\alpha^* C_\alpha M_{\mathcal{B}}^T M_{\mathcal{A}}^2 \right. \\ & \quad \left. + (\tau - \sigma) 2C_\alpha^* C_\alpha M_{\mathcal{A}}^2 M_{\mathcal{K}} + \sigma^\alpha \frac{(C_\alpha + C_\alpha^*) M_{\mathcal{A}} M_{1-\alpha}^A}{\alpha} + \sigma L \right\} \|g\|, \end{aligned}$$

for $\sigma \in [0, \tau]$ and $\tau \geq 0$. Setting:

$$\begin{aligned} Z_1 &:= \frac{2C_\alpha^* C_\alpha^2 \Lambda_\alpha M_{\mathcal{B}}^T M_{\mathcal{A}}^2}{1-\alpha}, & Z_2 &:= 2C_\alpha^* C_\alpha M_{\mathcal{B}}^T M_{\mathcal{A}}^2 + L, \\ Z_3 &:= 2C_\alpha^* C_\alpha M_{\mathcal{A}}^2 M_{\mathcal{K}}, & Z_4 &:= \frac{(C_\alpha + C_\alpha^*) M_{\mathcal{A}} M_{1-\alpha}^A}{\alpha}, \end{aligned}$$

we obtain:

$$\begin{aligned} & \|\mathcal{A}^{-\alpha} e^{-\sigma \mathcal{B}} (e^{-\sigma \mathcal{K}_0} \mathcal{B} - \mathcal{B} e^{-\sigma \mathcal{K}_0}) e^{-(\tau-\sigma)\mathcal{K}} \mathcal{A}^{-\alpha} g\| \\ & \leq \left\{ Z_1 \sigma (\tau - \sigma)^{1-\alpha} + Z_2 \sigma + Z_3 (\tau - \sigma) + Z_4 \sigma^\alpha \right\} \|g\|. \end{aligned} \quad (5.13)$$

From (5.6) we derive the representation:

$$\mathcal{A}^{-\alpha} (T(\tau) - e^{-\tau \mathcal{K}}) \mathcal{A}^{-\alpha} g = \int_0^\tau d\sigma \mathcal{A}^{-\alpha} e^{-\sigma \mathcal{B}} \left\{ e^{-\sigma \mathcal{K}_0} \mathcal{B} - \mathcal{B} e^{-\sigma \mathcal{K}_0} \right\} e^{-(\tau-\sigma)\mathcal{K}} \mathcal{A}^{-\alpha} g,$$

which yields the estimate:

$$\|\mathcal{A}^{-\alpha} (T(\tau) - e^{-\tau \mathcal{K}}) \mathcal{A}^{-\alpha} g\| \leq \int_0^\tau d\sigma \|\mathcal{A}^{-\alpha} e^{-\sigma \mathcal{B}} \left\{ e^{-\sigma \mathcal{K}_0} \mathcal{B} - \mathcal{B} e^{-\sigma \mathcal{K}_0} \right\} e^{-(\tau-\sigma)\mathcal{K}} \mathcal{A}^{-\alpha} g\|.$$

Inserting (5.13) into this estimate and using:

$$\int_0^\tau d\sigma (\tau - \sigma)^{1-\alpha} = \tau^{3-\alpha} \int_0^1 dx x(1-x)^{1-\alpha} = \tau^{3-\alpha} \frac{\Gamma(1-\alpha)}{\Gamma(2-\alpha)},$$

we find the estimate:

$$\|\mathcal{A}^{-\alpha}(T(\tau) - e^{-\tau\mathcal{K}})\mathcal{A}^{-\alpha}g\| \leq Z_1 \frac{\Gamma(1-\alpha)}{\Gamma(2-\alpha)} \tau^{3-\alpha} + \frac{Z_2 + Z_3}{2} \tau^2 + \frac{Z_4}{1+\alpha} \tau^{1+\alpha},$$

for $\tau \geq 0$. We have:

$$\|\mathcal{A}^{-\alpha}(T(\tau) - e^{-\tau\mathcal{K}})\mathcal{A}^{-\alpha}g\| \leq \left(Z_1 \frac{\Gamma(1-\alpha)}{\Gamma(2-\alpha)} \tau^{2-2\alpha} + \frac{Z_2 + Z_3}{2} \tau^{1-\alpha} + Z_4 \right) \tau^{1+\alpha},$$

for $\tau \geq 0$. Since $T(\tau) = 0$ and $e^{-\tau\mathcal{K}} = 0$ for $\tau \geq T$ we finally obtain:

$$\|\mathcal{A}^{-\alpha}(T(\tau) - e^{-\tau\mathcal{K}})\mathcal{A}^{-\alpha}g\| \leq \left(Z_1 \frac{\Gamma(1-\alpha)}{\Gamma(2-\alpha)} T^{2-2\alpha} + \frac{Z_2 + Z_3}{2} T^{1-\alpha} + Z_4 \right) \tau^{1+\alpha},$$

which proves the lemma. \square

Lemma 5.3. *Let $\alpha \in [0, 1)$. Then the estimates:*

$$\sum_{m=1}^{n-1} \frac{1}{m^\alpha} \leq \frac{n^{1-\alpha}}{1-\alpha} \quad \text{and} \quad \sum_{m=1}^{n-1} \frac{1}{(n-m)^\alpha m^\alpha} \leq \frac{2}{1-\alpha} n^{1-2\alpha}, \quad (5.14)$$

are valid for $n = 2, 3, \dots$.

Proof. The function $f(x) = x^{-\alpha}$, $x > 0$, is decreasing. Hence:

$$\sum_{m=1}^{n-1} \frac{1}{m^\alpha} \leq \int_0^{n-1} dx \frac{1}{x^\alpha} \leq \frac{(n-1)^{1-\alpha}}{1-\alpha} \leq \frac{n^{1-\alpha}}{1-\alpha},$$

for $n = 2, 3, \dots$. Further, we have:

$$\sum_{m=1}^{n-1} \frac{1}{(n-m)^\alpha m^\alpha} \leq 2 \frac{1}{n^\alpha} \sum_{m=1}^{n-1} \frac{1}{m^\alpha} \leq 2 \frac{1}{n^\alpha} \frac{n^{1-\alpha}}{1-\alpha} = \frac{2}{1-\alpha} n^{1-2\alpha},$$

and the claim follows. \square

5.2. The Trotter product formula in operator-norm topology

Now, we are able to prove and to estimate the rate of operator-norm convergence of the Trotter product approximation.

Theorem 5.4. *Let the assumptions (A1), (A2), and (A3) be satisfied. If the family of generators $\{B(t)\}_{t \in \mathcal{I}}$ is A -stable, then there exists a (depending on $\alpha \in (1/2, 1)$ and on the compact interval \mathcal{I}) constant $C_{\alpha, \mathcal{I}} > 0$ such that:*

$$\| (e^{-\tau\mathcal{B}/n} e^{-\tau\mathcal{K}_0/n})^n - e^{-\tau\mathcal{K}} \|_{\mathcal{B}(L^p(\mathcal{I}, X))} \leq \frac{C_{\alpha, \mathcal{I}}}{n^{1-\alpha}}, \quad (5.15)$$

for $\tau \geq 0$ and $n = 2, 3, \dots$.

Proof. Let $T(\sigma) := e^{-\sigma\mathcal{B}} e^{-\sigma\mathcal{K}_0}$ and $U(\sigma) := e^{-\sigma\mathcal{K}}$, $\sigma \geq 0$. Then the following identity holds:

$$\begin{aligned} T(\sigma)^n - U(\sigma)^n &= \sum_{m=0}^{n-1} T(\sigma)^{n-m-1} (T(\sigma) - U(\sigma)) U(\sigma)^m \\ &= T(\sigma)^{n-1} (T(\sigma) - U(\sigma)) + (T(\sigma) - U(\sigma)) U(\sigma)^{n-1} + \sum_{m=1}^{n-2} T(\sigma)^{n-m-1} (T(\sigma) - U(\sigma)) U(\sigma)^m \\ &= T(\sigma)^{n-1} \mathcal{A}^\alpha \mathcal{A}^{-\alpha} (T(\sigma) - U(\sigma)) + (T(\sigma) - U(\sigma)) \mathcal{A}^{-\alpha} \mathcal{A}^\alpha U(\sigma)^{n-1} \\ &\quad + \sum_{m=1}^{n-2} T(\sigma)^{n-m-1} \mathcal{A}^\alpha \mathcal{A}^{-\alpha} (T(\sigma) - U(\sigma)) \mathcal{A}^{-\alpha} \mathcal{A}^\alpha U(\sigma)^m, \end{aligned}$$

which yields the estimate:

$$\begin{aligned} & \|T(\sigma)^n - U(\sigma)^n\| \\ & \leq \|\overline{T(\sigma)^{n-1}\mathcal{A}^\alpha}\| \|A^{-\alpha}(T(\sigma) - U(\sigma))\| + \|(T(\sigma) - U(\sigma))\mathcal{A}^{-\alpha}\| \|A^\alpha U(\sigma)^{n-1}\| \\ & \quad + \sum_{m=1}^{n-2} \|\overline{T(\sigma)^{n-m-1}\mathcal{A}^\alpha}\| \|A^{-\alpha}(T(\sigma) - U(\sigma))\mathcal{A}^{-\alpha}\| \|A^\alpha U(\sigma)^m\|. \end{aligned}$$

From Lemma 5.1 we get the estimates:

$$\|\overline{T(\sigma)^{n-1}\mathcal{A}^\alpha}\| \leq Y_\alpha \left(\sigma^{1-2\alpha} + \frac{1}{((n-1)\sigma)^\alpha} \right), \quad n \geq 2,$$

as well as:

$$\|A^{-\alpha}(T(\sigma) - U(\sigma))\| \leq \Pi_\alpha \sigma \quad \text{and} \quad \|(T(\sigma) - U(\sigma))\mathcal{A}^{-\alpha}\| \leq \Pi_\alpha \sigma,$$

for $\sigma \in (0, \tau]$. Hence:

$$\|\overline{T(\sigma)^{n-1}\mathcal{A}^\alpha}\| \|A^{-\alpha}(T(\sigma) - U(\sigma))\| \leq \Pi_\alpha Y_\alpha \sigma^{1-\alpha} \left(\sigma^{1-\alpha} + \frac{1}{(n-1)^\alpha} \right),$$

and:

$$\|(T(\sigma) - U(\sigma))\mathcal{A}^{-\alpha}\| \|A^\alpha U(\sigma)^{n-1}\| \leq \frac{\Pi_\alpha \Lambda_\alpha}{(n-1)^\alpha} \sigma^{1-\alpha},$$

where we have used (5.1). Since:

$$\|A^{-\alpha}(T(\sigma) - e^{-\sigma\mathcal{K}})\mathcal{A}^{-\alpha}\|_{B(L^p(\mathcal{I}, X))} \leq Z_\alpha \sigma^{1+\alpha}, \quad \tau \in [0, \tau_0),$$

by Lemma 5.2 we obtain:

$$\begin{aligned} & \|\overline{T(\sigma)^{n-m-1}\mathcal{A}^\alpha}\| \|A^{-\alpha}(T(\sigma) - U(\sigma))\mathcal{A}^{-\alpha}\| \|A^\alpha U(\sigma)^m\| \\ & \leq Y_\alpha \left(\sigma^{1-2\alpha} + \frac{1}{((n-m-1)\sigma)^\alpha} \right) Z_\alpha \sigma^{1+\alpha} \Lambda_\alpha \frac{1}{(\sigma m)^\alpha} \\ & \leq Y_\alpha Z_\alpha \Lambda_\alpha \left(\sigma^{2-2\alpha} \frac{1}{m^\alpha} + \sigma^{1-\alpha} \frac{1}{(n-m-1)^\alpha m^\alpha} \right). \end{aligned}$$

Now, using Lemma 5.3 we get:

$$\begin{aligned} & \sum_{m=1}^{n-2} \|\overline{T(\sigma)^{n-m-1}\mathcal{A}^\alpha}\| \|A^{-\alpha}(T(\sigma) - U(\sigma))\mathcal{A}^{-\alpha}\| \|A^\alpha U(\sigma)^m\| \\ & \leq Z_\alpha \Lambda_\alpha Y_\alpha \sigma^{2-2\alpha} \sum_{m=1}^{n-2} \frac{1}{m^\alpha} + Z_\alpha \Lambda_\alpha Y_\alpha \sigma^{1-\alpha} \sum_{m=1}^{n-2} \frac{1}{(n-m-1)^\alpha m^\alpha} \\ & \leq \frac{Z_\alpha \Lambda_\alpha Y_\alpha}{1-\alpha} (n^{1-\alpha} \sigma^{2-2\alpha} + 2n^{1-2\alpha} \sigma^{1-\alpha}). \end{aligned}$$

Summing up, we find that:

$$\begin{aligned} \|T(\sigma)^n - U(\sigma)^n\| & \leq \Pi_\alpha Y_\alpha \sigma^{1-\alpha} \left(\sigma^{1-\alpha} + \frac{1}{(n-1)^\alpha} \right) + \frac{\Pi_\alpha \Lambda_\alpha}{(n-1)^\alpha} \sigma^{1-\alpha} + \\ & \quad \frac{Z_\alpha \Lambda_\alpha Y_\alpha}{1-\alpha} n^{1-\alpha} \sigma^{2-2\alpha} + \frac{2Z_\alpha \Lambda_\alpha Y_\alpha}{1-\alpha} n^{1-2\alpha} \sigma^{1-\alpha}. \end{aligned}$$

Note that setting $\sigma := \tau/n$, one obtains:

$$\begin{aligned} & \|T(\tau/n)^n - U(\tau/n)^n\| \\ & \leq \frac{\Pi_\alpha \Lambda_\alpha T^{2-2\alpha}}{(n-1)^{2-2\alpha}} + \frac{\Pi_\alpha \Lambda_\alpha}{n-1} + \frac{\Pi_\alpha \Lambda_\alpha T^{1-\alpha}}{(n-1)} + \frac{Z_\alpha \Lambda_\alpha Y_\alpha T^{2-2\alpha}}{1-\alpha} \frac{1}{n^{1-\alpha}} + \frac{2Z_\alpha \Lambda_\alpha Y_\alpha T^{1-\alpha}}{1-\alpha} \frac{1}{n^\alpha}, \end{aligned}$$

for $\tau \geq 0$ and $n = 2, 3, \dots$. Hence, there exists a constant $C_{\alpha, \mathcal{I}} > 0$ such that: (5.15) holds. \square

Remark 5.5. It is worth noting that this result depends only on the domains of the operators A and $B(t)$ and not on their concrete realization.

5.3. Operator-norm convergence of propagators

Theorem 5.4 allows to estimate the rate of approximation by the product formula of the solution operator (propagator) $\{U(t, s)\}_{(t,s) \in \Delta}$.

To this aim we note that due to Theorem 3.3 we have the identity:

$$\left(\left\{ \left(e^{-\frac{\tau}{n}B} e^{-\frac{\tau}{n}K_0} \right)^n - e^{-\tau(B+K_0)} \right\} g \right) (t) = \left\{ U_n(t, t - \tau) - U(t, t - \tau) \right\} \chi_{\mathcal{I}}(t - \tau) g(s - \tau),$$

for $(t, t - \tau) \in \Delta$ and $g \in L^p(\mathcal{I}, X)$, where:

$$U_n(t, s) := \prod_{j=1}^{n \leftarrow} G_j(t, s; n), \quad (t, s) \in \Delta,$$

where $G_j(t, s; n) := e^{-\frac{t-s}{n}B(s+j\frac{t-s}{n})} e^{-\frac{t-s}{n}A}$ and the product is increasingly ordered from the right to the left. Next, we introduce on $L^p(\mathcal{I}, X)$ the left-shift semigroup:

$$(L(\tau)f)(t) := \chi_{\mathcal{I}}(t + \tau) f(t + \tau), \quad f \in L^p(\mathcal{I}, X).$$

Theorem 5.6. *Let the assumptions (A1), (A2), and (A3) be satisfied. If the family of generators $\{B(t)\}_{t \in \mathcal{I}}$ is A -stable, then there is a constant $C_{\alpha, \mathcal{I}} > 0$:*

$$\operatorname{ess\,sup}_{(t,s) \in \Delta} \|U_n(t, s) - U(t, s)\|_{\mathcal{B}(X)} \leq \frac{C_{\alpha, \mathcal{I}}}{n^{1-\alpha}}, \quad n = 2, 3, \dots, \tag{5.16}$$

where the constant $C_{\alpha, \mathcal{I}}$ coincides with that one of Theorem 5.4.

Proof. We set:

$$S_n(t, s) := U_n(t, s) - U(t, s), \quad (t, s) \in \Delta, \quad n \in \mathbb{N},$$

and:

$$\mathcal{S}_n(\tau) := L(\tau) \left\{ \left(e^{-\frac{\tau}{n}B} e^{-\frac{\tau}{n}K_0} \right)^n - e^{-\tau(B+K_0)} \right\} : L^p(\mathcal{I}, X) \rightarrow L^p(\mathcal{I}, X),$$

for $\tau \geq 0$ and $n = 2, 3, \dots$. Then one gets:

$$(\mathcal{S}_n(\tau)g)(t) = S_n(t + \tau, t) \chi_{\mathcal{I}}(t + \tau) g(t), \quad t \in \mathcal{I}_0, \quad g \in L^p(\mathcal{I}, X).$$

Hence, for any $\tau \in \mathcal{I}$ and $n \in \mathbb{N}$, the operator $\mathcal{S}_n(\tau)$ is a multiplication operator on $L^p(\mathcal{I}, X)$ induced by the family $\{S_n(\cdot + \tau, \cdot) \chi_{\mathcal{I}}(\cdot + \tau)\}_{\tau \in \mathcal{I}}$ of bounded operators. Applying equation (7.27) of [7], we conclude that for $\tau \geq 0$ one has the identity:

$$\begin{aligned} \| \left(e^{-\frac{\tau}{n}B} e^{-\frac{\tau}{n}K_0} \right)^n - e^{-\tau(B+K_0)} \|_{\mathcal{B}(L^p(\mathcal{I}, X))} &= \| L(\tau) \left\{ \left(e^{-\frac{\tau}{n}B} e^{-\frac{\tau}{n}K_0} \right)^n - e^{-\tau(B+K_0)} \right\} \|_{\mathcal{B}(L^p(\mathcal{I}, X))} \\ &= \| \mathcal{S}_n(\tau) \|_{\mathcal{B}(L^p(\mathcal{I}, X))} = \operatorname{ess\,sup}_{t \in \mathcal{I}_0} \| S_n(t + \tau, t) \chi_{\mathcal{I}}(t + \tau) \|_{\mathcal{B}(X)} \\ &= \operatorname{ess\,sup}_{t \in \mathcal{I}_0} \| \{ U_n(t + \tau, t) - U(t + \tau, t) \} \chi_{\mathcal{I}}(t + \tau) \|_{\mathcal{B}(X)} \\ &= \operatorname{ess\,sup}_{t \in (0, T-\tau]} \| U_n(t + \tau, t) - U(t + \tau, t) \|_{\mathcal{B}(X)}. \end{aligned} \tag{5.17}$$

Now, taking into account Theorem 5.4, we find:

$$\operatorname{ess\,sup}_{t \in (0, T-\tau]} \| U_n(t + \tau, t) - U(t + \tau, t) \|_{\mathcal{B}(X)} \leq \frac{C_{\alpha, \mathcal{I}}}{n^{1-\alpha}}, \quad \tau \geq 0, \quad n \in 2, 3, \dots,$$

which yields (5.16). □

Remark 5.7.

(i) In the case of a Hilbert space Ichinose and Tamura proved in [6] that the convergence rate has order $O(\ln(n)/n)$ if one assumes that the operators A and $B(t)$ are positive and self-adjoint. On the other hand, the authors proved in [7] for Banach spaces that the convergence rate estimate is $O(n^{-(\beta-\alpha)})$ for any $\beta \in (\alpha, 1)$, assuming $\operatorname{dom}(A^*) \subset \operatorname{dom}(B(t)^*)$. We comment here that under the same conditions for *autonomous* case ($B(t) = B$) the estimate in a Banach has the form $O(\ln(n)/n^{1-\alpha})$, $0 < \alpha < 1$, see [8, Theorem 3.6].

(ii) The key identity (5.17) that makes a contact between the evolution semigroup and the solution operator (propagator) approaches to non-autonomous Cauchy problems, also shows that estimates (5.15) and (5.16) are equivalent.

(iii) We note that a priori the operator family $\{U_n(t, s)\}_{(t,s) \in \Delta}$ do not define a propagator since the co-cycle equation is in general not satisfied. But one can check that:

$$U_n(t, s) = U_{n-k} \left(t, s + \frac{k}{n}(t-s) \right) U_k \left(s + \frac{k}{n}(t-s), s \right),$$

is satisfied for $0 < s \leq t \leq T$, $n \in \mathbb{N}$ and any $k \in \{0, 1, \dots, n\}$.

6. Example: diffusion equation perturbed by a time-dependent potential

We investigate the diffusion equation perturbed by a time-dependent potential. On the Banach space $X = L^q(\Omega)$, where $\Omega \subset \mathbb{R}^d$ is a bounded domain with C^2 -boundary ($d \geq 2$) and $q \in (1, \infty)$, the equation reads:

$$\dot{u}(t) = \Delta u(t) - B(t)u(t), \quad u(s) = u_s \in L^q(\Omega), \quad t, s \in \mathcal{I}_0. \tag{6.1}$$

Δ denotes the Laplace operator on $L^q(\Omega)$ with Dirichlet boundary conditions defined on:

$$\Delta : \text{dom}(\Delta) = H_q^2(\Omega) \cap \dot{H}_q^1(\Omega) \rightarrow L^q(\Omega).$$

It turns out that $-\Delta$ is the generator of a holomorphic contraction semigroup on $L^q(\Omega)$ (cf. [11, Theorem 7.3.5/6]). $B(t)$ denotes a time-dependent scalar-valued multiplication operator given by:

$$(B(t)f)(x) = V(t, x)f(x), \quad \text{dom}(B(t)) = \{f \in L^q(\Omega) : V(t, x)f(x) \in L^q(\Omega)\},$$

where:

$$V : \mathcal{I} \times \Omega \rightarrow \mathbb{C}, \quad V(t, \cdot) \in L^q(\Omega).$$

For $\alpha \in (0, 1)$, the fractional power of $-\Delta$ are defined on the domain:

$$(-\Delta)^\alpha : \dot{H}_q^{2\alpha}(\Omega) \rightarrow L^q(\Omega).$$

Note, that for $2\alpha < 1/q$, it holds that $\dot{H}_q^{2\alpha}(\Omega) = H_q^{2\alpha}(\Omega)$. The adjoint operator of $(-\Delta)^\alpha$ is defined on the domain $\text{dom}(((-\Delta)^\alpha)^*) = \dot{H}_{q'}^{2\alpha}(\Omega) \subset L^{q'}(\Omega)$, where $1/q + 1/q' = 1$. The operators $B(t)$ are scalar-valued and hence $B(t)^* = \overline{B(t)} : \text{dom}(B(t)) \subset L^{q'}(\Omega) \rightarrow L^{q'}(\Omega)$. Moreover, one can show that $\mathcal{K}_0 = D_0 + \mathcal{A}$, i.e. the operator sum $D_0 + \mathcal{A}$ is already closed.

Now, we are going to verify the assumptions (A1)–(A3) in order to approximate the solution of (6.1). This means, we determine the required regularity in space and in time of the potential $V(\cdot, \cdot)$ to ensure the assumptions (A1)–(A3).

To guarantee that the operators $B(t)$ are generators, we assume that the potential $V(t, x)$ is positive, i.e.:

$$\text{Re}(V(t, x)) \geq 0, \quad \text{for a.e. } (t, x) \in \mathcal{I} \times \Omega.$$

Then, for any $t \in \mathcal{I}$ the operator $V(t, x)$ is a generator of a contraction semigroup on $X = L^q(\Omega)$ (cf. [5, Theorem I.4.11–12]). In particular, the operator family $B(t)$ is A -stable.

For fixed $d \geq 2$ and $\alpha \in (1/2, 1)$, we define the following values for the parameters $\tilde{r}, \tilde{\rho}, \tau$:

	$q \in \left(1, \frac{d}{2\alpha}\right)$	$q \in \left[\frac{d}{2\alpha}, \infty\right)$
$q' \in \left(1, \frac{d}{2\alpha}\right)$	$\tilde{r} \in \left[\frac{d}{2\alpha}, \infty\right], \tilde{\rho} \in \left[\frac{d}{2\alpha}, \infty\right],$ $\tau \in \left[\frac{d}{4\alpha}, \infty\right]$	$\tilde{r} \in (q, \infty], \tilde{\rho} \in \left[\frac{d}{2\alpha}, \infty\right],$ $\tau \in \left[\frac{d}{2\alpha + dq}, \infty\right]$
$q' \in \left[\frac{d}{2\alpha}, \infty\right)$	$\tilde{r} \in \left[\frac{d}{2\alpha}, \infty\right], \tilde{\rho} \in (q', \infty],$ $\tau \in \left[\frac{d}{2\alpha + dq'}, \infty\right]$	$\tilde{r} \in (q, \infty], \tilde{\rho} \in (q', \infty],$ $\tau \in (1, \infty]$

Take $\tilde{r}, \tilde{\rho}$ from the table above and define r, ρ via:

$$\frac{1}{r} + \frac{1}{\tilde{r}} = \frac{1}{q}, \quad \frac{1}{\rho} + \frac{1}{\tilde{\rho}} = \frac{1}{q'}. \tag{6.2}$$

Using Sobolev embeddings of the form:

$$H_{\gamma_1}^s(\Omega) \subset L^{\gamma_2}(\Omega) \text{ for } \begin{cases} \gamma_2 \in \left[\gamma_1, \frac{d}{s} \gamma_1 \right], & \text{if } \gamma_1 \in \left(1, \frac{d}{s} \right); \\ \gamma_2 \in [\gamma_1, \infty), & \text{if } \gamma_1 \in \left[\frac{d}{s}, \infty \right); \end{cases} \quad (6.3)$$

it is not hard to show $H_q^{2\alpha}(\Omega) \subset L^r(\Omega)$ and $H_{q'}^{2\alpha}(\Omega) \subset L^\rho(\Omega)$ on the one hand, and $L^r(\Omega), L^\rho(\Omega) \subset \text{dom}(B(t))$ on the other hand. This means, $\text{dom}((-\Delta)^\alpha) \subset \text{dom}(B(t))$ and $\text{dom}((-\Delta)^\alpha)^* \subset \text{dom}(B(t)^*)$. The operator $B(t)$ is a multiplication operator defined by $V(t, \cdot)$ and hence, following (6.2) the regularity of $V(t, \cdot)$ has to be at least $\varrho := \max\{\tilde{r}, \tilde{\rho}\}$. Hence, assuming $V \in L^\infty(\mathcal{I}, L^\varrho(\Omega))$, we have $\text{ess sup}_{t \in \mathcal{I}} \|B(t)(-\Delta)^\alpha\| \leq \infty$ and

$\text{ess sup}_{t \in \mathcal{I}} \|B(t)^*((-\Delta)^\alpha)^*\| \leq \infty$. Hence, (A1) and (A2) are satisfied.

Moreover, let:

$$F(t) := (-\Delta)^{-\alpha} B(t) (-\Delta)^{-\alpha} : L^q(\Omega) \rightarrow \dot{H}_q^{2\alpha}(\Omega).$$

For τ from the table above the relation:

$$\frac{1}{r} + \frac{1}{\tau} + \frac{1}{\rho} \leq 1 \quad (6.4)$$

holds. One can show that each $t \in \mathcal{I}$ the operator $F(t)$ is bounded for $V(t, \cdot) \in L^\tau(\Omega)$. Indeed, let $f \in L^q(\Omega)$ and $g \in L^{\rho'}(\Omega)$. Define $\tilde{f} = \Delta^{-\alpha} f \in \dot{H}_q^{2\alpha}(\Omega) \subset L^r(\Omega)$ and $\tilde{g} = (\Delta^{-\alpha})^* g = (\Delta^*)^{-\alpha} g \in \dot{H}_{q'}^{2\alpha}(\Omega) \subset L^\rho(\Omega)$. Then, we have for $t \in \mathcal{I}$:

$$\langle F(t)f, g \rangle = \langle (-\Delta)^{-\alpha} B(t) (-\Delta)^{-\alpha} f, g \rangle = \langle (-\Delta)^{-\alpha} f, B(t)^* (-\Delta^*)^{-\alpha} g \rangle = \langle \tilde{f}, B(t)^* \tilde{g} \rangle.$$

The boundedness of $\langle \tilde{f}, B(t)^* \tilde{g} \rangle$ is satisfied for $V(t, \cdot) \in L^\tau(\Omega)$. Assuming V to be Lipschitz continuous in time, i.e. assuming $V \in C^{\text{Lip}}(\mathcal{I}, L^\tau(\Omega))$, it follows that (A3) is satisfied. We remark that since we have $r \geq q$, it holds that $\tau \leq \tilde{\rho}$ and hence, $\tau \leq \varrho = \max\{\tilde{r}, \tilde{\rho}\}$.

The arguments that we collected above yield the following statement concerning our example (6.1):

Theorem 6.1. *Let $\Omega \subset \mathbb{R}^d$ be a bounded domain with C^2 -boundary, let $q \in (1, \infty)$ and let $\alpha \in (1/2, 1)$. Let $B(t)f = V(t, \cdot)f$ define a scalar valued multiplication operator on $L^q(\Omega)$ with:*

$$V \in L^\infty(\mathcal{I}, L^\varrho(\Omega)) \cap C^{\text{Lip}}(\mathcal{I}, L^\tau(\Omega)), \quad (6.5)$$

where $\varrho = \max\{\tilde{r}, \tilde{\rho}\}$ and $\tilde{r}, \tilde{\rho}, \tau$ is chosen from the above table. Moreover, let $\text{Re}(V(t, x)) \geq 0$ for $t \in \mathcal{I}$ and for a.e. $x \in \Omega$.

Then, the evolution problem (6.1) has a unique solution operator $U(t, s)$ which can be approximated in operator-norm by:

$$\sup_{(t,s) \in \Delta} \|U_n(t, s) - U(t, s)\|_{\mathcal{B}(L^q(\Omega))} = O(n^{-(1-\alpha)}),$$

where:

$$U_n(t, s) = \prod_{j=1}^n e^{-\frac{t-s}{n} V(\frac{n-j+1}{n}t + \frac{j-1}{n}s, \cdot)} e^{\frac{t-s}{n} \Delta}. \quad (6.6)$$

Proof. The claim follows, using Theorem 3.3 and Theorem 5.6. The ‘‘ess sup’’ becomes a ‘‘sup’’, since the solution operator and the approximating operator are continuous. \square

Remark 6.2.

(i) In [12], the existence of a solution operator for equation (6.1) is shown assuming weaker regularity in space and time for the potential. We assumed uniform boundedness of the function $t \mapsto \|B(t)(-\Delta)^\alpha\|_{\mathcal{B}(X)}$, which is indeed too strong but important for the considerations.

(ii) We focused on domains, which are bounded and have C^2 -boundaries. Our considerations can be extended to other domains, too.

(iii) Although the approximating propagator $\{U_n(t, s)\}_{(t,s) \in \Delta}$ defined in (6.6) looks elaborate, it has a simple structure. The semigroup of the Laplace operator on $L^q(\mathbb{R}^d)$ is given by the Gauss–Weierstrass semigroup (see for example [5, Chapter 2.13]) defined via:

$$(e^{t\Delta}u)(x) = (T(t)u)(x) = (4\pi t)^{-d/2} \int_{\mathbb{R}^d} e^{-\frac{|x-y|^2}{4t}} u(y) dy.$$

The terms $e^{-\tau V(t_j)}$ are scalar valued and can be easily computed.

Acknowledgments

The preparation of the paper was supported by the European Research Council via ERC-2010-AdG No. 267802 (“Analysis of Multiscale Systems Driven by Functionals”).

References

- [1] Kato T. Integration of the equation of evolution in a Banach space. *J. Math. Soc. Japan*, 1953, **5**, P. 208–234.
- [2] Phillips R.S. Perturbation theory for semi-groups of linear operators. *Trans. Amer. Math. Soc.*, 1953, **74**, P. 199–221.
- [3] Tanabe H. *Equations of evolution*. Pitman (Advanced Publishing Program), Boston, Mass.-London, 1979.
- [4] Trotter H.F. On the product of semi-groups of operators. *Proc. Amer. Math. Soc.*, 1959, **10**, P. 545–551.
- [5] Engel K.-J., Nagel R. *One-parameter semigroups for linear evolution equations*. Springer-Verlag, New York, 2000.
- [6] Ichinose T., Tamura H. Error estimate in operator norm of exponential product formulas for propagators of parabolic evolution equations. *Osaka J. Math.*, 1998, **35** (4), P. 751–770.
- [7] Neidhardt H., Stephan A., Zagrebnov V.A. Convergence rate estimates for the Trotter product approximations of solution operators for non-autonomous Cauchy problems, 2016, URL: <https://arxiv.org/abs/1612.06147>.
- [8] Cachia V., Zagrebnov V.A. Operator-norm convergence of the Trotter product formula for holomorphic semigroups. *J. Operator Theory*, 2001, **46**, P. 199–213.
- [9] Kato T. *Perturbation theory for linear operators*. Classics in Mathematics. Springer-Verlag, Berlin, 1995.
- [10] Neidhardt H., Zagrebnov V.A. Linear non-autonomous Cauchy problems and evolution semigroups. *Adv. Differential Equations*, 2009, **14** (3–4), P. 289–340.
- [11] Pazy A. *Semigroups of linear operators and applications to partial differential equations*. Springer-Verlag, New York, 1983.
- [12] Prüss J., Schnaubelt R. Solvability and maximal regularity of parabolic evolution equations with coefficients continuous in time. *J. Math. Anal. Appl.*, 2001, **256** (2), P. 405–430.

Unique continuation principles and their absence for Schrödinger eigenfunctions on combinatorial and quantum graphs and in continuum space

N. Peyerimhoff¹, M. Täufer², I. Veselić²

¹Department of Mathematical Sciences, Durham University, UK

²Fakultät für Mathematik, Technische Universität Dortmund, Germany

norbert.peyerimhoff@durham.ac.uk, mtaeuer@math.tu-dortmund.de, iveselic@math.tu-dortmund.de

DOI 10.17586/2220-8054-2017-8-2-216-230

For the analysis of the Schrödinger and related equations it is of central importance whether a unique continuation principle (UCP) holds or not. In continuum Euclidean space, quantitative forms of unique continuation imply Wegner estimates and regularity properties of the integrated density of states (IDS) of Schrödinger operators with random potentials. For discrete Schrödinger equations on the lattice, only a weak analog of the UCP holds, but it is sufficient to guarantee the continuity of the IDS. For other combinatorial graphs, this is no longer true. Similarly, for quantum graphs the UCP does not hold in general and consequently, the IDS does not need to be continuous.

Keywords: eigenfunctions, unique continuation, Schrödinger equation, Wegner estimate, Integrated density of states.

Received: 3 February 2017

Revised: 23 February 2017

1. Introduction

Unique continuation properties for various function classes have been studied for many years. They are of great importance when addressing uniqueness of solutions of partial differential equations, the propagation or regularity of solutions, and their growth behavior. More recently, they have been successfully applied in the spectral theory of random Schrödinger operators, for instance to prove Wegner estimates and establish regularity properties of the integrated density of states (IDS).

On the other hand it is well-known that for discrete Schrödinger operators on the lattice \mathbb{Z}^d the analog of the UCP does not hold. This poses a serious difficulty for the analysis of discrete Schrödinger operators. This is exemplified by the fact that there is still no proof of localization for the multidimensional Anderson model with Bernoulli disorder while this has been established for the seemingly more difficult analogous problem in continuum space in [1]. Nevertheless, a certain weaker version of unique continuation, namely non-existence of finitely supported eigenfunctions, allows one at least to conclude that the IDS of discrete Schrödinger operators on \mathbb{Z}^d is continuous. This, however, uses specific properties of the underlying combinatorial graph \mathbb{Z}^d and does not need to be true for Laplace or Schrödinger operators on other graphs. A prominent example of this phenomenon is the Laplace operator on a subgraph of \mathbb{Z}^d , generated by (random) percolation. Another example is the discrete Laplacian on the Kagome lattice which is a planar graph exhibiting eigenfunctions with finite support. In both examples, finitely supported eigenfunctions lead to jumps of the IDS. The two properties are actually in a sense equivalent. However, there is a condition on planar graphs, namely non-positivity of the so-called corner curvature, which excludes the existence of finitely supported eigenfunctions.

For quantum graphs, more precisely, for Schrödinger operators on metric graphs, the UCP does not hold in general as well. On the one hand, this can be understood as a consequence of the phenomenon encountered for planar graphs, since there is a way to “translate” spectral properties of equilateral quantum graphs to spectral properties of the underlying combinatorial graph. On the other hand, as soon as the underlying combinatorial graph has cycles, the Laplacian on the corresponding equilateral quantum graph carries compactly supported, so-called *Dirichlet* eigenfunctions on these cycles which can again lead to jumps in the IDS.

The paper is structured as follows: In Section 2 we discuss unique continuation principles for Schrödinger equations on subsets of \mathbb{R}^d . Then, in Section 3, we turn to analogous discrete equations on the Euclidean lattice graph \mathbb{Z}^d , where we present both positive and negative results concerning unique continuation. Section 4 is devoted to subgraphs of the Euclidean lattice \mathbb{Z}^d , generated by percolation, i.e. by random removing vertices. There, finitely supported eigenfunctions exist leading to jumps in the IDS. After that, in Section 5, we introduce the Kagome lattice as an example of a planar graph which exhibits finitely supported eigenfunctions and then present a combinatorial curvature condition which can ensure the non-existence of such finitely supported eigenfunctions. The final Section 6 is devoted to quantum graphs. We explain how properties from the underlying combinatorial graph translate to the lattice graph and study the IDS.

2. Unique continuation for solutions in continuum space

Throughout this article we will use the following notation: A measurable function f on a domain $A \subset \mathbb{R}^d$ is in $L^p(A)$, if $\|f\|_{L^p(A)} = \|f\|_p < \infty$, where $\|f\|_p = (\int_A |f|^p)^{1/p}$ if $1 \leq p < \infty$ and $\|f\|_\infty = \text{esssup}_A |f|$, the essential supremum with respect to the Lebesgue measure. If $B \subset A$, we write $\|f\|_{L^p(B)} = \|\chi_B f\|_{L^p(A)}$, where χ_B is the characteristic function of the set B , i.e. $\chi_B(x) = 1$ if $x \in B$ and 0 else. The function f is said to be in $H^{k,p}$, $k \in \mathbb{N}$, if f and all weak derivatives of f up to k -th order are in L^p . For a vector $x \in \mathbb{R}^d$, we will denote by $|x| = (x_1^2 + \dots + x_d^2)^{1/2}$ its Euclidean norm. The (open) ball of radius $r > 0$ around $x \in \mathbb{R}^d$ is denoted by $B(x, r) = \{y \in \mathbb{R}^d : |x - y| < r\}$. Furthermore, for $L > 0$ and $x \in \mathbb{R}^d$, we will call $\Lambda_L(x) = x + (-L/2, L/2)^d \subset \mathbb{R}^d$ the d -dimensional cube of side length L , centered at x . If $x = 0$, we will simply write Λ_L .

Definition 2.1. A class of functions \mathcal{F} on a connected domain $A \subset \mathbb{R}^d$ has the unique continuation property (UCP), if for every nonempty and open $U \subset A$ every $f \in \mathcal{F}$ vanishing on U must vanish everywhere. If every eigenfunction of a partial differential operator D has the UCP, then we say that the operator D has the UCP.

Standard examples of operators having the UCP include the Laplace operator Δ or elliptic operators with analytic coefficients. A breakthrough result was due to Carleman [2], who in 1939 proved that $-\Delta + V$ with $V \in L^\infty_{\text{loc}}$ has the UCP by using inequalities which are currently referred to as Carleman estimates. We shall first have a look at some unique continuation properties which at first sight are weaker than the above definition. In order to illustrate the mechanism how Carleman estimates imply unique continuation, let us recall a proof of the following result, see [3].

Proposition 2.2 (Unique continuation from a half space, [3]). *Let $d \geq 3$, $p = 2d/(d+2)$ and $V \in L^{d/2}(\mathbb{R}^d)$. Then, every $u \in H^{2,p}(\mathbb{R}^d)$ satisfying $|\Delta u| \leq |Vu|$ which vanishes on a half space must vanish everywhere.*

In fact, we are going to show a slightly stronger statement. By an infinite slab of width ϵ , we denote a set $S \subset \mathbb{R}^d$ which is a translation and rotation of:

$$\{x \in \mathbb{R}^d : 0 < x_1 < \epsilon, x_2, \dots, x_d \in \mathbb{R}\}.$$

In dimension $d = 2$, an infinite slab would be an infinite strip.

Proposition 2.3 (Unique continuation from a slab). *Let $d \geq 3$, $p = 2d/(d+2)$ and $V \in L^{d/2}(\mathbb{R}^d)$. Then, every $u \in H^{2,p}(\mathbb{R}^d)$ satisfying $|\Delta u| \leq |Vu|$ which vanishes on a infinite slab of width $\epsilon > 0$ must vanish everywhere.*

The proof relies on the following Carleman estimate, which can be found e.g. in [3].

Theorem 2.4. *Let $d \geq 3$, $p = 2d/(d+2)$ and $q = 2d/(d-2)$. Then there is a constant $C > 0$ such that for all $\nu \in \mathbb{R}^d$, all $\lambda \in \mathbb{R}$ and all u with $e^{\lambda \langle \nu, x \rangle} u \in H^{2,p}(\mathbb{R}^d)$ we have:*

$$\|e^{\lambda \langle \nu, x \rangle} u\|_{L^q(\mathbb{R}^d)} \leq C \|e^{\lambda \langle \nu, x \rangle} \Delta u\|_{L^p(\mathbb{R}^d)}.$$

Proof of Proposition 2.3. We choose $\rho > 0$ such that $\|V\|_{L^{d/2}(S_\rho)} \leq 1/(2C)$ for all infinite slabs S_ρ of width ρ where C is the constant from Theorem 2.4. By translation and rotation, we may assume that u vanishes on the slab $\{x \in \mathbb{R}^d : -\epsilon < x_1 < 0\}$ and it suffices to show $u \equiv 0$ in $S_\rho := \{x \in \mathbb{R}^d : 0 < x_1 < \rho\}$. Let now $\chi \in C^\infty(\mathbb{R}^d)$ such that $\chi \equiv 0$ if $x_1 < -\epsilon$ and $\chi \equiv 1$ if $x_1 > 0$. We estimate, using Hölder's inequality and $|\Delta u| \leq |Vu|$ to obtain for all $\lambda > 0$:

$$\begin{aligned} \|e^{-\lambda x_1} u\|_{L^q(S_\rho)} &\leq \|e^{-\lambda x_1} \chi u\|_{L^q(\mathbb{R}^d)} \\ &\leq C \|e^{-\lambda x_1} \Delta(\chi u)\|_{L^p(\mathbb{R}^d)} \\ &\leq C \|e^{-\lambda x_1} \Delta u\|_{L^p(S_\rho)} + C \|e^{-\lambda x_1} \Delta(\chi u)\|_{L^p(\mathbb{R}^d \setminus S_\rho)} \\ &\leq C \|e^{-\lambda x_1} V u\|_{L^p(S_\rho)} + C e^{-\lambda \rho} \|\Delta u\|_{L^p(\mathbb{R}^d)} \\ &\leq C \|V\|_{L^{d/2}(\mathbb{R}^d)} \cdot \|e^{-\lambda x_1} u\|_{L^q(S_\rho)} + C e^{-\lambda \rho} \|\Delta u\|_{L^p(\mathbb{R}^d)} \\ &\leq \frac{1}{2} \|e^{-\lambda x_1} u\|_{L^q(S_\rho)} + C e^{-\lambda \rho} \|\Delta u\|_{L^p(\mathbb{R}^d)}, \end{aligned}$$

where q is the exponent from Theorem 2.4. Subtracting the first summand on the right hand side and multiplying by $e^{\lambda \rho}$, one finds:

$$\|e^{\lambda(\rho - x_1)} u\|_{L^q(S_\rho)} \leq 2C \|\Delta u\|_{L^p(\mathbb{R}^d)},$$

for all $\lambda > 0$. This is only possible if $u \equiv 0$ in S_ρ . \square

Now, one is in the position to conclude unique continuation properties of other domains.

Proposition 2.5 (Outside-in and inside-out unique continuation, [3]). *Let $u \in H^{2,p}(\mathbb{R}^d)$ satisfy $|\Delta u| \leq |Vu|$ for a $V \in L^{d/2}(\mathbb{R}^d)$.*

- (1) *If u vanishes outside of an open ball of radius $\rho > 0$, it must vanish everywhere.*
- (2) *If u vanishes on an open ball of radius $\rho > 0$, it must vanish everywhere.*

Part (1) is a special case of Proposition 2.2, while the proof of Part (2) is based upon the transformation $u(x) \mapsto \tilde{u}(x) := u(x/|x|^2) \cdot |x|^{-(d-2)}$.

So far, we found that eigenfunctions vanishing on half-spaces, slabs, outside and inside of balls must vanish everywhere. In particular, the latter implies the notion of unique continuation as in Definition 2.1. The assumption $V \in L^{d/2}(\mathbb{R}^d)$ can be substantially relaxed, but we are not going to focus our attention on this issue and refer to the references [4–6]. We emphasize, however that we exploited rotational symmetry and the transformation $x \mapsto x/|x|^2$. On the lattice \mathbb{Z}^d , this will no longer work.

While unique continuation itself has turned out to be a useful tool for many applications [7, 8], in some situations, more information is required. We speak of *Quantitative unique continuation* if a function which is “small” on U cannot be “too large” on the whole domain A . Of course the notion of smallness needs some clarification. It can be formulated in terms of different norms, local maxima, etc. and there is a connection to vanishing speed of functions in the vicinity of their zero set. We are going to cite some cases of quantitative unique continuation principles and some resulting applications.

The first example concerns vanishing speed of solutions of the Laplace-Beltrami operator on compact manifolds with the explicit dependence $e^{\sqrt{E}}$ on the eigenvalue – a term that we will encounter later on. It is due to [9] and follows by combining Thm. 4.2 (i) with the second displayed formula on p. 174 in [9].

Theorem 2.6. *Let M be a closed, compact C^∞ Riemannian manifold. Then, there are constants $C_1, C_2 \geq 0$ such that for every $u \neq 0$ and $-\Delta u = Eu$ and every $x_0 \in M$, we have:*

$$\epsilon^{C_1 + C_2 \sqrt{E}} \cdot \max_{x \in M} |u(x)| \leq \max_{x \in B(x_0, \epsilon)} |u(x)| \quad \text{for small enough } \epsilon > 0,$$

i.e. u can at most vanish of order $C_1 + C_2 \sqrt{E}$.

In particular, if an eigenfunction u of the Laplace-Beltrami operator is zero in a non-empty open set, it certainly vanishes of infinite order and thus $u \equiv 0$, i.e. it has the UCP. In [10], similar results were proven for a larger class of second order differential operators which allowed for a potential and first order terms.

Now, we turn to vanishing properties at infinity. In this setting, one wants to understand the fastest possible rate at which a function can decay as the norm of its argument tends to infinity.

Theorem 2.7 (Quantitative UCP for eigenfunctions of Schrödinger operator, [1]). *Assume $\Delta u = Vu + \gamma$ in \mathbb{R}^d , $u(0) = 1$, $|u| \leq C$ and $\|V\|_\infty \leq C$. Then there are $C_1, C_2 > 0$ such that for every $x_0 \in \mathbb{R}^d$, we have*

$$\max_{|x-x_0| \leq 1} |u(x)| + \|\gamma\|_\infty > C_1 \exp\left(-C_2(\log|x_0|)|x_0|^{4/3}\right). \tag{1}$$

Theorem 2.7 was an essential ingredient in proving *spectral localization*, i.e. almost sure occurrence of dense pure point spectrum with exponentially decaying eigenfunctions for the *Anderson-Bernoulli model*:

$$H_\omega = -\Delta + V_\omega, \quad V(x) = \sum_{j \in \mathbb{Z}^d} \omega_j u(x-j),$$

where ω_j are independent and identically distributed Bernoulli random variables (i.e. they are either 0 or 1) and ϕ is a smooth, positive, compactly supported single-site potential.

While localization has been well established before in the case of the ω_j having an absolutely continuous (with respect to the Lebesgue measure) probability measure, see e.g. [11, 12], the case of Bernoulli distributed random variables has been more challenging and Theorem 2.7 turned out to be an essential component of the proof. In fact, since there is no lattice analogue of Theorem 2.7, the question of localization for the Anderson-Bernoulli model on the lattice \mathbb{Z}^d is still open, except in the case of dimension $d = 1$ where different methods are available, see [13], Theorem 2.1.

In order to formulate the next result, we need to define the density of states (DOS) and the integrated density of states (IDS). Let $V \in L^\infty(\mathbb{R}^d)$ and $H = -\Delta + V$ on $L^2(\mathbb{R}^d)$. For a d -dimensional cube Λ , we call H_Λ the restriction of H to $L^2(\Lambda)$ with Dirichlet boundary conditions (i.e. by prescribing the value 0 at the boundary of Λ).

Its spectrum consists of an increasing sequence of eigenvalues of finite multiplicity with the only accumulation point at $+\infty$. The finite volume density of states measure η_Λ is defined by:

$$\eta_\Lambda(B) := \frac{1}{|\Lambda|} \#\{\text{Eigenvalues of } H_\Lambda \text{ in } B\},$$

for any Borel set $B \subset \mathbb{R}$. Here and in the sequel we count eigenvalues according to their multiplicity. If the potential V is periodic, the density of states measure can be defined as the limit:

$$\eta(B) := \lim_{L \rightarrow \infty} \eta_{\Lambda_L}(B).$$

More generally, if we have an ergodic random family $\{V_\omega\}_{\omega \in \Omega}$ of potentials, there is convergence of the integrated density of states to a non-random function:

$$N(E) := \lim_{L \rightarrow \infty} \eta_{\Lambda_L f}((-\infty, E])$$

for almost every E and almost every $\omega \in \Omega$. For generic Schrödinger operators, η might not be well-defined but one can still define the density of states outer-measure as:

$$\eta^*(B) := \limsup_{L \rightarrow \infty} \sup_{x \in \mathbb{R}^d} \eta_{\Lambda_L(x)}(B).$$

In [14], a version of Theorem 2.7 was applied to prove continuity of the density of states (outer-)measure in dimension $d = 2, 3$. The case of dimension $d = 1$ had already been proved in [15].

Theorem 2.8 ([14]). *Let $H = -\Delta + V$ be a Schrödinger operator with bounded potential V and let the dimension $d \in \{1, 2, 3\}$. Then for every $E_0 \in \mathbb{R}$ there are constants C_1, C_2 , depending only on $E_0, \|V\|_\infty$ and d such that for every $E \leq E_0$ and every small enough ϵ :*

$$\eta^*([E, E + \epsilon]) \leq \frac{C_1}{(\log 1/\epsilon)^{C_2}},$$

i.e. the density of states outer-measure is continuous.

If $d = 1$, one can choose $C_2 = 1$ and $\epsilon \in (0, 1/2)$ cf. Theorem 5.1 in [15]. The restriction to dimension $d \leq 3$ is due to the exponent $4/3$ in (an analog of) ineq. (1) which originates from the particular Carleman inequality they use. In fact, if this exponent was to be replaced by $\beta > 1$, then Theorem 2.8 would hold for all dimensions $d < \beta/(\beta - 1)$, whence it is desirable to reduce the exponent $4/3$ in ineq. (1) to 1. However, there is a classic example [16] which shows that this will not be feasible using Carleman estimates, whence new approaches to unique continuation will be required in order to lift the proof of Theorem 2.8 to higher dimensions.

We will now study *scale-free* unique continuation, i.e. we will study quantitative unique continuation results which hold uniformly over a large number of scales and geometric settings. For that purpose, we introduce the following definition:

Definition 2.9. Let $0 < \delta < 1/2$. We say that a sequence $Z = \{z_j\}_{j \in \mathbb{Z}^d}$ is δ -*equidistributed*, if for every $j \in \mathbb{Z}^d$ we have $B(z_j, \delta) \subset j + \Lambda_1$. Corresponding to a δ -equidistributed sequence and $L > 0$, we define:

$$S_\delta(L) := \bigcup_{j \in \mathbb{Z}^d} B(z_j, \delta) \cap \Lambda_L.$$

The simplest example of a δ -equidistributed set would be \mathbb{Z}^d itself (see Fig. 1).

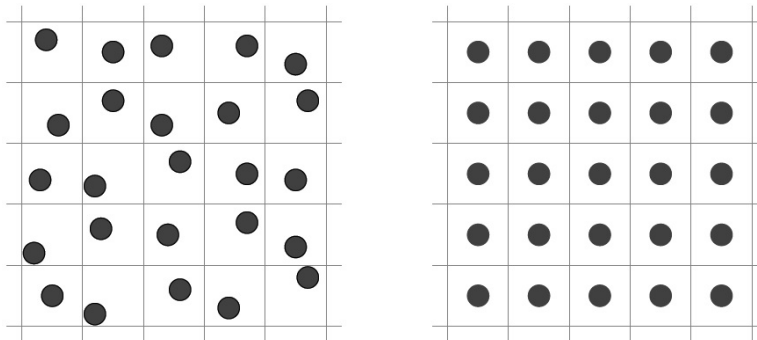


FIG. 1. Examples of $S_\delta(5)$ for different δ -equidistributed arrangements

Theorem 2.10 (Quantitative UCP for eigenfunctions, [17]). *Fix $K_V \in [0, \infty)$ and $\delta \in (0, 1/2)$. Then there is a constant $C > 0$ such that for all $L \in \mathbb{N}_{\text{odd}} = \{1, 3, \dots\}$, all measurable $V : \Lambda_L \rightarrow [-K_V, K_V]$ and all real-valued ψ in the domain of the Laplace operator on Λ_L with Dirichlet or periodic boundary condition satisfying:*

$$|\Delta\psi| \leq |V\psi|$$

we have:

$$\|\psi\|_{L^2(S_\delta(L))}^2 \geq \left(\frac{\delta}{C}\right)^{C+CK_V^{2/3}} \|\psi\|_{L^2(\Lambda_L)}^2.$$

Theorem 2.10 is called a *scale-free* unique continuation principle because the constant on the right hand side does not depend on the scale L . It has been used to study the spectrum of random Schrödinger operators, more precisely the *Delone-Anderson model*:

$$H_\omega = -\Delta + V_\omega, \quad V_\omega(x) = \sum_{y \in \mathcal{D}} \omega_y u(x-y) \quad (2)$$

where u is a compactly supported, positive and bounded function, the ω_y are independent and identically distributed, bounded random variables with a bounded density and $\mathcal{D} \subset \mathbb{R}^d$ is a *Delone set*. The latter means that there are $0 < L_1 < L_2$ such that for all $x \in \mathbb{R}^d$ we have $\#\{y \in \mathcal{D} \cup \Lambda_{L_1}\} \leq 1$ and $\#\{y \in \mathcal{D} \cup \Lambda_{L_2}\} \geq 1$. Every δ -equidistributed set is a Delone set and every Delone set can (after scaling) be decomposed into a δ -equidistributed set and some remaining set, see e.g. [17]. In [17], Theorem 2.10 was used to prove the following Wegner estimate:

Theorem 2.11. *Let $\{H_\omega\}_{\omega \in \Omega}$ be a Delone-Anderson Hamiltonian as in (2). For every E_0 there is a constant C_W such that for all $E \leq E_0$, all $\epsilon \leq 1/3$, all $L \in \mathbb{N}_{\text{odd}}$ we have:*

$$\mathbb{E} [\#\{\text{Eigenvalues of } H_{\omega, \Lambda} \text{ in } [E - \epsilon, E + \epsilon]\}] \leq C_W \cdot \epsilon \cdot |\ln \epsilon|^d \cdot |\Lambda_L|. \quad (3)$$

Wegner estimates serve as an induction anchor in the multi-scale analysis, an inductive process which establishes localization, i.e. the almost sure occurrence of pure point spectrum with exponentially decaying eigenfunctions for H_ω , at low energies. Note that the right hand side in Ineq. (3) is $o(\epsilon^\theta)$ as $\epsilon \rightarrow 0$ for every $\theta \in (0, 1)$. Therefore, if the integrated density of states of H_ω exists, it will be (locally) Hölder continuous with respect to any exponent $\theta \in (0, 1)$. Since, however, the Delone-Anderson model is not necessarily ergodic, existence of its IDS is a delicate issue, see [18].

In [17], the question had been raised if a similar statement as in Theorem 2.11 holds uniformly all for finite linear combination of eigenfunctions with eigenvalues below a threshold E_0 . Such results had been known before, cf. [19], albeit only in the special case where both the potential V and the Delone set D were \mathbb{Z}^d -periodic and without the explicit dependence on δ and K_V . They had led to Lipschitz continuity of IDS in the usual alloy-type or continuum Anderson model, cf. [20]. However, the proof of these unique continuation principles had relied on Floquet theory which only allowed for the periodic setting and a compactness argument which yielded no information on the influence of the parameters δ and K_V . A partially positive answer to the question raised in [17] was given in [21] where Theorem 2.10 was generalized to linear combinations of eigenfunctions with eigenvalues in a small energy interval. This allowed the dropping of the $\ln \epsilon$ term in (3). A full answer to the question raised in [17] was given by the following Theorem.

Theorem 2.12 ([22, 23]). *There is $N = N(d)$ such that for all $\delta \in (0, 1/2)$, all δ -equidistributed sequences, all measurable and bounded $V : \mathbb{R}^d \rightarrow \mathbb{R}$, all $L \in \mathbb{N}$, all $E_0 \geq 0$ and all $\phi \in \text{Ran}(\chi_{(-\infty, E_0]}(H_L))$ we have:*

$$\|\phi\|_{L^2(S_\delta(L))}^2 \geq \delta^N (1 + \|V\|_\infty^{2/3} + \sqrt{E_0}) \|\phi\|_{L^2(\Lambda_L)}^2. \quad (4)$$

Theorem 2.12 was a missing ingredient for treating new models of random Schrödinger operators such as the *standard breather model*: Let $\{\omega_j\}_{j \in \mathbb{Z}^d}$ be i.i.d. random variables on a probability space (Ω, \mathbb{P}) which are distributed according to the uniform distribution on the interval $[0, 1/2]$ and define the standard breather potential:

$$V_\omega(x) := \sum_{j \in \mathbb{Z}^d} \chi_{B(j, \omega_j)}(x),$$

where $\chi_{B(x, r)}$ denotes the characteristic function of a ball of radius r , centered at x . Then, the standard breather model is the family of operators $-\Delta + V_\omega$, $\omega \in \Omega$ on $L^2(\mathbb{R}^d)$ and can be seen as a prototype for a random Schrödinger operator where the random variables enter in a non-linear manner.

Theorem 2.13 (Wegner estimate for the standard breather model, [22,24]). *For every $E_0 \in \mathbb{R}$ there are $C > 0$, $0 < \theta < 1$ such that for every $E < E_0$, every $L \in \mathbb{N}$ and every small enough $\epsilon > 0$ we have:*

$$\mathbb{E} [\#\{\text{Eigenvalues of } H_{\omega, \Lambda_L} \text{ in } [E - \epsilon, E + \epsilon]\}] \leq C\epsilon^\theta L^d. \tag{5}$$

This implies (non-uniform) Hölder continuity at E of order θ of the corresponding IDS and can be used to establish localization for the standard breather model via multi-scale analysis.

Actually, Theorem 2.13 holds in a much more general setting, see [23]. We only mention here the (general) random breather model in which the characteristic functions of balls with random radii are replaced by random dilations of radially decreasing, compactly supported, bounded and positive function u :

$$V_\omega(x) = \sum_{j \in \mathbb{Z}^d} u\left(\frac{x-j}{\omega_j}\right).$$

Examples for u (see Fig. 2) are the smooth function:

$$u(x) = \exp\left(-\frac{1}{1-|x|^2}\right) \chi_{|x|<1},$$

or the hat potential:

$$u(x) = \chi_{|x|<1}(1-|x|).$$

Another application of Theorem 2.12 concerns decorrelation estimates and the spectral statistics of random Schrödinger operators in dimension 1, cf. [25].

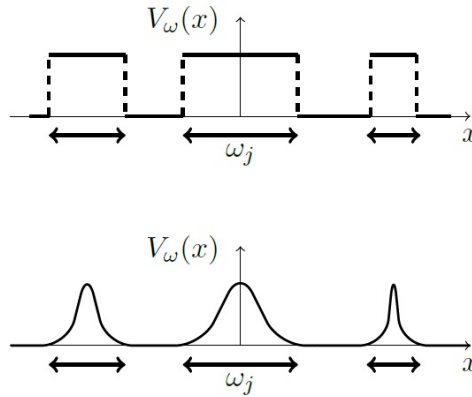


FIG. 2. Realizations of the standard breather potential and of a general random breather potential

Theorem 2.12 can also be applied in the context of control theory for the heat equation to show null controllability for the heat equation. More precisely, Theorem 2.12 can be used to give more explicit statements in the context of results obtained in [26], cf. [23].

3. Unique continuation problem for solutions on Euclidean lattice graphs

Definition 3.1 (Discrete Laplacian on \mathbb{Z}^d). We define the *discrete Laplacian* on functions $f : \mathbb{Z}^d \rightarrow \mathbb{C}$ as:

$$(\Delta f)(i) = \sum_{i \sim j} (f(j) - f(i)) = \sum_{i \sim j} f(j) - 2d \cdot f(i),$$

where $i \sim j$ means that i is a direct neighbor of j , i.e. $|i - j| = 1$.

Remark 3.2 (Why is this called ‘‘Laplacian’’?). If we think of $(f(i))_{i \in \mathbb{Z}^d}$ as evaluations of a function $f : \mathbb{R}^d \rightarrow \mathbb{C}$ on the points $i \in \mathbb{Z}^d$ and approximate the difference quotient $(f(x + \epsilon) - f(x))/\epsilon$ with $\epsilon = 1$, the minimal coarseness possible, we find:

$$f'(i + 1/2) \approx f(i + 1) - f(i) \quad \text{and} \quad f'(i - 1/2) \approx f(i) - f(i - 1),$$

whence

$$f''(i) \approx f'(i + 1/2) - f'(i - 1/2) \approx f(i - 1) - 2f(i) + f(i + 1).$$

In dimension d , this translates to:

$$(\Delta f)(i) \approx \sum_{i \sim j} f(j) - 2d \cdot f(i).$$

In the following examples we consider $-\Delta + V$ where $V : \mathbb{Z}^d \rightarrow \mathbb{R}$.

Example 3.3 (Unique Continuation from half spaces in \mathbb{Z}^d with border parallel to an axis, see Fig. 3). Let $f : \mathbb{Z}^d \rightarrow \mathbb{C}$ satisfy $(-\Delta + V)f = 0$ on \mathbb{Z}^d and $f(j) = 0$ for all $j = (j_1, \dots, j_d) \in \mathbb{Z}^d$ with $j_1 \leq 0$. Let $i \in \mathbb{Z}^d$ with $i_1 = 0$. Then:

$$-\sum_{j \sim i} f(j) + (2d + V(i))f(i) = 0,$$

but the only unknown term is $f((1, i_2, \dots, i_d))$ and therefore must be zero. We see that f must be zero on the slab $\{j \in \mathbb{Z}^d : j_1 = 1\}$. Inductively, we find $f \equiv 0$ in every slab of width 1 whence $f = 0$ on \mathbb{Z}^d . By the very same argument we establish unique continuation from a slab $\{(j_1, \dots, j_d) \in \mathbb{Z}^d : j_1 = k \text{ or } k + 1\}$ of width 2.

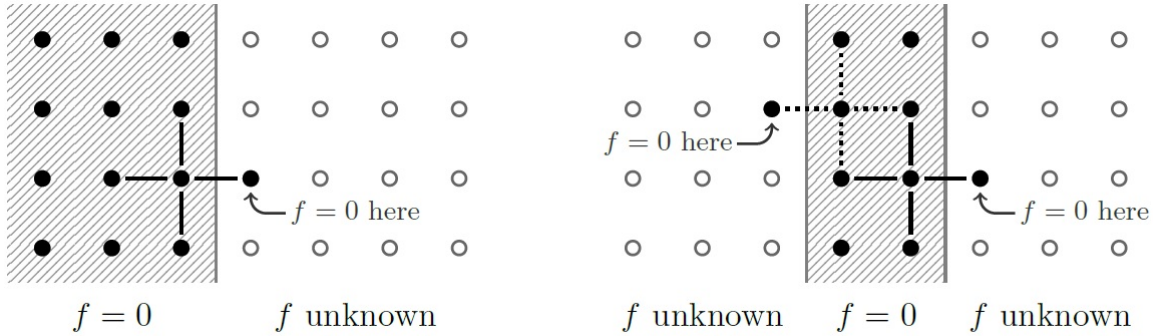


FIG. 3. Unique continuation from a half space and a double strip in dimension 2

Example 3.4 (No unique continuation from a double slab where one point has been omitted). For the one omitted point, we can prescribe any value. Then, there is a unique continuation (by induction over infinite slabs of width 1). Therefore, we have a 1-dimensional family of possible continuations.

Example 3.5 (No unique continuation from a double slab, where n points have been omitted). We prescribe values for the n points and find a unique continuation. Therefore, we have an n -dimensional family of possible continuations.

Example 3.6 (No unique continuation from a half space with border in a 45° angle to the axes). For simplicity, we consider the case $d = 2$ and $V \equiv 0$. Let $f : \mathbb{Z}^2 \rightarrow \mathbb{C}$ satisfy $\Delta f = 0$ on \mathbb{Z}^2 and $f \equiv 0$ on a diagonal half-space $\{(j_1, j_2) \in \mathbb{Z}^2 : j_1 + j_2 \leq 0\}$. This does not imply $f \equiv 0$ on \mathbb{Z}^d . In fact, as soon as a value of f on an additional point in the anti-diagonal line $\{(j_1, j_2) : j_1 + j_2 = 1\}$ is given, then the values on the whole anti-diagonal can be recovered successively from the equations

$$0 = \sum_{j \sim i} f(j) - 4f(i),$$

for i in $\{i \in \mathbb{Z}^2 : (i_1 + i_2) = 0\}$, cf. Fig. 4. Inductively, we find that there is one degree of freedom in every infinite anti-diagonal $\{(j_1, j_2) : j_1 + j_2 = k\}_{k \in \mathbb{N}}$ and we found an infinite dimensional family of possible continuations.

This illustrates the difference to the \mathbb{R}^d case: While \mathbb{R}^d is invariant under rotations, \mathbb{Z}^d is not whence some unique continuation properties only hold in certain directions. However, the next proposition shows that on \mathbb{Z}^2 , the half-spaces with border in a 45° angle to the axes are the only ones for which unique continuation fails.

Proposition 3.7 (Unique continuation in \mathbb{Z}^2 from half spaces in almost all directions). Let $f : \mathbb{Z}^2 \rightarrow \mathbb{C}$ satisfy $\Delta f = 0$ on \mathbb{Z}^2 and $f \equiv 0$ on a half-space $\{j \in \mathbb{Z}^2 : \langle j, \nu \rangle \leq \alpha\}$ where ν is not parallel to $(1, 1)$ or $(-1, 1)$, i.e. the border of the half-space is not in a 45° angle to an axis. Then $f \equiv 0$ on \mathbb{Z}^d .

Proof. By symmetry between the coordinate axes and reflection, we may assume $\nu = (1, \lambda)$ where $\lambda \in [0, 1)$. Similar considerations as in Example 3.6 show that u will vanish on the anti-diagonal line $\{j \in \mathbb{Z}^2 : j_1 + j_2 = c\}$ as soon as u vanishes on a set $Q_{c_1, c_2} := \{j \in \mathbb{Z}^2 : j_1 \leq c_1, j_2 \leq c_2\}$ with $c_1 + c_2 = c$. Hence, it suffices to show that for every $c \in \mathbb{Z}$, there is $(c_1, c_2) \in \mathbb{Z}^2$ with $c_1 + c_2 = c$ such that $Q_{c_1, c_2} \subset \{j \in \mathbb{Z}^2 : \langle j, \nu \rangle \leq \alpha\}$. This is the case if:

$$c_1 + \lambda c_2 \leq \alpha \quad \text{and} \quad c_1 + c_2 = c,$$

and a possible choice is $c_1 = c - \lceil (c - \alpha)/(1 - \lambda) \rceil$, $c_2 = c - c_1$, where $\lceil x \rceil$ denotes the least integer larger or equal than x . \square

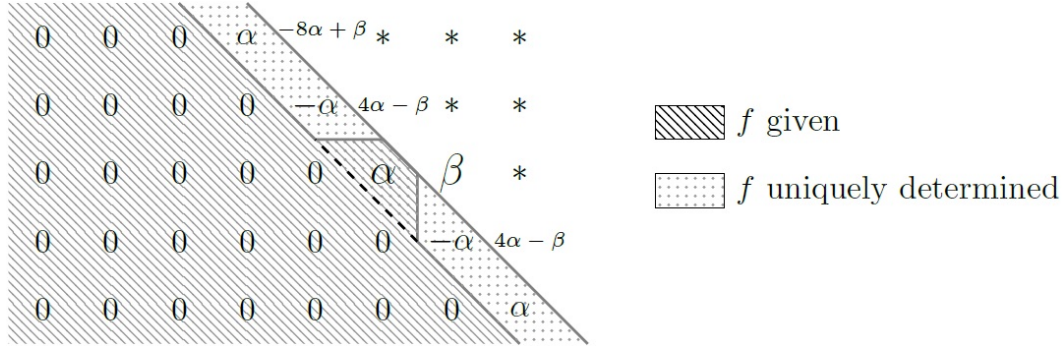


FIG. 4. No unique continuation from a half space with border in a 45° angle to the axes

Example 3.8 (Inside-out continuation does not work on \mathbb{Z}^d). If $(-\Delta + V)f = 0$ on \mathbb{Z}^d and $f = 0$ on a finite set $G \subset \mathbb{Z}^d$, we do not have $f = 0$ on \mathbb{Z}^d . In fact, G is contained in a half-space the border of which is in a 45° angle to a coordinate axis and even if f vanished on the entire half space, we have seen that this cannot ensure a unique continuation.

Example 3.9 (Outside-in continuation works on \mathbb{Z}^d). If however $(-\Delta + V)f = 0$ on \mathbb{Z}^d and f vanishes outside of a bounded set G , then f vanishes on a half-space (with borders parallel to the axes) and therefore must vanish everywhere.

So far, we have encountered a couple of negative examples in which properties valid on \mathbb{R}^d do not hold any more on \mathbb{Z}^d . Nevertheless, outside-in unique continuation which holds on \mathbb{Z}^d is sufficient to ensure continuity of the IDS of operators $-\Delta + V$ for ergodic $V : \mathbb{Z}^d \rightarrow \mathbb{R}$ on the Hilbert space $\ell^2(\mathbb{Z}^d) = \{f : \mathbb{Z}^d \rightarrow \mathbb{C} \mid \sum_{i \in \mathbb{Z}^d} |f(i)|^2 < \infty\}$, cf. [27]. Henceforth, when we speak about eigenfunctions, we always mean ℓ^2 -eigenfunctions. Let us explain their argument:

Outside-in continuation implies that there are no finitely supported eigenfunctions. In fact, if this was not true, one could take a large box which contains the support of the eigenfunction. Outside the function is 0, but by outside-in unique continuation, it follows that the function must be 0 everywhere. By linearity, this implies that every eigenfunction of $-\Delta + V|_{\Lambda_L}$ with eigenvalue E will be uniquely determined by its entries on $\partial_{(2)}\Lambda_L$, the set of sites in \mathbb{Z}^d with distance at most 2 to the complement of Λ_L . Now, continuity of the IDS at a point $E \in \mathbb{R}$ is equivalent to the vanishing of:

$$\lim_{L \rightarrow \infty} \frac{1}{|\Lambda_L|} \#\{\text{Eigenfunctions of } -\Delta + V|_{\Lambda_L} \text{ with eigenvalue } E\}, \tag{6}$$

where $-\Delta + V|_{\Lambda_L}$ denotes the restriction of $-\Delta + V$ to $\{j \in \mathbb{Z}^d : j \in \Lambda_L\}$ with *simple boundary conditions*, i.e. the finite submatrix of $\{\langle \delta_i, (-\Delta + V)\delta_j \rangle\}_{i,j \in \mathbb{Z}^d}$, corresponding to $i, j \in \Lambda_L \cap \mathbb{Z}^d$. By our considerations on unique continuation of eigenfunctions, the right hand side of Ineq. (6) is bounded from above by:

$$\lim_{l \rightarrow \infty} \frac{|\partial_{(2)}\Lambda_L|}{|\Lambda_L|} = 0.$$

For the sake of completeness, we also mention that in 1981, Wegner showed Lipschitz continuity of the IDS and boundedness of the DOS for the usual Anderson model on \mathbb{Z}^d :

$$(H_\omega f)_i = (-\Delta f)_i + \omega_i \cdot f_i \quad i \in \mathbb{Z}^d,$$

in the case where the random variables ω_j are distributed according to a probability measure with a bounded density, cf. [28]. Furthermore, with considerably more effort than in [27], Craig and Simon [29] established log-Hölder continuity of the IDS if the potential $V : \mathbb{Z}^d \rightarrow \mathbb{R}$ is a bounded, ergodic field. This includes in particular the Anderson model with i.i.d. Bernoulli random variables. Finally, in [13], Thm. 2.2 it is shown that in dimension $d = 1$, the IDS for the Anderson model with Bernoulli random variables is not absolutely continuous, i.e. it does indeed inherit some irregularity from the random variables.

4. Finitely supported eigenfunctions and the IDS on percolation graphs

We will now study site percolation on \mathbb{Z}^d . Let $\{q_j\}_{j \in \mathbb{Z}^d}$ be an i.i.d. collection of Bernoulli random variables on some probability space (Ω, \mathbb{P}) with parameter $p \in (0, 1)$, i.e.:

$$\mathbb{P}(q_j = 1) = p \quad \text{and} \quad \mathbb{P}(q_j = 0) = 1 - p.$$

We call $X(\omega) := \{j \in \mathbb{Z}^d : q_j = 1\} \subset \mathbb{Z}^d$ the set of *active* sites for the configuration $\omega \in \Omega$. We say that $i, j \in X(\omega)$ are direct neighbors if they are direct neighbors in \mathbb{Z}^d . $X(\omega)$ can be decomposed as a disjoint union of connected components, i.e. into subsets in which all sites are mutually joined by a path in $X(\omega)$ of direct neighbors.

The adjacency matrix H_ω on $X(\omega)$ is given by:

$$(H_\omega f)_i = \sum_{j \in X(\omega) : i \sim j} f_j.$$

For a finite box $G \subset \mathbb{Z}^d$ let $H_{\omega, G}$ denote the restriction of H_ω to $G \cap X(\omega)$. Then the finite volume normalized eigenvalue counting function on a box $\Lambda_L \subset \mathbb{Z}^d$ of side length L is defined as:

$$N_\omega^L(E) := \frac{\#\{\text{Eigenvalues } E_k \text{ of } H_{\omega, \Lambda_L} \text{ with } E_k \leq E\}}{|\Lambda_L|}.$$

Similarly to the continuum case, one can thus define the integrated density of states $N(E)$ as a limit of finite volume normalized eigenvalue counting functions, at least on the points where $N(E)$ is continuous. We present here some results taken from [30].

Theorem 4.1 ([30]). *There is $\Omega' \subset \Omega$ of full measure and a distribution function N (the IDS of H_ω) such that for all $\omega \in \Omega'$ and all continuity points of N we have:*

$$\lim_{L \rightarrow \infty} N_\omega^L(E) = N(E).$$

In contrast to the usual continuum Anderson model, the IDS for percolation graphs will be more irregular and have jumps. This is due to the fact that $X(\omega)$ almost surely contains finite connected components on which the restriction of H_ω will carry $\ell^2(\mathbb{Z}^d)$ -eigenfunctions of finite support. Hence, if an eigenfunction is zero outside some large box, the box might still contain a finite component of $X(\omega)$ on which we non-zero eigenfunctions can be found. Therefore, the outside-in unique continuation principle which had been used in the \mathbb{Z}^d case to show continuity of the IDS, fails.

Proposition 4.2 ([30,31]). *The set of discontinuity points of $N(E)$ is:*

$$\mathcal{D} = \{E \in \mathbb{R} : \exists \text{ finite } G \subset \mathbb{Z}^d \text{ and } f \in \ell^2(G) \text{ such that } H^G f = E f\},$$

which is an infinite subset of the algebraic numbers.

Now, one might wonder whether one can still expect some regularity of the IDS. We start with a statement on the finite volume approximations.

Theorem 4.3 ([30], Theorem 2.4). *The normalized finite volume eigenvalue counting functions N_ω^L are right log-Hölder continuous at $E \in \mathcal{D}$ uniformly in L , i.e. for every $E \in \mathcal{D}$ there is a constant C_E such that for all $\epsilon \in (0, 1)$, $L \in \mathbb{N}$ and $\omega \in \Omega$ we have:*

$$N_\omega^L(E + \epsilon) - N_\omega^L(E) \leq \frac{C_E}{\log(1/\epsilon)}.$$

This immediately implies right log-Hölder continuity of N and is actually sufficient to ensure the convergence of normalized finite volume eigenvalue counting functions.

Theorem 4.4 ([30], Corollary 2.5). *The IDS N is right log-Hölder continuous and the convergence $\lim_{L \rightarrow \infty} N_\omega^L(E) = N(E)$ holds for all $E \in \mathbb{R}$.*

We conclude our comments on the regularity of the IDS of percolation Hamiltonians by examining the effect of adding a random potential. Let

$$(V_\omega f)_i = \eta_i f_i, \quad i \in X(\omega),$$

where $\{\eta_j\}_{j \in \mathbb{Z}^d}$ is a process of positive, i.i.d. random variables independent of the percolation $\{q_j\}_{j \in \mathbb{Z}^d}$.

Theorem 4.5 ([30], Theorem 2.6). *If the probability measure corresponding to every η_j has no atoms then the IDS of $H_\omega + V_\omega$ is continuous.*

Most of the results of [30] hold for more general random operators defined on $\ell^2(G)$ where G is a countable amenable group (see also [32]). Furthermore, the pointwise convergence $\lim_{L \rightarrow \infty} N_{\omega}^L(E) = N(E)$ not only holds for all E , but actually uniformly in $E \in \mathbb{R}$, see [33] and the references given there. One can even give an estimate on the approximation error in supremum norm, see [34].

5. Existence of finitely supported eigenfunctions on planar graphs

The graph Laplacian on \mathbb{Z}^d , defined in Definition 3.1, has the following natural generalization to arbitrary graphs $G = (\mathcal{V}, \mathcal{E})$ with vertex set \mathcal{V} and edge set \mathcal{E} , with the only restriction of finite vertex degrees $|x| < \infty$ for all $x \in \mathcal{V}$: For a function $f : \mathcal{V} \rightarrow \mathbb{C}$, the (normalized) discrete Laplacian is given by:

$$\Delta_G f(x) = \frac{1}{|x|} \sum_{x \sim y} (f(x) - f(y)),$$

where $x \sim y$ means that $x, y \in \mathcal{V}$ are connected by an edge. The normalization by the vertex degree is just a scaling factor of the operator in the case of a regular graph (i.e., $|x|$ constant for all $x \in \mathcal{V}$) such as \mathbb{Z}^d . For the rest of this note, we will use the normalized Laplacian.

A particular family of graphs are the planar graphs, that is, graphs which have a realization in \mathbb{R}^2 with non-crossing edges (edges can be curved and do not need to be straight lines). For simplicity, we often identify planar realizations and their underlying discrete graphs. The faces of (a realization of) a planar graph G are the closures of the connected components of the complement $\mathbb{R}^2 \setminus G$. We have already seen that the planar graph \mathbb{Z}^2 with edges between nearest neighbours does not admit finitely supported eigenfunctions (the faces of this graph are the unit squares $[k, k + 1] \times [l, l + 1]$ with $k, l \in \mathbb{Z}$).

A particular planar graph admitting finitely supported eigenfunctions is the Kagome lattice. The Kagome lattice has attracted attention in the physics and mathematical physics community in connection with magnetic properties of certain crystal structures (see, e.g., [35,36]) and due to the emergence of butterfly spectra [37–39].

The Kagome lattice $K = (\mathcal{V}, \mathcal{E})$ can be described as follows (see, e.g., [40]): Let $w_1 = 1$ and $w_2 = e^{\pi i/3}$. Then the vertex set \mathcal{V} is given by the disjoint union:

$$\mathcal{V} = (2\mathbb{Z}w_1 + 2\mathbb{Z}w_2) \cup (w_1 + 2\mathbb{Z}w_1 + 2\mathbb{Z}w_2) \cup (w_2 + 2\mathbb{Z}w_1 + 2\mathbb{Z}w_2).$$

A pair $x, y \in \mathcal{V}$ is connected by a straight edge if and only if $|y - x| = 1$. The faces of this graph are regular triangles and hexagons, cf. Fig. 5.

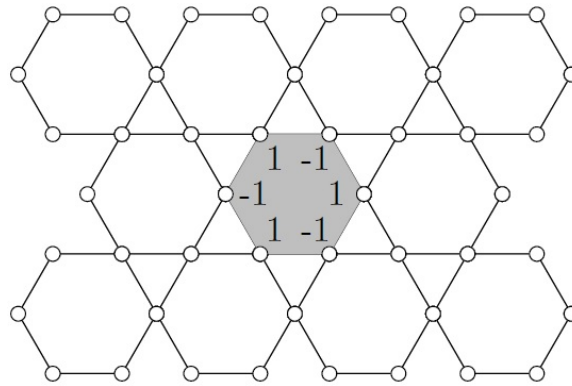


FIG. 5. The Kagome lattice and a finitely supported eigenfunction

It is easy to see that for a given hexagon:

$$H = \{x_0, x_1, \dots, x_5\} = \{z_0 + e^{k\pi i/3} \mid k = 0, 1, \dots, 5\},$$

with $z_0 \in (2\mathbb{Z} + 1)w_1 + (2\mathbb{Z} + 1)w_2$, the function

$$F_H(x) := \begin{cases} 0, & \text{if } x \in \mathcal{V} \setminus H, \\ (-1)^k, & \text{if } x \in H, \end{cases} \tag{7}$$

satisfies $-\Delta_K F_H = 3/2 F_H$. The following result tells us that, up to (infinite) linear combinations, these are the only ℓ^2 -eigenfunctions of the discrete Laplacian on the Kagome lattice:

Proposition 5.1 ([40] Prop. 3.1). [(a)]

- (1) Let $F : \mathcal{V} \rightarrow \mathbb{C}$ be a finitely supported eigenfunction of Δ_K . Then $-\Delta_K F = 3/2F$ and F is a linear combination of finitely many eigenfunctions F_H of the above type (7).
- (2) Let $H_i, i = 1, \dots, k$ be a collection of distinct, albeit not necessarily disjoint, hexagons. Then the set F_{H_1}, \dots, F_{H_k} is linearly independent.
- (3) If $g \in \ell^2(\mathcal{V})$ satisfies $-\Delta_K g = Eg$, then $E = 3/2$.
- (4) The space of $\ell^2(\mathcal{V})$ -eigenfunctions to the eigenvalue $-3/2$ is spanned by finitely supported eigenfunctions.

The next proposition shows that, similarly to the situation encountered in percolation, these finitely supported eigenfunctions give rise to a jump in the IDS.

There is a \mathbb{Z}^2 -action on the Kagome lattice via $T : \mathbb{Z}^2 \times \mathcal{V} \rightarrow \mathcal{V}$ via $T(\gamma, x) = T_\gamma(x) = 2\gamma_1 w_1 + 2\gamma_2 w_2 + x$ with combinatorial fundamental domain $Q = \{0, w_1, -w_2\}$. Any box $\Lambda_L \subset \mathbb{Z}^2$ gives rise to a set:

$$\Lambda_{Q,L} := \bigcup_{\gamma \in \Lambda_L} T_\gamma(Q).$$

Then Proposition 5.1 has the following consequence:

Proposition 5.2 ([40] Prop.3.3). Let K be the Kagome lattice with the \mathbb{Z}^2 action introduced above. Then the IDS:

$$N(E) = \lim_{L \rightarrow \infty} \frac{1}{|\Lambda_{Q,L}|} \#\{\text{Eigenfunctions of } -\Delta_K|_{\Lambda_{Q,L}} \text{ with eigenvalue } \leq E\},$$

exists and has the following properties: N vanishes on $(-\infty, 0]$, is continuous on $\mathbb{R} \setminus \{3/2\}$ and has a jump of size $1/3$ at $E = 3/2$. Moreover, N is strictly monotone increasing on $[0, 3/2]$ and $N(E) = 1$ for $E \geq 3/2$.

For the analysis of the IDS, in particular its jumps, an alternative formula is sometimes crucial:

$$N(E) = \frac{1}{|Q|} \mathbb{E} [\text{Tr} \chi_Q \chi_{(-\infty, E]}(\Delta_K)].$$

Here, χ_Q denotes the multiplication operator with the indicator function of the fundamental cell Q , whereas $\chi_{(-\infty, E]}(\Delta_K)$ is the spectral projector. Note that their product has finite trace.

An essential difference between the \mathbb{Z}^2 -lattice and the Kagome lattice can be seen via a suitable notion of discrete curvature, defined on certain planar graphs called planar tessellations: A *planar tessellation* $T = (\mathcal{V}, \mathcal{E}, \mathcal{F})$ is given by a realization of a planar graph with vertex set \mathcal{V} , edge set \mathcal{E} , and face set \mathcal{F} , satisfying the following properties:

- (1) Any edge is a side of precisely two different faces.
- (2) Any two faces are disjoint or have precisely either a vertex or a side in common.
- (3) Any face $f \in \mathcal{F}$ is a polygon (i.e., homeomorphic to a closed disk) with finitely many sides, where $|f|$ denotes the number of sides.
- (4) Every vertex $v \in \mathcal{V}$ has finite degree $|v|$.

We first define a curvature notion concentrated on the vertices. For this, we view the faces adjacent to a vertex $v \in \mathcal{V}$ as being represented by regular Euclidean polygons, that is, if $|f| = k$ its representation as regular k -gon has interior angles $(k - 2)\pi/k$. The *vertex curvature* $\kappa(v)$ in the vertex $v \in \mathcal{V}$ is then defined via the angle defect/excess to 2π of the polygons around v :

$$2\pi\kappa(v) = 2\pi - \sum_{f \ni v} \frac{|f| - 2}{|f|} \pi = 2\pi \left(1 - \frac{|v|}{2} + \sum_{f \ni v} \frac{1}{|f|} \right).$$

Unfortunately, this notion does not distinguish the Kagome lattice and the Euclidean lattice \mathbb{Z}^2 , since both tessellations have vanishing vertex curvature. A finer curvature notion is defined on the corners (cf. [41]). A *corner* of T is a pair $(v, f) \in \mathcal{V} \times \mathcal{F}$ such that v is a vertex of the polygon f . The set of all corners of T is denoted by $\mathcal{C} = \mathcal{C}(T)$. Then the *corner curvature* of the corner $(v, f) \in \mathcal{C}(T)$ is defined as:

$$\kappa(v, f) := \frac{1}{|v|} + \frac{1}{|f|} - \frac{1}{2}.$$

It is easy to see that we have:

$$\kappa(v) = \sum_{f \ni v} \kappa(v, f).$$

While \mathbb{Z}^2 has vanishing corner curvature in all corners, the Kagome lattice has corners with positive and negative corner curvature. There is the following general result:

Theorem 5.3 ([42]). *Let $T = (\mathcal{V}, \mathcal{E}, \mathcal{F})$ be a planar tessellation with non-positive corner curvature, that is, $\kappa(v, f) \leq 0$ for all $(v, f) \in \mathcal{C}(T)$. Then Δ_T does not admit finitely supported eigenfunctions.*

Note that Theorem 5.3 gives another proof of the fact that \mathbb{Z}^2 does not admit finitely supported eigenfunctions.

Remark 5.4. In fact, Theorem 5.3 holds for a much larger class of operators, called elliptic or nearest neighbour operators. Furthermore, it has been generalised to arbitrary connected, locally finite planar graphs in [43] and to so-called polygonal complexes with planar substructures in [44].

6. Compactly supported eigenfunctions on quantum graphs

In this section, we introduce quantum graphs and study properties of the IDS in the particular example of the quantum graph associated to the Kagome lattice both in the equilateral and random setting. The results in the equilateral setting are based on the appearance of compactly supported eigenfunctions. The main reference for this section is [40], providing further details. We start with some relevant definitions.

Definition 6.1. A metric graph (X, ℓ) associated to a directed graph $G = (\mathcal{V}, \mathcal{E})$ with maps $\partial_{\pm} : \mathcal{E} \rightarrow \mathcal{V}$ describing the direction of the edges (i.e., $\partial_-(e)$ is the source node and $\partial_+(e)$ the target node of the edge $e \in \mathcal{E}$) consists of disjoint intervals $I_e = [0, \ell(e)]$ for each edge $e \in \mathcal{E}$ which are identified at their end points in agreement with G (for example, $0 \in I(e)$ is identified with $\ell(e') \in I_{e'}$ if $\partial_-(e) = \partial_+(e')$). The vertices and edges of (X, ℓ) are denoted by $\mathcal{V}(X)$ and $\mathcal{E}(X)$.

Note that every metric graph (X, ℓ) is automatically also a metric space. The (one-dimensional) volume of a metric subgraph (X_0, ℓ) of (X, ℓ) with a finite number of edges is defined as:

$$\text{vol}(X_0, \ell) = \sum_{e \in \mathcal{E}(X_0)} \ell(e),$$

and the boundary ∂X_0 consists of all vertices of X_0 which are adjacent to vertices in $\mathcal{V}(X) \setminus \mathcal{V}(X_0)$.

Functions on a given metric graph (X, ℓ) are functions $f = \bigoplus_{e \in \mathcal{E}} f_e$ with $f_e : I_e \rightarrow \mathbb{C}$, and there is a natural Laplacian defined as follows:

$$\Delta_{X, \ell} f = \bigoplus_{e \in \mathcal{E}} f_e''.$$

A metric graph (X, ℓ) equipped with the Laplacian $\Delta_{X, \ell}$ is called a quantum graph.

The relevant function spaces $C(X)$, $L^2(X)$, and Sobolev spaces $H^{2,2}(X)$ are defined in a natural way (for details, see, e.g., [40]). Note that for

$$H^{2,2}(X) \ni f = \bigoplus_{e \in \mathcal{E}} f_e \in \bigoplus_{e \in \mathcal{E}} H^{2,2}(I_e),$$

the values $f_e(v), f_e'(v)$ for all $e \in \mathcal{E}$ and $v \in \{\partial_{\pm}(e)\}$ are well defined. To guarantee self-adjointness of the Laplacian, we assume a uniform positive lower bound on the edge lengths and assume appropriate vertex conditions for the functions f_e at their end-points. For simplicity, we only consider Kirchhoff vertex conditions (other vertex conditions can be found, e.g., in [40]): For all $v \in \mathcal{V}$, we require:

- (1) $f_e(v) = f_{e'}(v)$ for all $e, e' \in \mathcal{E}$ adjacent to v ,
- (2) $\sum_{\partial_+(e)=v} f_e'(v) = \sum_{\partial_-(e)=v} f_e'(v)$.

Later, when we define the IDS via an exhaustion procedure, we will also need Dirichlet conditions on certain vertices $v \in \mathcal{V}$, which are defined by $f_e(v) = 0$ for all $e \in \mathcal{E}$ adjacent to v . In this survey, we restrict our considerations to the Laplacian, but the results hold also in the more general setting of Schrödinger operators.

In the case of an equilateral quantum graph, there is a well-known relation between the spectral components of the Laplacian $\Delta_{X, \ell}$ and the discrete graph Laplacian Δ_G , by associating to a function $f \in H^{2,2}(X)$ with Kirchhoff boundary conditions the function $F \in \ell^2(\mathcal{V})$ via $F(v) = f(v)$:

Proposition 6.2. (see, e.g., [45–47]) *Let (X, ℓ) with Kirchhoff Laplacian $\Delta_{X, \ell}$ be a quantum graph associated to the combinatorial graph $G = (\mathcal{V}, \mathcal{E})$ with $\ell(e) = 1$ for all $e \in \mathcal{E}$ and Δ_G be the normalized discrete Laplacian. Then we have the following correspondence between the spectra:*

$$E \in \sigma_{\bullet}(\Delta_{X, \ell}) \iff 1 - \cos(\sqrt{E}) \in \sigma_{\bullet}(\Delta_G),$$

for all $E \notin \Sigma^D = \{(\pi k)^2 \mid k = 1, 2, \dots\}$, where $\bullet \in \{\emptyset, \text{pp}, \text{disc}, \text{ess}, \text{ac}, \text{sc}, \text{p}\}$.

The values in Σ^D above play a special role, since the quantum graph may have eigenfunctions $\Delta_{X,\ell} f = E f$ vanishing on all vertices (so-called *Dirichlet eigenfunctions*). They will appear as soon as the undirected underlying graph G contains a cycle and must be of the form $(\pi k)^2$ for some $k = 1, 2, \dots$. More precisely, the multiplicity of $(\pi k)^2$ is related to the global topology of the graph, as explained in [48]. Related multiplicity calculations for quantum graphs were carried out in [49].

Note that the Kagome lattice, given in Fig. 5 as a subset of \mathbb{R}^2 , can be viewed as the corresponding metric graph (X, ℓ) with constant side length $\ell(e) = 1$ for all $e \in \mathcal{E}$. The map T defined earlier can be extended to $T : \mathbb{Z}^2 \times \mathbb{R}^2 \rightarrow \mathbb{R}^2$, $T_\gamma(x) = 2\gamma_1 w_1 + 2\gamma_2 w_2 + x$, and induces a natural \mathbb{Z}^2 -action on (X, ℓ) as a subset of \mathbb{R}^2 . The closure of a fundamental domain of this \mathbb{Z}^2 -action is given in Fig. 6 and is the induced metric subgraph (Y, ℓ) with vertex set $\{0, w_1, 2w_1, 2w_1 - w_2, -w_2, -2w_2, -2w_2 + w_1\}$. Any box $\Lambda_L \subset \mathbb{Z}^2$ gives rise to a metric subgraph $(\Lambda_{Y,L}, \ell)$, defined as:

$$\Lambda_{Y,L} := \bigcup_{\gamma \in \Lambda_L} T_\gamma(Y).$$

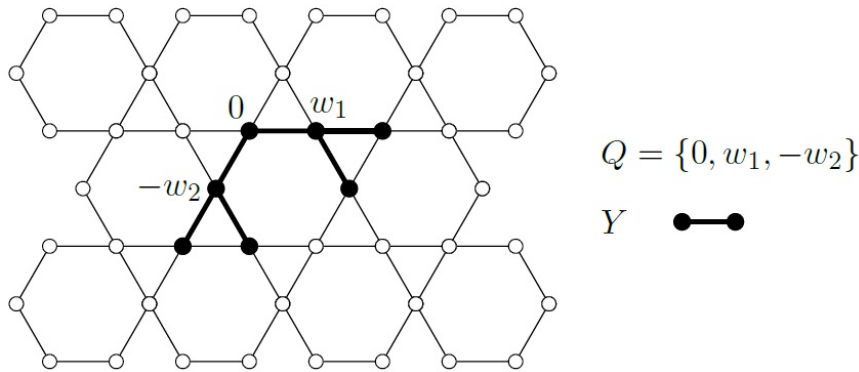


FIG. 6. Combinatorial fundamental domain $Q = \{0, w_1, -w_2\}$ of the Kagome lattice and the metric subgraph Y , introduced in Section 6

Using the above spectral correspondence, it can be shown that Proposition 5.2 has the following analog in the equilateral quantum graph on the Kagome lattice:

Proposition 6.3. *Let (X, ℓ) be the metric graph associated to the Kagome lattice $K = (\mathcal{V}, \mathcal{E})$ with $\ell(e) = 1$ for all $e \in \mathcal{E}$. Then the IDS:*

$$N(E) = \lim_{L \rightarrow \infty} \frac{1}{\text{vol}(\Lambda_{Y,L})} \#\{\text{Eigenfunctions of } -\Delta_{X,\ell} |_{\Lambda_{Y,L}} \text{ with eigenvalue } \leq E\},$$

exists, where $\Delta_{X,\ell} |_{X_0}$ is the restriction of $\Delta_{X,\ell}$ to the metric subgraph (X_0, ℓ) with Dirichlet vertex conditions on ∂X_0 . Furthermore, all discontinuities of $N : \mathbb{R} \rightarrow [0, \infty)$ are:

- (1) at $E = (2k + 2/3)^2 \pi^2$, $k \in \mathbb{Z}$, with jumps of size $1/6$,
- (2) at $E = k^2 \pi^2$, $k \in \mathbb{N}$, with jumps of size $1/2$.

Moreover, N is strictly increasing on the absolutely continuous spectrum of $\Delta_{X,\ell}$, which is explicitly given in [40, Cor. 3.4].

Remark 6.4. Note that there are two types of compactly supported eigenfunctions on a general equilateral quantum graph (X, ℓ) associated to a graph $G = (\mathcal{V}, \mathcal{E})$:

- (1) eigenfunctions corresponding to finitely supported eigenfunctions of the discrete Laplacian Δ_G ,
- (2) Dirichlet eigenfunctions which appear as soon as the graph G has cycles. For such a cycle of length n in G , the corresponding cycle in the quantum graph (X, ℓ) can be canonically identified with the interval $[0, n]$ where the end-points are identified, and any eigenfunction $\sin(k\pi)$ on $[0, n]$ gives rise to a corresponding Dirichlet eigenfunction with eigenvalue $k^2 \pi^2$. Note that if n is odd, $k \in \mathbb{Z}$ needs to be even.

As a consequence, even though there are no jumps of the IDS of $\Delta_{\mathbb{Z}^d}$ in the discrete lattice \mathbb{Z}^d , jumps of the IDS of $\Delta_{X,\ell}$ appear in the equilateral quantum graph (X, ℓ) associated to \mathbb{Z}^d , due to the compactly supported eigenfunctions in (2), in dimension $d \geq 2$.

Now we introduce randomness on the edge lengths of our metric Kagome lattice (X, ℓ) . Let $0 < \ell_{\min} < \ell_{\max} < \infty$ and $(\omega_e)_{e \in \mathcal{E}}$ be a process of i.i.d. random variables on a probability space (Ω, \mathbb{P}) with support in $[\ell_{\min}, \ell_{\max}]$ and assume that every ω_e has a probability density $h \in C^1(\mathbb{R})$. For every $\omega \in \Omega$, we consider the metric graph (X, ℓ_ω) , where $\ell_\omega(e) = \omega_e$ for all $e \in \mathcal{E}$. This induces a random family of quantum graphs, called the *random length model* associated to the Kagome lattice, consisting of $(X, \ell_\omega)_{\omega \in \Omega}$ with associated Laplacians Δ_{X, ℓ_ω} . Then the following Wegner estimate, linear in energy and volume, holds:

Theorem 6.5. *Let $(X, \ell_\omega)_{\omega \in \Omega}$ be the random length model associated to the Kagome lattice $K = (\mathcal{V}, \mathcal{E})$ and $u > 1$. Then there exists a constant $C > 0$, only depending on $u, \ell_{\min}, \ell_{\max}, \|h\|_\infty, \|h'\|_\infty$, such that, for all intervals $I \subset [1/u, u]$ and $L \in \mathbb{N}$,*

$$\mathbb{E} (\#\{\text{Eigenfunctions of } -\Delta_{X, \ell_\omega} |_{\Lambda_{Y, L, \omega}} \text{ with eigenvalue in } I\}) \leq C \cdot |I| \cdot |E(\Lambda_{Y, L})|,$$

where $(\Lambda_{Y, L, \omega}, \ell_\omega)$ is a metric subgraph of (X, ℓ_ω) defined analogously to the definition of $\Lambda_{Y, L}$ above.

A related Wegner estimate for the quantum graph associated to the lattice \mathbb{Z}^d with random edge lengths and its application to localization was shown in [50]. The above Wegner estimate implies that randomness improves regularity of the IDS, as the next corollary states.

Corollary 6.6. *Let $(X, \ell_\omega)_{\omega \in \Omega}$ be the random length model associated to the Kagome lattice $K = (\mathcal{V}, \mathcal{E})$. Then there is a unique function $N : \mathbb{R} \rightarrow [0, \infty)$ such that for almost every $\omega \in \Omega$, the IDS corresponding to the quantum graph $(X, \ell_\omega, \Delta_{X, \ell_\omega})$ agrees with N . Moreover, N is continuous on \mathbb{R} and even locally Lipschitz continuous on $(0, \infty)$.*

Remark 6.7. In fact, the result presented for the Kagome lattice holds in the much more general setting of a *random length covering model*, as explained in [40], where \mathbb{Z}^2 is replaced by a (not necessarily abelian) amenable group, acting cocompactly and isometrically on a connected, noncompact equilateral quantum graph and the boxes $\Lambda_L \subset \mathbb{Z}^2$ are replaced by a tempered Følner sequence.

Acknowledgements

This work was partially financially supported by the Deutsche Forschungsgemeinschaft through the grants VE 253/6-1 *Unique continuation principles and equidistribution properties of eigenfunctions* and VE 253/7-1 *Multiscale version of the Logvinenko-Sereda Theorem*. While writing part of this article, NP and MT enjoyed the hospitality of the Isaac Newton Institute during the programme *Non-Positive Curvature Group Actions and Cohomology*, supported by the EPSRC Grant EP/K032208/1. We would like to thank Michela Egidi for reading a previous version of the manuscript.

References

- [1] Bourgain J. and Kenig C. E. On localization in the continuous Anderson-Bernoulli model in higher dimension. *Invent. Math.*, 2005, **161**(2), P. 389–426.
- [2] Carleman T. Sur un problème d'unicité pour les systèmes d'équations aux dérivées partielles à deux variables indépendantes. *Ark. Mat. Astron. Fysik*, 1939, **26B**(17), P. 1–9.
- [3] Kenig C.E., Ruiz A., and Sogge C.D. Uniform Sobolev inequalities and unique continuation for second order constant coefficient differential operators. *Duke Math. J.*, 1987, **55**, P. 329–347.
- [4] Koch H. and Tataru D. Carleman estimates and unique continuation for second-order elliptic equations with nonsmooth coefficients. *Comm. Pure Appl. Math.*, 2001, **54**(3), P. 339–360.
- [5] Wolff T. H. Note on counterexamples in strong unique continuation problems. *Proc. Amer. Math. Soc.*, 1992, **114**(2), P. 351–356.
- [6] Wolff T. H. Recent work on sharp estimates in second order elliptic unique continuation problems. In *Fourier analysis and partial differential equations (Miraflores de la Sierra, 1992)*, Stud. Adv. Math., pages 99–128. CRC, Boca Raton, FL, 1995.
- [7] Escuriaza L., Kenig C. E., Ponce G. and Vega L. Uniqueness properties of solutions to Schrödinger equations. *Bull. Amer. Math. Soc. (N.S.)*, 2012, **49**(3), P. 415–442.
- [8] Jerison D. and Kenig C.E. Unique continuation and absence of positive eigenvalues for Schrödinger operators. *Ann. of Math. (2)*, 1985, **121**(3), P. 463–494. With an appendix by E. M. Stein.
- [9] Donnelly H. and Fefferman C. Nodal sets of eigenfunctions on Riemannian manifolds. *Invent. math.*, 1988, **93**(1), P. 161–183.
- [10] Bakri L. Carleman estimates for the Schrödinger operator. Applications to quantitative uniqueness. *Commun. Part. Diff. Eq.*, 2013, **38**(1), P. 69–91.
- [11] Germinet F. and Klein A. A comprehensive proof of localization for continuous Anderson models with singular random potentials. *J. Eur. Math. Soc.*, 2013, **15**(1), P. 53–143.
- [12] Stollmann P. *Caught by disorder: Bound States in Random Media*, volume 20 of *Progress in Mathematical Physics*. Birkhäuser, 2001.
- [13] Carmona R., Klein A., and Martinelli F. Anderson localization for Bernoulli and other singular potentials. *Commun. Math. Phys.*, 1987, **108**, P. 41–66.
- [14] Bourgain J. and Klein A. Bounds on the density of states for Schrödinger operators. *Invent. Math.*, 2013, **194**(1), P. 41–72.

- [15] Craig W. and Simon B. Subharmonicity of the Lyapunov index. *Duke Math. J.*, 1983, **50**(2), P. 551–560.
- [16] Meshkov V.Z. On the possible rate of decay at infinity of solutions of second order partial differential equations. *Math. USSR Sb.*, 1992, **72**(2), P. 343–361.
- [17] Rojas-Molina C. and Veselić I. Scale-free unique continuation estimates and application to random Schrödinger operators. *Commun. Math. Phys.*, 2013, **320**(1), P. 245–274.
- [18] Germinet F., Müller P., and Rojas-Molina C. Ergodicity and dynamical localization for Delone-Anderson operators. *Rev. Math. Phys.*, 2015, **27**(9), P. 1550020,36.
- [19] Combes J.-M., Hislop P. D., and Klopp F. Hölder continuity of the integrated density of states for some random operators at all energies. *Int. Math. Res. Not.*, 2003, **4**, P. 179–209.
- [20] Combes J.-M., Hislop P. D., and Klopp F. An optimal Wegner estimate and its application to the global continuity of the integrated density of states for random Schrödinger operators. *Duke Math. J.*, 2007, **140**(3), P. 469–498.
- [21] Klein A. Unique continuation principle for spectral projections of Schrödinger operators and optimal Wegner estimates for non-ergodic random Schrödinger operators. *Commun. Math. Phys.*, 2013, **323**(3), P. 1229–1246.
- [22] Nakić I., Täufer M., Tautenhahn M., and Veselić I. Scale-free uncertainty principles and Wegner estimates for random breather potentials. *C. R. Math.*, 2015, **353**(10), P. 919–923.
- [23] Nakić I., Täufer M., Tautenhahn M., and Veselić I. Scale-free unique continuation principle, eigenvalue lifting and Wegner estimates for random Schrödinger operators. arXiv:1609.01953 [math.AP], 2016.
- [24] Täufer M. and Veselić I. Conditional Wegner estimate for the standard random breather potential. *J. Stat. Phys.*, 2015, **161**(4), P. 902–914. arXiv:1509.03507.
- [25] Shirley C. Decorrelation estimates for some continuous and discrete random Schrödinger operators in dimension one, without covering condition. 2015. <https://hal.archives-ouvertes.fr/hal-01149320>
- [26] Le Rousseau J. and Lebeau G. On Carleman estimates for elliptic and parabolic operators. Applications to unique continuation and control of parabolic equations. *ESAIM Contr. Optim. Ca.*, 2012, **18**(3), P. 712–747.
- [27] Delyon F. and Souillard B. Remark on the continuity of the density of states of ergodic finite-difference operators. *Commun. Math. Phys.*, 1984, **94**, P. 289–291.
- [28] Wegner F. Bounds on the density of states in disordered systems. *Z. Phys. B*, 1981, **44**, P. 9–15.
- [29] Craig W. and Simon B. Log Hölder continuity of the integrated density of states for stochastic Jacobi matrices. *Commun. Math. Phys.*, 1983, **90**, P. 207–218.
- [30] Veselić I. Spectral analysis of percolation Hamiltonians. *Math. Ann.*, 2005, **331**(4), P. 841–865. <http://arxiv.org/math-ph/0405006>.
- [31] Chayes J. T., Chayes L., Franz J. R., Sethna J. P., and Trugman S. A. On the density of states for the quantum percolation problem. *J. Phys. A*, 1986, **19**(18), P. L1173–L1177.
- [32] Antunović T. and Veselić I. Spectral asymptotics of percolation Hamiltonians on amenable Cayley graphs. Volume 186 of *Operator Theory: Advances and Applications*, pages 1–29. Birkhäuser, 2008. <http://arxiv.org/abs/0707.4292>.
- [33] Lenz D. and Veselić I. Hamiltonians on discrete structures: jumps of the integrated density of states and uniform convergence. *Math. Z.*, 2009, **263**(4), P. 813–835.
- [34] Schumacher Ch., Schwarzenberger F., and Veselić I. A Glivenko–Cantelli theorem for almost additive functions on lattices. *Stoch. Proc. Appl.*, 2016, **127**(1), P. 179–208. <https://arxiv.org/abs/1606.07664>.
- [35] Chaudhury R.P., Chu C.W., Galstyan E., Galstyan E., Lorenz B., Sun Y.Y., Wang Y.Q., and Yen F. Magnetic phase diagrams of the kagome?? staircase compound. *Physica B: Condensed Matter*, 2008, **403**(5-9), P. 1487–1489. Proceedings of the International Conference on Strongly Correlated Electron Systems.
- [36] Lawes G., Harris A.B., Kimura T., Rogado N., Cava R.J., Aharony A., Entin-Wohlman O., Yildirim T., Kenzelmann M., Broholm C., and Ramirez A.P. Magnetically driven ferroelectric order in $\text{Ni}_3\text{V}_2\text{O}_8$. *Phys. Rev. Lett.*, 2005, **95**(Aug), P. 087205.
- [37] Helffer B., Kerdelhué P., and Royo-Letelier J. Chambers’s formula for the graphene and the Hou model with kagome periodicity and applications. *Ann. Henri Poincaré*, 2016, **17**(4), P. 795–818.
- [38] Hou J.M. Light-induced hofstadter’s butterfly spectrum of ultracold atoms on the two-dimensional kagomé lattice. *Chinese Physics Letters*, 2009, **26**(12), P. 123701.
- [39] Kerdelhué P. and Royo-Letelier J. On the low lying spectrum of the magnetic Schrödinger operator with kagome periodicity. *Rev. Math. Phys.*, 2014, **26**(10), P. 1450020,46.
- [40] Lenz D., Peyerimhoff N., Post O., and Veselić I. Continuity of the integrated density of states on random length metric graphs. *Math. Phys. Anal. Geom.*, 2009, **12**(3), P. 219–254.
- [41] Baues O. and Peyerimhoff N. Geodesics in non-positively curved plane tessellations. *Adv. Geom.*, 2006, **6**(2), P. 243–263.
- [42] Klassert S., Lenz D., Peyerimhoff N., and Stollmann P. Elliptic operators on planar graphs: unique continuation for eigenfunctions and nonpositive curvature. *Proc. Amer. Math. Soc.*, 2006, **134**(5), P. 1549–1559.
- [43] Keller M. Curvature, geometry and spectral properties of planar graphs. *Discrete Computational. Geom.*, 2011, **46**(3), P. 500–525.
- [44] Keller M., Peyerimhoff N., and Pogorzelski F. Sectional curvature of polygonal complexes with planar substructures. arXiv:1407.4024 [math.MG], 2015.
- [45] Cattaneo C. The spectrum of the continuous Laplacian on a graph. *Monatsh. Math.*, 1997, **124**(3), P. 215–235.
- [46] Pankrashkin K. Spectra of Schrödinger operators on equilateral quantum graphs. *Lett. Math. Phys.*, 2006, **77**(2), P. 139–154.
- [47] Post O. Equilateral quantum graphs and boundary triples. In *Analysis on graphs and its applications*, volume 77 of *Proc. Sympos. Pure Math.*, pages 469–490. Amer. Math. Soc., Providence, RI, 2008.
- [48] Lledó F. and Post O. Eigenvalue bracketing for discrete and metric graphs. *J. Math. Anal. Appl.*, 2008, **348**(2), P. 806–833.
- [49] J. von Below. A characteristic equation associated to an eigenvalue problem on c^2 -networks. *Linear Algebra Appl.*, 1985, **71**, P. 309–325.
- [50] Klopp F. and Pankrashkin K. Localization on quantum graphs with random edge lengths. *Lett. Math. Phys.*, 2009, **87**(1-2), P. 99–114.

Electrical conductivity model for quasi-one-dimensional structures

S. A. Botman, S. B. Leble

Immanuel Kant Baltic Federal University,
ul. Aleksandra Nevskogo, 14, Kaliningrad, 236016, Russia
sbotman@innopark.kantiana.ru, sleble@kantiana.ru

PACS 03.65.Nk, 05.60.k

DOI 10.17586/2220-8054-2017-8-2-231-235

The electron-impurity scattering coefficient of Bloch waves for one dimensional Dirac comb potential is used for calculating the temperature dependence of conductivity within kinetic theory. We restrict ourselves by scattering on impurities that is also modelled by zero-range potential. The conductivity is obtained by standard averaging in momentum space, it is expressed by integral that is evaluated within temperature expansion.

Keywords: Dirac comb, resistivity, kinetic equation, Bloch wave scattering.

Received: 14 January 2017

Revised: 7 February 2017

1. Introduction

Quasi one-dimensional structures such as nanowires, nanorods and nanoribbons are important due to wide range of applications, particularly as photodetectors, logic devices, thermoelectric coolers, chemical and biological sensors etc. Knowledge of the electronic properties for this class of materials is essential for practical application.

The latest theoretical and experimental results in the field of transport in low-dimensional structures have demonstrated that by changing particular conditions and parameters of such objects, the conductivity properties in low-dimensional materials can be drastically changed from highly conductive to that of the insulator regime. The transport properties of low dimensional systems is of intense interest for the physics of condensed matter and has been the subject of investigation by many physicists and mathematicians for more than 50 years [1, 2]. Recent progress raises both general academic questions and technological demands in the understanding of transport phenomena through low-dimensional and nanosystems.

In order to elaborate an understanding in the challenging problem of transport in low-dimensional and nanosystems, a theoretical model should be created. Although various methods of calculation may give reasonable results for conductivity in some cases, they do not provide insight into the basic concepts of transport properties in these types of systems.

There are nanoobjects, whose transport properties non-trivially depend on the temperature and diameter of samples [3–6]. These phenomena still need more general theoretical consideration. In pure single crystal nanowires, boundary scattering processes are believed to be dominant. Thus, at low temperatures (up to 300 K) phonon contribution to resistivity is not crucial. One may conclude that scattering on defects determine general resistivity properties of the system.

The aim of this work is to create and verify general model for quasi 1D systems, based on zero range potential (ZRP) model for atomic network and its irregularities, revealing conduction dependence on temperature and structure parameters of real quasi 1D nanoobject. As the nodal element of our model, we take the electron-surface impurity scattering coefficient of Bloch waves.

2. Conductivity calculation

2.1. 1D model

If one of the crystal lattice axis is aligned with nanowire direction, one can treat it as a series of homogeneous atom layers. In order to investigate properties of electrons moving longitudinally though such a nanowire, let us use Dirac comb potential – i.e. potential of equidistant Dirac delta functions:

$$\hat{V} = \beta\delta(x - na), \quad n = 0, \pm 1, \dots \quad (1)$$

where β – parameter of potential, a – period of cell, x – longitudinal axis coordinate, n – number of transversal layer of atoms.

To enhance the 1D model, we propose to use the fact that defects of a wire are primarily concentrated in the vicinity of the surface. The origin of such phenomenon is due to “contradiction” between the crystal-like net of atoms inside and the cylindrical geometry of the surface. So, going to the 1D model, we transfer all action of such surface deformation to the plane of the wire and model it by 1D ZRP posed at x_0 . Next, we introduce total number of electrons also considering 3D wire geometry. Translational symmetry of the model allows us to introduce Bloch wave basis set [9] and corresponding set up quantum scattering problem within this basis. It was shown [7] that scattering probability for a Bloch wave for (1) on point impurity with potential $\gamma\delta(x - x_0)$ can be expressed as follows:

$$W = (1 - |b_-|^2) \left| \frac{(b_+ e^{ikx_0} + e^{-ikx_0})^2 \gamma m}{(b_- - b_+)(i\hbar^2 k + \gamma m) + \gamma m (b_- b_+ e^{2ikx_0} + e^{-2ikx_0})} \right|^2, \quad (2)$$

where $k = \sqrt{2mE}/\hbar$ – electron wave number, m – electron rest mass, \hbar – Planck constant, γ – impurity strength, x_0 – impurity position and b_{\pm} stands for:

$$b_{\pm} = \frac{e^{\pm iKa} e^{-ika} - 1}{e^{\pm iKa} e^{ika} - 1}. \quad (3)$$

Here, $K = K(E)$ is momentum energy dispersion relation.

2.2. Kolmogorov equation

Thus, in order to study conductivity of nanostructures It’s more convenient to use Kolmogorov equation as defects scattering process prevalent for them. The Kolmogorov [8] equation is a kinetic equation which describes evolution of a distribution function $f(\mathbf{k}, \mathbf{r}, t)$ in phase space. Generally, It can be written as:

$$\frac{\partial f}{\partial t} + \dot{\mathbf{k}} \frac{\partial f}{\partial \mathbf{k}} + \dot{\mathbf{r}} \frac{\partial f}{\partial \mathbf{r}} = \frac{\partial f}{\partial t} \Big|_{coll}, \quad (4)$$

where \mathbf{r} – particle position vector, \mathbf{k} – particle momentum vector.

There are two factors which cause f to evolve: scattering which causes discontinuous changing of \mathbf{k} (right side of equation) and acceleration of the particles (left side of equation). Taking into account semi-classical equations of motions: $\dot{\mathbf{r}} = \mathbf{v}$ and $\hbar \dot{\mathbf{k}} = \mathbf{F}$, and assuming electro-magnetic field with components \mathbf{E} and \mathbf{H} applied to a system, equation (4) for electron moving in this field can be written as:

$$\frac{\partial f}{\partial t} + \mathbf{v} \frac{\partial f}{\partial \mathbf{r}} - e \left(\mathbf{E} + \frac{1}{c} [\mathbf{v} \times \mathbf{H}] \right) \frac{\partial f}{\partial \mathbf{k}} = I_{coll}(f), \quad (5)$$

where $f = f(\mathbf{k}, \mathbf{r})$ is ensemble average nonequilibrium distribution function, $I_{coll}(f)$ is a collision integral. For scattering on static potential one may use:

$$I_{coll}(f) = \sum_{\mathbf{k}'} W(\mathbf{k}, \mathbf{k}') [f(\mathbf{k}') - f(\mathbf{k})], \quad (6)$$

where $W(\mathbf{k}, \mathbf{k}')$ is a collision probability.

Let’s rewrite equation (5) for electrons in solid making several simplifications. First, we will assume that the applied field is electrostatic ($\mathbf{H} = \mathbf{0}$). Second, we will focus on the static conductivity problem ($\frac{\partial f}{\partial t} = 0$).

Third, we will adopt homogeneous current hypothesis ($\frac{\partial f}{\partial \mathbf{r}} = 0$). Fourth, we will assume that the deviation of the distribution function from its equilibrium is small ($f = f_0 + f_1$, $|f_1| \ll f_0$). Because the equilibrium distribution function f_0 is \mathbf{k} -symmetric, it has no impact on the collision integral.

Applying all aforementioned simplifications, one can rewrite (5) as follows:

$$-e\mathbf{E} \frac{\partial f_0}{\partial \mathbf{k}} = \sum_{\mathbf{k}'} W(\mathbf{k}, \mathbf{k}') [f_1(\mathbf{k}') - f_1(\mathbf{k})]. \quad (7)$$

For the one dimensional case ($W(\mathbf{k}, \mathbf{k}') = W(k, -k) = W$, $f_1(-k) = -f_1(k)$), further simplification is possible:

$$f_1 = \frac{1}{2W} e\mathbf{E} \frac{\partial f_0}{\partial \mathbf{k}}. \quad (8)$$

Solution of this equation gives us the non-equilibrium distribution function for a given external field \mathbf{E} and collision mechanism $I(f)$, which in turn can be used to determine electric current (in form of electron quasiparticle propagation studied by Drude, Sommerfeld, Bloch, Landau):

$$\mathbf{j} = -\frac{e}{V} \sum_k \mathbf{v}_k f, \quad (9)$$

where summation is performed over quasiparticle states k , \mathbf{v}_k is group velocity $\mathbf{v}_k = \frac{1}{\hbar} \frac{\partial \varepsilon_k}{\partial \mathbf{k}}$, V is sample volume. For real systems, it is useful to transform sum in (9) into integral. Thus, one can find conductivity of the system using (8), (9) and classical definition of conductivity $\mathbf{j} = \sigma \mathbf{E}$:

$$\sigma = -\frac{e^2}{\pi \hbar} \int \frac{1}{W} \frac{\partial f_0}{\partial k} dE. \quad (10)$$

The equilibrium distribution function is the Fermi-Dirac distribution function.

2.3. Evaluation of integral for low temperatures

Let's consider integral in the following form:

$$I = \int_0^{\infty} F(E) n'_f(E, T) dE, \quad (11)$$

where $F(E)$ – some function of energy, $n'_f(E, T)$ – first derivative of the Fermi-Dirac distribution function:

$$n_f(E, T) = \left(e^{\frac{E-\mu}{k_B T}} + 1 \right)^{-1}, \quad (12)$$

where μ – chemical potential, k_B – Boltzmann constant. The chemical potential can be found from the normalization condition for total numbers of electrons: $N_e = \int n_f(E, T) \rho(E) dE$, where $\rho(E)$ is density of states.

It's known, that at low temperatures $n'_f(E, T)$ has a sharp peak at $E = \mu$. Taking this into consideration, we replace the lower integration limit with $-\infty$ and expand $F(E)$ to a Taylor series at μ point. Thus, for the integral, we have:

$$I = \int_0^{\infty} F(E) n'_f(E, T) dE = \sum_0^{\infty} \frac{F^{(n)}(\mu)}{n!} \int_{-\infty}^{\infty} n'_f(E, T) (E - \mu)^n dE. \quad (13)$$

Next, we introduce new variable: $z = \frac{E - \mu}{k_B T}$:

$$I = - \sum_0^{\infty} \frac{F^{(n)}(\mu)}{n!} \int_{-\infty}^{\infty} \frac{e^z}{(e^z + 1)^2} (zk_B T)^n dz. \quad (14)$$

Obviously, $e^z / (e^z + 1)^2 = 1/2(\cosh(z) + 1)$ is an even function and $(zk_B T)^n$ is either odd or even depending on number n . Thus, integral can be transformed into:

$$I = -F(\mu) - \sum_1^{\infty} \frac{F^{(2n)}(\mu) (k_B T)^{2n}}{2n!} \int_0^{\infty} \frac{e^z}{(e^z + 1)^2} z^{2n} dz. \quad (15)$$

Equation (15) describes how integral (11) behaves at low temperatures. The first order approximation gives us a quadratic temperature dependence.

It can be shown using integration by parts that:

$$\int_0^{\infty} \frac{e^z}{(e^z + 1)^2} z^{2n} dz = \left(\frac{2^{2n} - 2}{2^{2n}} \right) \zeta(2n) \Gamma(2n), \quad (16)$$

where $\Gamma(n)$ – Gamma function, $\zeta(n)$ – Riemann zeta function:

$$\Gamma(n) = \int_0^{\infty} z^{n-1} e^{-z} dz = (n-1)!, \quad (17)$$

$$\zeta(n) = \sum_{m=1}^{\infty} \frac{1}{m^n}. \quad (18)$$

Further, one can rewrite (16) in terms of Bernoulli numbers. It can be shown, that for integer n :

$$\zeta(2n) = (-1)^{n+1} (2\pi)^{2n} \frac{B_{2n}}{2(2n)!}, \quad (19)$$

where B_n – n -th Bernoulli number.

Thus, combining (16), (18) and (19) one may obtain first order approximation of integral (11) for low temperatures:

$$I = \int_0^{\infty} F(E) n'_f(E, T) dE \approx -F(\mu) - \frac{F''(\mu) (k_B T)^2}{8} \pi^2 B_2. \quad (20)$$

Applying obtained expression (20) to conductivity calculation one may obtain the following expression:

$$\sigma = -\frac{e^2}{\pi \hbar} \int \frac{1}{W(E)} \frac{\partial n_f}{\partial k} dE \approx \frac{e^2}{\pi} \sqrt{\frac{2}{m}} \left[\frac{\sqrt{\mu}}{W(\mu)} + \left(\frac{\sqrt{E}}{W(E)} \right)'' \Big|_{E=\mu} \frac{\pi^2 B_2}{8} (k_B T)^2 \right]. \quad (21)$$

3. Results and discussion

In order to test the model, one has to substitute parameters according to Bi nanowire experimental data [3] and calculate conductivity plots. Within the given model, conductivity plots were obtained (Fig. 1). For certain model parameters σ/σ_0 peak can be clearly seen. Thus, the model can exhibit behavior similar to that of real systems. There are two different ways of model implementation: a) choose model parameters in the way that certain basic physical quantities of real systems agrees with ones of model, b) fit model parameters to resemble experimental resistance behavior.

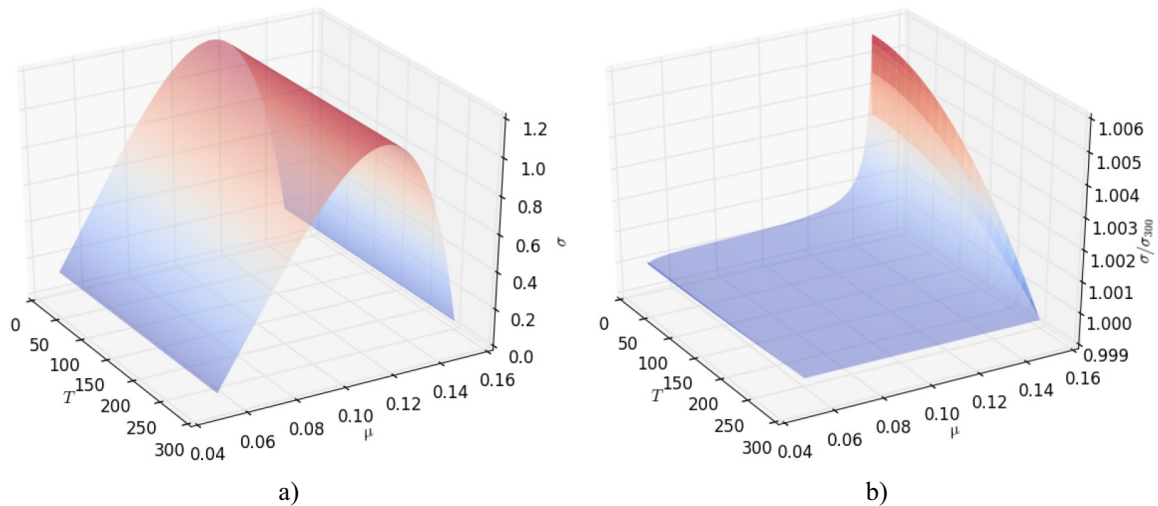


FIG. 1. Results of numerical experiments for a) conductivity and b) conductivity normalized by values at $T = 300$. Model parameters for both pictures are: $a = 10$, $\beta = -0.25$, $x_0 = a/2$, $\gamma = -0.1$

The main features of this work are as follows: obtained temperature dependence of conductivity, impurity scattering was implied as main source of electron scattering, result was obtained for Bloch waves. In previous work [11], the expression for d. c. conductivity was obtained for Umklapp processes within memory matrix approach. The first non-constant term of conductivity temperature expansion (21) is quadratic which agrees

with [11]. Depending on the parameters of the model conductivity can either increase or decrease, but there is not enough data to compare results quantitatively [13].

It's known that for low temperatures (up to room temperatures) main contribution to resistivity is made by defect scattering. There is the possibility to choose the 1D model parameters on base of 3D picture, linking its values with cylindrical geometry of a wire. For a regular structure of quasi 1D nanoobject, surface irregularities can be treated as defect which has had its position shifted with respect to the net. Considering nanoobject has length l and diameter d , the parameters diameter dependence is as follows: $\beta = \text{const}$, $\gamma = \gamma(d) \sim \pi d l$. One other parameter, which depends on d and l is the full number of electrons (which is essential for Fermi energy and chemical potential calculation): $N_e = N_e(d) \sim \pi d^2 l/4$.

The model approbation showed promising results. The next step of the research will be two-dimensional model with cylindrical symmetry assumed. For one of important direction of a development of the theory we would mention [10] where a model of point-like interaction between electrons with spin account and bosons was considered.

References

- [1] Dingle R.B. The electrical conductivity of thin wires. *Proceedings of the Royal Society of London. Series A, Mathematical and Physical Sciences*, 1950, **201** (1067), P. 545.
- [2] Lal R. Effect of electron-phonon interaction on the resistivity of metallic nanowires. *Physical Review B*, 2003, **68** (11), P. 115417.
- [3] Zhang Z., Sun X., et al. Electronic transport properties of single-crystal bismuth nanowire arrays. *Physical Review B*, 2000, **61** (7), P. 4850–4861.
- [4] Lin Y., Sun X., Dresselhaus M.S. Theoretical investigation of thermoelectric transport properties of cylindrical Bi nanowires. *Physical Review B*, 2000, **62** (7), P. 4610.
- [5] Wen W., Brongersma S.H., Van Hove M., Maex K. Influence of surface and grain-boundary scattering on the resistivity of copper in reduced dimensions. *Applied physics letters*, 2004, **84** (15), P. 2838–2840.
- [6] Natelson D., Willett R.L., West K.W., Pfeiffer L.N. Molecular-scale metal wires. *Solid State Communications*, 2004, **115** (5), P. 269–274.
- [7] Botman S., Leble S. Bloch wave – ZRP scattering as a key element of solid state physics computation: 1D example. *TASK Quarterly*, 2016, **20** (2), P. 197–206.
- [8] Kolmogoroff A. Über die analytischen Methoden in der Wahrscheinlichkeitsrechnung *Mathematische Annalen*, 1931, **104** (1), P. 415–458.
- [9] Newton R.G. Bloch-wave scattering by crystal defects. *Journal of mathematical physics*, 1991, **32** (2), P. 551–560.
- [10] Boitsev A., Neidhardt H., Popov I. Dirac operator coupled to bosons. *Nanosystems: Physics, Chemistry, Mathematics*, 2016, **7** (2), P. 332–339.
- [11] Rosch A., Andrei N. Conductivity of a clean one-dimensional wire. *Physical review letters*, 2000, **85** (5), P. 1092.
- [12] Popov I., Kurasov P., et al. A distinguished mathematical physicist Boris S. Pavlov. *Nanosystems: Physics, Chemistry, Mathematics*, 2016, **7** (2), P. 782–788.
- [13] Bid A., Bora A., Raychaudhuri A.K. Temperature dependence of the resistance of metallic nanowires of diameter ≥ 15 nm: Applicability of Bloch-Grüneisen theorem. *Physical Review B*, 2006, **74** (3), P. 035426.

Mathematical modeling of sedimentation of nanoparticles in the vessel of finite depth

S. I. Ezhenkova

ITMO University, Kronverkskiy, 49, St. Petersburg, 197101, Russia
sveta.ejenkova@yandex.ru

DOI 10.17586/2220-8054-2017-8-2-236-238

The sedimentation of nanoparticles in a liquid considering their Brownian diffusion was investigated by using mathematical modeling. The main purpose of this work is investigation of the particles' behavior in the area adjoining to the bottom of the vessel – the boundary layer.

Keywords: sedimentation, diffusion, the Newton polygon.

Received: 15 January 2017

Revised: 8 March 2017

1. Introduction

The problem of the influence of Brownian diffusion of nanoparticles on their sedimentation remains relevant [1]. Since the experiment of Robert Brown (the movement of pollen particles in a liquid drop), many scientists have studied the behavior of particles in different types of environments. The method of nanoparticle synthesis plays an important role in the distribution of nanoparticles' sizes [2]. Theoretical investigation of the sedimentation of nanoparticles is described in [3,4], Brownian motion of nanoparticles is described in [5–7].

In this work, we discuss the effect of the nanoparticles' diffusion on their sedimentation along the lower boundary of the vessel bottom, called the boundary layer [8]. To find the solution of the diffusion equation, the Newton polygon method is used – a method allowing one to find the solution of the equation with perturbed coefficients.

2. The calculation of particles density distribution in the boundary layer

We consider the sedimentation process of spherical nanoparticles in a liquid taking into account the Brownian diffusion between them. The equation of convective diffusion has the form:

$$\frac{\partial f}{\partial t} + v(R)\frac{\partial f}{\partial x} = D(R)\frac{\partial^2 f}{\partial x^2}, \quad (1)$$

where $v(R)$ is the velocity of sedimentation, f is the particle distribution function, D is the diffusion coefficient, x is the coordinate, t is the time of sedimentation.

The initial condition:

$$f|_{t=0} = f_0(R)\Theta(x),$$

where $f_0(R)$ is the size distribution function, $\Theta(x)$ is the coordinate distribution function (the Heaviside step function).

The boundary conditions:

$$\begin{aligned} j|_{x=0} &= 0, \\ j|_{x=L} &= 0, \end{aligned} \quad (2)$$

where $j = v(R)f - D\frac{df}{dx}$ is the particles' flux density, L is the height of the vessel.

To find the solution inside the boundary layer, we transform (1) into dimensionless form. For this, we introduce the dimensionless parameters for variables x , t and some small parameter ε :

$$x = L\bar{x}, \quad t = T\bar{t}, \quad \varepsilon = \frac{D(R)}{v(R)L},$$

where $T = \frac{L}{v(R)}$, $v(R) = \gamma R^2 = \frac{2g(\rho - \rho_p)}{9\mu} R^2$ is the velocity of sedimentation, ρ, ρ_p is the liquid density and particle density, μ is the viscosity, $D = \frac{k_B T}{6\pi\mu R}$ is the diffusion coefficient, where k_B is the Boltzmann constant, T is the temperature, R is the radius of particle, g is the gravitational constant.

Here, the value of ε is a small considering the fact that the diffusion of the particles is small: the larger the radius of the particle, the lower its diffusion.

Then, we rewrite the equation in the new form:

$$\varepsilon \frac{\partial^2 f}{\partial \bar{x}^2} - \frac{\partial f}{\partial \bar{x}} - \frac{\partial f}{\partial \bar{t}} = 0,$$

and introduce a new coordinate $\xi = e^{-\lambda}(1 - \bar{x})$, where λ is the indefinite parameter.

After all this transformation, (1) takes the form:

$$\varepsilon^{1-2\lambda} \frac{\partial^2 f}{\partial \xi^2} + \varepsilon^{-\lambda} \frac{\partial f}{\partial \xi} - \varepsilon^0 \frac{\partial f}{\partial \bar{t}} = 0. \quad (3)$$

For sewing the solution $f^p(\xi)$ inside the boundary layer with the solution $f^0(\bar{x}, \bar{t})$ outside the boundary layer, the following asymptotic equality must hold:

$$\lim_{\bar{x} \rightarrow 1} f^0(\bar{x}, \bar{t}) = \lim_{\xi \rightarrow \infty} f^p(\xi). \quad (4)$$

Firstly, we consider the behavior of individual members of (3) taking into account $\varepsilon \rightarrow 0$ for different values of λ . For this, we use the Newton polygon.

- (1) When $0 < \lambda < 1$, the leading term of the equation has the degree $-\lambda$. In this case, the solution of (3) has only one arbitrary constant and satisfies only one of two boundary conditions (2);
- (2) When $\lambda > 1$ the leading term of the equation has the degree $1 - 2\lambda$. In this case, the solution of (3) has two arbitrary constants and is satisfied by two boundary conditions (2), but in this case $\lim_{\xi \rightarrow \infty} f^p(\xi)$, does not exist for this solution. Consequently, this solution cannot be sewed with the solution outside the boundary layer;
- (3) When $\lambda = 1$ there are two leading terms with the degrees $1 - 2\lambda$ and $-\lambda$ which satisfy (2).

After this, we find the solution of (3) outside the boundary layer:

$$f^0(x, t) = AR e^{-\lambda R^2} \Theta(\bar{x} - \bar{t}),$$

and the solution of (3) inside the boundary layer:

$$f^p(\xi) = A + B e^{-\xi},$$

where $A = f_0(R)\Theta(1 - \bar{t})$, $B = \frac{f_0(R)\Theta(1 - \bar{t})}{\varepsilon^{-1} + 1}$, $\lambda = 1$, and carry out the sewing of this solutions in accordance with (4).

In the result, we have the final formula for the particle size distribution:

$$f = f_0(R)\Theta\left(1 - \frac{tv(R)}{L}\right) \left(1 + \frac{D(R)}{D(R) + v(R)L} e^{-\frac{v(R)}{D(R)}(L-x)}\right). \quad (5)$$

This equation allows us to see influence of diffusion localization along the lower boundary at the bottom of the vessel. The exponential dependence of the concentration of particles on the coordinate arises in the localization region, while in an area remote from the bottom, conventional particle sedimentation occurs. The order of the width of the boundary layer is $\frac{D(R)}{v(R)}$ for different particle sizes. Sedimentation velocity and diffusion are the functions of the particles radius. In this regard, if the thickness of the boundary layer is visually observed (optically, for example), then it makes it possible to estimate the particle sizes without taking measurements.

Acknowledgements

This work was partially supported financially by grant 074-U01 of the Government of the Russian Federation, by grant MK-5161.2016.1 of the President of the Russian Federation, by grant 16-11-10330 of Russian Science Foundation.

References

- [1] Vahedi Tafreshi H., Piseri P., Barborini E., Benedek G. and Milani P. Simulation on the effect of Brownian motion on nanoparticle trajectories in a pulsed microplasma cluster source. *Journal of Nanoparticle Research*, 2002, **4**(6), P. 511–524.
- [2] Almjasheva O.V. Formation and structural transformations of nanoparticles in the TiO₂-H₂O system. *Nanosystems: Physics, Chemistry, Mathematics*, 2016, **7**(6), P. 1031–1049.
- [3] Gangulya S., Chakraborty S. Sedimentation of nanoparticles in nanoscale colloidal suspensions. *Physics Letters A*, 2011, **375**, P. 2394–2399.
- [4] Demeler B., Tich-Lam Nguyen, Gorbet G.E., Schirf V., Brookes E.H., Mulvaney P., El-Ballouli A.O., Pan J., Bakr O.M., Demeler A.K., Hernandez Uribe B.I., Bhattarai N., Whetten R.L. Characterization of size, anisotropy and density heterogeneity of nanoparticles by sedimentation velocity. *Analytical Chemistry*, 2014, **86**, P. 7688–7695.
- [5] Eun Chul Cho, Qiang Zhang, Younan Xia. The effect of sedimentation and diffusion on cellular uptake of gold nanoparticles. *Nature Nanotechnology*, 2011, **6**, P. 385–391.
- [6] Ezhenkova S.I., Chivilikhin S.A. Mathematical modeling of sedimentation process of nanoparticles in gradient medium. *Journal of Physics: Conference Series*, 2015, **643**, P. 012111.1–012111.6.
- [7] Fisenko S.P., Shnip A.I. *Physics, chemistry and applications of nanostructures*. World Scientific, Singapore, 2003, 596 pp.
- [8] Nayfeh A.H. *Perturbation Methods*. Wiley-Interscience, USA, 1973, 425 pp.

Quantum random number generator based on homodyne detection

A. E. Ivanova, S. A. Chivilikhin, A. V. Gleim

ITMO University, Kronverkskiy, 49, St. Petersburg, 197101, Russia
newiva@mail.ru, sergey.chivilikhin@gmail.com, aglejm@yandex.ru

PACS 03.67.-a

DOI 10.17586/2220-8054-2017-8-2-239-242

A quantum random number generator (QRNG) based on the quantum nature of vacuum fluctuations allows one to obtain random bit sequences that can be used in applications that require a high degree of randomness. In that type of quantum random generation system, optical beam splitters with two inputs and two outputs are normally used. A comparison of Y-splitter and spatial beam splitters shows that for two types of optical splitters, the quantum mathematical description of output signals is identical. This allows the use of fiber Y-splitters in practical QRNG schemes. The possibility of generating true random bits was demonstrated experimentally by using quantum random number generator based on homodyne detection.

Keywords: quantum random number generation, beam splitter, Y-splitter, vacuum fluctuations.

Received: 14 January 2017

Revised: 1 February 2017

1. Introduction

The need to generate random numbers arises in many scientific and engineering disciplines. There are many types of random number generators with different entropy sources. Historically, two approaches for random number generation have been developed. According to the first method, random numbers can be generated algorithmically, but the resulting sequences in that case are pseudorandom and not suitable for applications in which a high degree of randomness is needed, such as classical or quantum cryptography [1]. These applications require true random numbers obtained by the second method, used indeterminate physical processes. For example, physical random number generators can use quantum processes. All QRNGs provide the necessary physical randomness for generated sequences that can be used in applications requiring high quality random numbers.

Existing approaches to quantum random number generation include different implementations: using separation of radiation [2], entangled photon states [3], quantum noise of lasers [4, 5] and photon emission and detection processes [6]. In alternative QRNG systems, quantum vacuum fluctuations are used as the entropy source. In this work, we investigate QRNG is based on quantum vacuum fluctuations [7–9] in which classical detectors are used, however, they can also measure quantum values. The principle of this type of QRNG is based on extracting randomness from quantum noise that appears upon subtracting the balanced detector signals received from beam splitter outputs. To first splitter input (Fig. 1a) a vacuum state is sent, and to other input – a coherent state from laser. On beam splitter these two signals are mixed, then signals from outputs of beam splitter come to balanced detector. One signal from the output of beam the splitter is subtracted from the other and the obtained signal is quantum noise, which can be processed using a PC.

A beam splitter is a key element for quantum random number generation schemes based on vacuum fluctuations [7–9]. Mathematical description of a beam splitter, when a strong laser signal, described by the Poisson distribution, arrives at one of its inputs and a vacuum state arrives to other, has been obtained in our previous research [10, 11] in the operator form. Also, we obtained mathematical description for fiber Y-splitter (Fig. 1b) and this, with the exception of phase shift, coincided with the previously-obtained expression for the beam splitter [10, 11]. Thus, as description for beam splitter and Y-splitter are equal, we can use Y-splitter for quantum random number generation system, based on homodyne detection.

2. Scheme and postprocessing methods

The scheme for our experimental setup is shown in Fig. 2a. During the research, a linear relationship between the laser power and the noise level was observed, which confirms that noise has quantum nature.

Quantum noise (Fig. 2b) obtained from our system had the following characteristics: mean value of fluctuations $\mu = 7 \cdot 10^{-6}$, standard deviation $\sigma = 0.03$, asymmetry coefficient $S = \frac{\mu_3}{\sigma^3} = -4.38 \cdot 10^{-3}$ (where μ_3 – third central moment of the noise distribution), kurtosis (a measure of sharpness of the random variable maximum) $K = \frac{\mu_4}{\sigma^4} = -3.87 \cdot 10^{-3}$ (where μ_4 – fourth central moment of the noise distribution), probability of the most

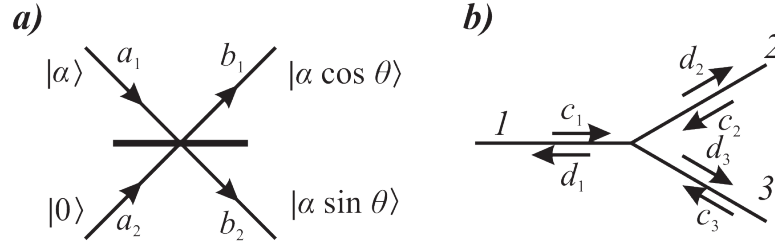


FIG. 1. a) Scheme of a beamsplitter with angle θ , where to the 1st splitter input a_1 a coherent state is sent, and to other input a_2 – a vacuum state. b) Scheme of optical Y-splitter, where c_1, c_2, c_3 – input signals of 1st, 2nd and 3rd ports, respectively, d_1, d_2, d_3 – output signals from the splitter

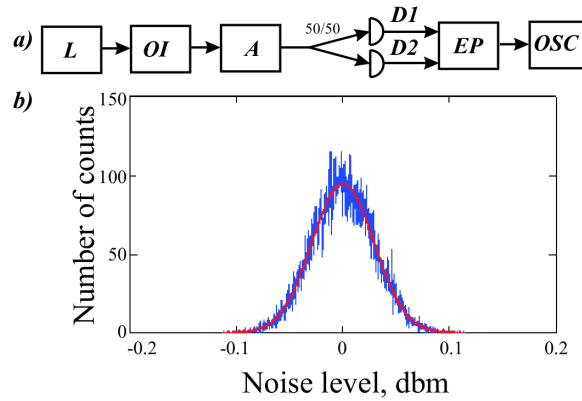


FIG. 2. a) Block diagram of the experimental setup. L – laser, OI – optical isolator, A – controllable attenuator, D1, D2 – detectors, EP – electronic processing system, OSC – oscilloscope; b) Distribution of samples on noise level

likely outcome $\max(P_i) = 3.02 \cdot 10^{-3}$ (where P_i – probability of the i -th realization of random discrete variable), min-entropy $H_{\min} = -\log_2(\max(P_i)) = 8.27$.

In our research, we used four methods to convert samples to sequences of bits:

- A) If noise level in count is above 0, then we write “1”, otherwise – “0” (Fig. 3a);
- B) We apply XOR to sequence, obtained by the first method (Fig. 3a);
- C) We generate three bits from one sample [9] (convert initial Gaussian distribution to uniform distribution, applying Gaussian error function, as shown in Fig. 3b);
- D) We discard most significant bits after analog-to-digital conversion (Fig. 3c).

3. Randomness tests

Knowing the probability properties of a truly random sequence, we can verify how much of the generated sequence is genuinely random. To do this, we select the appropriate statistics for each test [12] and then compare its value for the ideal sequence and the generated sequence. If experimental sequence does not satisfy the criteria, then it is considered to be non-random. In our research we used five tests: monobit test, twobit test, “poker” test, autocorrelation test and runs test.

Monobit test is the simplest of all used tests. It is based on how equally frequent “0” and “1” appear in an ideal random number generator. If we denote the number of bits in the experimental sequence as L , quantity of “1” – n_1 , quantity of “0” – n_0 , then in this test, we can calculate next value:

$$X_1 = \frac{(n_0 - n_1)^2}{L}. \quad (1)$$

If the value X_1 exceeds a certain threshold (which depends on the confidence level of p , indicating the probability that test will reject a good generator, in our case $p = 0.01$), then the generator does not pass the test. Since X_1 has approximately χ^2 -distribution with one degree of freedom, then the number 6.63 was taken as the threshold.

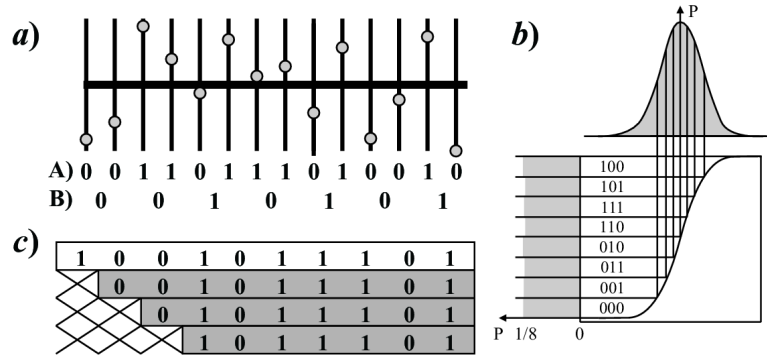


FIG. 3. Illustration of the four postprocessing methods for obtained samples: a) Illustrations of methods A and B; b) Illustration of method C, then convert one count to three bits; c) Illustration of method D, where most significant bits are discarding

In the *twobit test*, not only quantities of “0” and “1” are calculated, but also quantities of bit pairs “00”, “01”, “10” and “11”. Numbers of this combinations we denote as n_1 , n_0 , n_{00} , n_{10} , n_{01} , n_{11} respectively. The function used in this test is as follows:

$$X_2 = \frac{4}{L-1} (n_{00}^2 + n_{01}^2 + n_{10}^2 + n_{11}^2) - \frac{2}{L} (n_0^2 + n_1^2) + 1, \quad (2)$$

which has χ^2 – distribution with two degrees of freedom. Therefore, the threshold for X_2 was chosen to be 9.21.

When we use the *“poker” test* the experimental sequence is divided into blocks with length m . This test is based on fact that in an ideal random sequence, all bits have equal probability. If we denote n_i as quantity of m -bit blocks, which have a binary representation of i , then we can consider the next statistics function:

$$X_3 = \frac{2^m}{k} \left(\sum_{i=1}^{2^m} n_i^2 \right) - k, \quad (3)$$

where $k = L/m$ is the total number of m -bit blocks in the investigated sequence. Since the X_3 has the distribution χ^2 with $2m - 1$ degrees of freedom, for $m = 4$ we need to choose a threshold of 30.6.

Runs test measures the number of occurrences of identical bits series (runs) with different lengths. In an ideal random number sequence, the average quantity of series with length i is equal $l_i = \frac{L-i+3}{2i+2}$. If we denote B_i and G_i as numbers of single and zero runs in tested sequences with length i , then we can calculate statistics:

$$X_4 = \sum_{i=1}^n \frac{(B_i - l_i)^2}{l_i} + \sum_{i=1}^n \frac{(G_i - l_i)^2}{l_i}, \quad (4)$$

which has the distribution χ^2 with $2n - 2$ degrees of freedom, and we choose a threshold equal to 32.

Autocorrelation test is based on the fact that repetitive subsequences should not be in an ideal random sequence. In this test, we calculate the number of matching bits in the original and shifted by N_{shift} bit sequences. The statistics function is shown in the next formula:

$$X_5 = \frac{1}{\sqrt{L - N_{\text{shift}}}} \left(2 \left(\sum_{i=0}^{L-N_{\text{shift}}-1} \text{XOR}(b_i, b_{i+N_{\text{shift}}}) \right) - L + N_{\text{shift}} \right), \quad (5)$$

where $b_i - i$ -th bit of sequence. Since X_5 has a normal distribution with zero mean and variance equal to 1, the threshold is 2.33.

The results of randomness tests applied to sequences, which were obtained by four different post processing techniques, are shown in Table 1. We can see that the optimal postprocessing technique for our scheme is to discard two or three of the most significant bits.

4. Conclusion

We use Y-splitter for experimental implementation of QRNG systems based on quantum vacuum fluctuations. In our research, we considered four postprocessing methods to convert experimental samples to bits and after testing, we concluded that the optimal postprocessing technique for our system is to discard two or three of the most significant bits after analog-to-digital conversion.

TABLE 1. Results of randomness tests applied to sequences, obtained by different post processing techniques. “+” – test passed, “-” – test failed

Generation method	Method A	Method B	Method C	Method D. Discarding N MSB			
				$N = 1$	$N = 2$	$N = 3$	$N = 4$
Monobit test	+	+	+	+	-	+	+
Twobit test	-	+	+	-	-	+	+
“Poker” test	-	-	+	-	-	+	+
Runs test	+	+	-	-	-	+	+
Autocorrelation test	-	-	-	-	-	+	+

Acknowledgements

This work was financially supported by Government of Russian Federation, Grant 074-U01 and by the Ministry of Education and Science of Russian Federation (projects No. 14.578.21.0112, No. 02.G25.31.0229).

References

- [1] Scarany V., Bechmann-Pasquinucci H., et al. The security of practical quantum key distribution. *Rev. Mod. Phys.*, 2009, **81**, P. 1301–1350.
- [2] Jennewein T., Achleitner U., et al. A fast and compact quantum random number generator. *Rev. Sci. Instrum.*, 2000, **71** (4), P. 1675–1680.
- [3] Kwon O., Cho Y.-W., Kim Y.-H. Quantum random number generator using photon-number path entanglement. *Appl. Opt.*, 2009, **48**, P. 1774–1778.
- [4] Qi B., Chi Y.-M., et al. High-speed quantum random number generation by measuring phase noise of a single-mode laser. *Optics Letters*, 2010, **35**, P. 312–314.
- [5] Reidler I., Aviad Y., Rosenbluh M., Kanter I. Ultrahigh-Speed Random Number Generation Based on a Chaotic Semiconductor Laser. *Phys. Rev. Lett.*, 2009, **103**, P. 024102.
- [6] Dynes J.F., Yuan Z.L., et al. A high speed, post-processing free, quantum random number generator. *Appl. Phys. Lett.*, 2008, **93**, P. 031109.
- [7] Shen Y., Tian L., Zou H. Practical quantum random number generator based on measuring the shot noise of vacuum states. *Phys. Rev. A*, 2010, **81**, P. 063814.
- [8] Gabriel C., Wittmann C., et al. A generator for unique quantum random numbers based on vacuum states. *Nature Phot.*, 2010, **4**, P. 711–715.
- [9] Symul T., Assad S.M. and Lam P.K. Real time demonstration of high bitrate quantum random number generation with coherent laser light. *Appl. Phys. Lett.*, 2011, **98**, P. 231103.
- [10] Ivanova A.E., Chivilikhin S.A., Gleim A.V. Using of optical splitters in quantum random number generators, based on fluctuations of vacuum. *Journal of Physics: Conference Series*, 2016, **735**, P. 012077(1–4).
- [11] Ivanova A.E., Chivilikhin S.A., Gleim A.V. The use of beam and fiber splitters in quantum random number generators based on vacuum fluctuations. *Nanosystems: Physics, Chemistry, Mathematics*, 2016, **7**, P. 378–383.
- [12] Menezes A., van Oorschot P., Vanstone S. *Handbook of Applied Cryptography*. CRC Press, 1996, 816 p.

Stability of Grover's algorithm in respect to perturbations in quantum circuit

K. V. Gubaidullina, S. A. Chivilikhin

ITMO University, Kronverkskiy, 49, St. Petersburg, 197101, Russia

ksenya-gbd@yandex.ru, sergey.chivilikhin@gmail.com

PACS 03.67.-a

DOI 10.17586/2220-8054-2017-8-2-243-246

Grover's algorithm is a quantum algorithm for searching specified elements in an unsorted list. It has many valuable applications. The utilization of Grover's algorithm, to adapt it to accelerate the works of well-known classical algorithms, is very promising, and it is one of the fastest algorithms to solve such problems like global optimization and graph coloring. In this regard, it is very important to study the stability of the Grover's algorithm, to know how distortion of the circuit's elements affects on it results. This work presents the results of the simulation of Grover's algorithm, research of its stability with respect to perturbations of quantum logic circuit elements and its dependencies from the number of qubits, used in quantum circuit. Another part of this research was realized on IBM quantum processor and shows the stability of the 2-qubit Grover's algorithm.

Keywords: Grover's algorithm, quantum computations, quantum algorithms, IBM quantum processor.

Received: 23 January 2017

Revised: 4 March 2017

1. Introduction

Quantum computing uses a special kind of superposition, which allows exponentially many logical states simultaneously. This is a powerful feat, and no classical computer can achieve it. Quantum computer can solve many famous problems that classical computers cannot. For example, the problem of searching in unsorted list in classical algorithm actually reduces to sequential scan of N values, and uses on average $N/2$ steps. For a quantum computer, however, we can find the marked element use \sqrt{N} steps using Grover's algorithm [1].

The algorithm is performed on a search condition that is enclosed in a quantum oracle operator. This condition could be equal to some exact value, or we can for example find the minimum in some array. Such problem is relevant in searching for the optimal path on the graph [2] when it is necessary to find the shortest path between two vertices. In the classic case, many different methods of finding the minimum [3] could be used, and Dürr and Høyer in 1996 presented the method based on Grover's algorithm for finding the minimum with quantum enhancement [4].

We now describe the general stages of Grover's algorithm. At the initial time, the system is in the zero state. The Hadamard gate transforms the system into a state of superposition. After this transform, the followed iterative process consists of two functions: the first – phase rotation controlled by a search condition, which is enclosed in a quantum oracle operator; and the second – diffusion function makes a calculation of the amplitudes relative to its average. In the literature, this function is referred to as an inversion-about-average operator [5,6].

The number of Grover's iterations must be strictly defined, otherwise the algorithm returns erroneous results. This quantity was calculated through formula (1) and it is enough to reach highest probability for algorithm with defined number of qubits n :

$$I = \frac{\pi}{4} \sqrt{2^n} \quad (1)$$

The need to know in advance the number of values is a drawback of this algorithm - such situation in dealing with applications is quite rare. However, in the article [7,8] an algorithm was proposed for finding suitable search condition values that do not require an exact number of such values. Grover's algorithm is most effective with a large amount of data.

2. Stability of multiqubit schemes

The 3-qubit Grover's algorithm was simulated in article [9] and its stability to the effects of quantum logic circuit elements' perturbations was verified. Increasing perturbation values were shown to increase the probability of detecting the wrong state, but even the 3-qubit algorithm has good stability to the effects of quantum logic circuit element perturbations. The goal of this work was to simulate Grover's algorithm with more than 3 qubits, to study how doing this changes the probability of detection states and distortion impact. For example, a system

with 11 qubits consists of 2048 states and needs 35 iterations, so this research helps one to know how the number of qubits affects the stability of Grover’s algorithm.

The ways to affect the amplitude values of the states can be divided into two groups – light and strong deviations [9]. A histogram for the light deviations (Fig. 1) shows that the probability of detecting the marked state decreases with increased perturbation values.

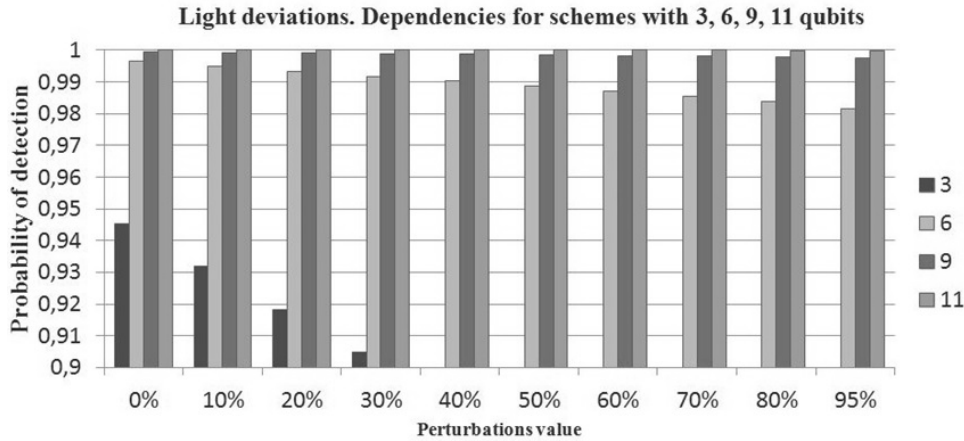


FIG. 1. Dependencies of detection probability and perturbation values for different number of qubits and light deviations

Correspondingly, the probability of detecting other (wrong) states increases, causing an increase in the frequency erroneous results. A larger number of qubits makes the algorithm more stable because of the number of necessary iterations that can be calculated by the formula (1) – a larger number of qubits requires a larger number of iterations. For example, 11 qubits with light deviations has extremely little distortion for very high value of perturbations.

Simulation of strong deviations (Fig. 2) is similar – the algorithm is more stable with a large number of qubits.

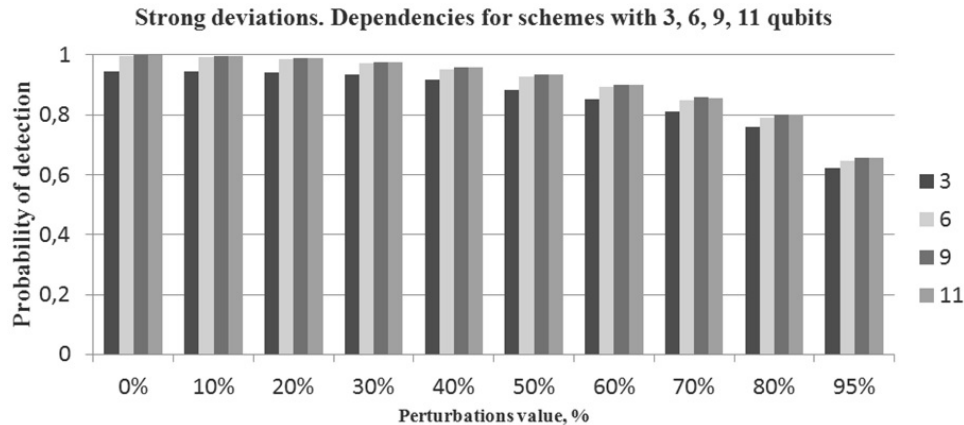


FIG. 2. Dependencies of detection probability and perturbation values for different numbers of qubits and strong deviations

In addition, it should be noted that the values of the probabilities for large systems is close to each other when error values increase. This is because the ideal values of the probabilities of these systems, when perturbation values are 0 %, are very close to one and respectively to each other. The stabilities of Grover’s algorithm in these schemes are almost equal.

3. IBM quantum experience

IBM allows researchers to gain access to their 5-qubit quantum computer called IBM Quantum Experience (IBM QE). They use fixed-frequency superconducting transmon qubit [10] and the quantum processor itself is

contained inside of a printed circuit board package. This package is mounted inside of a light-tight, magnetic-field shielding can, which sits at the coldest stage at the bottom of a dilution refrigerator, contained in IBM's Quantum Computing lab [11].

To perform the calculations, there is the Quantum Composer – a graphical user interface where the necessary quantum circuit can be created. Fig. 3 shows a representation of the platform with the scheme of Grover's algorithm for 2 qubits and marked state $|11\rangle$.

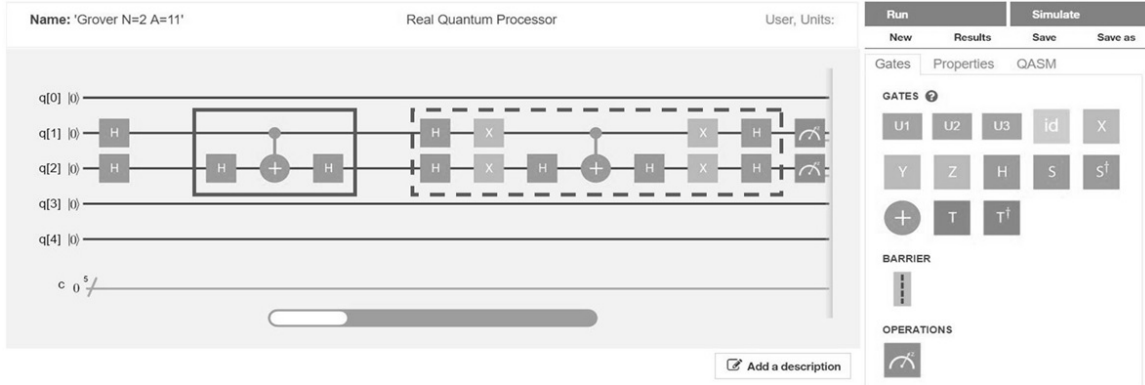


FIG. 3. Image of 5-qubit Quantum Composer and 2-qubit Grover's algorithm. Solid line box is a block of quantum oracle operator, and inside the dashed box - inversion-about-average operator

It is possible to run algorithms in simulation or on a real processor. Exploring the algorithm's running on a real quantum processor platform, its real stability with respect to circuit distortions can be seen and compared with theoretical calculations. There is also the opportunity to personally introduce distortions in the scheme collected by available gates and study their impact on the operation of the algorithm.

Topology of represented processor may allow the study only of the 2-qubit algorithm, so to compare the results in Fig. 4, the simulation of perturbation for 2-qubit Grover algorithm is presented. This is a histogram of average values for the strong and light deviation types.

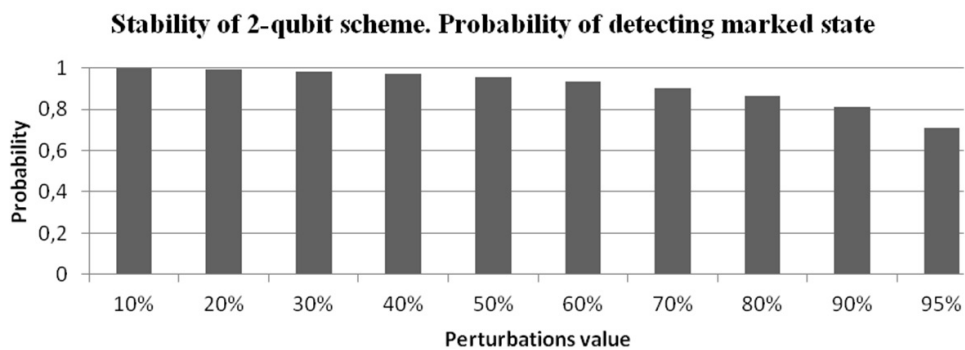


FIG. 4. Theoretical research of the distortion of 2-qubit Grover's algorithm

In an ideal 2-qubit circuit without any distortion, algorithm finds the right solution in 1 iteration in 100% of the cases. Due to the probabilistic nature of quantum algorithms and the existence of even the slightest noise in the circuit, which also affects the distribution of initial amplitudes, such a high proportion of correct answer detection is greatly reduced in the real computer. The algorithm was run by 8192 shots, and the results of every shot were considered to build a Fig. 5 – histogram of probability of detecting quantum states on the real quantum processor IBM.

The probability of detecting the correct state has decreased to 81.8 %. For theoretical simulation results in Fig. 4, this value corresponds to perturbations of the initial state amplitudes of about 80–85 %. Based on the fact that there is not only the distortion introduced by deviation of initial amplitudes, but other perturbations in the circuit, it can be concluded that this kind of deviation does not exceed 85 %.

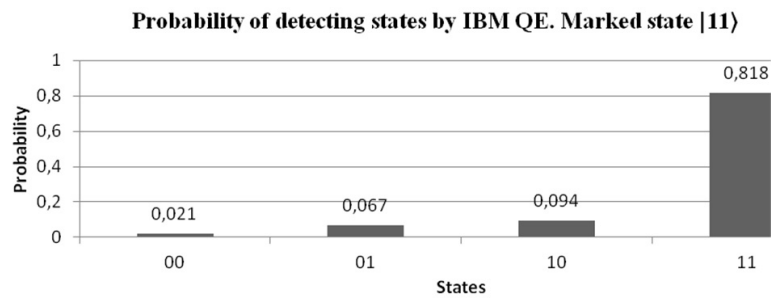


FIG. 5. Results for Grover's algorithm that have been computed by real quantum processor

4. Conclusion

By experimentation using the IBM quantum processor, computation of Grover's algorithm has been reviewed and compared with the theoretical results for a 2-qubit circuit. Theoretical simulation helps one to know how the number of qubits affects the stability of Grover's algorithm. It was shown that larger number of qubits and iterations makes the algorithm more stable. Another useful observation obtained from the results, is that stability of Grover's algorithm for schemes with large number of qubits is very similar. Thus, we can assume the stability of the algorithm on a larger number of qubits, which couldn't be calculated due to the insufficient computing power of classical computers.

Acknowledgments

This work was partially financially supported by the Government of the Russian Federation (grant 074U01).

References

- [1] Grover L.K. A fast quantum mechanical algorithm for database search *Proc. 28th Ann. ACM Symp. Theory of Computing (STOC)* New York, ACM Press, 1996, P. 212–221.
- [2] Aghaei M.R.S., Zukarnain Z.A., Mamat A., Zainuddin H. A hybrid algorithm for finding shortest path in network routing. *J. Theoretical and Applied Inform. Technol.*, 2009, P. 360–365.
- [3] Koistinen O.-P., Maras E., Vehtari A., J'onsson H. Minimum energy path calculations with Gaussian process regression. *Nanosystems: Physics, Chemistry, Mathematics*, 2016, 7(6), P. 925–935.
- [4] Dürr C., Hoyer P. A quantum algorithm for finding the minimum *arXiv preprint quant-ph/9607014*, 1996.
- [5] Linington I.E., Ivanov P.A., Vitanov N.V. Quantum search in a nonclassical database of trapped ions. *Phys. Rev. A*, 2009, 79, P. 012322.
- [6] Nakahara M., Ohmi T. *Quantum Computing: From Linear Algebra to Physical Realizations*. CRC Press, 2008.
- [7] Boyer M., Brassard G., Hoyer P., Tapp A. Tight bounds on quantum searching. *arXiv preprint quant-ph/9605034*, 1996.
- [8] Toyama F.M., Dijk W., Nogami Y. Quantum search with certainty based on modified Grover algorithms: optimum choice of parameters. *Quantum Inf Process*, 2013, 12, P. 1897–1914.
- [9] Gubaidullina K.V., Chivilikhin S.A. Theoretical research of the distortion of quantum circuit in Grover's algorithm *Journal of Physics: Conference Series*, 2016, 735, P. 012074-1–012074-6.
- [10] Koch J., Yu T.M., et al. Charge-insensitive qubit design derived from the Cooper pair box. *Phys. Rev. A*, 2007, 76, P. 042319.
- [11] IBM Research Quantum Experience. URL: www.research.ibm.com/quantum.

Kolmogorov equation for Bloch electrons and electrical resistivity models for nanowires

S. B. Leble

Immanuel Kant Baltic Federal University,
ul. Aleksandra Nevskogo, 14, Kaliningrad, 236016, Russia
leble@mif.pg.gda.pl

PACS 02.30.Mv, 02.60.Nm, 05.20.Dd, 73.23.b

DOI 10.17586/2220-8054-2017-8-2-247-259

The problem of a nanowires conductivity is studied from a kinetic point of view for quasiclassical Bloch electrons in an electric field. Few statements of problems with cylindrical symmetry for the integro-differential Kolmogorov equation are formulated: the dynamic Cauchy problem and two stationary boundary regime ones. The first is for an empty cylinder with scattering of the conduction electrons on walls, the second takes into account scattering on defects inside the wire. The integro-differential equations are transformed to integral ones and solved iteratively. There are two types of expansions with the leading terms in the right and left sides. The iteration series is constructed and its convergence studied.

Keywords: Kolmogorov kinetic equation, N-fold series, Bloch electrons, electrical resistivity, nanowires.

Received: 14 January 2017

Revised: 2 February 2017

1. Introduction

We consider a problem of a solid nanowires conductivity, which demonstrates an intriguing dependence on temperature and wire diameter that is fundamentally different from its bulk counterpart (e.g. for (Bi) see [1–3]). Conductivity is a non-equilibrium phenomenon, therefore we will use a kinetic description of charge carriers, following the idea of Bloch electrons as quasiclassical particles [4]. Having in mind the key element of the theory, a Bloch wave scattering problem [9], the distribution function (DF) f is interpreted as either a density number of electrons or probability density in phase space Γ with continuous wavenumbers (velocities) approximation.

There are few parameters, typical for electrons in solids, those are:

1. de Broglie wavelength $\lambda = h/p$;
2. v – typical velocity, e.g. one that enters Fermi–Dirac distribution function (FDF) as parameter;
3. τ_r – transport relaxation time;
4. mean free path: $l = v\tau_r$.

It is convenient to use dimensionless variables in the phase space Γ . In the next sections, we will imply that the position coordinates are measured in free path l units, while the velocity components are measured in units of v . One of aims of such description may be evaluation of correction to ballistic formula, or, more generally, to reproduce the Landauer regime [4].

The main *motivation* of this study is to link the conductivity parameters with temperature, that is achieved by a statement of problem formulation in such form, which includes the FDF distribution as an initial condition or a boundary one. A statement of the problem naturally implies that the conductor geometry is cylindrical for nanowires or other interesting cases, for example a point contact for tunnel microscopy.

For the distribution function, we take the integro-differential Kolmogorov equation [5] that was applied in [7] to the LIDAR problem, in [6] to the neutrons and to X-rays scattering [8]. Its form is presented in Sec. 2, where the collision terms are specified.

As the main mathematical tool of the basic equation solution, we derive an expansion in N -fold scattering series of the Bloch electron distribution function in a conducting domain. We also present a transition to integral equations and compact formulas for the distribution function, in particular, for the first and second iterations in this expansion. We consider a nanowire as a cylindrical waveguide via the choice of the domain geometry and reflective scattering by the walls.

In the Sec. 3, we describe the method of solution via the iterative scheme for the basic integro-differential equation, using the characteristic variables for the differential part, that allows us to transform the equation to an integral one. This problem admits studying transition regimes of switching and pulses of current.

In Sec. 4, we simplify the problem, by switching to the stationary case, which needs different characteristic variables to transform the differential part. We also formulate two problems, one for an empty cylinder with reflecting wall for the case in which the scattering inside the wire is much smaller than at boundary (Subsec. 4.2).

The second problem is closer to the normal temperature regime, when scatterers (e.g. phonons) fill the volume homogenously (Subsec. 4.3). To solve the problem, we expand the DF in series by number of collisions and derive the operator that links the neighboring terms (Subsec 4.5). In this problem, we choose the leading FDF term in the differential part as in [4] which results in the Fredholm equation for the next (first) term for the expansion.

Sec. 5 is devoted to the general iterative construction for the case of $\epsilon = 0$, specified to 1-fold and two-fold scattering solutions. Its explicit form allows one to evaluate the averaged values that give the formula for a current through a wire. The paper is concluded by a series convergence theorem at some conditions, that may permit one to estimate the number of terms and error of the corresponding calculation (Sec. 6).

2. Problem formulation

2.1. Kinetic equation and boundary conditions

Let us define the *collision integral* by the sum of losses by scattering with eventual account of absorption:

$$I_- = -f(\vec{r}, \vec{v}) \int \sigma(\vec{r}, \vec{v} \rightarrow \vec{v}') d\vec{v}' = -\sigma_t(\vec{r})f, \quad (1)$$

and the return term:

$$I_+ = \int \sigma(\vec{r}, \vec{v}' \rightarrow \vec{v}) f(\vec{r}, \vec{v}') d\vec{v}', \quad (2)$$

so that *Kolmogorov kinetic equation* for Bloch electron in the phase space $\{\vec{r}, \vec{v}\} \in \Gamma$ under action of electric field \vec{E} , directed along z , have the form:

$$\frac{\partial f}{\partial t} + \frac{e}{m} E \frac{\partial f}{\partial v_z} + \vec{v} \cdot \nabla f = -\sigma_t(z)f + I_+, \quad (3)$$

where $f(t, \vec{r}, \vec{v})$ is the probability density function over phase space $\{\vec{r}, \vec{v}\} \in \Gamma$, $\vec{v} = (v \sin \theta \cos \phi, v \sin \theta \sin \phi, v \cos \theta)$ and $\sigma_t(z)$, $\sigma(\vec{r}, \vec{v}' \rightarrow \vec{v}) = \sigma(\gamma, z)$ are total and differential cross section densities per unit volume of a medium. In spherical coordinates of incident θ, ϕ and scattered θ', ϕ' particles the scattering angle is characterized as follows:

$$\cos \gamma = \cos \theta \cos \theta' + \sin \theta \sin \theta' \cos(\phi - \phi'); \quad (4)$$

for elastic scattering ($v = v'$). We will discuss two problems: initial and boundary regime ones.

Initial problem. The function $f(t, \vec{r}, \vec{v})$ is used as a distribution (generalized function) defined by action on the Schwartz space $\psi(\vec{r}, v, \theta, \phi) \in \mathbf{S}$, via continuous linear functional $(f, \psi) \in \mathbb{R}$. The initial condition for (3) is also represented by a distribution. For example, for an initiation point with fixed velocity, we take:

$$f(0, \vec{r}, v, \theta, \phi) = V \delta(\vec{r}) \delta(\theta), \quad (5)$$

with a constant V as normalization factor. This means that we built a solution for the probability density as a weak limit (when $t \rightarrow 0$) to the δ -function at $t = 0$. The distribution $\delta(\theta)$ is chosen as:

$$(\delta(\theta), \psi(\vec{r}, v, \theta, \phi)) = \int_0^{2\pi} \psi(\vec{r}, v, 0, \phi) d\phi, \quad (6)$$

$\psi \in \mathbf{S}$, and, in a conventional mode, $\delta(\vec{r}) = \delta(x)\delta(y)\delta(z)$.

Boundary problem may be used when a conductor is in electric contact with a metal, that is characterized by some given FDF:

$$f(t, x, y, 0, \vec{v}) = f_F(x, y, \vec{v}). \quad (7)$$

2.2. Distribution averaging. Electric current as number of particles rate

This is derived in direct applications as an integral by space variables which enter the solution as parameters, used as a receiver (anode) geometry description. Thus, we are concerned with:

$$J(\Delta, t) = \int_{\theta_0}^{\theta_1} (f(t, \vec{r}, v, \theta, \phi), \psi) d\theta. \quad (8)$$

The action of the distribution f on \mathbf{S} in the case of segmented continuous functions implies the integration with respect to ϕ, x, y, z . The applications relate to observations (measurements) as the result of averaging procedure, defined by (8). The expression (8) defines number of particles within a finite domain (Δ) of a measurement apparatus and having velocity direction between θ_0 and θ_1 restricted by aperture related to the apparatus window direction.

Our particular aim is the evaluation of number of particles per unit time which enter the round area of radius ρ_0 laying in the plane $z = z_c$ (receiver) with center in $x = y = 0$ and having velocity vectors inclined to z-axis within the angle interval $\theta \in [0, \theta_0]$. Here, an aperture angle θ_0 , restricts possible velocities of particles directions. In the sample case we take here, the receiver domain Δ has cylindrical symmetry and for the initial direction along z , the function ψ does not depend on θ, ϕ , so it is defined as zero outside the receiver, and $\psi(x, y, z) = 1$ for internal points of the domain $x^2 + y^2 \leq \rho_0^2, z_0 \leq z \leq z_0 + \Delta t |\cos \theta|$ and zero outside, being z_0 the coordinate of anode interface, Δt – reaction time; for instant reaction:

$$I(t) = e \lim_{\Delta t \rightarrow 0} \frac{1}{\Delta t} \int_0^{\rho_0} \int_0^{\theta_0} \int_0^{2\pi} v_z (f(t, \rho, z, \theta, \phi), \psi(x, y, z)) \sin \theta d\phi d\theta d\rho. \quad (9)$$

Similar geometry was used in [8] for application to the problem of X-ray scattering.

3. Method of solution. N-fold scattering expansion

3.1. Cylindrical coordinates

A solution method depends on the conductor geometry and problem symmetry, that in our case of nanowires we have chosen as cylindrical one. Let the scattering cross section depend only on ρ and γ . For such a problem, we take (3) in cylindric coordinates neglecting $\frac{\partial f}{\partial \phi}$ term, having:

$$Lf = \frac{\partial f}{\partial t} + \epsilon \frac{\partial f}{\partial v_z} + v_z \frac{\partial f}{\partial z} + v_\rho \frac{\partial f}{\partial \rho} = -\sigma_t(\rho)f + \int_0^\pi \sigma(\gamma, \rho)f d\gamma, \quad (10)$$

with $\epsilon = \frac{e}{m}E$, $\cos \gamma = (\vec{v}, \vec{v}')/v^2$.

For the first (Cauchy) problem, we take an initial condition, if the external field E is switched on at $t = 0$:

$$f(0, \rho, v_z, v_\rho) = f_F(\vec{v})\theta(\rho_0 - \rho), \quad (11)$$

where f_F is the FDF, θ – step (Heaviside) distribution.

A solution is searched as a N -fold scattering expansion:

$$f = f_0 + f_1 + f_2 + \dots \quad (12)$$

We choose for the leading term f_0 the equation:

$$Lf_0 = \frac{\partial f_0}{\partial t} + \epsilon \frac{\partial f_0}{\partial v_z} + v_z \frac{\partial f_0}{\partial z} + v_\rho \frac{\partial f_0}{\partial \rho} = -\sigma_t(\rho)f_0, \quad (13)$$

which accounts only for losses, and initial condition:

$$f_0(0, \vec{v}, v_z, v_\rho) = f_F(\vec{v})\theta(\rho_0 - \rho). \quad (14)$$

The general approach for solution to the kinetic equation uses the transition to *characteristic variables*. Let us change variables in (13), putting $t' = t$, $v'_\rho = v_\rho$, and

$$v'_z = v_z + \epsilon(z - t) - v_z^2/2, \quad (15a)$$

$$\rho' = \rho - v_\rho t, \quad (15b)$$

$$z' = -\epsilon z + v_z^2/2. \quad (15c)$$

Equation (13) is transformed as:

$$\frac{\partial f_0}{\partial t'} = -\sigma_t(\rho' + v'_\rho t')f_0, \quad (16)$$

which is directly integrated including arbitrary *functional parameter* G :

$$f_0 = G(\vec{r}', \vec{v}') \exp \left[- \int_0^{t'} \sigma_t(\rho' + v'_\rho \tau) d\tau \right]. \quad (17)$$

It is useful to introduce a function Q via:

$$Q(t, \rho, v_\rho) = \exp \left[- \int_0^t \sigma_t(\rho + v_\rho \tau) d\tau \right]. \quad (18)$$

Going back to the original variables results in:

$$f_0 = G(-\epsilon z + v_z^2/2, \rho - v_\rho t, v_z + \epsilon(z - t) - v_z^2/2, v_\rho) \exp \left[- \int_0^t \sigma_t(\rho - v_\rho(t - \tau)) d\tau \right]. \quad (19)$$

At $t = 0$,

$$f_0 = G(-\epsilon z + v_z^2/2, \rho, v_z + \epsilon z - v_z^2/2, v_\rho). \quad (20)$$

The function G is found from initial conditions (14):

$$G(-\epsilon z + v_z^2/2, \rho, v_z + \epsilon z - v_z^2/2, v_\rho) = f_F(\vec{v})\theta(\rho_0 - \rho). \quad (21)$$

3.2. Iterations construction

For $n \geq 0$, the expansion is defined by:

$$\frac{df_{n+1}}{dt'} = -\sigma_t f_{n+1} + \int_0^\pi \sigma(\gamma, \rho) f_n d\gamma, \quad (22)$$

$n = 0, 1, \dots$, with zero initial conditions for $n > 0$:

$$f_n|_{t=0} = 0. \quad (23)$$

Transforming (22) by (15) and plugging its inverse:

$$v_z = v'_z + z' + \epsilon t', \quad (24a)$$

$$\rho = \rho' + v'_\rho t', \quad (24b)$$

$$z = \epsilon^{-1} (-z' + (v'_z + z' + \epsilon t')^2/2), \quad (24c)$$

$$t = t', \quad (24d)$$

into the r.h.s. of (22) yields:

$$\begin{aligned} \frac{\partial f_{n+1}}{\partial t'} &= -\sigma_t(\rho' + v'_\rho t') f_{n+1} \\ &+ \int_0^\pi \sigma(\gamma, \rho' + v'_\rho t') f_n(t', \epsilon^{-1} (-z' + (v'_z + z' + \epsilon t')^2/2), \rho' + v_\rho t', v'_z + z' + \epsilon t', v'_\rho) d\gamma. \end{aligned} \quad (25)$$

To have a more compact form, we define $f_{n+1} = Q \hat{f}_{n+1}$, which gives:

$$\frac{d\hat{f}_{n+1}}{dt'} = Q^{-1} \int_0^\pi \sigma(\gamma, \rho' + v'_\rho t') f_n(t', \epsilon^{-1} (-z' + (v'_z + z' + \epsilon t')^2/2), \rho' + v_\rho t', v'_z + z' + \epsilon t', v'_\rho) d\gamma, \quad (26)$$

where the definition of $Q(t', \rho', v_\rho')$ by (18) and the relation $\frac{\partial Q}{\partial t'} = -\sigma_t Q$ are used. After integration, one has:

$$\begin{aligned} \hat{f}_{n+1} &= Q^{-1} f_{n+1} = \int_0^{t'} \exp \left[\int_0^\tau \sigma_t(\rho' + v'_\rho \tau') d\tau' \right] \int_0^\pi \sigma(\gamma, \rho' + v'_\rho \tau) \\ &f_n(\tau, \epsilon^{-1} (-z' + (v'_z + z' + \epsilon \tau)^2/2), \rho' + v_\rho \tau, v'_z + z' + \epsilon \tau, v'_\rho) d\gamma d\tau. \end{aligned} \quad (27)$$

In the original variables, it reads as:

$$\begin{aligned} f_{n+1} &= Q \int_0^t \exp \left[\int_0^\tau \sigma_t(\rho - v_\rho(t - \tau')) d\tau' \right] \int_0^\pi \sigma(\gamma, \rho - v_\rho(t - \tau)) \\ &f_n(\tau, \epsilon^{-1} (\epsilon z - v_z^2/2 + (v_z - \epsilon(t - \tau))^2/2), \rho - v_\rho(t - \tau), v_z - \epsilon(t - \tau), v_\rho) d\gamma d\tau. \end{aligned} \quad (28)$$

4. Stationary case

4.1. Boundary regime problem

For the next topic, *boundary regime problem*, we study the *stationary kinetic equation* in cylindrical coordinates:

$$v_z \frac{\partial f}{\partial z} + v_\rho \frac{\partial f}{\partial \rho} + \epsilon \frac{\partial f}{\partial v_z} = -\sigma_t(\vec{\rho})f + \int \sigma(\vec{\rho}, \vec{v}', \vec{v})f(\vec{\rho}, \vec{v}')d\vec{v}', \quad (29)$$

where $\frac{e}{m}E = \epsilon$, $f(z, \rho, \vec{v})$ is a DF over phase space $\{\vec{\rho}, \vec{v}\} \in \Gamma$, $\vec{v} = (v_z, v_\rho)$, $\vec{\rho} = (z, \rho)$ and $\sigma_t(z)$, $\sigma(\vec{\rho}, \vec{v}', \vec{v})$ are total and differential cross section densities per unit volume. The function $f(\vec{\rho}, \vec{v})$ is used as a distribution defined by action on the Schwartz space $\psi(\vec{\rho}, \vec{v}) \in \mathbf{S}$, via continuous linear functional $(f, \psi) \in \mathbb{R}$. The boundary conditions for (29) is represented by a distribution, this paper choice is restricted by:

$$f(0, \rho, v_z, v_\rho) = f_F(\vec{v})\theta(\rho_0 - \rho), \quad (30)$$

where $f_F = \left(\exp \left[\frac{H - H_F}{k_B T} \right] + 1 \right)^{-1}$ is the Fermi–Dirac electron DF. The energy $H = mv^2/2$ for quasi free Bloch electron, H_F – Fermi energy, T – temperature. This means that we have constructed a solution for the probability density with the boundary conditions as a weak limit (when $z \rightarrow 0$).

4.2. Stationary problem solution for empty cylinder with reflecting wall

Let us change the variables in (29) as:

$$z' = z - \epsilon\rho + v_\rho v_z, \quad (31a)$$

$$\rho' = \epsilon\rho - v_\rho v_z, \quad (31b)$$

$$v'_z = v_z^2 - 2\epsilon z. \quad (31c)$$

The inverse transformation reads as:

$$z = z' + \rho', \quad (32a)$$

$$\rho = \epsilon^{-1} \left(\rho' + v_\rho \sqrt{v'_z + 2\epsilon(z' + \rho')} \right), \quad (32b)$$

$$v_z = \sqrt{v'_z + 2\epsilon(z' + \rho')}. \quad (32c)$$

Hence, for a homogeneous along z elastic scattering at the cylinder wall $\rho = \rho_0$, with the differential cross-section:

$$\sigma(\rho, v_z, v_\rho, \dots) = s\delta(\rho - \rho_0)\delta(v_z - v'_z)\delta(v_\rho + v'_\rho), \quad (33)$$

as a function of the parameter v_ρ , simplifies the collision integral, giving the equation:

$$\begin{aligned} Lf(z, \rho_0, v_z, v_\rho) &= \epsilon \frac{\partial f}{\partial v_z} + v_z \frac{\partial f}{\partial z} + v_\rho \frac{\partial f}{\partial \rho} = \\ &= -s\delta(\rho - \rho_0)f + \int s\delta(\rho - \rho_0)\delta(v_z - v'_z)\delta(v_\rho + v'_\rho)f(\vec{\rho}, \vec{v}')d\vec{v}' = \\ &= s\delta(\rho - \rho_0)[f(z, \rho_0, v_z, -v_\rho) - f(z, \rho_0, v_z, v_\rho)]. \end{aligned} \quad (34)$$

Taking the equation at the opposite v_ρ point and combining the results, yields:

$$\begin{aligned} L[f(z, \rho_0, v_z, v_\rho) + f(z, \rho_0, v_z, -v_\rho)] &= Lf^+ = 0, \\ L[f(z, \rho_0, v_z, v_\rho) - f(z, \rho_0, v_z, -v_\rho)] &= Lf^- = \\ 2s\delta(\rho - \rho_0)[f(z, \rho_0, v_z, -v_\rho) - f(z, \rho_0, v_z, v_\rho)] &= 2s\delta(\rho - \rho_0)f^-. \end{aligned} \quad (35)$$

Transition to the variables (31) first gives:

$$\frac{\partial f^+}{\partial z'} = 0, \quad (36)$$

and, secondly:

$$\frac{\partial f^-}{\partial z'} = 2s \frac{\delta \left(\epsilon^{-1}(\rho' + v_\rho \sqrt{v'_z + 2\epsilon(z' + \rho')}) - \rho_0 \right)}{\sqrt{v'_z + 2\epsilon(z' + \rho')}} f^- \left(z' + \rho', \rho_0, \sqrt{v'_z + 2\epsilon(z' + \rho')}, v_\rho \right). \quad (37)$$

The direct integration results in the first case as:

$$f^+ = \Phi^+(\rho', v'_z, v_\rho), \quad (38)$$

while the second one yields in:

$$f^- = \int_0^{z'} \frac{s \delta \left(\epsilon^{-1} (\rho' + v_\rho \sqrt{v_z' + 2\epsilon(\tau + \rho')}) - \rho_0 \right)}{\sqrt{v_z' + 2\epsilon(\tau + \rho')}} f^- \left(z' + \rho', \rho_0, \sqrt{v_z' + 2\epsilon(\tau + \rho')}, v_\rho \right) d\tau + \Phi^-(\rho', v_z', v_\rho). \quad (39)$$

Solving the equation:

$$\rho' + v_\rho \sqrt{v_z' + 2\epsilon(\tau + \rho')} - \epsilon \rho_0 = 0$$

with respect to τ , we obtain:

$$\tau_0 = z - \epsilon \rho + v_\rho v_z + \frac{\epsilon}{2} \left\{ \frac{(\rho_0 - \rho)}{v_\rho} \right\}^2 - v_z \frac{(\rho_0 - \rho)}{v_\rho},$$

which defines the only zero value of the δ -function argument. We plug it into (40), using $\delta(f(\tau)) = \frac{\delta(\tau - \tau_0)}{|f'(\tau_0)|}$, while:

$$\frac{d}{d\tau} \left[\epsilon^{-1} \left(\rho' + v_\rho \sqrt{v_z' + 2\epsilon(\tau + \rho')} \right) - \rho_0 \right] = \frac{v_\rho}{\sqrt{v_z' + 2\epsilon(\tau + \rho')}},$$

and return to original variables by (32):

$$\begin{aligned} f^- &= \int_0^{z'} \frac{s \delta \left(\epsilon^{-1} \left(\rho' + v_\rho \sqrt{v_z' + 2\epsilon(\tau + \rho')} \right) - \rho_0 \right)}{\sqrt{v_z' + 2\epsilon(\tau + \rho')}} f^- \left(z' + \rho', \rho_0, \sqrt{v_z' + 2\epsilon(\tau + \rho')}, v_\rho \right) d\tau \\ &= \begin{cases} \frac{s}{v_\rho} f^- \left(z, \rho_0, \frac{\epsilon \rho_0 - \epsilon \rho + v_\rho v_z}{v_\rho}, v_\rho \right), & \text{if } \tau_0 \in [0, z - \epsilon \rho + v_\rho v_z] \\ 0, & \text{otherwise.} \end{cases} \end{aligned} \quad (40)$$

We introduce $\hat{t} = \frac{\rho_0 - \rho}{v_\rho}$, then, inside the interval $\tau_0 \in [0, z - \epsilon \rho + v_\rho v_z]$, we write:

$$f^- (z, \rho, v_z, v_\rho) = \frac{s}{v_\rho} f^- (z, \rho_0, v_z + \epsilon \hat{t}, v_\rho), \quad (41)$$

and

$$\tau_0 = z - \epsilon \rho + v_\rho v_z + \frac{\epsilon}{2} \hat{t}^2 - v_z \hat{t}.$$

Its border values are:

$$\tau_0 = z - \epsilon \rho + v_\rho v_z + \frac{\epsilon}{2} \hat{t}^2 - v_z \hat{t} = z - \epsilon \rho + v_\rho v_z,$$

and

$$\tau_0 = z - \epsilon \rho + v_\rho v_z + \frac{\epsilon}{2} \hat{t}^2 - v_z \hat{t} = 0.$$

The first one gives the condition:

$$\frac{\epsilon}{2} \hat{t}^2 - v_z \hat{t} = 0,$$

which is equivalent to either relation: $\hat{t} = 0$, that fix the point

$$\rho = \rho_0,$$

or defines a hyperbolic curve in velocity space for each ρ

$$\frac{\epsilon}{2} \frac{\rho_0 - \rho}{v_\rho} - v_z = 0.$$

The second one also defines the curve:

$$v_z = \frac{z - \epsilon \rho + \frac{\epsilon}{2} \hat{t}^2}{\hat{t} - v_\rho}. \quad (42)$$

Both curves determine the integration domain for a mean value of DF in velocity subspace evaluation as in Sec. 2.3.

The symmetry of the boundary regime with respect to reflection $v_\rho \rightarrow -v_\rho$ yields:

$$f^-(0, \rho, v_z, v_\rho) = 0, \quad (43)$$

while (30) gives:

$$f^+(z, \rho, v_z, v_\rho) = \Phi^+ (\epsilon\rho - v_\rho v_z, v_z^2 - 2\epsilon z, v_\rho) = 2f_F(\vec{v})\theta(\rho_0 - \rho).$$

Taking the functional equation (40) at the point $z = 0$, at $\tau_0 \in [0, z - \epsilon\rho + v_\rho v_z]$, the condition (45) reads:

$$f^-(0, \rho, v_z, v_\rho) = \frac{s}{v_\rho} f^-(0, \rho_0, v_z + \epsilon\hat{t}, v_\rho) = 0. \quad (44)$$

The final step gives the DF:

$$f = (f^- + f^+)/2. \quad (45)$$

4.3. Stationary problem for cylinder filled with scatterers

In this section, we suppose that the scattering inside the wire admits homogeneous distribution along z ($l \ll \lambda_B$), looking for the further simplification. Let $f(\rho, v_z, v_\rho)$ be a distribution function for Bloch electrons, that solves the equation (cf. (29)):

$$\epsilon \frac{\partial f}{\partial v_z} + v_\rho \frac{\partial f}{\partial \rho} = -\sigma_t(\vec{\rho})f + \int \sigma(\vec{\rho}, \vec{v}', \vec{v})f(\vec{\rho}, \vec{v}')d\vec{v}'. \quad (46)$$

Adding to the expression (33) the term that model elastic scattering with a given dependence on the only scattering angle inside the cylinder, we have:

$$\sigma(\rho, v_z, v_\rho, \dots) = s\delta(\rho - \rho_0)\delta(v_z - v'_z)\delta(v_\rho + v'_\rho) + \sigma_0(\gamma)\delta(v - v')\theta(\rho - \rho_0). \quad (47)$$

Simplifying the model by $\sigma_0(\gamma) = \sigma_0$ and plugging (47) in (29) gives:

$$\begin{aligned} \epsilon \frac{\partial f}{\partial v_z} + v_\rho \frac{\partial f}{\partial \rho} = & -[s\delta(\rho - \rho_0) + \sigma_0\theta(\rho - \rho_0)]f(\rho, v_z, v_\rho) - \\ & s\delta(\rho - \rho_0) \int \delta(v_z - v'_z)\delta(v_\rho + v'_\rho)f(\rho, v'_z, v'_\rho)dv'_z dv'_\rho + \\ & \sigma_0\theta(\rho_0 - \rho) \left[f(\rho, v_z, v_\rho) + \int \delta(v^2 - v'^2)f(\rho, v'_z, v'_\rho)dv'_z dv'_\rho \right]. \end{aligned} \quad (48)$$

After integration, in collision terms with $\delta(f(\tau)) = \sum_j \frac{\delta(\tau - \tau_j)}{|f'(\tau_j)|}$ account, we write:

$$\begin{aligned} \epsilon \frac{\partial f}{\partial v_z} + v_\rho \frac{\partial f}{\partial \rho} = & s\delta(\rho - \rho_0)[f(\rho, v_z, v_\rho) - f(\rho, v_z, -v_\rho)] + \\ & \sigma_0\theta(\rho_0 - \rho) \left[f(\rho, v_z, v_\rho) + \int \frac{f(\rho, v'_{z+}, v'_\rho) + f(\rho, v'_{z-}, v'_\rho)}{2\sqrt{v_\rho^2 + v_z^2 - v_\rho'^2}} dv'_\rho \right], \end{aligned} \quad (49)$$

where:

$$v'_{z\pm} = \pm \sqrt{v_\rho^2 + v_z^2 - v_\rho'^2}. \quad (50)$$

For this case, the *characteristic variables* are defined by the direct transform:

$$\rho' = \rho/v_\rho, \quad v'_z = v_z - \epsilon\rho/v_\rho, \quad (51)$$

and the inverse one as:

$$\rho = \rho'v_\rho, \quad v_z = v'_z + \epsilon\rho'. \quad (52)$$

This gives:

$$\begin{aligned} \frac{\partial f}{\partial \rho'} = & s\delta(\rho'v_\rho - \rho_0)[f(\rho'v_\rho, v'_z + \epsilon\rho', v_\rho) - f(\rho'v_\rho, v'_z + \epsilon\rho', -v_\rho)] + \\ & \sigma_0\theta(\rho_0 - \rho'v_\rho) \left[f(\rho'v_\rho, v'_z + \epsilon\rho', v_\rho) + \int \frac{f(\rho'v_\rho, v'_{z+}, v'_\rho) + f(\rho'v_\rho, v'_{z-}, v'_\rho)}{2\sqrt{v_\rho^2 + v_z^2 - v_\rho'^2}} dv'_\rho \right], \end{aligned} \quad (53)$$

where now:

$$v'_{z\pm} = \pm \sqrt{v_\rho^2 + (v'_z + \epsilon\rho')^2 - v_\rho'^2}. \quad (54)$$

Integrating, we arrive at the integral equation:

$$f(\rho', v'_z, v_\rho) = s \int_0^{\rho'} \delta(rv_\rho - \rho_0) \left[f(rv_\rho, v'_z + \epsilon r, v_\rho) - f(rv_\rho, v'_z + \epsilon r, -v_\rho) \right] dr + \\ \sigma_0 \int_0^{\rho'} \theta(rv_\rho - \rho_0) \left[f(rv_\rho, v'_z + \epsilon r, v_\rho) + \int \frac{f(rv_\rho, v'_{z+}, v'_\rho) + f(rv_\rho, v'_{z-}, v'_\rho)}{2 \left| \sqrt{v_\rho^2 + (v'_z + \epsilon r)^2 - v_\rho'^2} \right|} dv'_\rho \right] dr. \quad (55)$$

Now

$$v'_{z\pm} = \pm \sqrt{v_\rho^2 + (v_z - \epsilon \rho / v_\rho + \epsilon r)^2 - v_\rho'^2}. \quad (56)$$

In primary variables, it is:

$$f(\rho, v_z, v_\rho) = s \int_0^{\rho/v_\rho} \delta(rv_\rho - \rho_0) \left[f(rv_\rho, v_z - \epsilon(\rho/v_\rho - r), v_\rho) - f(rv_\rho, v_z - \epsilon(\rho/v_\rho - r), -v_\rho) \right] dr + \\ \sigma_0 \int_0^{\rho/v_\rho} \theta(\rho_0 - rv_\rho) \int \frac{f(rv_\rho, v'_{z+}, v'_\rho) + f(rv_\rho, v'_{z-}, v'_\rho)}{2 \left| \sqrt{v_\rho^2 + (v_z - \epsilon \rho / v_\rho + \epsilon r)^2 - v_\rho'^2} \right|} dv'_\rho dr. \quad (57)$$

Changing the variable of integration as $rv_\rho = t$, $v_\rho > 0$, yields:

$$f(\rho, v_z, v_\rho) = \\ \frac{s}{v_\rho} \int_0^\rho \delta(t - \rho_0) \left[f\left(t, v_z - \frac{\epsilon}{v_\rho}(\rho - t), v_\rho\right) - f\left(t, v_z - \frac{\epsilon}{v_\rho}(\rho - t), -v_\rho\right) \right] dt + \\ \frac{\sigma_0}{v_\rho} \int_0^\rho \theta(\rho_0 - t) \int \frac{f(t, v'_{z+}, v'_\rho) + f(t, v'_{z-}, v'_\rho)}{2 \left| \sqrt{v_\rho^2 + \left(v_z + \epsilon \frac{t - \rho}{v_\rho}\right)^2 - v_\rho'^2} \right|} dv'_\rho dt = \\ \begin{cases} \frac{\sigma_0}{2v_\rho} \int_0^\rho \int \frac{f(t, v'_{z+}, v'_\rho) + f(t, v'_{z-}, v'_\rho)}{\left| \sqrt{v_\rho^2 + \left(v_z + \epsilon \frac{t - \rho}{v_\rho}\right)^2 - v_\rho'^2} \right|} dv'_\rho dt, & \text{if } \rho < \rho_0, \\ \frac{s}{2} \left[f(\rho_0, v_z, v_\rho) - f(\rho_0, v_z, -v_\rho) \right], & \text{if } \rho = \rho_0, \end{cases} \quad (58)$$

with v_{z+} under square root.

4.4. Alternative expansion for stationary case

Neglecting the longitudinal inhomogeneity (the second term) in (34) let us study it as the basic equation. The structure of the integro-differential equation and physical sense of its terms in conditions of constant current suggest an alternative expansion with the leading term in the l.h.s. [4]. A solution is searched as an expansion (12), but we choose for the link between f_0 and f_1 , the equation:

$$Lf_0 = \epsilon \frac{\partial f_0}{\partial v_z} + v_\rho \frac{\partial f_0}{\partial \rho} = -\sigma_t f_1 + \int \sigma(\vec{\rho}, \vec{v}', \vec{v}) f_1(\vec{\rho}, \vec{v}') d\vec{v}, \quad (59)$$

taking the FDF distribution for f_0 inside the cylinder of radius ρ_0 :

$$f_0(\rho, v_z, v_\rho) = f_F(v_z, v_\rho) \theta(\rho_0 - \rho). \quad (60)$$

Differentiating in the l.h.s., and switching to angle variables in collision integral as in (13), one has:

$$\epsilon \frac{\partial f_F(v_z, v_\rho)}{\partial v_z} \theta(\rho_0 - \rho) + v_\rho f_F(v_z, v_\rho) \delta(\rho - \rho_0) = -\sigma_t f_1 + \int_0^\pi \sigma(\vec{\rho}, \gamma) f_1(\vec{\rho}, \vec{v}') d\gamma. \quad (61)$$

Equation (61) is the Fredholm II integral equation with continuous kernel for the function f_1 . The theory of such equations guarantee the existence and methods of its solution outside the integral operator spectrum, which depends

on details of the kernel $\sigma(\vec{\rho}, \gamma)$ behavior and needs special investigation after the kernel (cross-section) is specified for given material.

5. Approximate solutions

5.1. N -fold iteration ($\epsilon = 0$)

In this section, we consider the problem of zero field transport for conductors contact pulse current excitations as a Cauchy problem. Let us return to the spherical coordinates for the basic equation (3). Integration and transformation yields:

$$f_{n+1}(x, y, z, \theta, \phi) = \int_0^t Q(\tau, z, \theta) \int_0^\pi \int_0^{2\pi} \sigma(\cos \gamma, z - \tau \cos \theta) f_n(t - \tau, x - \tau \sin \theta \cos \phi, y - \tau \sin \theta \sin \phi, z - \tau \cos \theta, \theta', \phi') \sin \theta' d\theta' d\phi' d\tau, \quad (62)$$

where

$$Q(t, z, \theta) = \exp \left[- \int_0^t \sigma_t(z - \tau \cos \theta) d\tau \right] \quad (63)$$

This expression defines the recurrence operator:

$$f_{n+1} = K_n f_n, \quad (64)$$

the form of which determines the properties of approximate solutions and convergence of the multiple scattering series (12). The basic equation for f_0 is integrated as:

$$f_0 = G(\vec{r}, \vec{v}) \exp \left[- \int_0^t \sigma_t(z') d\tau \right]. \quad (65)$$

The functional parameter G is found from initial conditions (see (5)), modeling a point pulse contact:

$$f_0(0, \vec{r}, \theta, \phi) = V \delta(x) \delta(y) \delta(z) \delta(\theta), \quad (66)$$

that results in:

$$f_0(t, \vec{r}, \theta, \phi) = V \delta(z - t) \delta(x) \delta(y) \delta(\theta) Q(t, z, \theta). \quad (67)$$

For the first iteration, f_1 one obtains from (62):

$$f_1 = V \int_0^t Q(\tau, z, \theta) E(t - \tau, z - \tau \cos \theta, 0) \sigma(\cos \theta, z - \tau \cos \theta) \delta(x - \tau \cos \theta - (t - \tau)) \delta(y - \tau \sin \theta \sin \phi) \delta(z - \tau \sin \theta \cos \phi) d\tau. \quad (68)$$

Similar expressions are obtained and interpreted in the case of N -fold scattering terms, the two-fold one is presented in the following sections.

5.2. One-fold scattering for a point receiver

As mentioned above, the integrand in (68) is considered as distributions on Schwartz space \mathbf{S} of functions x, y, z which depend on ϕ, θ, τ as parameters. For example, f_1 acts on an element $\psi(\vec{r}) \in \mathbf{S}$ as:

$$\left(f_1(t, \vec{r}, \theta, \phi), \psi \right) = V \int_0^{2\pi} \int_0^t Q(\tau, \tau \cos \theta + t - \tau, \theta) E(t - \tau, t - \tau, 0) \sigma(\cos \theta, \tau \cos \theta + t - \tau) \psi(\tau \sin \theta \cos \phi, \tau \sin \theta \sin \phi, \tau \cos \theta + t - \tau) d\tau d\phi, \quad (69)$$

where ψ describes a receiver. It is determined in Sec. (2.2) as $\psi(\vec{r}) = 1$ at:

$$x^2 + y^2 \leq \rho_0^2, \quad z_0 \leq z \leq z_0 + \Delta t |\cos \theta|$$

and zero outside, being z_0 the boundary coordinate of the cylindrical contact.

From the definition (8) for the forward scattering and aperture angle θ_0 we have:

$$J_1(t) = \int_0^{\theta_0} (f_1, \psi) \sin \theta d\theta. \quad (70)$$

Therefore, we get for (68) when going to the intensity of a point receiver that we do as the limit:

$$I_{1p}(t, 0, 0, z_0) = - \lim_{\Delta t \rightarrow 0} \lim_{\rho_0 \rightarrow 0} \int_{z_0}^{z_0 + \cos \theta_0 \Delta t} \int_0^{2\pi} \int_0^{\rho_0} \int_0^{\theta_0} \int_0^t Q(\tau, z_0, \theta) \int \sigma(\cos \theta \cos \theta', z - \tau \cos \theta) f_0(t - \tau, x - \tau \sin \theta \cos \phi, y - \tau \sin \theta \sin \phi, z - \tau \cos \theta, \theta) \sin \theta' d\theta' d\tau d\theta d\rho d\phi dz, \quad (71)$$

or, plugging f_0 , one has:

$$I_{1p}(t) = - \lim_{\Delta t \rightarrow 0} \lim_{\rho_0 \rightarrow 0} \frac{1}{\Delta t} \int_0^{\rho_0} \int_0^{\theta_0} \int_0^t \int_{z_0}^{z_0 + \cos \theta_0 \Delta t} Q(\tau, z, \theta_0) Q(t - \tau, z - \tau \cos \theta_0, \theta_0) \int \sigma(\cos \theta_0 \cos \theta', z - \tau \cos \theta_0) \psi(\tau \sin \theta_0 \cos \phi, \tau \sin \theta_0 \sin \phi, \tau \cos \theta_0) \sin \theta' d\theta' d\tau d\phi d\rho dz. \quad (72)$$

The area of integration lies between the horizontal lines $z = z_0$, $z_0 + \Delta z$ and inclined lines $z = \cos \theta_0 + a$ and $z = \cos \theta_0 + b$, where a , b are boundaries of domain, filled with scatterers under consideration: e.g. a “cloud” of defects. The vertical line marks a current pulse arrival time $z = t$. In the case of a fixed angle θ_0 , $z' = \tau(\cos \theta_0 - 1) + t$, $\tau = (\cos \theta_0 - 1)^{-1}(z' - t)$, hence the argument of the δ -function is:

$$z_0 + t - \tau - z' = z_0 + t - (\cos \theta_0 - 1)^{-1}(z' - t) - z' = z_0 - bt + az' = a \left(z' - \frac{b}{a} \right) t + \frac{z_0}{a},$$

where

$$a = -1 - (\cos \theta_0 - 1)^{-1} = \frac{\cos \theta_0}{1 - \cos \theta_0}, \quad b = 1 + (\cos \theta_0 - 1)^{-1}.$$

The second argument of the scattering amplitude σ is therefore:

$$z_0 - \tau \cos \theta_0 = z_0 - (\cos \theta_0 - 1)^{-1}(z' - t) \cos \theta_0.$$

The result of 1-fold scattering for zero angle for the point receiver is almost trivial from a geometrical point of view, the arriving pulse is infinitely short. The expression for intensity contains natural spherical divergence, exponential decay due to absorption and forward scattering in a level inside the layer:

$$J_1^p(t) = \lim_{\Delta_i \rightarrow 0} \frac{1}{\prod \Delta_i} \int_{\theta_0}^{\pi} \int_0^{2\pi} (f_1, \psi) \sin \theta d\phi d\theta, \quad i = 1, 2, 3, \quad (73)$$

where the function ψ have nonzero components if:

$$|x| \leq \Delta x = \Delta_1, \quad |y| \leq \Delta y = \Delta_2, \quad |z| \leq \Delta t |\cos \theta| = \Delta_3,$$

and 0 outside the domain. Plugging f_1 from (68) yields:

$$J_1^p(t) = \lim_{\Delta_i \rightarrow 0} \frac{1}{\prod \Delta_i} \int_{\theta_0}^{\pi} \int_0^{2\pi} \int_0^t E(\tau, \tau \cos \theta + t - \tau, \theta) E(t - \tau, t - \tau, 0) \sigma(\cos \theta, \tau \cos \theta + t - \tau) \psi(\tau \sin \theta \cos \phi, \tau \sin \theta \sin \phi, \tau \cos \theta + t - \tau) d\tau \sin \theta d\phi d\theta. \quad (74)$$

5.3. Alternative variables of integration. One- and two-fold solutions for a point receiver

Let us change the variables of integration, having in mind more convenient (compared to [7]) description of the integration domain and limiting procedure:

$$\begin{aligned} x &= \tau \sin \theta \cos \phi, \\ y &= \tau \sin \theta \sin \phi, \\ x &= \tau \cos \theta + t - \tau. \end{aligned} \quad (75)$$

The inverse ones are found as:

$$\begin{aligned}\tau &= \frac{x^2 + y^2 + z^2 - 2zt + t^2}{2(t-z)}, \\ \cos \phi &= \frac{x}{\sqrt{x^2 + y^2}}, \\ \cos \theta &= \frac{x^2 + y^2 + z^2 - 2zt + t^2 - 2(t-z)^2}{x^2 + y^2 + z^2 - 2tz + t^2}.\end{aligned}\quad (76)$$

We calculate the Jacobian:

$$J \sin \theta = \frac{2}{x^2 + y^2 + z^2 - 2zt + t^2}.\quad (77)$$

Let us define the integration intervals by means of:

$$\begin{aligned}0 \leq \tau \leq t, \quad 0 \leq \phi \leq 2\pi, \quad \pi - \theta_0 \leq \theta \leq \pi, \\ 0 \leq \tau \cos \theta + t - \tau \leq \Delta t, \\ |\tau \sin \theta \cos \phi| \leq \Delta x, \quad |\tau \sin \theta \sin \phi| \leq \Delta y, \quad t - \tau + \tau \cos \theta \geq 0,\end{aligned}\quad (78)$$

then $|x| \leq \Delta x$, $|y| \leq \Delta y$, $0 \leq z \leq \Delta t$.

1-fold again. The explicit expression for the integral J_1 , corresponding to (74), in new variables takes the form:

$$J_1 = \lim \frac{1}{2\Delta x \Delta y \Delta z} \int_{-\Delta x}^{\Delta x} \int_{-\Delta y}^{\Delta y} \int_0^{\Delta t} \frac{Q' Q'' \sigma}{x^2 + y^2 + z^2 - 2zt + t^2} dx dy dz,\quad (79)$$

where $Q' = Q(\tau, z, \theta)$, $Q'' = Q(t - \tau, z - \tau \cos \theta, 0)$, is defined by (63). In arguments of Q' , Q'' , σ the variables τ , θ expressed in new ones (76).

Performing the limiting transition $\Delta x \rightarrow 0$, $\Delta y \rightarrow 0$, $\Delta z \rightarrow 0$, $\Delta t \rightarrow 0$ for a point receiver, we obtain the simple formula for back scattering:

$$I_1^p(t) = \frac{2}{t^2} E' \left(\frac{t}{2}, 0, \pi \right) E'' \left(\frac{t}{2}, \frac{t}{2}, 0 \right) \sigma \left(-1, \frac{t}{2} \right).\quad (80)$$

This reproduces the one-fold LIDAR formula for a small receiver in convenient form.

The dependence of $I_1(t)$ is shown for the homogeneous distribution of scatterers at Fig. 1 and for a layer of scatterers and for a layer of scatterers at Fig. 2.

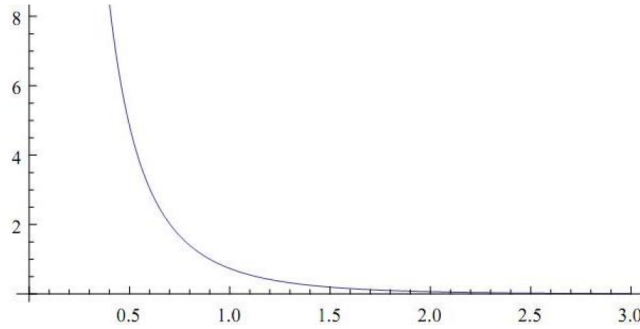


FIG. 1. Homogeneous scatterers distribution case $I_1(t)$

5.4. 2-fold case

From (62), similar to (68), when using the correspondingly modified transformations (75), (76), one arrives at the distribution term f_2 :

$$\begin{aligned}f_2 = \int_0^t Q(\tau_2, z, \theta) \int_0^{2\pi} \int_0^\pi \sigma(\cos \gamma, z - \tau_2 \cos \theta) \int_0^{t-\tau_2} Q_1(\tau, z - \tau_2 \cos \theta, \theta') Q(t - \tau_2 - \tau, t - \tau - \tau_2, 0) \sigma(\cos \theta', t - \tau - \tau_2) \\ \delta(x - \tau_2 \sin \theta \cos \phi - \tau \sin \theta' \cos \phi') \delta(y - \tau_2 \sin \theta \sin \phi - \tau \sin \theta' \sin \phi') \\ \delta(z - \tau_2 \cos \theta - \tau \cos \theta' - (t - \tau_2 - \tau)) d\tau \sin \theta' d\theta' d\phi' d\tau_2.\end{aligned}\quad (81)$$

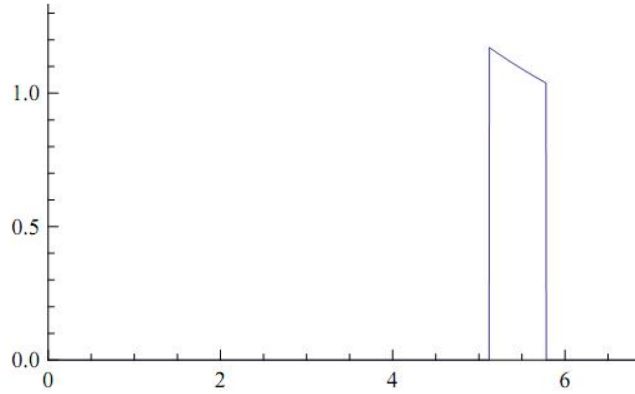


FIG. 2. $I_1(t)$, 1-fold scattering from a layer of scatterers

In new variables, (75) the integral J_2 takes the form:

$$J_2 = \lim_{\Delta V \rightarrow 0} \frac{1}{2\Delta x \Delta y \Delta z} \int_{-\Delta x}^{\Delta x} \int_{-\Delta y}^{\Delta y} \int_0^{\Delta t} \int_0^{t/2} \int_0^{2\pi} \int_{\pi-\theta_0}^{\pi} \frac{Q^* \sigma(\cos \gamma, \tau_1(\cos \theta_1 - 1) + t - \tau_2) \sigma(\cos \theta_1, t - \tau_1 - \tau_2)}{(\tau_2 \sin \theta_2 \cos \phi_2 - x)^2 + (\tau_2 \sin \theta_2 \sin \phi_2 - y)^2 + (t - (1 - \cos \theta_2)\tau_2 - z)^2} \sin \theta_2 d\theta_2 d\phi_2 d\tau_2 dz dx dy, \quad (82)$$

where:

$$Q^* = Q(\tau, z - \tau_2 \cos \theta, \theta') Q(t - \tau_2 - \tau, t - \tau - \tau_2, 0). \quad (83)$$

The corresponding intensity from 2-fold scattering for a layer of scatterers is shown at Fig. 3.

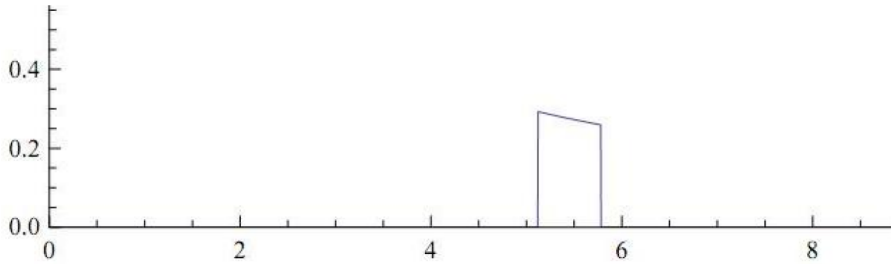


FIG. 3. $I_2(t)$, intensity: 2-fold scattering from a layered medium

6. Convergence theorem

6.1. Resulting estimation

Let the norm of σ be denoted as $\|\sigma\| = \max_{\gamma, z} \sigma$:

$$J_N \leq 2^{3n-1} \|\sigma\|^n \exp[-\sigma_{\min} t] \pi^{n-1} t^{n-3} \frac{(n-1)^2}{((n-1)!)^{1/3}} \theta_0^{2/3}. \quad (84)$$

The series generated by r.h.s. of the inequality (84) converge because:

$$\lim_{n \rightarrow \infty} \sqrt[n]{2^{3n-1} \|\sigma\|^n \exp[-\sigma_{\min} t] \pi^{n-1} t^{n-3} \frac{(n-1)^2}{((n-1)!)^{1/3}}} \rightarrow 0. \quad (85)$$

(root test). Therefore, the radius of convergence is infinity.

On proof. Divide the integration domain D to subdomains D_1, D_2 so that for a positive ϵ_n , the following holds:

$$\begin{aligned} \left(t - \sum_2^n \tau_i (1 - \cos \theta_i) \right)^2 + \left(\sum_2^n \tau_i \cos \theta_i \sin \phi_i \right)^2 + \left(\sum_2^n \tau_i \cos \theta_i \cos \phi_i \right)^2 \\ \leq \epsilon_n \sim D_1, \\ \geq \epsilon_n \sim D_2. \end{aligned} \quad (86)$$

This determines the choice of ϵ_n .

6.2. Error estimation

If $8\pi\|\sigma\|t < 1$, the following estimate for error is the following:

$$\left| I(t) - \sum_1^n I_k(t) \right| \leq 4\|\sigma\|e^{-\sigma_{\min}t}\theta_0^{2/3}t^2 \sum_{k=n}^{\infty} (8\pi\|\sigma\|t)^{k-1} = 4t^2\theta_0^{2/3}\|\sigma\| \frac{e^{-t\sigma_{\min}}}{1 - 8\pi\|\sigma\|t}. \quad (87)$$

Having such an estimation, one can decide what number of N -fold contributions should be taken into account for a given error.

7. Conclusion

We do understand that the approximations for the differential cross-sections as (47) are too rough. We have chosen such models to move the theory in explicit form as far as possible. Modifications of the formulas should improve the description and may be compared with the presented results. The convergence theorem is certainly generalized for nonzero field.

In transport problems, the electron *Bloch wave* scatters either on phonons or on a solid crystal lattice inhomogeneities (point defects or dislocations). Such contribution may be incorporated into the suggested scheme. One of the simplest, to say a “textbook” version of the model, accomplished in a sense of possibility to plot the dependences of the conductivity on temperature and wire radius, see our contribution with Botman, see also [9].

Account of electron-electron scattering implies transition to Boltzmann equation. The quantum corrections also use its generalizations [10].

Acknowledgment

The kinetic method based on the distributions application was inspired by fruitful discussions with B. S. Pavlov and I. Y. Popov [11].

References

- [1] Heremans J., Thrush C.M., et al. Bismuth nanowire arrays: Synthesis, galvanomagnetic properties. *Phys. Rev. B*, 2000, 61, P. 2921–2930.
- [2] Hong K., Yang F.Y., et al. Giant positive magnetoresistance of Bi nanowire arrays in high magnetic fields. *J. Appl. Phys. A*, 1999, 85, P. 6184–6186.
- [3] Lin Y.-M., Cronin S.B., et al. Transport properties of Bi nanowire arrays. *Appl. Phys. Lett.*, 2000, 76, P. 3944–3946.
- [4] Gal’perin Y.M. *Introduction to Modern Solid State Physics*. FYS 448, Oslo, 2009.
- [5] Kolmogoroff A. Über die analytischen Methoden in der Wahrscheinlichkeitsrechnung. *Math. Ann.*, 1931, 104, P. 415.
- [6] Kolchuzhkin A.M., Uchaikin V.V. *Introduction into the Theory of Particle Penetration through a Matter*. Moscow, Atomizdat, 1978 (in Russian).
- [7] Buzdin A., Leble S. Lidar Problem Solution in Double-Scattering Approximation. arXiv:1112.3297v1 [math-ph], 2011.
- [8] Guarao M., Leble S. Modeling of X-ray attenuation via photon statistics evolution. *TASK Quarterly*, 2014, 18 (2), P. 187–203.
- [9] Botman S., Leble S. Bloch Wave - ZRP Scattering as a Key Element of Solid State Physics Computation: 1D Example. *TASK Quarterly*, 2016, 20 (2), P. 185–194.
- [10] Kailasvuori J., Lüffe M.C. Quantum corrections in the Boltzmann conductivity of graphene and their sensitivity to the choice of formalism. *J. Stat. Mech.*, 2010, P. 06024.
- [11] Popov I.Y., Kurasov P.A., et al. A distinguished mathematical physicist Boris S. Pavlov. *Nanosystems: Physics, Chemistry, Mathematics*, 2016, 7, P. 782–788.

Asymptotic solution of ultrasonic near-field levitation problem

I. F. Melikhov

ITMO University, Kronverkskiy, 49, St. Petersburg, 197101, Russia
ivan.melikhov@gmail.com

PACS 43.25.Uv

DOI 10.17586/2220-8054-2017-8-2-260-265

Ultrasonic near-field levitation allows suspension of a moderately large object at a height of tens of microns above sound actuator. We developed an asymptotic approach to describe the air dynamics in the gap between an acoustic source and the levitating object. The suggested method allows computation of the lifting force. Due to resolving of both viscous and inertial effects, it remains applicable across a wide range of levitation distances. The paper explains theoretical background of the model and presents a numerical solution of the obtained equations. The results are compared to published numerical and experimental data showing very good agreement.

Keywords: ultrasonic levitation, acoustic streaming, asymptotic analysis.

Received: 13 January 2017

Revised: 19 January 2017

1. Introduction

This work focuses on a specific kind of acoustic levitation, which is called ultrasonic near-field levitation. This name comes from the observed small levitation heights: from 5 μm to 500 μm . The phenomenon is employed in contactless transportation systems. The suspension of an object at extremely small distance was reported in 1964 by Salbu [1]. The first implementation of this technology for transport systems was utilized soon thereafter. A system based on flexural traveling waves of a guideline were studied in [2,3]. The works [4,5] suggested another approach: they used a trolley with ultrasonic source.

The theoretical base of acoustic levitation was founded by Lord Rayleigh [6,7], who considered acoustic pressure in inviscid fluid. His theory was finally finished much later in the papers [8,9]. This approach was used for lifting force estimation in the works [2,3]. However, this method is not applicable for small levitation distances. The reason is that for the heights comparable with acoustic boundary layer thickness, viscous effects begin to play a larger role. There is a plenty of purely viscous approaches. The absence of inertia terms is beneficial in terms of analysis. In some particular cases, it allows exact analytical description of flow in a domain with distributed velocity on the border [10]. However, the most wide-spread method is based on lubrication theory. In particular, this theory was used in the works [4,5] for lifting force estimation. The papers [12–14] also discuss this matter in greater detail. Unfortunately, the lubrication theory is limited to very small levitation heights.

Direct numerical simulation is more accurate. There are many computational methods for wave propagation in a medium (i.e. one is based on the cellular automation rules [11]). However, the most studied are mesh-based methods, such as finite differences or finite element methods. The paper [15] suggests a numerical scheme which gives results in good agreement with those obtained experimentally. A similar study was carried out in [16]. These papers also show that simplified approaches, e.g. purely acoustic and purely viscous, are much less accurate than numerical solution; however, the latter requires enormous computation resources.

The present paper suggests a new semi-analytical approach which allows one to resolve both inertial (acoustic) and viscous effects. The implemented model covers a wide range of levitation distances but remains computationally easy.

The next section describes the problem and gives basic equations of fluid dynamics. In section 3, the governing equations are derived. We sequentially carry out scaling analysis, asymptotic analysis and Fourier analysis. The results are discussed in the section 4, and then are summed up in conclusion.

2. Problem statement

We study the levitation of a rigid disk of radius R , as shown in the Fig. 1. Consider a flat ultrasonic transducer which vibrates with amplitude a and circular frequency ω . Displacement of the radiating face is described by:

$$H_s(t) = a \cos(\omega t). \quad (1)$$

The levitating disk is assumed to be motionless and floating at the levitation height H_0 . Then, the gap thickness is given by:

$$h(t) = H_0 - H_s(t). \quad (2)$$

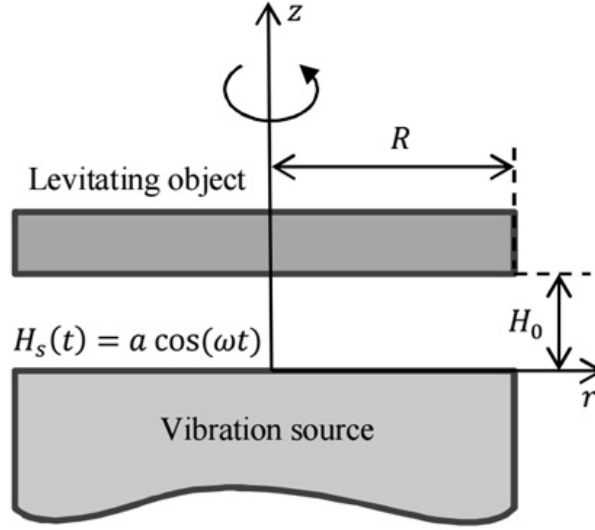


FIG. 1. Levitation of a disk

We start with basic equations of fluid dynamics (e.g. see [17]). First, we consider Navier–Stokes equations for a compressible fluid:

$$\rho(\partial_t \mathbf{v} + (\mathbf{v} \cdot \nabla) \mathbf{v}) = \nabla \cdot (-p \mathbf{I} + \boldsymbol{\tau}), \quad (3a)$$

$$\partial_t \rho + \nabla \cdot (\rho \mathbf{v}) = 0, \quad (3b)$$

where ρ is the gas density, $\mathbf{v} = (v_r, v_z)$ is the velocity vector, p is the pressure, \mathbf{I} is the unit tensor, and $\boldsymbol{\tau}$ is the viscous stress tensor given by:

$$\boldsymbol{\tau} = \mu \left[\nabla \mathbf{v} + (\nabla \mathbf{v})^T \right] + \left(\mu^b - \frac{2}{3} \mu \right) (\nabla \cdot \mathbf{v}) \mathbf{I}, \quad (4)$$

with μ for the dynamic viscosity of gas, and μ^b for the bulk viscosity.

The dynamic equations have to be accompanied by the energy equation:

$$\rho T (\partial_t s + \mathbf{v} \cdot \nabla s) = \nabla \cdot (k \nabla T) + \Phi, \quad (5)$$

where T is the temperature, s is the gas entropy, k is the thermal conductivity of the gas, and Φ describes viscous dissipation of energy:

$$\Phi = \tau_{jk} \frac{\partial v_i}{\partial x_k}.$$

In addition, the viscosity-temperature dependence is given by Sutherland's law [18]:

$$\mu = \mu_0 \left(\frac{T}{T_0} \right)^{3/2} \frac{T_0 + C}{T + C}, \quad (6)$$

where μ_0 , T_0 , C are empirical constants.

Finally, we assume that the pressure, density and temperature are connected by the ideal gas law:

$$p = \rho \frac{\mathcal{R}}{\mathcal{M}} T, \quad (7)$$

where \mathcal{R} is the universal gas constant, and \mathcal{M} is the molar mass of the gas.

The lifting force is computed by integration of σ_{zz} over the disk's surface:

$$F = - \iint (\sigma_{zz}|_{z=H}) dx_1 dx_2, \quad (8)$$

where

$$\sigma_{zz} = -p + \mu \left[2 \frac{\partial v_z}{\partial z} + \left(\mu^b - \frac{2}{3} \mu \right) \nabla \cdot \mathbf{v} \right]. \quad (9)$$

3. Governing equations

The general equations may be significantly simplified in a few steps. First, scaling analysis is performed. Doing so allows us to neglect some terms in the equations. Then, the dimension of the continuity equation is reduced by averaging it through the thickness. After that, we introduce a small parameter, the ratio of the vibration amplitude a to the gap thickness H_0 , and seek solution in the form of an asymptotic series. Finally, we focus on the stationary part of the solution, which creates time-independent lifting force. In addition, non-reflective boundary conditions are developed on the gap's edge.

3.1. Scaling analysis

We introduce dimensionless variables:

$$\begin{aligned} \tilde{r} &= \frac{r}{R}, & \tilde{z} &= \frac{z}{H_0}, & \tilde{t} &= \omega t, & \tilde{v} &= \frac{v_z}{\omega H_0}, & \tilde{u} &= \frac{v_r}{\omega R}, \\ \tilde{p} &= \frac{p}{p_0}, & \tilde{\rho} &= \frac{\rho}{\rho_0}, & \tilde{\mu} &= \frac{\mu}{\mu_0}, & \tilde{s} &= \frac{s}{c_v}, & \tilde{T} &= \frac{T}{T_0}, \end{aligned}$$

where c_v is the specific heat capacity at constant volume, and p_0 , ρ_0 , μ_0 , T_0 are pressure, density, viscosity, and temperature at normal conditions.

The developed theory relies on the following assumptions:

- the gap thickness is much smaller than the acoustic wavelength;
- the gap thickness is much smaller than its length;
- the vibration amplitude is much smaller than the gap thickness.

For ultrasonic near-field levitation, the typical gap thickness is 20–400 μm , acoustic wavelength at 20 kHz is about 2 cm, and the disk radius is 1–10 cm; the vibration amplitude varies in the range 1–10 μm . Therefore, the first two assumptions always hold. The third one will be used to introduce a small parameter.

The given assumptions allow significant simplification of the governing equations. First, the energy equation (5) is reduced to the adiabatic relation:

$$\tilde{\rho} = \tilde{p}^{1/\gamma}. \quad (10)$$

Using the ideal gas law (7) and viscosity-temperature dependence (6), one expresses viscosity in terms of pressure.

The dynamic equations (3a)–(3b) take simpler form as well:

$$\partial_{\tilde{z}} \tilde{p} = 0, \quad (11a)$$

$$\gamma K^2 \tilde{\rho} (\partial_{\tilde{t}} \tilde{u} + (\tilde{u} \partial_{\tilde{r}} \tilde{u} + \tilde{v} \partial_{\tilde{z}} \tilde{u})) = -\partial_{\tilde{r}} \tilde{p} + \Sigma \partial_{\tilde{z}} (\tilde{\mu} \partial_{\tilde{z}} \tilde{u}), \quad (11b)$$

$$\partial_{\tilde{t}} \tilde{\rho} + \tilde{\nabla} \cdot (\tilde{\rho} \tilde{\mathbf{v}}) = 0, \quad (11c)$$

where $K^2 = \omega^2 R^2 \gamma^{-1} \rho_0 / p_0$ is the squared dimensionless acoustic wavenumber, and $\Sigma = \mu_0 \omega R^2 / (p_0 H_0^2)$ is the so-called squeeze number.

The equation (11a) implies constant pressure across the gap. Together with (10), (7), (6) it results in z -independence of density, temperature, and viscosity.

There are no-slip boundary conditions on the sound source's and disk's surfaces:

$$\tilde{u}|_{\tilde{z}=\tilde{H}_s} = \tilde{u}|_{\tilde{z}=1} = 0, \quad (12a)$$

$$\tilde{v}|_{\tilde{z}=\tilde{H}_s} = -\partial_{\tilde{t}} \tilde{h} = -a/H_0 \sin(\tilde{t}), \quad \tilde{v}|_{\tilde{z}=\tilde{H}} = 0. \quad (12b)$$

Further, we will omit tilde over the dimensionless variables.

In addition, it is convenient to average the continuity equation (11c) across the gap:

$$\frac{\partial}{\partial t} (\rho h) + \frac{1}{r} \frac{\partial}{\partial r} (r \rho h \bar{u}) = 0, \quad (13)$$

where the gap-averaged velocity is:

$$\bar{u} = \frac{1}{h} \int_{H_s}^1 u dz. \quad (14)$$

3.2. Asymptotic analysis

We introduce the small parameter $\varepsilon = a/H_0$ – ratio of the vibration amplitude to the average gap thickness. The solution is sought in the form of asymptotic series:

$$\begin{aligned}\rho &= 1 + \varepsilon\rho^{(1)} + \varepsilon^2\rho^{(2)} + O(\varepsilon^3), & p &= 1 + \varepsilon p^{(1)} + \varepsilon^2 p^{(2)} + O(\varepsilon^3), \\ \mu &= 1 + \varepsilon\mu^{(1)} + \varepsilon^2\mu^{(2)} + O(\varepsilon^3), & u &= 0 + \varepsilon u^{(1)} + \varepsilon^2 u^{(2)} + O(\varepsilon^3), \\ & & v &= 0 + \varepsilon v^{(1)} + \varepsilon^2 v^{(2)} + O(\varepsilon^3), \\ & & h &= 1 + \varepsilon h^{(1)}(t), \quad h^{(1)}(t) = -\cos(t).\end{aligned}$$

The equations (10) and (6) give expressions for the density terms:

$$\rho^{(1)} = \frac{1}{\gamma} p^{(1)}, \quad \rho^{(2)} = \frac{1}{\gamma} p^{(2)} - \frac{\gamma-1}{2\gamma^2} (p^{(1)})^2, \quad (15)$$

and the viscosity term:

$$\mu^{(1)} = \frac{(\gamma-1)T_0 + 3C}{2\gamma} \frac{T_0 + 3C}{T_0 + C} p^{(1)} = Mp^{(1)}. \quad (16)$$

Since we focus on the steady levitation process, it is natural to look for solution in the form of the Fourier series:

$$p^{(m)} = \sum_{n=1}^{\infty} p_n^{(m)} e^{int}, \quad u^{(m)} = \sum_{n=1}^{\infty} u_n^{(m)} e^{int}, \quad (17)$$

$$h^{(1)} = \sum_{n=1}^{\infty} h_n^{(1)} e^{int} = -\cos(t) = -\frac{1}{2} (e^{it} + e^{-it}). \quad (18)$$

Substituting these expressions into the equations above we get the system on the coefficient of the Fourier series (17). The first order gives non-trivial solution only for the terms with numbers $n = \pm 1$. However, the time-averaged lifting force is zero. Therefore, a second-order solution is required. In order to compute the time-averaged lifting force, it is enough to study only zero-harmonic solution of the second-order problem.

The final governing equations which describe fluid flow in the gap are listed below. First-order continuity equation has the form:

$$\frac{i}{\gamma} p_1^{(1)} + \frac{1}{r} \frac{\partial}{\partial r} (r\bar{u}) = \frac{i}{2}. \quad (19)$$

It is equipped with non-reflective boundary condition on pressure on the edge of the gap. This condition allows propagation of outgoing acoustic waves outside the gap:

$$\partial_r p_1^{(1)} \Big|_{r=1} = iK p_1^{(1)}. \quad (20)$$

The momentum equation with its boundary conditions are written as:

$$i\gamma K^2 u_1^{(1)} = -\partial_r p_1^{(1)} + \Sigma \partial_{zz}^2 u_1^{(1)}, \quad (21a)$$

$$u_1^{(1)} \Big|_{z=0} = 0, \quad u_1^{(1)} \Big|_{z=1} = 0, \quad (21b)$$

$$\bar{u}_1^{(1)} = \int_0^1 u_1^{(1)} dz, \quad (21c)$$

and the transversal velocity is given by:

$$v_1^{(1)} = \frac{i}{2} - \int_0^z \left(\frac{i}{\gamma} p_1^{(1)} + \frac{1}{r} \frac{\partial}{\partial r} (r u_1^{(1)}) \right) dz'. \quad (22)$$

The second-order equations for time-averaged (zero harmonic) values are the following. The continuity equation with the pressure boundary condition are

$$\frac{1}{r} \frac{\partial}{\partial r} (r \bar{u}_0^{(2)} + r [(p^{(1)}/\gamma - h^{(1)}) \bar{u}^{(1)}]_0) = 0, \quad (23a)$$

$$p_0^{(2)} \Big|_{r=1} = 0, \quad (23b)$$

and velocity can be found from:

$$iK^2 \left[np_n^{(1)} u_{-n}^{(1)} \right]_0 + \gamma K^2 \left[u^{(1)} \partial_r u^{(1)} + v^{(1)} \partial_z u^{(1)} \right]_0 = -\partial_r p_0^{(2)} + \Sigma \left(\partial_{zz}^2 u_0^{(2)} + M \left[p^{(1)} \partial_{zz}^2 u^{(1)} \right]_0 \right), \quad (24a)$$

$$u_0^{(2)} \Big|_{z=0} = \left[h^{(1)} \partial_z u^{(1)} \right]_0, \quad u_0^{(2)} \Big|_{z=1} = 0, \quad (24b)$$

$$\bar{u}_0^{(2)} = \int_0^1 u_0^{(2)} dz - \left[h^{(1)} \bar{u}^{(1)} \right]_0, \quad (24c)$$

where $[\cdot]_0$ denotes zero harmonic of the expression (e.g. $\left[\left(p^{(1)} \right)^2 \right]_0 = p_1^{(1)} p_{-1}^{(1)} + p_1^{(-1)} p_1^{(1)}$).

The first-order equations (19), (21a) with the boundary conditions (20), (21b) are solved first. Then, one can calculate the transversal velocity (22). Substituting the first-order solution into the second-order equations: (23a), (24a) with the boundary conditions (23b), (24b), one obtains the time-averaged pressure.

Finally, the total lifting force can be calculated as:

$$F_0 = -2\pi \int \sigma_{zz} \Big|_{z=1} r dr = 2\pi \int p_0^{(2)} r dr. \quad (25)$$

4. Results and discussion

The governing equations show that there are two mechanisms of ultrasonic near-field levitation: inertial (acoustic) and viscous. Their intensity is described by the wavenumber K and squeeze number Σ respectively. The ratio of γK^2 to Σ , which is included into equations (21a), (24a), is proportional to squared ratio of the gap thickness to the acoustic boundary layer thickness:

$$\Pi = \frac{\gamma K^2}{\Sigma} = \frac{H_0^2 \omega \rho_0}{\mu_0} = 2 \left(\frac{H_0}{\delta} \right)^2, \quad (26)$$

where $\delta = \sqrt{2\mu_0/(\omega\rho_0)}$ is the boundary layer thickness [17]. Its value is $\delta \approx 15$ μm in the case of air and 20 kHz vibration frequency. When the gap is large, $\Pi \gg 1$, inertial effects are more important and acoustic models can be used; otherwise, when the gap is smaller than boundary layer, $\Pi \ll 1$, viscous effects dominate and viscous models are applicable. For intermediate regimes, $\Pi \approx 1$, both effects are important, and the presented model resolves them.

The obtained equations were solved by FEM in COMSOL Multiphysics software.

Figure 2 shows the comparison of the presented approach with a full numerical simulation and experimental data from the work [15]. The agreement is very good. However, our model requires the solution of 5 linear time-independent PDEs which is much easier computationally than direct simulation based on the general fluid dynamics equations.

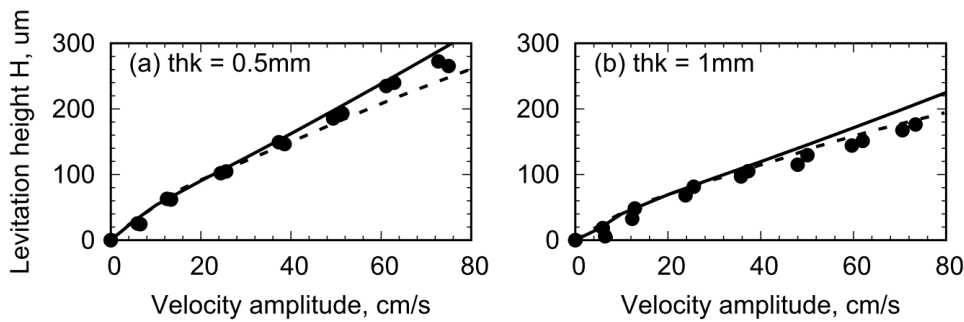


FIG. 2. Levitation height as a function of velocity of vibrating face. Disk radius 20 mm, disk thickness $d = 0.5 - 1$ mm, frequency 19.5 kHz. Solid lines denote the presented model; dashed line corresponds to numerical results of [15]; dots represent experimental data from [15]

5. Conclusion

We presented a new approach for modeling of ultrasonic near-field levitation. In comparison to existing analytical works, our method covers a wide range of levitation distances and resolves both viscous and acoustic effects. However, it remains computationally simple in contrast to straightforward numerical simulation.

Our approach allows us to distinguish three regimes of levitation: viscous one for small levitation heights; acoustic one for large levitation distances; and intermediate visco-acoustic for moderate heights.

The model was successfully validated against published modeling and experimental results.

Acknowledgements

This work was partially financially supported by the Government of the Russian Federation (grant 074-U01), by grant MK-5161.2016.1 of the President of the Russian Federation, by grant 16-11-10330 of Russian Science Foundation.

References

- [1] Salbu E.O.J. Compressible Squeeze Films and Squeeze Bearings. *Journal of Basic Engineering, ASME*, 1964, **86**, P. 355–364.
- [2] Hashimoto Y., Koike Y., Ueha S. Near-field acoustic levitation of planar specimens using flexural vibration. *The Journal of the Acoustical Society of America*, 1996, **100**, P. 2057–2061.
- [3] Hashimoto Y., Koike Y., Ueha S. Transporting objects without contact using flexural traveling waves. *The Journal of the Acoustical Society of America*, 1998, **103**, P. 3230–3233.
- [4] Yoshimoto S., Anno Y., Sato Y., Hamanaka K. Float Characteristics of Squeeze-Film Gas Bearing with Elastic Hinges for Linear Motion Guide. *JSME International Journal Series C*, 1997, **40**, P. 353–359.
- [5] Yoshimoto S., Kobayashi H., Miyatake M. Float characteristics of a squeeze-film air bearing for a linear motion guide using ultrasonic vibration. *Tribology International*, 2007, **40**, P. 503–511.
- [6] Lord Rayleigh. On the pressure of vibrations *Philosophical Magazine Series 6*, 1902, **3**, P. 338–346.
- [7] Lord Rayleigh. On the momentum and pressure of gaseous vibrations, and on the connexion with the virial theorem. *Magazine Series 6*, 1905, **10**, P. 364–374.
- [8] Chu B.-T., Apfel R.E. Acoustic radiation pressure produced by a beam of sound. *The Journal of the Acoustical Society of America*, 1982, **72**, P. 1673–1687.
- [9] Lee C.P., Wang T.G. Acoustic radiation pressure. *The Journal of the Acoustical Society of America*, 1993, **94**, P. 1099–1109.
- [10] Makeev I.V., Popov I.Yu. Steady Stokes flow between confocal semi-ellipses. *Nanosystems: Phys. Chem. Math.*, 2016, **7** (2), P. 324–331.
- [11] Yamazaki Y., Ohmori S. Ultradiscretization of reaction-diffusion type partial differential equations exhibiting pulse propagation. *Nanosystems: Phys. Chem. Math.*, 2017, **8** (1), P. 38–41.
- [12] Minikes A., Bucher I. Coupled dynamics of a squeeze-film levitated mass and a vibrating piezoelectric disc: numerical analysis and experimental study. *Journal of Sound and Vibration*, 2003, **263**, P. 241–268.
- [13] Minikes A., Bucher I., Haber S. Levitation force induced by pressure radiation in gas squeeze films. *The Journal of the Acoustical Society of America*, 2004, **116**, P. 217–226.
- [14] Ilssar D., Bucher I. On the slow dynamics of near-field acoustically levitated objects under High excitation frequencies. *Journal of Sound and Vibration*, 2015, **354**, P. 154–166.
- [15] Nomura H., Kamakura T., Matsuda K. Theoretical and experimental examination of near-field acoustic levitation. *The Journal of the Acoustical Society of America*, 2002, **111**, P. 1578–1583.
- [16] Minikes A., Bucher I. Comparing numerical and analytical solutions for squeeze-film levitation force. *Journal of Fluids and Structures*, 2006, **22**, P. 713–719.
- [17] Landau L.D., Lifshitz E.M. *Fluid Mechanics*, 2nd ed., Vol. 6, Pergamon Press, Oxford, 1987, 532 p.
- [18] Sutherland W. The viscosity of gases and molecular force. *Philosophical Magazine Series 5*, 1893, **36**, P. 507–531.

Correlation between structure and resistance of composites based on polystyrene and multilayered graphene oxide

M. N. Nikolaeva¹, T. D. Anan'eva¹, A. N. Bugrov^{1,2}, A. T. Dideikin³, E. M. Ivankova^{1,3}

¹Institute of macromolecular compounds RAS, Bolshoy pr. 31, 199004 St. Petersburg, Russia

²Saint Petersburg Electrotechnical University "LETI",
ul. Professora Popova 5, 197376 St. Petersburg, Russia

³Ioffe Institute RAS, Polytechnicheskaya ul., 26 St. Petersburg, 194021, Russia

marianna_n@mail.ru, anthracene@hq.macro.ru, alexander.n.bugrov@gmail.com, dideikin@mail.ioffe.ru,
elena.Ivankova@mail.ioffe.ru

PACS 36.20.-r; 68.65.Pq; 71.20.Rv; 72.80. Tm; 74.78.-w, 68.37.Hk, 73.40.-c

DOI 10.17586/2220-8054-2017-8-2-266-271

The correlation between the structure, resistance and UV-irradiation impact on conductivity of polystyrene-based composites with multilayered graphene oxide flakes was observed. It is established that composites structure and conducting properties depend on concentration, surface modification and the methods by which graphene oxide was incorporated into the polystyrene matrix.

Keywords: graphene oxide flakes, polystyrene, composite, conductivity, UV-irradiation.

Received: 3 February 2017

Revised: 24 February 2017

1. Introduction

It is known polymer/graphene nanocomposites show superior electrical properties in comparison to unfilled polymers [1–4], so the conductivity level for polystyrene/graphene nanocomposites can reach even more than $20 \text{ S}\cdot\text{m}^{-1}$ [4]. Moreover, recent experimental observations demonstrate that the graphene-based composite synthesized in [5] displays superconducting features at temperatures higher than that of liquid helium and even in the structures Cu/Graphene-based composite/Cu [6, 7] without superconducting electrodes. Since graphene is a monolayer of graphite, it is important to compare the electrical properties of graphene with those of graphite. To date, a significant number of indirect experiments indicating the existence of a superconducting state up to room temperature in graphite-based compounds have been reported [8–12]. The main problem of these indirect observations lies in the fact that the superconducting regions occupy only a small areas of carbon materials, and for this reason, the observable effects of superconductivity are negligible in bulk samples [9]. Evidence for superconductivity in graphite lamellae at temperatures above 150 K has been demonstrated in [13]. Considering graphene, the classical theory of superconductivity does not predict the occurrence of intrinsic superconductivity in such low-dimensional structure without doping. To promote intrinsic superconductivity in graphene, the authors of [14] suggested reconstructing the electronic density of states by inducing elastic deformations. The strain field in graphene can probably be created by introducing it into a polymer host material [6] when chemical bonds are formed between the graphene and polymer. In this case, one can expect graphene flakes with a variety of different deformations. These specific deformations of graphene may be the reason of superconducting state in graphene-based polymer composites.

The aim of this work was to determine why high conductivity and superconductivity arise in polystyrene (PS)-based films with graphene oxide flakes (GF). Polystyrene was used as a polymer matrix because electrization is most expressed in polymers with high resistivity [15, 16]. Multilayered GF after heat treatment in an aqueous medium [17] becomes semiconductor and can even have a zero bandgap. After special treatment, GF may copolymerize with styrene [5].

2. Experimental

The methods, described in [17, 18] was used for GF production. Natural crystalline graphite was used as a starting material. After series of chemical reactions in liquid medium, the prepared GF was extracted from an aqueous suspension by aerobic drying at a room temperature. As a result, multilayered GF were obtained (Fig. 1). Surface modification of the GF was carried out by treating 3-(trimethoxysilyl)propyl methacrylate (TMPMA) for subsequent reaction with styrene [5, 19]. Polystyrene and polymer-GF composites ((PS/TMPMA/GF)^{syn} and (PS/GF)^{syn}) were synthesized by free radical polymerization in solution [5]. In order to produce the composites, 3 ampoules were used and 19.5 mg of 2,2'-azobis(2-methylpropionitrile) (AIBN) was dissolved in 4 ml mixture of styrene and toluene (1:1 by volume). The prepared solution (1 ml) was dispensed into each ampoule containing 4.8 mg (1 wt.%), 4.8 mg (1 wt.%) and 14 mg (3 wt.%) of functionalized GF correspondingly. Then ampoules were purged with argon for 10 min and sealed, after that the ampoules were sonicated for 0.5 hour. Polymerization was carried out for 28 hours at 70°C. Polystyrene was prepared in an analogous manner. Polymer yield was 70 %. Molecular mass average weight of synthesized polystyrene was determined using viscosimetry method and formulae from [19] as 50000. These composites were also obtained by mechanical mixing of PS with GF and PS with functionalized GF: (PS/GF)^{mix} and (PS/TMPMA/GF)^{mix}.

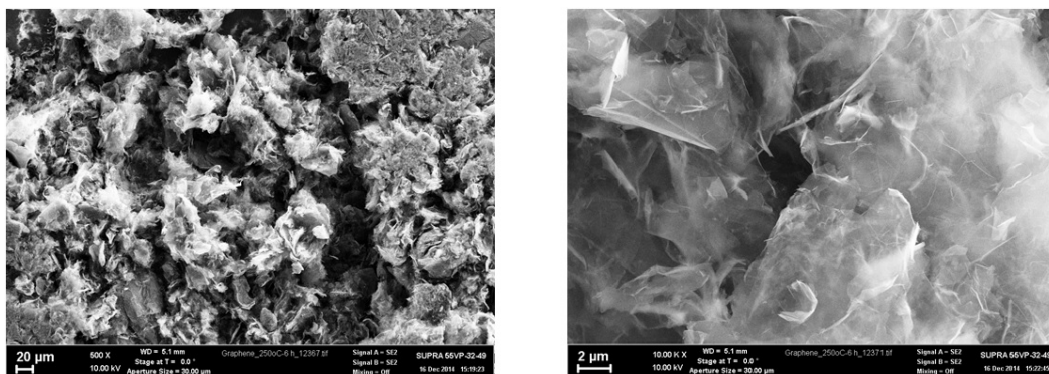


FIG. 1. SEM images of graphene oxide flakes

The distribution and agglomeration of GF particles in a polystyrene matrix was investigated by Zeiss Supra 55VP field emission scanning electron microscope (Germany). Cross sections of polystyrene-GF films for SEM investigation were prepared by cryofracture in liquid nitrogen.

Films of the polymer composite were deposited on copper electrodes through the dispenser by casting from the 1 wt.% solution. Thickness of the films was controlled by the interference microscope using the method described in [20–22]. Current-voltage characteristics of the metal-composite-metal structures were obtained by the modified two-probe method. The area of electrodes was 1 cm². Measurements were carried out at the pressure not higher than 1 kg/cm². The resistive nature of obtained current-voltage characteristics exclude the presence of a breakdown in films which have been investigated.

UV- irradiation of the composite films was performed by full spectrum of Hg-lamp DKB-9 with energy 220 kW and having effective wavelength range of 185–270 nm.

3. Results and discussion

The surfaces of polystyrene films are rather smooth, even for very thin films. The surface of polystyrene films without graphene oxide is presented in Fig. 2a,b. The conductivity of polystyrene films for was observed only on thickness not higher than 0.02 μm. Surface topographies of (PS/GF) mix film cleavages are presented in Fig. 2c,d. For (PS/GF)^{syn} and (PS/TMPMA/GF)^{mix}, SEM images are similar. As revealed by SEM (Fig. 2f,g) in the case of the (PS/TMPMA/GF)^{syn} composite with 1 wt.% of GF, the inclusions of GF are distributed rather evenly in the polystyrene matrix obviously due to the formation of chemical bonds between the graphene and polystyrene. For the mechanically-mixed (PS/TMPMA/GF)^{mix} and composite with 3 wt.% of functionalized GF (PS/TMPMA/GF-3)^{syn}, the GF particles are not distributed in significant amount on the surface of the composite film (Fig. 2c,d,h,i). Therefore, the conductivity values for these films do not increase significantly compared to pure polystyrene, as it can be seen from current-voltage characteristics (Fig. 3). Apparently, GF particles in (PS/TMPMA/GF)^{mix}, (PS/GF)^{mix} and (PS/GF)^{syn} composites have a large chemical affinity for the polymer

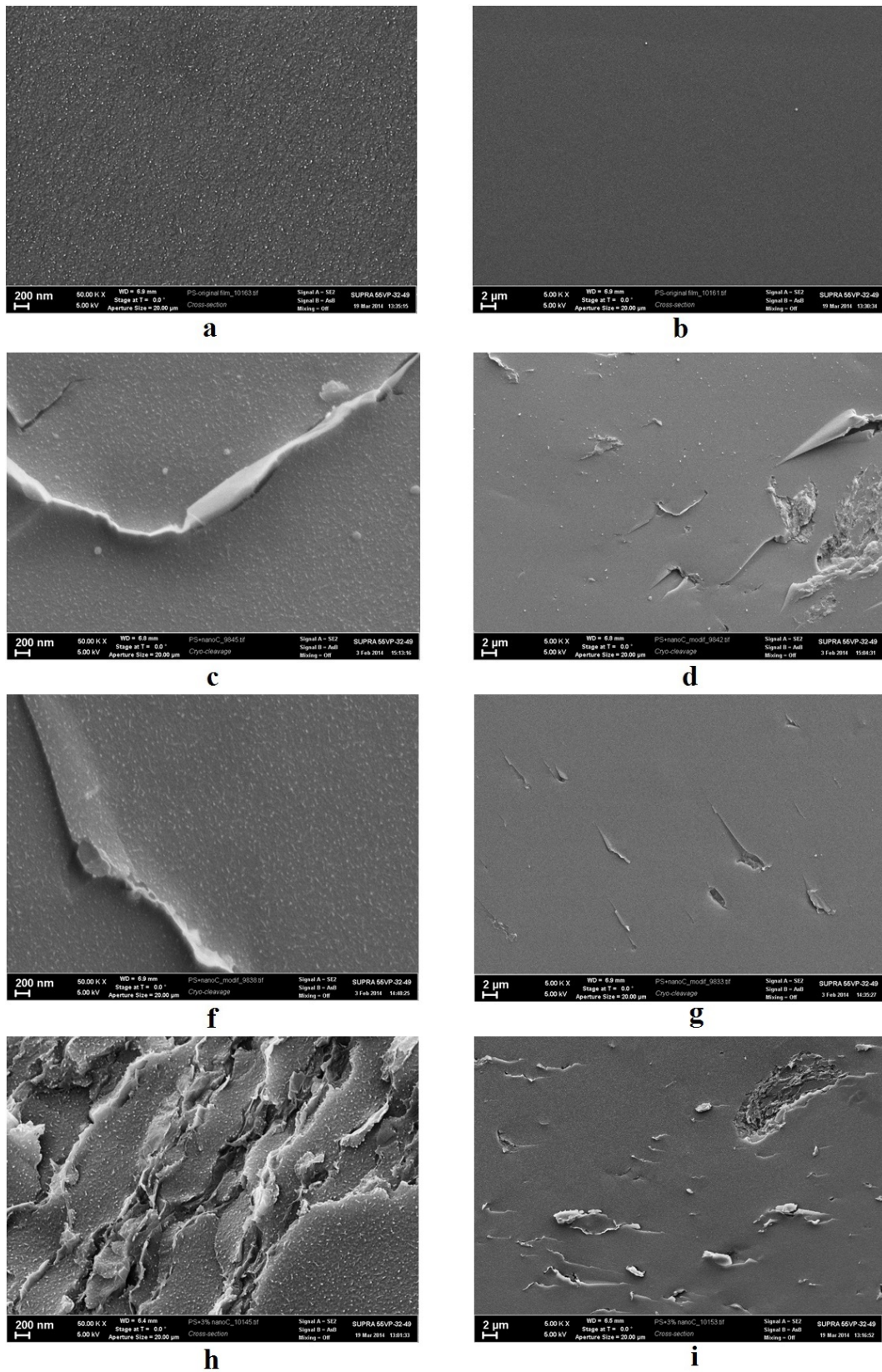


FIG. 2. SEM images of the polystyrene (a, b), (PS/GF)^{mix} (c, d), (PS/TMPMA/GF)^{syn} (f, g), (PS/TMPMA/GF-3)^{syn} (h, i) films

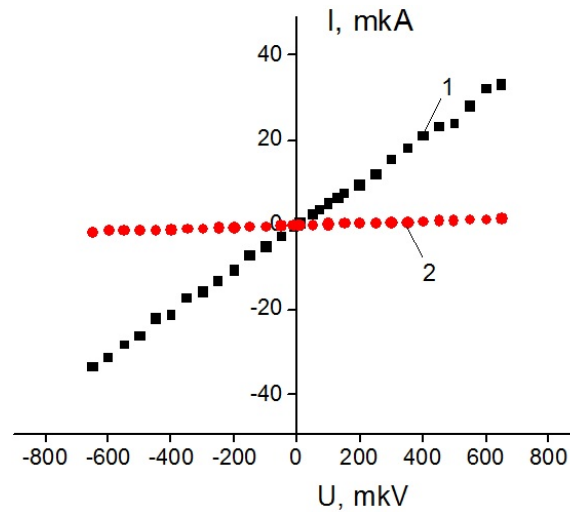


FIG. 3. Typical current-voltage characteristics for Cu/GF composite/Cu systems, 1 – for $(\text{PS}/\text{TMPMA}/\text{GF})^{\text{syn}}$ and 2 – for $(\text{PS}/\text{GF})^{\text{syn}}$, films thickness $2 \mu\text{m}$

matrix of polystyrene and are preferentially immersed in it completely, simultaneously leaving defects on the polymer surface. Films of $(\text{PS}/\text{GF})^{\text{mix}}$ demonstrate random GF inclusions on the surface which are fully covered by polystyrene (Fig. 2c,d). The surface topography of $(\text{PS}/\text{TMPMA}/\text{GF}-3)^{\text{syn}}$ at the same time drastically changes from that of others composites' surfaces probably due to the excess of GF which did not form covalent bonds with polystyrene matrix completely and directed to agglomeration under van der Waals forces. For the case of composites $(\text{PS}/\text{GF})^{\text{syn,mix}}$ as also for $(\text{PS}/\text{TMPMA}/\text{GF})^{\text{mix}}$, conductivity was low as it can be seen from current-voltage characteristics (Fig. 3, curve 2). It is worth noting that the GF concentration rise in $(\text{PS}/\text{TMPMA}/\text{GF})^{\text{syn}}$ (from 1 to 3 wt.%) significantly increased films resistance up to values of tens of $\text{k}\Omega$ as it was for $(\text{PS}/\text{TMPMA}/\text{GF})^{\text{mix}}$, $(\text{PS}/\text{GF})^{\text{mix}}$ and $(\text{PS}/\text{GF})^{\text{syn}}$ composites. To the contrary as it was shown earlier [19], composite films $(\text{PS}/\text{TMPMA}/\text{GF})^{\text{syn}}$ with thickness less than $3 \mu\text{m}$ conduct electric current and for $(\text{PS}/\text{TMPMA}/\text{GF})^{\text{syn}}$ ohmic behavior of current-voltage characteristic is observed indicating a metallic type of conductivity.

Observations of the composites' SEM images and their resistance values show that in fact the systems under considerations could be divided into 3 categories: 1) polystyrene, 2) $(\text{PS}/\text{TMPMA}/\text{GF})^{\text{syn}}$ and 3) $(\text{PS}/\text{TMPMA}/\text{GF})^{\text{mix}}$, $(\text{PS}/\text{GF})^{\text{mix}}$, $(\text{PS}/\text{GF})^{\text{syn}}$, $(\text{PS}/\text{TMPMA}/\text{GF}-3)^{\text{syn}}$. So we can suppose resistance of composite films is dependent on composites structure and consequently on surface topography. The preparation methods of composites obviously also have an influence on the formation of films' surface. Composite $(\text{PS}/\text{TMPMA}/\text{GF})^{\text{syn}}$ with low resistance demonstrates specific distribution of GF on films surface that substantiate the formation of chemical bonds between styrene and GF during synthesis. Obviously in this case, the chemical bonds formed between GF and PS prevent mutual adhesion of graphene sheets and create substantial stretches and deformations for erasing high conductivity. The scheme of GF modification and evident chemical reaction with styrene is shown in Fig. 4.

After that, measurements of resistance of GF composites films were performed before and after UV-irradiation. UV-irradiation was carried out for 2 hours for films of $2 \mu\text{m}$ thickness. The resistance was lowered by 1 order of magnitude for composites $(\text{PS}/\text{TMPMA}/\text{GF})^{\text{syn}}$, being reduced from 20 to 2Ω . This result correlates with measurements of resistance for UV-irradiated graphite in [23]. For $(\text{PS}/\text{GF})^{\text{syn,mix}}$, $(\text{PS}/\text{TMPMA}/\text{GF})^{\text{mix}}$ as for individual GF, the influence of UV-irradiation on films' resistance has not been observed. Resistance value remained unchanged and was near $30 \text{ k}\Omega$ for $(\text{GF}/\text{PS})^{\text{mix,syn}}$ and $(\text{PS}/\text{TMPMA}/\text{GF})^{\text{mix}}$ composites. This effect can be explained as the impact of UV-irradiation on GF directly when some edges of GF are situated on films' surface as in the case of $(\text{PS}/\text{TMPMA}/\text{GF})^{\text{syn}}$.

These above-presented results for $(\text{PS}/\text{TMPMA}/\text{GF})^{\text{syn}}$ can be explained by the formation of covalent bonds firmly holding GF particles in given positions; then some edges of the GF are distributed on the surface of polystyrene film. Additionally, during the synthesis and formation of covalent bonds between the polystyrene and GF special mechanical stresses can be created. As known, they contribute to the emergence of superconductivity [6, 7], predicted for graphite [8–12].

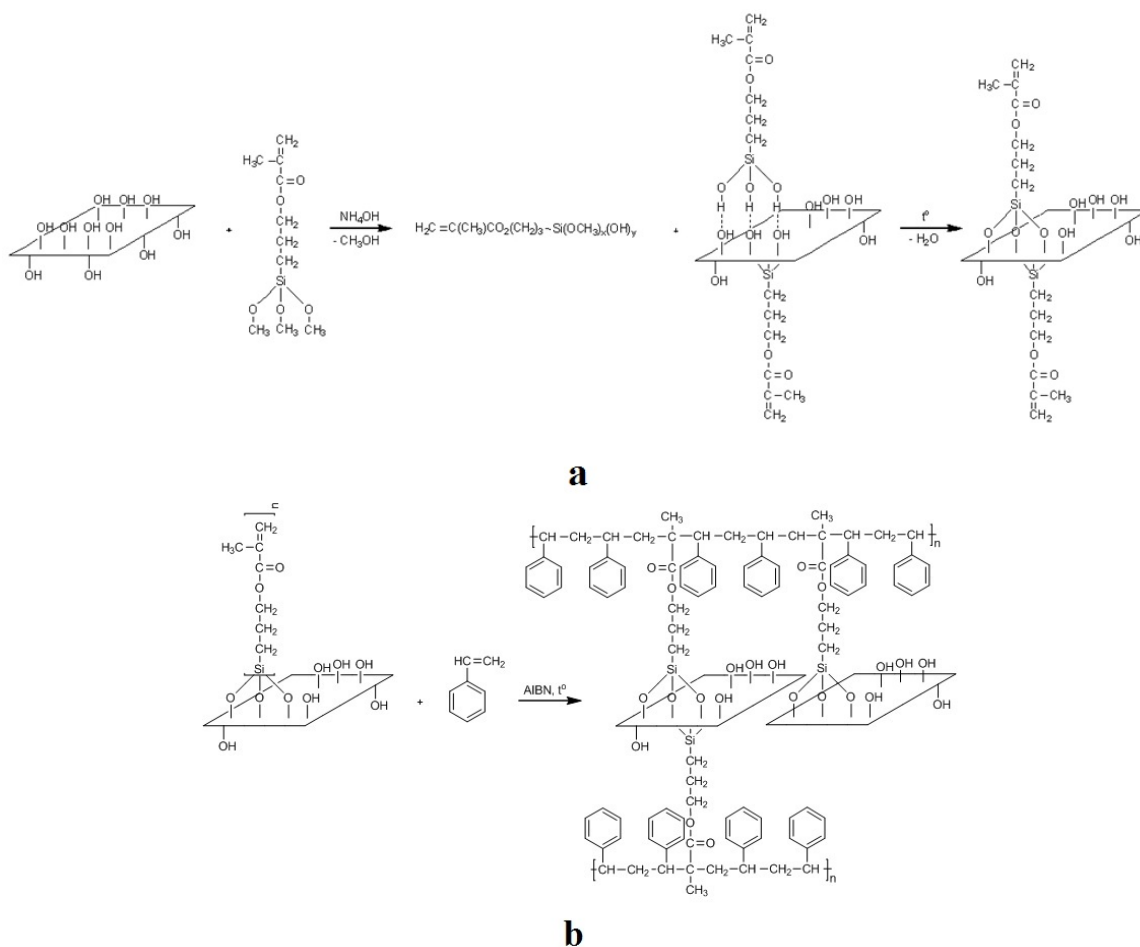


FIG. 4. Procedure of GF surface modification (a) and subsequent synthesis with styrene (b)

4. Conclusions

The differences in the conductivity of composites based on polystyrene with chemically bonded and unbonded GF have been determined. The films of $(\text{PS}/\text{TMPMA}/\text{GF})^{\text{syn}}$ composite with chemically bonded GF showed metallic type conductivity and demonstrated low resistance up to $2 \mu\text{m}$ thickness. All other composite films had rather high resistance because of lack of conducting GF particles on the surface. Thus, a correlation between the structure of the films and conductive properties was observed. The influence of UV-radiation exposure on the composite films was also found for $(\text{PS}/\text{TMPMA}/\text{GF})^{\text{syn}}$, where the direct absorption of radiation by graphene flakes is possible.

References

- [1] Stankovich S., Dikin D.A., et. al. Graphene-based composite materials. *Nature*, 2006, **442**(7100), P. 282–288.
- [2] Eda G., Chhowalla M. Graphene-based composite thin films for electronics. *Nano Lett.*, 2009, **9**(2), P. 814–822.
- [3] Abramov D., Arakelian S., et al. Interaction of femtosecond laser radiation with carbon materials: exfoliation of graphene structures and synthesis of low-dimensional carbon structures. *Nanosystems: Physics, Chemistry, Mathematics*, 2016, **7**(1), P. 220–225.
- [4] Deepak A., Shankar P. Exploring the properties of lead oxide and tungsten oxide based graphene mixed nanocomposite films. *Nanosystems: Physics, Chemistry, Mathematics*, 2016, **7**(3), P. 502–505.
- [5] Nikolaeva M.N., Bugrov A.N., et al. Conductive properties of the composite films of graphene oxide based on polystyrene in a metal-polymer-metal structure. *Russ. J. Appl. Chem.*, 2014, **87**(8), P. 1151–1155.
- [6] Ionov A.N. Josephson current-voltage characteristic of a composite based on polystyrene and graphene oxide. *Tech. Phys. Lett.*, 2015, **41**(7), P. 651–653.
- [7] Ionov A.N. Josephson-like behaviour of the current-voltage characteristics of multi-graphene flakes embedded in polystyrene. *J. Low Temp. Phys.*, 2016, **182**(3/4), P. 107–114.
- [8] Antonowicz K. Possible superconductivity at room temperature. *Nature*, 1974, **247**(5440), P. 358–360.
- [9] Esquinazi P., Garcia N., et. al. Indications for intrinsic superconductivity in highly oriented pyrolytic graphite. *Phys. Rev. B.*, 2008, **78**(13), P. 134516(1–8).

- [10] Scheike T., Böhlmann W., et al. Can doping graphite trigger room temperature superconductivity? Evidence for granular high-temperature superconductivity in water-treated graphite powder. *Advanced Materials*, 2012, **24**(43), P. 5826–5831.
- [11] Lebedev S.G. Evidence of Josephson-like behaviour of thin granular carbon films. *International Review of Physics*, 2008, **2**(5), P. 312–328.
- [12] Felner I., Kopelevich Y. Magnetization measurement of a possible high-temperature superconducting state in amorphous carbon doped with sulfur. *Phys. Rev. B*, 2009, **79**(23), P. 233409(1–4).
- [13] Ballestar A., Barzola-Quiquia J., et al. Josephson-coupled superconducting regions embedded at the interfaces of highly oriented pyrolytic graphite. *New J. Phys.*, 2013, **15**(5), P. 023024.
- [14] Uchoa B., Barlas Y. Superconducting states in pseudo-Landau levels of strained graphene. *Phys. Rev. Lett.*, 2013, **111**(4), P. 046604(1–5).
- [15] Lowell J., Rose-Innes A.C. Contact electrification. *Adv. Phys.*, 1980, **29**(6), P. 947–1023.
- [16] Duke C.B., Fabish T.J. Charge-induced relaxation in polymers. *Phys. Rev. Lett.*, 1976, **37**(16), P. 1075–1078.
- [17] Mikoushkin V.M., Shnitov V.V., Nikonov S.Yu., et al. Controlling graphite oxide bandgap width by reduction in hydrogen. *Tech. Phys. Lett.*, 2011, **37**(10), P. 942–945.
- [18] Aleksenskii A.E., Brunkov P.N., Dideikin A.T., et al. Single-layer graphene oxide films on a silicon surface. *Tech. Phys.*, 2013, **58**(11), P. 1614–1618.
- [19] Khairullin A.R., Nikolaeva M.N., Bugrov A.N. Resistance of the composite films based on polystyrene and graphene oxide. *Nanosystems: Physics, Chemistry, Mathematics*, 2016, **7**(6), P. 1055–1058.
- [20] Nikolaeva M., Boiko Y., Martynenkov A. Supramolecular structure and conductive properties of dielectric polymers in metal/polymer/metal systems. *Int. J. Polym. Mat.*, 2013, **62**(13), P. 706–710.
- [21] Nikolaeva M.N., Anan'eva T.D., et al. Influence of chemical structure and chain length on conducting properties of dielectric polymers in metal/polymer/metal structures. *Rus. J. Appl. Chem.*, 2013, **86**(5), P. 756–759.
- [22] Nikolaeva M.N., Martynenkov A.A., et al. Resistance of dielectric polymer films with fillers in metal-polymer-metal systems. *Rus. J. Appl. Chem.*, 2014, **87**(5), P. 646–650.
- [23] Smirnov V.A., Arbuzov A.A., Shul'ga Yu.M., et al. Photoreduction of graphite oxide. *Chemistry of high energies*, 2011, **45**(1), P. 60–64.

Error analysis in circuits building at the quantum computing platform IBM Quantum Experience

E. O. Samsonov

ITMO University, Kronverkskiy, 49, St. Petersburg, 197101, Russia

Edi.samsonov@gmail.com

PACS 03.65.Yz, 03.67.-a

DOI 10.17586/2220-8054-2017-8-2-272-276

There are many quantum computing systems, some of which are still being developed today. To develop quantum calculation systems, IBM provides access to the 5-qubit quantum computer ‘IBM Quantum Experience’. Quantum computers must deal with the loss of information due to environmental disturbances. Quantum systems cannot be completely isolated. Noise can be a cause of different errors in the quantum circuits. In this work, we observe distortions in quantum circuits and investigate the noise stability of different quantum gates. We investigate a method for calculating the quantum state of the superconducting qubit, used in ‘IBM Quantum Experience’, after an interaction with a quantum operator.

Keywords: quantum computing, quantum information, IBM Quantum Experience, distortions of quantum circuits.

Received: 14 January 2017

Revised: 18 February 2017

1. Introduction

Quantum systems have interactions with the environment. These interactions are presented as noise in quantum computing systems. The loss of information due to environmental disturbances is termed decoherence [1]. We need to develop an understanding of these noise processes so that they may be better controlled.

The evolution of the quantum system is considered in [2,3]. For different types of quantum computing systems, there are several ways to increase the system stability with respect to the effect of noise. Interactions between superconducting quantum systems, used in ‘IBM Quantum Experience’, and the most significant sources of noise, are investigated in [4–7]. The effect of noise in quantum circuits is considered in [8–10]. The errors may result in distortions of quantum algorithms. Research on the Grover’s algorithm stability with respect to perturbations of quantum logic circuit elements is represented in [11]. Quantum computers use quantum error correction to protect information from decoherence errors and other quantum noise. Quantum error correction is considered in [8, 10].

In this work, we use an open access to the ‘IBM Quantum Experience’ computer [12], to investigate distortions of quantum circuits. This gives us the opportunity to observe known quantum circuits with respect to noise. Various circuits can be used for implementation of the same quantum gate. We consider different circuits for implementation of the same well-known quantum single-qubit and two-qubit gates, such as NOT and CNOT. Also, we investigate the NOT gate and two types of controlled NOT gate, such as CNOT and ‘Toffoli’ gates with respect to noise stability.

A superconducting qubit called ‘transmon’ is used in ‘IBM Quantum Experience’ [4]. We investigate a method for calculating the quantum state of this superconducting qubit after interaction with the quantum operator, which includes a source of noise. Thus, we can calculate the quantum state without using the quantum computer and investigate the qubit with respect to noise stability.

2. Quantum circuits

A graphical user interface for programming a quantum processor in ‘IBM Quantum Experience’ is ‘Quantum Composer’ [12]. There are single-qubit gates in ‘Quantum Composer’, such as Pauli operators and Clifford operators. Also, it contains a two-qubit gate CNOT. We will consider different circuits for implementation of the same X gate, which is equivalent to a classical NOT, and different circuits for implementation of the same CNOT gate.

The single-qubit X gate is a Pauli operator, which represents bit-flip. The X gate is represented in the library of ‘Quantum Composer’. If the initial state is $|0\rangle$, after an interaction with the X gate, the probability of the expected state $|1\rangle$ is 0.976. We can observe that there are some errors, which are due to noise processes in the circuit.

We can create a circuit which works like the X gate. $X = HZH$, where Z – Pauli operator, H – Hadamard gate. If the initial state is $|0\rangle$, after an interaction with this circuit for implementation of the X gate, the probability of the expected state $|1\rangle$ is 0.934.

Two different circuits for implementation of the same quantum gate with respect to the noise stability can be compared. We notice that the quantum circuit for implementation of the X gate is worse with respect to the noise stability than the X gate which is represented in the library of ‘Quantum Composer’.

The two-qubit CNOT gate functions as an exclusive OR gate in conventional digital logic. If the initial state is $|00\rangle$, after an interaction with the CNOT gate, the probability of the expected state $|00\rangle$ is 0.913. In this experiment, there are more decay channels, and there is the interaction between two qubits.

We can create a circuit for a controlled- V operation if we can find three circuits A, B, C , such that $ABC=I$ and $e^{ia}AXBXC=V$ [13]. We have added a control qubit to X gate to implement a controlled- X operation, which is an equivalent to a CNOT. For the controlled- X operation $e^{ia}AXBXC=X$, where $a = \pi/2$, the circuits A, B, C , is given by the Pauli and Clifford gates: $A=HY, B=HXT, C=T$. Combining these circuits as shown in [13], we will obtain the controlled- X gate (Fig. 1).

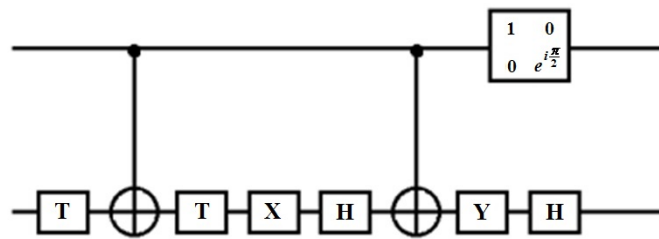


FIG. 1. Controlled- X operation

If the initial state is $|00\rangle$, after an interaction with this controlled- X gate, the probability of the expected state $|00\rangle$ is 0.901.

After this experiment, we compare different circuits for implementation of the same quantum gate with respect to the noise stability. The quantum circuit for implementation of the CNOT gate, which was created, is worse with respect to the noise stability than the CNOT gate, which is represented in the library of ‘Quantum Composer’. But we can see that the values from the second experiment approximately equal the values from the first experiment.

Also, it is interesting to investigate the NOT gate and two types of controlled NOT gates, such as CNOT and Toffoli, with respect to the noise stability.

The set of allowed connections is defined by the schematic of the device. We cannot use the known three-qubit CCNOT gate, however, we can use another circuit for implementation of the quantum three-qubit gate CCNOT. It is important to investigate this quantum circuit with respect to the noise stability. The CCNOT gate is illustrated in the Fig. 2 [8, 13].

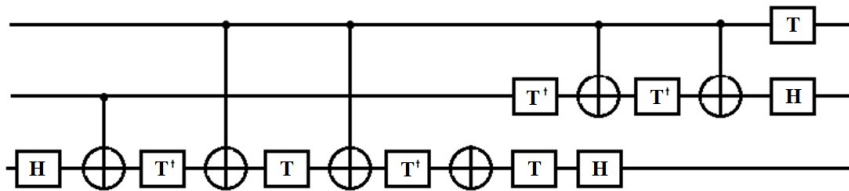


FIG. 2. Circuit for implementation of the quantum three-qubit CCNOT gate

If the initial state is $|00\rangle$, after the interaction with the circuit for implementation of the quantum three-qubit gate CCNOT gate, the expected state $|00\rangle$ is 0.746. The probability of the expected state after the X gate is 0.976, and the probability of the expected state after the CNOT gate is 0.913. We can notice a significant decrease in the noise stability of the quantum circuit for implementation of the quantum three-qubit gate.

3. Interaction with an external field

A promising type of a quantum bit is the Josephson-junctions based quantum bit. There are three types of these qubits: phase [5]; flux [6]; and charge [5, 7, 14]. These types of qubits have a great scalability, advanced

capabilities for managing states, relatively high coherence time. Such macroscopic quantum systems have been described previously [5]. The impact of the most significant sources of noise is considered in [4–7]. A new type of superconducting qubit was introduced in [4]. They proposed a superconducting qubit called a ‘transmon’. The ‘transmon’ is closely related to the ‘Cooper pair box’ qubit; it has a superconducting ‘island’ with two Josephson junctions (with Josephson energy E_j , which can be controlled by an external magnetic field) and gates capacitance, which control the charge energy E_c for one Cooper pair. If there is only one or zero Cooper pair in the ‘island’, we can get a two-level system (qubit). The Hamiltonian for this system [4,5] is given by:

$$\mathbf{H}_0 = -\frac{1}{2}B_z\sigma_z - \frac{1}{2}B_x\sigma_x, \quad (1)$$

where B_z – is determined by the charging energy E_c , B_x – is determined by the Josephson energy E_j and the magnetic field through a superconducting ring. σ_z and σ_x are the Pauli operators. The ‘transmon’ is designed to operate in a regime of significantly increased ratio of Josephson energy to the charging energy of E_j/E_c . Its charge dispersion decreases exponentially with the E_j/E_c . Analysis of the full system in [4] shows that this benefit is not compromised by the increased noise in other channels. This type of qubit is used in IBM Quantum Experience.

It is interesting to investigate the dynamics of a superconducting qubit proposed in [4]. We present a method for calculating the quantum state of this superconducting qubit, after interaction with the quantum operator which includes a source of noise.

We will observe the interaction between the qubit and the external field. The impact of the external field can change the qubit state. Firstly we consider the ideal unitary evolution, which is represented by the logical operator NOT.

Evolution of the quantum system with time is given by:

$$i\hbar \frac{\partial |\phi(t)\rangle}{\partial t} = \mathbf{H}_0 |\phi(t)\rangle. \quad (2)$$

If we integrate this equation, we get:

$$|\phi(t)\rangle = e^{-\frac{i}{\hbar}t\mathbf{H}_0} |\phi(t)\rangle. \quad (3)$$

Here, the \mathbf{H}_0 , Hamiltonian of the system with a spin 1/2 is given by (1).

Then the operator of the evolution is given by:

$$e^{-\frac{i}{\hbar}t\mathbf{H}_0} = \exp\left[\frac{i}{2\hbar}t(B_z\sigma_z + B_x\sigma_x)\right] = \mathbf{E}. \quad (4)$$

If only the external field B_x is applied to the system, \mathbf{E} will be given by:

$$\mathbf{E}(\psi) = \exp\left[\frac{itB_x\sigma_x}{2\hbar}\right] = \begin{pmatrix} \cos\frac{\psi}{2} & i\sin\frac{\psi}{2} \\ i\sin\frac{\psi}{2} & \cos\frac{\psi}{2} \end{pmatrix}, \quad (5)$$

where $\psi = B_x t/\hbar$.

In other words, we can obtain a unitary evolution. For certain B_x and t values, we can get the operator \mathbf{X} accurate to a phase factor.

There is some noise in real quantum systems. Control pulses create unwanted external fluctuations. In contact with its surroundings, the coherence decays with time in a process called quantum decoherence. The time evolution of a system with noise can be described with the master equations [8]. Secondly, we consider the interaction between the system and a control pulse with a Gaussian noise as a reversible process [2]. In work [15], the minimum energy path was calculated with Gaussian process regression for transitions such as spin rearrangements.

We will consider evolution of system, which is represented by the logical operator NOT with some noise. We write Hamiltonian of the system $\mathbf{H}(t)$ as a sum \mathbf{H}_0 and the component $\sigma_x V(t)$, which describes the time-dependent noise field $V(t)$ [5]. For the system, which is observed, the noise field can be created by the externally applied flux [2]:

$$\mathbf{H}(t) = \mathbf{H}_0 + \sigma_x V(t). \quad (6)$$

Evolution of the system is given by:

$$|\phi(t)\rangle = e^{-\frac{i}{\hbar}t\mathbf{H}_0} |\phi(t)_I\rangle, \quad (7)$$

$e^{-\frac{i}{\hbar}t\mathbf{H}_0} = \mathbf{E}(\psi)$, where $\psi = 1.57$. Thus, this evolution operator, accurate to the phase factor, equals the Pauli operator \mathbf{X} . Thus, $|\phi(t)_I\rangle$ is the state vector in the interaction picture, and $|\phi(t)_I\rangle$ is given by:

$$|\phi(t)_I\rangle = e^{\frac{i}{\hbar}t\mathbf{H}_0} V(t) |\phi(0)\rangle, \quad (8)$$

where $|\phi(0)\rangle = |\phi(0)_I\rangle$,

$$|\phi(t)_I\rangle = \mathbf{U}(t)_I |\phi(0)_I\rangle, \quad (9)$$

where $\mathbf{U}(t)_I = e^{-\frac{i}{\hbar}t\mathbf{H}_0}\mathbf{U}(t)$.

Then:

$$\mathbf{U}(t) = e^{-\frac{i}{\hbar}t\mathbf{H}_0}\mathbf{U}(t)_I. \quad (10)$$

This quantum operator describes the system with a unitary evolution operator, which has been described, and a time-dependent noise field.

From the equation for the motion of the operator $\mathbf{U}(t)$, we obtain:

$$i\hbar\frac{\partial\mathbf{U}(t)}{\partial t} = (\mathbf{H}_0 + \boldsymbol{\sigma}_x V(t)) e^{-\frac{i}{\hbar}t\mathbf{H}_0}\mathbf{U}(t)_I. \quad (11)$$

Then:

$$i\hbar\frac{\partial\mathbf{U}(t)_I}{\partial t} = \mathbf{V}(t)_I \mathbf{U}(t)_I, \quad (12)$$

where $\mathbf{V}(t)_I = \boldsymbol{\sigma}_x V(t)$. If we integrate this equation, we will get an accurate, to the second order, small parameter $\varepsilon = \frac{1}{\hbar} \int_0^t V(\tau) d\tau$:

$$\mathbf{U}(t)_I = \mathbf{I} - \frac{i}{\hbar}\boldsymbol{\sigma}_x \int_0^t V(\tau) d\tau + \frac{1}{2} \left(-\frac{i}{\hbar}\boldsymbol{\sigma}_x \int_0^t V(\tau) d\tau \right)^2. \quad (13)$$

Then, $\mathbf{U}(t)$ is given by:

$$\mathbf{U}(t) = i\boldsymbol{\sigma}_x + \frac{1}{\hbar}\mathbf{I} \int_0^t V(\tau) d\tau - \frac{i}{\hbar^2 2} \boldsymbol{\sigma}_x \left(\int_0^t V(\tau) d\tau \right)^2. \quad (14)$$

We consider $V(\tau)$ as a Gaussian process [5], $\mathbf{U}(t)$ will be random, the expected value of the variable part in (14) is the integral of the expected value of $V(\tau)$. Typical parameters of the system: the flux field magnitude is $\approx 10^{-6} \Phi_0$, where Φ_0 is the magnetic quantum flux [2, 6], and the interaction time t is 1 ns [2]. Thusly, we derive the evolution operator:

$$\mathbf{U} = \begin{pmatrix} 0.196 & 0.981 \\ 0.981 & 0.196 \end{pmatrix}. \quad (15)$$

We have obtained the operator NOT with a bit flip channel. There are errors in a circuit because of the interaction with an external field.

If the initial state is $|0\rangle$, we get:

$$\mathbf{U}|0\rangle = a|0\rangle + b|1\rangle, \quad (16)$$

where $a = 0.196$, $b = 0.981$. The probability of the state $|0\rangle$ is $|a|^2 = 0.038$, the probability of the state $|1\rangle$ is $|b|^2 = 0.962$. We have calculated the quantum state of this superconducting qubit, after the interaction with the quantum operator, which includes a source of noise. These values are approximately equal to the values from the experiment, which we have got from the quantum computing platform. If the initial state is $|0\rangle$, after an interaction with the \mathbf{X} gate, the probability of the state $|0\rangle$ is 0.024, and the probability of the expected state $|1\rangle$ is 0.976. So, we have calculated the quantum state without using the quantum computer and investigate the qubit with respect to the noise stability.

4. Acknowledgments

This work was partially financially supported by the Government of the Russian Federation (grant 074U01).

References

- [1] Zurek W.H. Decoherence, einselection, and the quantum origins of the classical. *Rev. Mod. Phys.*, 2003, **75**, P. 715–775.
- [2] Blum K. *Density matrix theory and applications*. Plenum press, New York, 1981, 242 pp.
- [3] Gardiner C. *Stochastic methods for natural sciences*. Springer Science, New York, 2004, 538 pp.
- [4] Koch J., Yu T.M., Gambetta J., Houck A. A., Schuster D. I., Majer J., Blais A., Devoret M. H., Girvin S. M., Schoelkopf R.J. Charge-insensitive qubit design derived from the Cooper pair box. *Phys. Rev. A*, 2007, **76**, P. 042319/1–19.
- [5] Makhlin Yu. *Quantum coherence in mesoscopic superconducting systems and quantum computing*. Doctor dissertation, Landau Institute for Theoretical Physics, Moscow, 2004.
- [6] Yoshihara F., Harrabi K., Niskanen A.O., Nakamura Y., Tsai J.S. Decoherence of flux qubits due to 1/f flux noise. *Phys. Rev.*, 2006, **97**, P. 167001.

- [7] Averin D.V., Ruggiero B., Silvestrini P. *Macroscopic Quantum Coherence and Quantum Computing*. Springer Science and Business Media, New York, 2001, 460 pp.
- [8] Nielsen M.A., Chuang I.L. *Quantum Computation and Quantum Information*. Cambridge University Press, Cambridge, 2001, 670 pp.
- [9] Aharonov D., Kitaev A., Nisan N. *Quantum circuits with mixed states*. Proceedings of 'The thirtieth annual ACM symposium on Theory of computing'. Dallas, May 24–26, ACM New York, 1998, P. 20–30.
- [10] Kitaev A.Yu. Quantum computations: algorithms and error correction. *Uspekhi Mat. Nauk*, 1997, **52**(5), P. 53–112.
- [11] Gubaidullina K.V., Chivilikhin S.A. Theoretical research of the distortion of quantum circuit in Grover's algorithm. *Journal of Physics. Conference Series*, 2016, **735**, P. 012074-1–012074-6.
- [12] Retrieved from <https://quantumexperience.ng.bluemix.net/qstage/#/community>.
- [13] Barenco A., Bennett C.H., Cleve R., DiVincenzo D.P., Margolus N., Shor P., Sleator T., Smolin J.A., Weinfurter H. Elementary gates for quantum computation. *Phys. Rev. A*, 1995, **52**, P. 3457–3467.
- [14] Makhlin Y., Shnirman A. Dephasing of Solid-State Qubits at Optimal Points. *Phys. Rev.*, 2004, **92**, P. 178301.
- [15] Koistinen O-P., Maras E., Vehtari A., J'onsson H. Minimum energy path calculations with Gaussian process regression. *Nanosystems: Physics, Chemistry, Mathematics*. 2016, **7**(6), P. 925–935.

Two eccentric cylinders in a uniform electric field

A. S. Starkov, K. V. Korzenkov, K. A. Starkov

ITMO University, Kronverkskiy, 49, St. Petersburg, 197101, Russia

starkovalexandr@corp.ifmo.ru, korund607@yandex.com, ferroelectrics@ya.ru

PACS 77.84.Lf, 77.22.d, 65.80.g

DOI 10.17586/2220-8054-2017-8-2-277-281

The present study examines the electric field distribution in the structure made of two eccentric dielectric cylinders. In order to find the potential of electric field, we employ a bipolar coordinate system. The obtained results allow one to quantify the impact of the eccentricity on effective characteristics of a periodic set of eccentric cylinders. Special attention is paid to the analysis of the structure polarizability.

Keywords: Eccentric cylinders, polarizability, Maxwell-Garnett approximation, effective dielectric constant.

Received: 11 December 2016

Revised: 23 February 2017

1. Introduction

Currently, composites are one of the most promising materials for use in new technologies [1, 2]. The most widespread are laminates, fibrous (reinforcing component – the fibrous structure), and filled materials (the reinforcing component – particles). In turn, compared with laminated composites, cylindrical composites (fibers) have more compact structure, which is beneficial for device miniaturization [3, 4]. Such composites are usually modeled by periodic sets of cylinders made of one material (filler) and placed in the second material (matrix). The calculation of effective parameters of the composite medium is based, as a rule, on the solution of the problem for the single cylinder (inclusion) in the surrounding external field and subsequent averaging procedure [5]. To be more precise, for the description of corresponding inclusions it is necessary to use the equations considering interactions of all possible fields: electromagnetic, elastic and thermal.

The surface and nonlocal effects start to play a significant role for the inclusions of size about one nanometer. Therefore, in general there is a need to solve the integro-differential equations. In our work, an average diameter of inclusions is assumed to be tens of nanometers and, thus, we can restrict ourselves by differential equations. Moreover, we analyze the case where the electrical properties of composites can be considered independently of the elastic ones. That is, it is sufficient to find the electric potential by means of the Laplace equation. In a classic work by Rayleigh [6], the electric potential was computed for a conducting composite consisting of a periodic array of inclusions (cylinders and spheres). More complex core-shell structures, which have appeared in recent years, allow one to improve the desired properties of composites. However, these structures complicate the determination of their properties even in the elementary cases [7–9].

Future prospects for the development of composites are associated with the finding of non-smooth fillings of untypical shapes. As already well known [9], the presence of peaks or edges of a filling leads to the appearance of singularities in the electric field that has a strong impact on the effective permittivity. The numerical calculation of such structures is not an easy task and requires skilled techniques for its solution (see, e.g. [9, 10]). In this study, we investigate the possibility to control the dielectric constant by changing the distance between the boundaries of the different layers (shells). We consider the electric potential in the medium consisting of cylindrical inclusion in which one more cylinder is placed (see, Fig. 1). In other words, two dielectric cylinders are considered. If the cylinders have no common points, then the solution of an electrostatic problem can be found in [9, 11]. Summing it up, this paper examines a cylinder completely immersed inside another one. A case of intersecting cylinders remains unexplored.

Note that due to the analogy between the stationary electric and thermal fields, the effective thermal capacity of a composite with inclusions in the form of eccentric cylinders can be determined by the same procedure.

2. The solution of the general problem

2.1. The problem statement

As a starting point, we consider an electric field in the system illustrated in Fig. 1. Inclusion consists of two eccentric circles of radii of r_1 and r_2 which centers are located at distance d from each other. The surfaces of

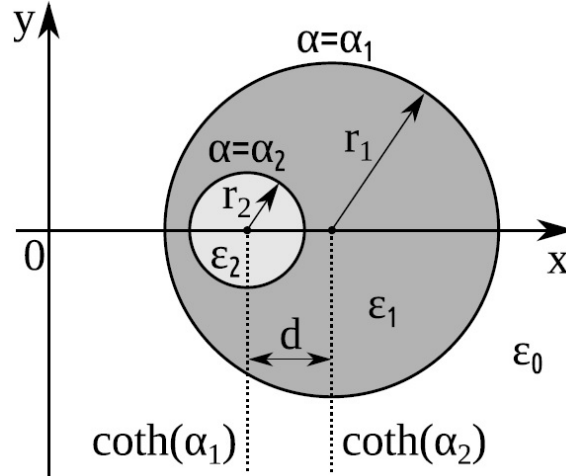


FIG. 1. The mutual arrangement of two dielectric cylinders

circles are $S_{1,2}$. To describe electrostatic field, we employ a Cartesian coordinate system (x, y) . By ϵ_1, ϵ_2 we denote dielectric permeability of circles and dielectric permeability of external space (matrix) by ϵ_0 .

Similarly, we will use the subscripts 1, 2 to identify quantities related to circles and subscript 0 for the matrix parameters. In the absence of any subscript, the expression is fulfilled in all environments. The intensity of the external electric field is supposed to be a constant vector of length E . In the solution of our problem it is necessary to find the potential u , which satisfies the two-dimensional Laplace equation:

$$\Delta u = 0, \tag{1}$$

and is continuous at the interfaces $S_{1,2}$ together with the normal component of the electric displacement:

$$u_0 \Big|_{S_1} = u_1 \Big|_{S_1}, \quad \epsilon_1 \frac{\partial u_0}{\partial n} \Big|_{S_1} = \epsilon_2 \frac{\partial u_1}{\partial n} \Big|_{S_1}, \quad u_1 \Big|_{S_2} = u_2 \Big|_{S_2}, \quad \epsilon_1 \frac{\partial u_1}{\partial n} \Big|_{S_2} = \epsilon_2 \frac{\partial u_2}{\partial n} \Big|_{S_2}. \tag{2}$$

Moreover, at the distance far from the inclusion, the potential u tends to the potential of the external field:

$$u_0 \rightarrow -E_0(x \cos \gamma + y \sin \gamma). \tag{3}$$

Here, n is normal to the surfaces $S_{1,2}$, E_0 is the electric stress, and γ is an angle between the external field and the x -axis. Because of the lack of symmetry, the solution of Eqs. (1)-(3) depends on the angle γ .

If we introduce the potential U that tends to $U_0 = x + iy$ at large distances from the inclusion, then the desired potential u can be expressed in terms of U as:

$$u = -E_0(\text{Re}U \cos \gamma + \text{Im}U \sin \gamma). \tag{4}$$

Further, it is reasonable to switch to a bipolar coordinate system (α, β) [12] associated with the Cartesian by the relations:

$$x + iy = c \tanh \left(\frac{\alpha + i\beta}{2} \right). \tag{5}$$

If we define the parameters α_1, α_2 and c from:

$$\cosh \alpha_j = \frac{r_1^2 - r_2^2 + (-1)^j d^2}{2r_j d}, \quad c = r_1 \sinh \alpha_1, \tag{6}$$

then the circles' boundaries are the coordinate lines $\alpha = \alpha_{1,2}$. The solution of the stated problem will be sought in the form:

$$\begin{aligned}
U_0 &= x + iy + \sum_{n=1} a_{0n} e^{n(\alpha - 2\alpha_1 + i\beta)}, \\
U_1 &= \sum_{n=1} \left[a_{1n} e^{n(\alpha - 2\alpha_1)} + b_{1n} e^{-n\alpha} \right] e^{in\beta}, \\
U_2 &= \sum_{n=1} b_{2n} e^{in\beta - n\alpha}.
\end{aligned} \tag{7}$$

The Fourier coefficients a_{jn} and b_{jn} in Eq. (7) are uniquely determined by taking into account boundary conditions. In particular

$$a_{0n} = 2c(-1)^n \frac{\lambda_n - 1}{\lambda_n + 1}, \quad \lambda_n = \frac{\varepsilon_1 \delta_n + 1}{\varepsilon_0 \delta_n - 1}, \quad \delta_n = \frac{\varepsilon_2 + \varepsilon_1}{\varepsilon_2 - \varepsilon_1} e^{2n(\alpha_2 - \alpha_1)}. \tag{8}$$

The coefficients a_{1n} and $b_{1,2n}$ have a similar form. For simplicity we do not write down explicit equations for these coefficients.

2.2. The Maxwell–Garnett theory

Let us now discuss the influence of the cylinder eccentricity on the effective characteristics of the medium. First, we consider the main principles of the Maxwell–Garnett theory for the set of identical inclusions randomly arranged in the matrix. Each of these inclusions consists of n dielectric layers with permeabilities ε_i , $i = 1, 2, \dots, n$. The effective dielectric constant ε_{eff} can be defined from:

$$\langle \mathbf{D} \rangle = \varepsilon_{eff} \langle \mathbf{E} \rangle, \tag{9}$$

where \mathbf{D} is the electric displacement and the symbol $\langle \cdot \rangle$ denotes averaging of corresponding values. If we introduce quantities f_j characterizing volume part of the j -th layer and $f_0 = 1 - \sum f_j$ for the matrix, then the average electric displacement and electric field are given by:

$$\langle \mathbf{D} \rangle = \sum_{j=1}^n f_j \varepsilon_j \langle \mathbf{E}_j \rangle + f_0 \varepsilon_0 \mathbf{E}_0, \quad \langle \mathbf{E} \rangle = \sum_{j=1}^n f_j \langle \mathbf{E}_j \rangle + f_0 \mathbf{E}_0. \tag{10}$$

By the linearity of the electrostatic problem, the values of average electric field strength are proportional to the external electric field $\langle \mathbf{E}_j \rangle = p_j \langle \mathbf{E}_m \rangle$ with coefficients of proportionality p_j . According to Eqs. (9)–(10) the expression for the effective dielectric permittivity is approximately given by:

$$\varepsilon_{eff} = \frac{\sum_{j=1}^n f_j \varepsilon_j p_j + f_m \varepsilon_m}{\sum_{j=1}^n f_j p_j + f_0}. \tag{11}$$

For $n = 1$ Eq. (11) is known as the Maxwell–Garnett formula [5]. More accurate results can be obtained with the T-matrix method [13]. In the case of concentric circles and $n = 2$ we have [7]

$$p_1 = \frac{2\varepsilon_m(\varepsilon_1 + \varepsilon_2)}{(\varepsilon_1 + \varepsilon_2)(\varepsilon_0 + \varepsilon_1) + (r_2/r_1)^2(\varepsilon_1 - \varepsilon_2)(\varepsilon_0 - \varepsilon_1)}, \tag{12}$$

$$p_2 = \frac{4\varepsilon_m \varepsilon_1}{(\varepsilon_1 + \varepsilon_2)(\varepsilon_0 + \varepsilon_1) + (r_2/r_1)^2(\varepsilon_1 - \varepsilon_2)(\varepsilon_0 - \varepsilon_1)}. \tag{13}$$

It is possible to define the polarizability of a two-layer system as a $p = (p_1 f_1 + p_2 f_2)/(f_1 + f_2)$. Exactly this quantity is included in Eq. (11) for the effective dielectric constant. After performing numerical averaging of the series (7) and taking into account [12]

$$dx dy = \frac{c^2}{(\cosh \alpha + \cos \beta)^2} d\alpha d\beta, \tag{14}$$

we find the polarizability p . The dependencies of p on the distance between the cylinders centers and relative dielectric constants $\varepsilon_1/\varepsilon_0$ are shown in Fig. 2.

From these graphs follows that if the distance between the cylinders centers d is not too large, then the polarizability $p(d)$ is close to its value $p(0)$ for the concentric cylinders. Significant changes in polarizability have place only in the case where the outer and inner circles are almost touching each other. The proximity of

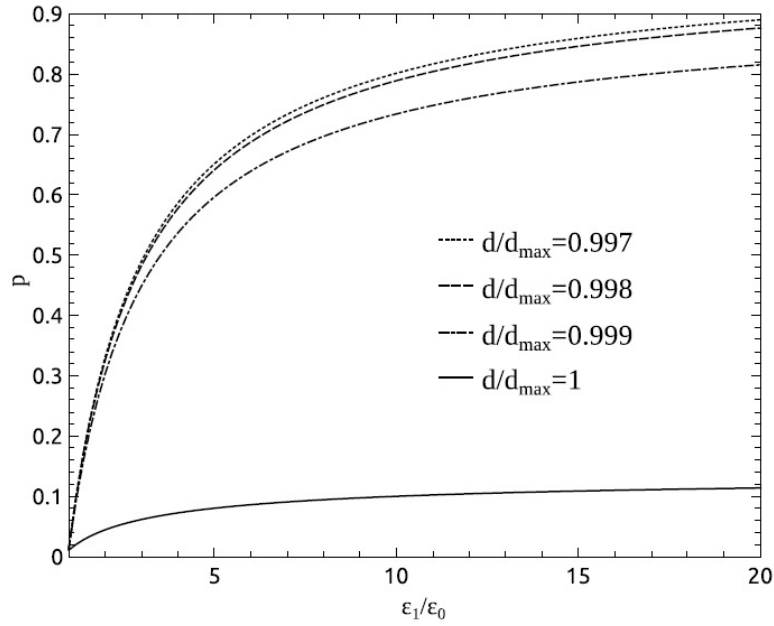


FIG. 2. The dependence of the polarizability p on the ratio $\varepsilon_1/\varepsilon_0$ for the different relative distance d between the cylinders centers

the cylinders boundaries leads to a noticeable decrease in the polarizability. The polarizability dependence on the dielectric constant of the inner cylinder is shown in Fig. 3.

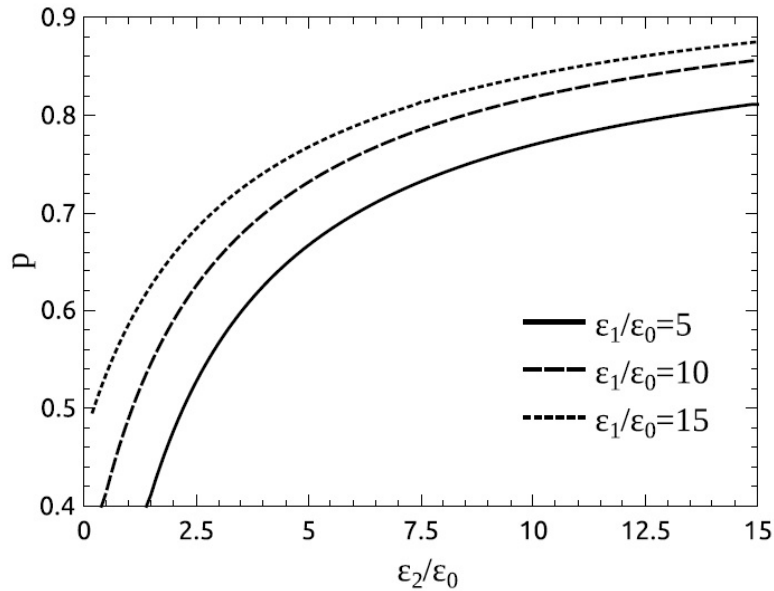


FIG. 3. The dependence of the polarizability p on the ratio $\varepsilon_2/\varepsilon_0$

3. Conclusion

We have presented a new approach to describe the effective characteristics of a periodic set of eccentric cylinders. If the distance between the axes of the cylinder is small ($d/d_{\max} < 0.997$), the effective dielectric constant depends only on volume fractions of fillers. In this case it is possible to use the Maxwell-Garnett approximation. In turn, if the cylinders are almost touching each other ($d/d_{\max} > 0.003$), then the Maxwell-Garnett method cannot be employed and the effective dielectric constant depends on the interaxial distance d . This

dependence allows one to control the permittivity of composites. Perhaps, such a mechanism is realized in living cells. The cell nucleus might move inside the cell volume [14] and change its thermal and electrical conductivity when approaching the cell surface.

Also note that the dependence of the properties of eccentric cylinders on d specifies the need for major modifications of classical averaging methods as Maxwell–Garnett, Bruggeman, etc. In these techniques, the effective dielectric constant depends only on the specific volume of the composite component. In more complex cases, however, the surface area of each component also can be taken into account (the Maxwell–Wagner effect). The change in the effective dielectric constant, as discussed in this paper, occurs at identical volumes and surface areas of each component. In addition, in our opinion, the angles of the edges and vertices at the boundaries of the various components need to be entered in the generalization of the formula for the effective permittivity of composites. Since no assumptions about the reality or positivity of cylinder dielectric constants (ε_1 and ε_2) have been made, the resulting expressions are applicable for calculation of the metal cylinders with a complex permittivity and cylinder of metamaterials. It is also important also to emphasize, that the solution of piezoelectricity equations for eccentric circular fibrous composites under the generalized anti-plane shear deformation [15] may be constructed in precisely the same manner.

Acknowledgements

The research leading to the results exposed has received funding from the Government of Russian Federation, Grant 074-U01.

References

- [1] Lagarkov A. N., Matytsin S. M., Rozanov K. N., Sarychev A. K. Dielectric properties of fiber-filled composites. *J. Appl. Phys.*, 1998, **84**(7), P. 3806–3814.
- [2] Dang Z. M., Yuan J. K., Zha J. W., Zhou T., Li S. T., Hu G. H. Fundamentals, processes and applications of high-permittivity polymer-matrix composites. *Progress in Materials Science*, 2012, **57**(4), P. 660–723.
- [3] Alekseev A. V., Predtechenskiy M. R. Aluminum foil reinforced by carbon nanotubes. *Nanosystems: Physics, Chemistry, Mathematics*, 2016, **7**(1), P. 185–189.
- [4] Khodke M. R., Joshi S. V. An investigative study on application of carbon nanotubes for strain sensing. *Nanosystems: Physics, Chemistry, Mathematics*, 2016, **7**(4), P. 755–758.
- [5] Garnett J. C. M. Colours in metal glasses, in metallic films, and in metallic solutions. II *Philosophical Transactions of the Royal Society of London, Series A*, 1906, **203**, P. 237–288.
- [6] Rayleigh L. LVI. On the influence of obstacles arranged in rectangular order upon the properties of a medium. *The London, Edinburgh, and Dublin Philosophical Magazine and Journal of Science*, 1892, **34**(211), P. 481–502.
- [7] Zhang H., Shen Y., Xu Y., Zhu H., Lei M., Zhang X., Xu M. Effective medium theory for two-dimensional random media composed of core-shell cylinders, *Opt. Comm.*, 2013, **306**, P. 9–16.
- [8] Starkov I. A., Starkov A. S. Effective parameters of nanomatryoshkas. *Journal of Nanophotonics*, 2016, **10**(3), P. 033503–033503.
- [9] Grinberg G. A., *Selected Topics in the Mathematical Theory of Electrical and Magnetical Phenomena*. Acad. of Sci. USSR, Leningrad, 1948, 733 pp.
- [10] Chaumet P. C., Dufour J. P. Electric potential and field between two different spheres. *Journal of electrostatics*, 1998, **43**(2), P. 145–159.
- [11] Balagurov B. Y. On the polarizability of a pair of cylinders in a transverse electric field. *Technical Physics*, 2003, **48**(8), P. 945–951.
- [12] Lebedev N. N., Skalskaya I. P., Uflyand Y. S. *Worked Problems in Applied Mathematics*. Dover, New York, 2010, 420 pp.
- [13] Kiselev A. D., Plutenko D. O. Light scattering of Laguerre-Gaussian beams: near-field structures and symmetries. *Nanosystems: Physics, Chemistry, Mathematics*, 2016, **7**(2), P. 349–370.
- [14] Bunge R. P., Bunge M. B., Bates M. Movements of the Schwann cell nucleus implicate progression of the inner (axon-related) Schwann cell process during myelination. *The Journal of Cell Biology*, 1989, **109**(1), P. 273–284.
- [15] Xiao J., Xu Y., Zhang F. A generalized self-consistent method for nano composites accounting for fiber section shape under antiplane shear. *Mechanics of Materials*, 2015, **81**, P. 8194–8200.

Layer-by-layer capsules as smart delivery systems of CeO₂ nanoparticle-based theranostic agents

N. R. Popova¹, A. L. Popov¹, A. B. Shcherbakov², V. K. Ivanov^{3,4}

¹Institute of theoretical and experimental biophysics of the Russian Academy of Sciences, Institutskaya, 3, Pushchino 142290, Russia

²Zabolotny Institute of Microbiology and Virology, National Academy of Sciences of Ukraine, Str. Zabolotnogo, 154, Kyiv D0368, Ukraine

³Kurnakov Institute of General and Inorganic Chemistry of the Russian Academy of Sciences, Leninsky av, 31, Moscow 119991, Russia

⁴National Research Tomsk State University, Lenin str., 36, Tomsk 634050, Russia

nellipopovaran@gmail.com, antonpopovleonid@gmail.com, carotene@igic.ras.ru, van@igic.ras.ru

PACS 68.65.-k, 81.07.Pr, 81.16.Be, 87.85.Qr

DOI 10.17586/2220-8054-2017-8-2-282-289

Modern methods of cancer treatment include chemotherapy and radiotherapy, but they are often characterized by low efficacy and high toxicity. The effectiveness of cancer therapy is often limited by a lack of effective systems for drug delivery to the tumor site. Cerium oxide nanoparticles are able to act as radioprotectors and as radiosensitizers exhibiting selective toxicity in the tumor microenvironment, providing for their tremendous potential in treating cancer. However, methods for controlled delivery of CeO₂ nanoparticles to the tumor have not been investigated nor described yet. In this article, we consider different approaches to the development of new ceria nanoparticle-based theranostic agents. Modification of polyelectrolyte microcapsules with nano-ceria appears to be the most promising method. Our design proposals are based on the synergistic pharmacological action of ceria-based nanomaterials and anticancer pharmaceuticals with the ability to control and visualize their sites of localization.

Keywords: cerium oxide nanoparticles, polyelectrolyte microcapsules, theranostics agents, radiation therapy.

Received: 9 January 2017

Revised: 18 January 2017

1. Introduction

Radiation therapy is one of the leading methods of cancer treatment [1]. According to WHO recommendations, radiation therapy is advised for more than 70 % of cancer patients within a particular plan of treatment or as part of combined and complex therapy. Treatment of patients with locally advanced tumors corresponding to stages III–IV is particularly difficult due to their sheer numbers of 54–68 % (even when modern diagnostic tools are used) [2]. Radiation therapy is often the only possible means of medical care for these patients. Apart from a purely technical solution to the problem by improving radiotherapy techniques today, much attention is paid to the control of tissue radiosensitivity, i.e. to the development of methods for selective effect on the radiosensitivity of tumor and normal tissue to expand the boundaries of a radiotherapy interval. Prospects for the combination of radiotherapy and chemotherapy for patients with locally advanced tumors are associated with the development of radiochemotherapy. Radiochemotherapy treatment is a method in which radiation and chemical substances are used simultaneously, wherein the special drugs have not only cytostatic effects but also exhibit radiosensitizing properties [3, 4]. The procedure for selecting chemotherapy drugs as photosensitizers, their dosages, optimal modes of administration, as well as the development of adequate dose fractionation schemes of ionizing radiation are still relevant. Methods of administering already known radiomodifiers that increase efficiency and reduce toxic side effects also need improvement.

The present level of nanotechnology development allows the synthesis of new multifunctional nanomaterials with unique physical and chemical properties which are widely used in biomedical applications, including the radiotherapy of tumors. For example, heavy metal nanoparticles (mostly gold nanoparticles) are used in radiotheranostics (radiodiagnostics and radiotherapy) of tumors [5–8]. Bismuth oxide nanoparticles have also been shown to enhance the effect upon irradiation [9] and can replace gold nanoparticles. Multifunctional bismuth sulfide nanocapsules can be used in combined ultrasonic and radiation therapy [10]. The complex therapy uses magnetic iron oxide particles that also have low toxicity [11], and dextran-coated iron oxide nanoparticles decrease tumor growth in a breast cancer model by the combined action of hyperthermia and radiation [8]. Gadolinium oxide nanoparticles (Gd₂O₃) are also considered an alternative to gold nanoparticles. Ultra-small Gd₂O₃ nanoparticles are

accumulated in brain tumors after intravenous injection and can be used for visualization by MRI and subsequent radiation therapy [12]. Hafnium oxide nanoparticles increase the destructive effect of radiation due to the emission of Auger electrons and increase the generation of ROS [13]. The intratumoral injections of 50-nm-sized HfO₂ followed by radiation therapy sessions have shown good results in Phase 1 clinical trials with locally advanced soft tissue sarcoma patients [14].

One of the most promising materials having a multifaceted mechanism of radioprotective action is nanosized cerium oxide [15,16]. Cerium oxide nanoparticles have SOD-mimetic activity and inactivate superoxide radicals [17], and their ability to inactivate hydrogen peroxide is comparable to that of catalase [18,19]. Using a variety of surface modifiers and synthetic methods allows one to vary the size, shape, and charge of cerium oxide nanoparticles that affect their physical and chemical characteristics, including the level of antioxidant activity, and consequently intracellular biological effects [16,20–22]. The presence of oxygen vacancies (defects in a crystal lattice) and auto-regenerative oxidation-reduction cycle ($\text{Ce}^{3+} \longleftrightarrow \text{Ce}^{4+}$) enable the use of cerium oxide nanoparticles as broad-spectrum antioxidant drugs at the neutral pH found in healthy tissues [23,24]. Conversely, in the tumor, cerium oxide nanoparticles are able to perform as both peroxidase (effective pro-oxidant) and a radiosensitizer. The key external condition determining the pathway of the biological activity for cerium oxide nanoparticles in cancer therapy is the pH of the medium [16,25–29] and the power of X-rays used [30]. Previously, it was shown [21] that cerium oxide nanoparticles significantly reduce the level of ROS and increase cell survival in the non-malignant normal cells ($\text{pH} \geq 7$) after exposure to ionizing radiation, while emerging as strong pro-oxidants in cancer cells of the pancreas ($\text{pH} \leq 7$) increasing cell death. On the other hand, Briggs et al. [30] showed that the use of radiation of different intensities may have a different impact on the radioprotective properties of cerium oxide nanoparticles. When exposed to low-intensity X-rays (150 kVp), cerium oxide nanoparticles do not exhibit radioprotective properties and increase cell death, generating additional Auger electrons that act as radiosensitizers. However, when high-intensity X-ray radiation (10 MV) is used, cerium oxide nanoparticles exhibit a strong radioprotective effect by inactivating a broad range of ROS and free radicals produced by radiolysis, i.e. work as radioprotectors. The key factor determining the effectiveness of radiation therapy of cancer is the localization of cerium oxide nanoparticles while the development of the targeted delivery of cerium oxide nanoparticles is an urgent task of modern biomedicine.

In this article, we propose the use of biodegradable polyelectrolyte microcapsules modified with cerium oxide nanoparticles, other comprising functional components and anticancer pharmaceutical preparations (Fig. 1) for complex therapy of cancer. This microcapsule structure will provide a synergistic effect for the encapsulated anticancer drug and cerium oxide nanoparticles in a combined therapy of oncological diseases. The presence of specific antigens on the surface of the microcapsules will facilitate its targeted delivery to tumor cells.

2. The hypothesis assessment and review

Polyelectrolyte microcapsules are one of the most promising means for effective controlled delivery of substances to target organs and tissues. Previously it was shown that they can be used for encapsulating proteins [20], DNA [31], RNA [32], pharmaceutical formulations [33] and other compounds. A layer-by-layer method of synthesizing polyelectrolyte microcapsules is based on the use of differently charged polyelectrolytes that are alternately adsorbed on an organic (polymeric) or inorganic (oxides, calcium carbonate) substrate [34]. For example, a positively charged substrate is placed in a solution of polyanions, the deposition of which leads to recharging the surface, and the substrate becomes negatively charged preventing further adsorption of polyanions. Adsorptive saturation occurs and the molecular layer is formed with a thickness of about 1 nm. The substrate is then rinsed in water and placed in a solution of positively charged macromolecules. Polycations are deposited, forming ionic bonds between oppositely charged ionic groups, and then they again recharge the surface. These mild synthetic conditions allow the encapsulation of biologically active materials (proteins, peptides, pharmaceuticals, etc.) while retaining their native properties. Thus, a bilayer is formed which can be repeated a number of times. The stratified character of polyelectrolyte microcapsule formation provides ample opportunities for managing their physical and chemical properties. The degradation rate of microcapsules and release of the contents into the cell can be adjusted by varying the type of polyelectrolyte and the number of adsorbed layers. Using a polyelectrolyte matrix can also maintain the physicochemical properties and biological activity of its constituent nanoparticles.

Cerium oxide nanoparticles can be introduced into the microcapsule by a variety of ways (Fig. 1): as a component of the polyelectrolyte shell (A), core (B), or the gap between the core and the shell (C).

The layer-by-layer method allows the integration of CeO₂ nanoparticles by replacing one of the polyanion or polycation layers (Fig. 1, A). In [35], the authors used a similar approach to introduce titanium dioxide into microcapsule shells. Using photoactive TiO₂ nanoparticles allows one to control the release rate of the microcapsules' contents by irradiation. The incorporation of magnetic particles into the shell (e.g. iron oxide) allows control

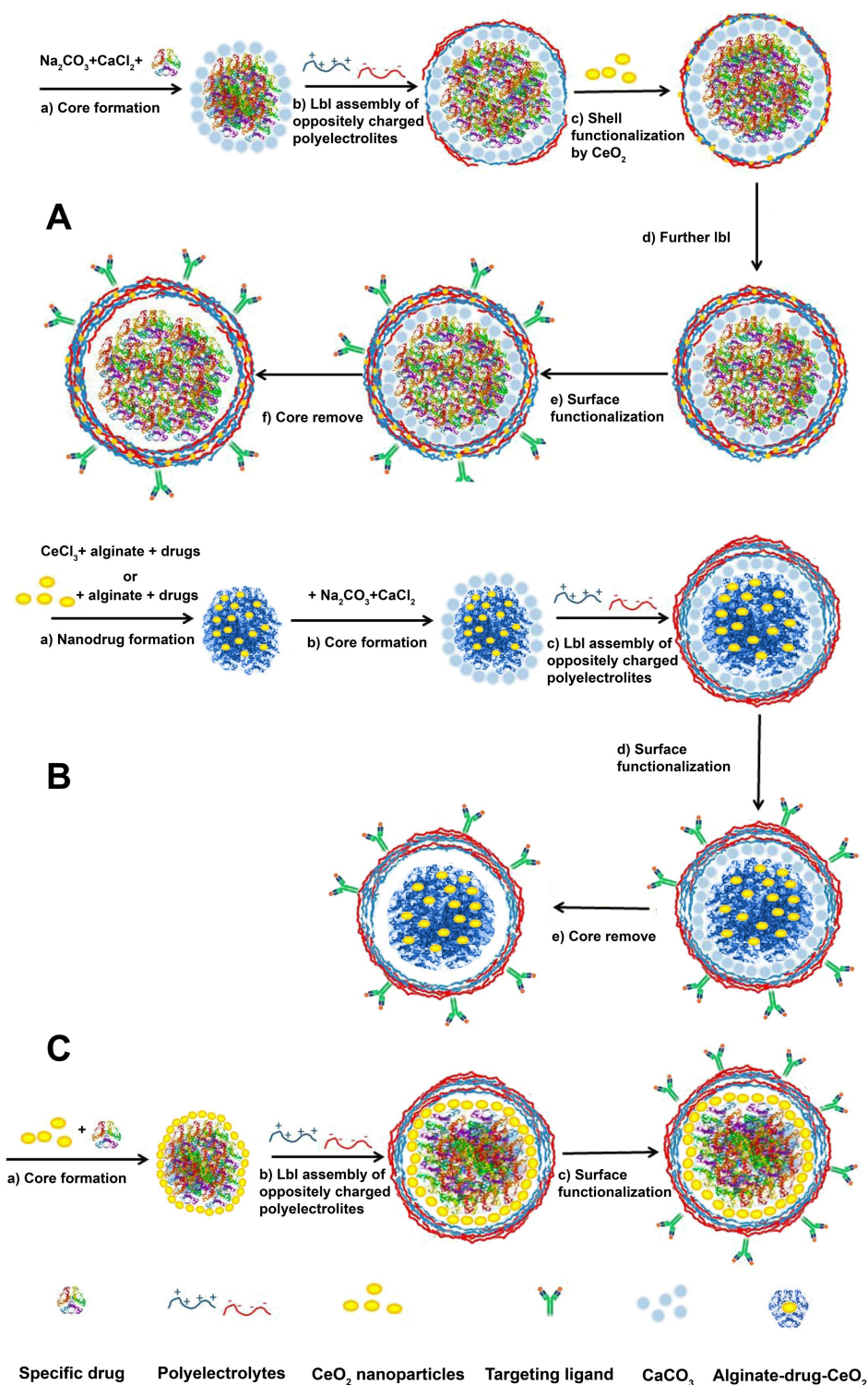


FIG. 1. Possible synthetic scheme of biodegradable polyelectrolyte microcapsules by LbL (layer-by-layer) assembly with cerium oxide nanoparticles: (A) located in shell; (B) located in core and (C) covering the core. A – Encapsulation of anticancer drug (a), step-by-step deposition of differently charged polyelectrolytes (b, d), their modification by cerium oxide nanoparticles (c) functionalization by antibody (e), and removal of the core supporting shell (f). B – Formation of hybrid particles consisting of a drug, cerium oxide nanoparticles and binding polymer (alginate or alginate + chitosan) (a) encapsulation of anticancer drug (b), step-by-step deposition of differently charged polyelectrolytes (s), functionalization by specific antibodies (d) and removal of the core supporting shell (e). C – Encapsulation of anticancer drug with cerium oxide nanoparticles (a), step-by-step deposition of differently charged polyelectrolytes (b) and functionalization by antibodies (c).

over the delivery. In the latter case, the shell modification may be carried out using both previously synthesized magnetite nanoparticles [36] and *in situ* formation of Fe₃O₄ nanoparticles directly on the capsule shell [37,38]. In the first case, because of the mutual repulsion of charged nanoparticles, their adsorption is limited. In the second case, the nanoparticles formed in the solution are adsorbed on the surface of the polyelectrolyte capsules wherein they are partially stabilized by the shell's polymers. Silver nanoparticles have also been incorporated into microcapsules' shells by the *in situ* method [39]. To introduce CeO₂ nanoparticles into the shell of the microcapsules, both approaches can be used (via pre-synthesized nanoparticles and *in situ* approach). The techniques described herein allow control of the final nanoparticle concentration in each microcapsule up to 1 unit.

Unstabilized ("naked") cerium oxide nanoparticles in solution have a positive ζ -potential (ca. 40 mV) [40], and thus, can replace a polycation layer during microcapsule synthesis. Conversely, polycarboxylic (citric, polyacrylic) acids normally used for the stabilization of cerium oxide nanoparticles provide a negative ζ -potential (ca. -15 mV) [41,42], and these particles can be incorporated into the microcapsule shell in place of one of the polyanion layers. In terms of electrostatic interaction and the DLVO theory (a physical theory of stability of colloidal systems), with an increase in the particle charge, the rate of adsorption equilibrium increases, but the amount of adsorbed particles per cycle application decreases (fewer particles are required to compensate the charge of a previous layer). Thus, using CeO₂ sols with different ζ -potentials (both in sign and in absolute value) allows one to adjust the loading of a microcapsule with nanoparticles during its synthesis as well as the rate of nanoparticle release during its degradation.

To implement the approach *in situ* after the next polyanionic layer is applied, microcapsules must be transferred into a solution with a predetermined amount of cerium ions in the form of a soluble Ce(III) salt, then, after the adsorption equilibrium is achieved the medium should be made alkaline. At pH > 7, the Ce(III) salts are hydrolyzed and rapidly oxidized by dissolved oxygen to Ce(IV), and cerium oxide nanoparticles are generated on the surface of the microcapsule. Subsequently, microcapsules can be transferred into a solution of polyanion to generate additional layers.

If the therapeutic agent and the cerium oxide nanoparticles are chemically compatible, (as happens in most cases), then, the latter can be introduced into the core of the microcapsule together with the drug (Fig. 1, B). The use of an auxiliary binder polymer allows the formation of the core of hybrid organic-inorganic particles. Thus, alginic acid is often used as a biologically acceptable binding carrier polymer (the compound is a heteropolysaccharide formed by residues of polyuronic acid). The water-soluble alginate forms solid insoluble particles and films in the presence of polyvalent metal ions (calcium salts are most commonly used). Introduction of the cationic polymer (chitosan, poly-L-arginine or poly-L-lysine) can adjust the size of the particles formed. For example, 250–850 nm (depending on the alginate concentration) particles were synthesized as drug carriers; these particles are formed in solution by adding sodium alginate, calcium chloride and then poly-L-lysine [43]. The particle size can also be controlled by the volume of "nanoreactors" (micelles); reverse micelles were successfully used to synthesize nanocarriers (from alginate and calcium salts) with an average size of about 80 nm in diameter exhibiting a high degree of endocytosis by NIH 3T3 cells [44]. It is also possible to combine the surfactant and the cationic polymer to tune the size of alginate particles. In [45], a weakly polar natural polyphenol curcumin (diferulometan) which is widely used in cancer treatment (including radiotherapy) and prevention was encapsulated into 100±20 nm calcium alginate particles. Cationic polymers (chitosan and a non-ionic surfactant (Pluronic)) were used as auxiliary compounds, and their absorption by HeLa cancer cells was recorded using curcumin fluorescence. In a series of preliminary experiments, we found that sols of ceria nanoparticles ("naked" or stabilized by citrate) can be successfully used instead of calcium salts for alginate gelation. In addition, water-soluble salts of cerium may also be used for that purpose. Alginate+CeO₂ nanoparticles systems can serve as a template for the storage and transport of biologically active compounds. Furthermore, the resulting combined nanodrug can be used as a constituent in the formation of an LbL-microcapsule core (Fig. 1, B).

Finally, cerium oxide nanoparticles can be used as a microcapsule core coating and as the basis for the application of polyionic layers (Fig. 1, C). For this purpose, the drug (a part of the microcapsule core) can be treated with a solution of cerium salt or a sol of cerium oxide nanoparticles prior to addition of the polyelectrolyte. Moreover, if the drug has an acidic functional group and is insoluble in water or if the drug is a slightly polar liquid (a slightly polar solid soluble in non-polar or weakly polar liquid), then the particles capable of performing the function of the microcapsule core can be formed directly in the sol of ceria by injection/homogenization (to form a Pickering emulsion [46]). In the literature, there are many examples of the preparation of drug-based sols using nanoparticles. The above mentioned curcumin was successfully stabilized in the aqueous sol by SiO₂ nanoparticles (the sol's stability is 100 times higher than in water) [47]; silica+curcumin composite has great promise in cancer therapy [48]. Our preliminary studies have shown that stability of the aqueous curcumin sols in the presence of

cerium oxide nanoparticles also increases. The resulting hybrid particle may be used as an LbL-microstructure core (Fig. 1, C).

Polyelectrolyte microcapsules may be functionalized by specific surface ligands or antibodies to a particular type of receptor on the surface of cancer cells (Fig. 1, A–C). For example, for the treatment of breast cancer polyelectrolyte microcapsules can be functionalized by selective antibody to the HER2 antigen which is over-expressed on the surface of this type of cancer cells [49]. Antibodies to *HORMAD1*, *CXorf61*, *ACTL8*, *PRAME*, *MAGE* and *CSAG* antigens [50] can be used for treating testicular cancer (those are also over-expressed on the surface of tumor cells of this type). The level of expression varies, depending on the stage of tumor development; however, there is the possibility of selecting both specific antibodies and an encapsulated pharmaceutical preparation at a particular stage of development of the disease.

It was earlier noted that the pro- and antioxidant activity of cerium oxide nanoparticles correlates with the concentration of oxygen vacancies and lattice defects in CeO_2 . This parameter can be adjusted, for example, via the introduction of CeO_2 nanoparticles doped with other rare earth elements [51]. The use of gadolinium is quite promising indeed [52–54]. Gadolinium doped cerium oxide nanoparticles not only demonstrate superior antioxidant properties but also can serve as a contrast agent in tumor diagnostics (X-ray CT and enhanced MRI). The microcapsules designed with the use of gadolinium doped cerium oxide nanoparticles could thus serve both therapeutic and diagnostic purposes.

The functionality of microcapsules can be increased by fluorescent label introduction. Organic luminophores or nanoparticles of rare earth elements oxides doped by europium or terbium ions can be used as such a label.

For example, if in a microcapsule design one polyanionic layer is replaced with a fluorescein isothiocyanate-dextran conjugate (FITC-Dextran) or if a layer of polycation is replaced with a rhodamine isothiocyanate-dextran conjugate (RITC-Dextran), these microcapsules will become luminescent. Additionally, the behavior of these microcapsules in the cell can be monitored from the time of administration (accumulation) to degradation. If cerium oxide nanoparticles functionalized with calcein are included in the composition of the microcapsules, these microcapsules will exhibit fluorescent properties only when reacting with active oxygen species [55], which would permit their monitoring during therapy. Moreover, if those luminophores have different emission wavelengths (e.g., calcein in nanoparticles and rhodamine in the shell), this combination would allow monitoring the pharmacokinetics and pharmacodynamics at all stages of the introduction, distribution and degradation of microcapsules.

As nanocrystalline luminophores for microcapsules, it is preferable to use yttrium or gadolinium orthovanadate doped with europium ($\text{Gd/YVO}_4:\text{Eu}$) [56,57] or cerium fluoride doped by terbium ($\text{CeF}_3:\text{Tb}$) [58]. In the synthesis of “smart” multi-layered microcapsules, it is expedient to replace one ionic nanoparticle layer with $\text{CeF}_3:\text{Tb}$ [58] or polyacrylic acid with $\text{YVO}_4:\text{Eu}$ nanoparticles synthesized in [56] to visualize the nanoparticles of cerium oxide doped with gadolinium. In addition to the fluorescent properties, these compounds exhibit an independent antioxidant and radioprotective activity [57–59]. Similar to CeO_2 , nanocrystalline CeF_3 is involved in redox processes (and in some cases is even superior to cerium oxide nanoparticles in its protective effect [58]). Cerium fluoride is one of the most efficient scintillators [60]. The use of CeF_3 (and $\text{CeF}_3:\text{Tb}$) nanoparticles in radiological diagnostics and therapy has great promise. For example, in microcapsule construction, a photosensitizer (of porphyrin or phthalocyanine series) can be placed near to cerium fluoride nanoparticles so that during radiotherapy under the influence of light emitted by the scintillator the photosensitizer will generate oxygen radicals and singlet oxygen. Reactive oxygen species will accelerate the degradation of the microcapsule shell, releasing its contents during radiotherapy, as well as provide additional damaging factors in tumor cells through photodynamic (radio dynamic) action.

Figure 2 shows one possible mode of action for smart polyelectrolyte microcapsules in tumor cells. Due to the presence of surface ligands (antibodies), microcapsules can be selectively accumulated at the site of oncogenesis, making it possible to define the size and location of the tumor (A) and to select a subsequent procedure of radiotherapy (B) using diagnostic methods (CT and MRI). Once inside the tumor cell, the microcapsules will be destroyed releasing the anti-cancer drug and cerium oxide nanoparticles into the cytoplasm of a cancer cell. Further irradiation of the cells by low-intensity X-rays will cause the surface of ceria oxide nanoparticles to generate secondary Auger electrons, and the anti-cancer drug will provide a specific effect inhibiting the metabolism of cancer cells. The acidic pH of “tumor microenvironment” promotes the pro-oxidant activity of cerium oxide nanoparticles and the generation of reactive oxygen species. This multifaceted effect of all components of the polyelectrolyte microcapsules should result in a rapid accumulation of reactive oxygen species in cancer cells and in their DNA damage that ultimately leads to the destruction of malignant tumors.

This article describes possible methods for the synthesis and functionalization of the polyelectrolyte microcapsules by cerium oxide nanoparticles to form novel drug delivery and theranostic systems. However, detailed

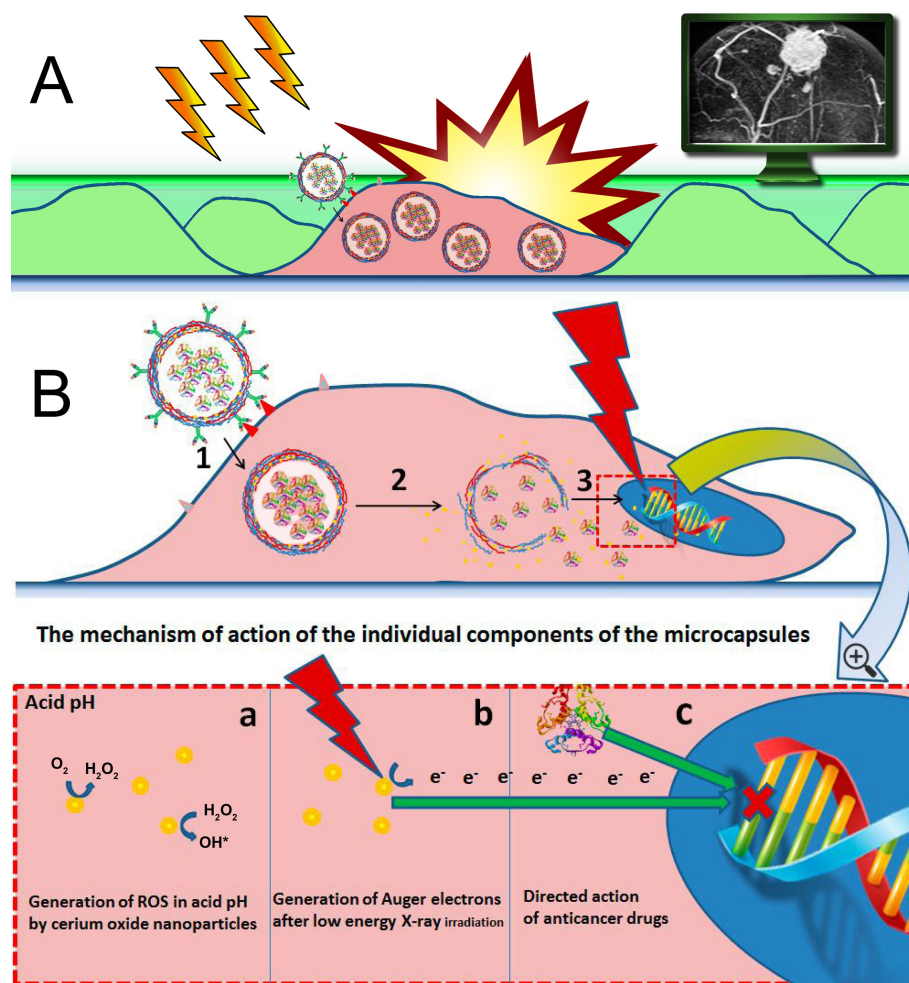


FIG. 2. Role of “smart” polyelectrolyte microcapsules in a cancer cell in radiation diagnostics (A) and treatment (B). Targeted entry into the cell (1), degradation of the microcapsules, and release of cerium oxide nanoparticles and encapsulated anticancer drug (2), the effect of low-intensity X-rays (3). The mechanism of action of polyelectrolyte microcapsules in a cancer cell: a – pro-oxidant properties of cerium oxide nanoparticles in the site of carcinogenesis; b – generation of Auger electrons by cerium oxide nanoparticles; c – chemotherapy by anti-cancer drug.

research is required to determine cytotoxicity and effectiveness *in vitro* and *in vivo* as well as confirm the mechanism of action.

3. Conflict of interest

The authors declare no conflict of interest.

Acknowledgements

The reported study was funded by RFBR and the Moscow City Government according to research project No. 15-34-70019 and RFBR project No. 16-34-60248. Ceria-based hybrid materials for cancer theranostics were designed with the support from the Russian Science Foundation (project No. 14-13-01373).

References

- [1] URL: <http://www.cancer.gov/about-cancer/treatment/types/radiation-therapy>.
- [2] Smart D.R. *Physician Characteristics and Distribution in the U.S.* IMV Medical Information Division, 2010.
- [3] Contreras J.L., Bilbao G., et al. Cytoprotection of pancreatic islets before and soon after transplantation by gene transfer of the anti-apoptotic Bcl-2 gene. *Transplantation*, 2011, **71**, P. 1015–1023.
- [4] Rivera C., Voipio J., et al. The K/Cl co-transporter KCC2 renders GABA hyperpolarizing during neuronal maturation. *Nature*, 1999, **397**, P. 251–255.

- [5] Ahn S., Jung S., Lee S. Gold nanoparticle contrast agents in advanced X-ray imaging technologies. *Molecules*, 2013, **18** (5), P. 5858–5890.
- [6] Li J., Gupta S., Li C. Research perspectives: gold nanoparticles in cancer theranostics. *Quant. Imaging Med. Surg.*, 2013, **3** (6), P. 284–291.
- [7] Liang H., Tian H., Deng M., Chen X. Gold Nanoparticles for Cancer Theranostics. *Chinese J. Chem.*, 2015, **33** (9), P. 1001–1010.
- [8] Cooper D.R., Bekah D., Nadeau J.L. Gold nanoparticles and their alternatives for radiation therapy enhancement. *Front. Chem.*, 2014, **2**, P. 86.
- [9] Alqathami M., Blencowe A., et al. Enhancement of radiation effects by bismuth oxide nanoparticles for kilovoltage x-ray beams: A dosimetric study using a novel multi-compartment 3D radiochromic dosimeter. *J. Phys.: Conf. Ser.*, 2013, **444** (1), P. 012025.
- [10] Yao M., Yao M., et al. Multifunctional Bi₂S₃/PLGA nanocapsule for combined HIFU/radiation therapy. *Biomater.*, 2014, **35** (28), P. 8197–8205.
- [11] Maier-Hauff K., Ulrich F., et al. Efficacy and safety of intratumoral thermotherapy using magnetic iron-oxide nanoparticles combined with external beam radiotherapy on patients with recurrent glioblastoma multiforme. *J. Neurooncol.*, 2011, **103** (2), P. 317–324.
- [12] Miladi I., Le Duc G., et al. Biodistribution of ultra-small gadolinium-based nanoparticles as theranostic agent: Application to brain tumors. *J. Biomater. Appl.*, 2013, **28** (3), P. 385–394.
- [13] Maggiorella L., Barouch G., et al. Nanoscale radiotherapy with hafnium oxide nanoparticles. *Future Oncology*, 2012, **8** (9), P. 1167–1181.
- [14] Pottier A., Borghi E., Levy L. The future of nanosized radiation enhancers. *Br. J. Radiol.*, 2015, **88**, P. 0171.
- [15] Xu P., Maidment B., et al. Cerium Oxide Nanoparticles: A Potential Medical Countermeasure to Mitigate Radiation-Induced Lung Injury in CBA/J Mice. *Radiat Res.*, 2016, **185** (5), P. 516–526.
- [16] Shcherbakov A.B., Zholobak N.M., Spivak N.Ya., Ivanov V.K. Advances and Prospects of Using Nanocrystalline Ceria in Cancer Theranostics. *Russ. J. Inorg. Chem.*, 2014, **59**, P. 1556–1575.
- [17] Heckert E., Karakoti A., Sudipta S., Self W.T., The role of cerium redox state in the SOD mimetic activity of nanoceria. *Biomater.*, 2008, **29** (18), P. 2705–2709.
- [18] Asati A., Santra S., Kaittanis C., Perez J.M. Surface-charge-dependent cell localization and cytotoxicity of cerium oxide nanoparticles. *ACS Nano*, 2010, **4**, P. 5321–5331.
- [19] Pirmohamed T., Dowding J.M., et al. Nanoceria exhibit redox state-dependent catalase mimetic activity. *Chem. Commun.*, 2010, **46** (16), P. 2736–2738.
- [20] Popov A., Popova N., et al. Cerium oxide nanoparticles stimulate proliferation of primary mouse embryonic fibroblasts in vitro. *Mater. Sci. Eng. C*, 2016, **68**, P. 406–413.
- [21] Wason M.S., Colon J., et al. Sensitization of pancreatic cancer cells to radiation by cerium oxide nanoparticle-induced ROS production. *Nanomed.*, 2013, **9** (4), P. 558–569.
- [22] Zholobak N.M., Ivanov V.K., et al. UV-shielding property, photocatalytic activity and photocytotoxicity of ceria colloid solutions. *J. Photochem. Photobiol. B*, 2011, **102**, P. 32–38.
- [23] Das S., Dowding J.M., et al. Cerium oxide nanoparticles: applications and prospects in nanomedicine. *Small*, 2009, **5** (24), P. 2848–2856.
- [24] Popov A.L., Selezneva I.I., et al. Study of CeO₂ nanoparticle interactions with biological cells and lipid bilayers. *J. Biol. Phys. Chem.*, 2014, **14**, P. 6–10.
- [25] Asati A., Santra S., et al. Oxidase-like activity of polymer-coated cerium oxide nanoparticles. *Angew. Chem. Int. Ed.*, 2009, **48**, P. 2308–2312.
- [26] von Montfort C., Alili L., Teuber-Hanselmann S., Brenneisen P. Redox-active cerium oxide nanoparticles protect human dermal fibroblasts from PQ-induced damage. *Redox Biol.*, 2015, **4**, P. 1–5.
- [27] Dowding J.M., Dosani T., et al. Cerium oxide nanoparticles scavenge nitric oxide radical (NO). *Chem. Commun.*, 2012, **48**, P. 4896–4898.
- [28] Korsvik C., Patil S., Seal S., Self W.T. Superoxide dismutase mimetic properties exhibited by vacancy engineered ceria nanoparticles. *Chem. Commun.*, 2007, **14**, P. 1056–1058.
- [29] Zhang L., Jiang H., Selke M., Wang X. Selective cytotoxicity effect of cerium oxide nanoparticles under UV irradiation. *J. Biomed. Nanotechnol.*, 2014, **10** (2), P. 278–286.
- [30] Briggs A., Corde S., et al. Cerium oxide nanoparticles: influence of the high-Z component revealed on radioresistant 9L cell survival under X-ray irradiation. *Nanomed.*, 2013, **9** (7), P. 1098–1105.
- [31] Jewell C., Lynn D.M. Multilayered polyelectrolyte assemblies as platforms for the delivery of DNA and other nucleic acid-based therapeutics. *Adv. Drug Deliv. Rev.*, 2008, **60** (9), P. 979–999.
- [32] Zhang X., Chabot D., et al. Target-molecule-triggered rupture of aptamer-encapsulated polyelectrolyte microcapsules. *ACS Appl. Mater. Interfaces*, 2013, **5** (12), P. 5500–5507.
- [33] Palamà I.E., Coluccia A.M., Gigli G. Uptake of imatinib-loaded polyelectrolyte complexes by BCR-ABL(+) cells: a long-acting drug-delivery strategy for targeting oncoprotein activity. *Nanomed.*, 2014, **9** (14), P. 2087–2098.
- [34] Kuklo L.I., Tolstoy V.P. Successive ionic layer deposition of Fe₃O₄@H_xMoO₄·nH₂O composite nanolayers and their superparamagnetic properties. *Nanosyst. Phys. Chem. Math.*, 2016, **7** (6), P. 1050–1054.
- [35] Demina P., Degtyareva V., Kuzmicheva G.M., Bukreeva T.V. Polyelectrolyte microcapsules modified with nanoscale titanium dioxide for targeted drug delivery. *Fine Chem. Technol.*, 2014, **9** (4), P. 73–79.
- [36] Gorin D.A., Portnov S.A., et al. Magnetic/gold nanoparticle functionalized biocompatible microcapsules with sensitivity to laser irradiation. *Phys. Chem. Chem. Phys.*, 2008, **10**, P. 6899–6905.
- [37] Shchukin D.G., Sukhorukov G.B., Möhwald H. Smart Inorganic/Organic Nanocomposite Hollow Microcapsules. *Angew. Chem. Int. Ed.*, 2003, **42**, P. 4471–4475.
- [38] Nakamura M., Katagiri K., Koumoto K. Preparation of hybrid hollow capsules formed with Fe₃O₄ and polyelectrolytes via the layer-by-layer assembly and the aqueous solution process. *J. Colloid Interface Sci.*, 2010, **341**, P. 64–68.
- [39] Shirtach A.G., Antipov A.A., Shchukin D.G., Sukhorukov G.B. Remote activation of capsules containing Ag-nanoparticles and IR dye by laser light. *Langmuir*, 2004, **20**, P. 6988–6992.
- [40] Ivanov V.K., Polezhaeva O.S., et al. Hydrothermal microwave synthesis of nanocrystalline cerium dioxide. *Doklady Chem.*, 2009, **426** (2), P. 2131–2133.
- [41] Ivanova O., Shekunova T., et al. One-stage synthesis of ceria colloid solutions for biomedical use. *Doklady Chem.*, 2011, **437** (2), P. 103–105.

- [42] Ivanov V.K., Polezhaeva O.S., et al. Synthesis and thermal stability of nanocrystalline ceria sols stabilized by citric and polyacrylic acids. *Russ. J. Inorg. Chem.*, 2010, **55** (3), P. 328–332.
- [43] Rajaonarivony M., Vauthier C., et al. Development of a new drug carrier made from alginate. *J. Pharm. Sci.*, 1993, **82** (9), P. 912–917.
- [44] You J.-O., Peng C.-A. Calcium Alginate Nanoparticles Formed by Reverse Microemulsion as Gene Carriers. *Macromol. Symp.*, 2005, **219** (1), P. 147–153.
- [45] Das R.K., Kasoju N., Bora U. Encapsulation of curcumin in alginate-chitosan-pluronic composite nanoparticles for delivery to cancer cells. *Nanomedicine*, 2010, **6** (1), P. 153–160.
- [46] Chevalier Y., Bolzinger M.A. Emulsions stabilized with solid nanoparticles: Pickering emulsions. *Colloids Surf. A*, 2013, **439**, P. 23–34.
- [47] Tikekar R.V., Pan Y., Nitin N. Fate of curcumin encapsulated in silica nanoparticle stabilized Pickering emulsion during storage and simulated digestion. *Food Res. Int.*, 2013, **51** (1), P. 370–377.
- [48] Gangwar R.K., Tomar G.B., et al. Curcumin conjugated silica nanoparticles for improving bioavailability and its anticancer applications. *J. Agric. Food Chem.*, 2013, **61** (40), P. 9632–9637.
- [49] Correa I., Plunkett T. Update on HER-2 as a target for cancer therapy: HER2/neu peptides as tumor vaccines for T cell recognition. *Breast Cancer Res.*, 2001, **3**, P. 399–403.
- [50] Yao J., Caballero O.L., et al. Tumor Subtype-Specific Cancer Testis Antigens as Potential Biomarkers and Immunotherapeutic Targets for Cancers. *Cancer Immunol. Res.*, 2014, **2**, P. 37.
- [51] Celardo I., De Nicola M., Mandoli C. et al. Ce³⁺ ions determine redox-dependent anti-apoptotic effect of cerium oxide nanoparticles. *ACS Nano*, 2011, **5** (6), P. 4537–4549.
- [52] Dolgoplova E.A., Ivanova O.S., et al. Microwave-hydrothermal synthesis of gadolinium-doped nanocrystalline ceria in the presence of hexamethylenetetramine. *Russ. J. Inorg. Chem.*, 2012, **57** (10), P. 1303–1307.
- [53] Shcherbakov A.B., Zholobak N.M., et al. Synthesis and antioxidant activity of biocompatible maltodextrin-stabilized aqueous sols of nanocrystalline ceria. *Russ. J. Inorg. Chem.*, 2012, **57** (11), P. 1411–1418.
- [54] Ivanova O.S., Gasylova G.A., et al. Polyol-mediated synthesis of nanocrystalline ceria doped with neodymium, europium, gadolinium, and ytterbium. *Doklady Chem.*, 2012, **443** (1), P. 82–85.
- [55] Zholobak N.M., Shcherbakov A.B., et al. Direct monitoring of the interaction between ROS and cerium dioxide nanoparticles in living cells. *RSC Adv.*, 2014, **4** (93), P. 51703–51710.
- [56] Dolgoplova E.A., Ivanova O.S., et al. Preparation of aqueous sols of Ce_{1-x}Gd_xO_{2-δ}, Y_{0.9}Eu_{0.1}VO₄ and nanocomposites Ce_{1-x}Gd_xO_{2-δ}/Y_{0.9}Eu_{0.1}VO₄ stabilized by polyacrylic acid. *Russ. J. Inorg. Chem.*, 2013, **58** (11), P. 1287–1293.
- [57] Mamotyuk E.M., Klochkov V.K., et al. Radioprotective Effect of CeO₂ and GdEuVO₄ Nanoparticles in “In Vivo” Experiments. In *Nanoscience Advances in CBRN Agents Detection, Information and Energy Security*, 2015, P. 193–197.
- [58] Shcherbakov A.B., Zholobak N.M., et al. Cerium fluoride nanoparticles protect cells against oxidative stress. *Mater. Sci. Eng. C*, 2015, **50**, P. 151–159.
- [59] Averchenko K.A., Kavok N.S., et al. Effect of inorganic nanoparticles and organic complexes on their basis on free-radical processes in some model systems. *Biopolym. Cell*, 2015, **31** (2), P. 138–145.
- [60] Moses W.W., Derenzo S.E. Cerium fluoride, a new fast, heavy scintillator. *IEEE Trans. Nucl. Sci.*, 1989, **36** (1), P. 173–176.

A surface and catalytic investigation of ceria by laser desorption ionization mass spectrometry

I. V. Zagaynov¹, A. K. Buryak²

¹A. A. Baikov Institute of Metallurgy and Materials Science, Leninskii pr. 49, Moscow, Russia

²A. N. Frumkin Institute of Physical Chemistry and Electrochemistry, Leninskii pr. 31, Moscow, Russia

¹igorscience@gmail.com

PACS 61.46.-w, 68.43.-h

DOI 10.17586/2220-8054-2017-8-2-290-295

Gd_{0.1}Ti_{0.1}Zr_{0.1}Ce_{0.7}O₂ solid solution with crystallite size of 10 nm, specific surface area of 85 m²/g and pore size of 2–6 nm has been prepared by a simple co-precipitation method with sonication and characterized by several methods. Among the characterization methods was laser desorption ionization-time of flight mass spectrometry (LDI-TOF) which was used to characterize the surface of the catalyst (fresh and used in CO oxidation) and thereby determine the catalytic sites (active sites of oxidation).

Keywords: ceria, solid solution, CO oxidation, LDI-TOF.

Received: 17 November 2016

Revised: 14 December 2016

1. Introduction

Nanocrystalline ceria based materials are playing an important role in environmental and energy related applications, especially in areas such as catalysis. Doped ceria materials are considered as more promising solid solutions for the use in these applications. The choice of a suitable dopant however, still remains a major challenge to the scientific community in terms of oxygen storage capacity, thermal stability, and economical considerations. Substitution of Ce⁴⁺ by other dopants in ceria leads to solid solutions which are found to increase both the oxygen storage capacity (OSC) and ionic conductivity as well as directly impact the catalytic activities. The activity is also dependent on other parameters such as the size, morphology and type of dopants. The presence of oxygen vacancies, especially for occurring interface reactions, in ceria-based materials is one of the key factors in oxidation reactions. Therefore, the investigation and characterization of the surface (interface) is an important goal [1–5]. To explore this key factor, the structural and morphological properties of fresh and spent catalysts were examined using XPS, EXAFS, XANES and other techniques. At the same time, mass spectrometry is widely used to measure molecular mass by ionizing the sample and report information [6,7], but did not in catalyst surface characterization. To obtain information on the nanoparticle's surface, they have to not undergo decomposition during ionization and detection. Clusters or nanodomains [8] of reduced ceria in the form of nonstoichiometric phase over the surface, likely originated from the reduction of ceria at the ceria interface, are giving direct evidence of the important role of the redox of ceria based materials. This means that the use of “soft ionization” methods to study such labile structures cannot be overestimated, it remains the only available method to accurately determine the mass, the number of atoms and molecules inside the nanodomain (cluster). Therefore, laser desorption ionization-time of flight mass spectrometry (LDI-TOF) method was used in this work to characterize the surface and establish active sites of oxidation [9,10]. This method can be used to characterize the surface of nanoparticles, bulk materials, ceramics and other relevant materials.

2. Material and methods

2.1. Synthesis

Ce(NO₃)₃·6H₂O, ZrO(NO₃)₂·6H₂O, Gd(NO₃)₃·6H₂O, TiCl₄ (Acros Organics) were used as metal precursors. Appropriate amounts of salts were dissolved in 500 mL distilled water containing of nitric acid (pH = 2) to give total concentrations of metals of 0.04 M. Then, the co-precipitation of hydroxides was carried out by addition of aqueous ammonia up to pH 10 at 30 °C under stirring. Ultrasonic processing (10 min, 35 kHz, 150 W, Sapphire UZV-4.0) was used during dissolution of salts in distilled water and after precipitation. The resulting precipitates were filtered, washed with distilled water-ethanol solution (H₂O/C₂H₅OH = 9 vol.), dried at 150 °C for 12 h, and calcined in static air by heating at a rate of 4 °C/min from room temperature to 500 °C and kept at 500 °C for 1 h in a muffle furnace.

2.2. Characterization

Powder XRD data were collected at room temperature (Rigaku MiniFlex 600) with $\text{CuK}\alpha$ radiation. Particle size (^dXRD) was calculated by Scherrer equation taking into account the instrumental broadening using germanium as reference; ^dXRD was calculated from (111), (220), (311) peaks. Quantitative phase analysis was calculated by the Rietveld method.

Specific surface area (^sBET) of the powders was measured by a conventional nitrogen adsorption method at 77 K (TriStar 3000 Micromeritics). Pore-size distributions were calculated from desorption isotherm, using BJH method. Samples were degassed at 120 °C for 5 h prior to measurement.

TEM analyses were conducted on an Omega Leo-912AB transmission electron microscope with accelerating voltage of 100 kV.

The XPS spectra were measured on an Axis Ultra DLD spectrometer (Kratos Analytical) using a monochromatic $\text{AlK}\alpha$ source (1486.6 eV, 150 W). The spectrometer was operated in fixed analysis energy mode, with a pass energy of 20 eV for high resolution spectra and 160 eV for survey spectra. The photoelectron spectra were recorded with 0.1 eV increments. The energy scale of spectrometer was calibrated according to the standard procedure with respect to Au $4f_{7/2}$, Ag $3d_{5/2}$, and Cu $2p_{3/2}$ photoelectron peaks of pure metals at 83.96, 368.21 and 932.62 eV, respectively. The surface charging effect in the spectra was compensated against the C–H states in the C 1 s spectra with the energy assumed to be 285.0 eV. The measurements were carried out at a pressure of 10^{-7} Pa at room temperature. Quantitative surface chemical analyses were calculated from the high-resolution core-level spectra, following the removal of a non-linear Shirley background.

Mass spectrometric analysis was performed using a MALDI-TOF mass spectrometer (Bruker UltraFlex 2) equipped with a 337 nm 110 μJ nitrogen laser. All measurements were performed in the linear mode by detecting positive and negative ions. Mass spectra were recorded with a laser power of 80–95 % of maximum. “Shots” were carried out in different parts of the samples. At the target, a surface double-sided tape was placed on stainless steel, on which the samples were applied and then dried at room temperature. On the basis of the molecular-mass isotope distribution patterns, formulas of proposed compounds corresponding to the m/z ratios are proposed.

The catalytic activity of the synthesized samples in the oxidation of CO was determined by the flow method at atmospheric pressure. The process was conducted in a U-shaped quartz reactor at a gas hourly space velocity of 1800 h^{-1} within a temperature range of 20–500 °C. The temperature was measured with a thermocouple placed in the center of the catalytic bed. The model gas mixture had the following composition, vol. %: CO – 4.2; O₂ – 9.6; N₂ – balance. The concentrations of gases were measured on a Konik-Tech HRGC 5000B gas chromatograph.

3. Results and discussion

XRD patterns (Fig. 1a) of fresh and used catalysts are perfectly indexed as the pure cubic phase, indicating the formation of solid solutions by the incorporation of respective dopant ions into the ceria lattice and stability of this system during catalysis. According to TEM (Fig. 1b), the images reveal that the particle size is about 10 nm and nearly spherical in shape with an agglomerated structure. All samples have IV type adsorption curves with a hysteresis loop of H₂, indicating the presence of mesopores in the systems [11]. The pore size distribution of samples (polymodal distribution of pores, 2–6 nm) is presented in Fig. 1c. Table 1 traces the evolution of the microstructure of the catalysts before and after catalytic test. It is clearly demonstrated that no phase and morphological changes were observed and the catalyst was stable.

TABLE 1. Main characteristics of ceria-based catalysts

No	Sample	^dXRD , nm	^dTEM , nm	^sBET , m^2g^{-1}	Pore diameter, nm	T ₅₀ (T ₁₀₀) CO conversion, °C
fresh	$\text{Gd}_{0.1}\text{Ti}_{0.1}\text{Zr}_{0.1}\text{Ce}_{0.7}\text{O}_2$	9	6–12	83	2–6	210 (263)
used		10	7–13	82	2–6	—

Ce 3d photoelectron peaks displayed a complex nature of spectrum originated from the existence of multiple oxidation states and overlapping of Ce 4f levels with O 2p states during the primary photoemission process. According to XPS data [12] Ce, Ti, and Zr cations have charge +4, and Gd has +3; also the existence of another phase or cation coordination on the surficial region is possible that can be interpreted in terms of the interaction between dopant and cerium species, i.e. Ce–O–Me bond formation, which induced more number of oxygen defects at the interface by the substitution of Ce^{4+} with the dopant. XPS spectrum indicated the absence of the Ce^{3+} state in these spectra in contrast to other many works, and significant changes were not observed [12].

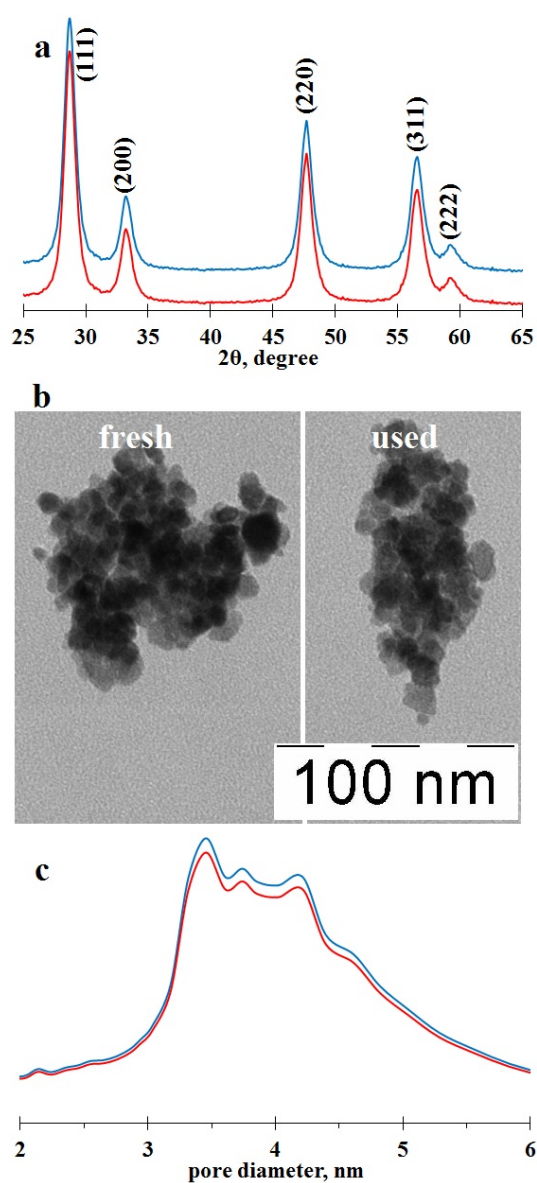


FIG. 1. XRD pattern (a), TEM images (b) and pore size distribution (c) of samples. Blue – before catalysis, red – after catalysis

Figure 2 shows LDI-TOF spectra of the samples in the positive and negative ion recording modes. The positive spectra are almost identical, and no evident changes were observed after the catalytic reaction. The main structural cationic fragments in the mass spectra (besides collateral fragments, containing of Na, K, Mg, Ca... , being only impurities) are presented in Table 2. Fragments of Ce with other dopants are detected. Gd-containing fragments are difficult to identify due to equal m/z ratio of Gd (157) and CeOH (157) fragments. Also the repeatability of $\text{CeO}(\text{CeO}_2)_n$ and $(\text{CeO}_2)_n$ fragments (see example in Fig. 2a) are presented. Another situation is in negative spectra (Fig. 2b). The cleaning of surface by CO was occurred during catalysis. MeO_4^- fragments are detected, and Cl- and (Na, K, Mg, Ca) CO_3^- -containing fragments are not. Fig. 3 shows interesting area of the spectra: CeO_4^- fragment, CO_2 and H_2O adsorbed molecules on it were presented in the fresh sample, but after catalytic test CeO and CeO_2 fragments with CO_3^- functional group (CeOCO_3^- and $\text{CeO}_2\text{CO}_3^-$ fragments, accordingly) were. This is in agreement with a redox mechanism where ceria reduction is initiated at the contact-interface area, forming reduced ceria (active catalytic site (special domains [8], like CeO_4^-) and transforms to used site (CeOCO_3^- and $\text{CeO}_2\text{CO}_3^-$), which is then oxidized by gas-phase oxygen and transforms again to CeO_4^- . So, it can be assumed that the vicinity of the oxidized sites, promoting the adsorption of CO, and reduced sites, promoting the dissociative adsorption of O_2 , can accelerate the reaction, provided that the reaction limiting step is the reaction of adsorbed

CO and dissociative adsorbed oxygen, thus results in a Langmuir-Hinshelwood model, or the chemisorption of CO takes place on the surface, while the lattice oxygen in ceria also involves in the reaction, thus resulting in a Mars van-Krevelen model [13]. Therefore, based on previous and presented LDI-TOF spectra data the proposed steps of the reaction can be suggested (Fig. 4). During the CO oxidation Ce^{4+} is reduced to Ce^{3+} , accompanied by extraction of oxygen from the lattice, which is consumed to oxidize CO to CO_2 . The defect mobility of oxygen on the surface has a large influence on the CO oxidation activity and is determined critically by the structure, size and morphology of catalyst. The nanosize ceria contributes a high surface area to volume ratio, and doping with transition metal oxides could create even more active defect sites and lead to enhanced CO conversion [14].

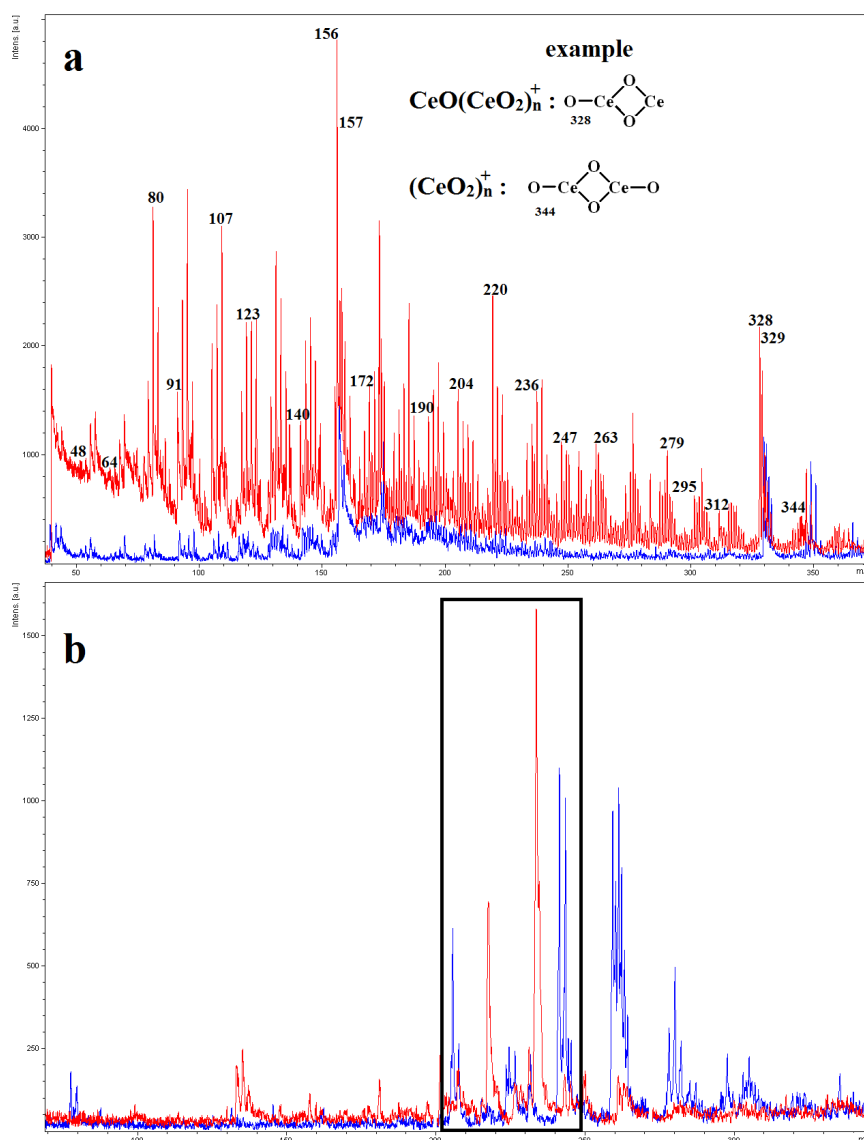


FIG. 2. LDI-TOF spectra of the samples in positive (a) and negative (b) ion recording modes. Blue – before catalysis, red – after catalysis

4. Conclusions

Mesoporous materials based on nanosized ceria were synthesized by a sonochemical method and characterized by complex methods. The method of laser desorption ionization-time of flight mass spectrometry (LDI-TOF) was used to characterize the surface of fresh and used after CO oxidation catalyst and thereby determine the catalytic sites. It was demonstrated that the active sites of oxidation could be proposed by using LDI-TOF data of positive and negative ion fragments and probable steps (possible mechanism) of the reaction could be suggested. Consequently, this work demonstrated that the LDI-TOF mass spectrometry is a promising method for these goals.

TABLE 2. The main structural cationic fragments in the mass spectra

ions	m/z, Da	ions	m/z, Da
Ti ⁺	48	CeOZr ⁺	247
TiO ⁺	64	OCeOOTiO ⁺	252
TiO ₂ ⁺	80	CeOOTi ⁺	263
Zr ⁺	91	OCeOOZr ⁺	279
ZrO ⁺	107	OCeOOZrO ⁺	295
ZrO ₂ ⁺	123	CeOOCe ⁺	312
Ce ⁺	140	CeOGd ⁺	313
CeO ⁺	156	CeOOCeO ⁺	328
CeOH ⁺	157	CeOOCeOH ⁺	329
Gd ⁺	157	CeOOGd ⁺	329
CeO ₂ ⁺	172	OCeOOCeO ⁺	344
GdO ⁺	173	OCeOOCeO ⁺	345
CeO ₂ ·H ₂ O ⁺	190	CeOOGdO ⁺	345
CeOTi ⁺	204	CeO(CeO ₂) _n ⁺	
CeOOTi ⁺	220	(CeO ₂) _n ⁺	
OCeOOTi ⁺	236		

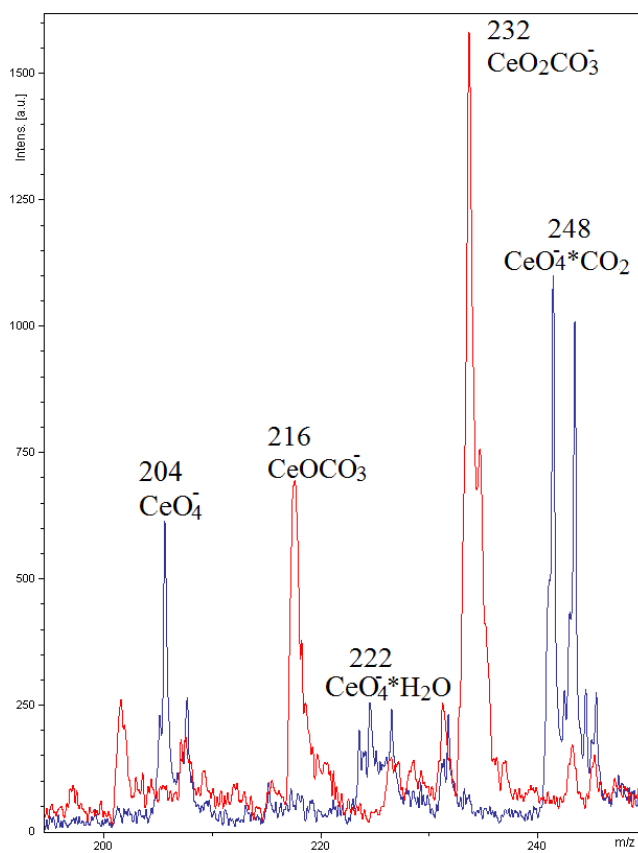


FIG. 3. LDI-TOF spectra of the samples in negative ion recording mode (delineated area in Fig. 1b). Blue – before catalysis, red – after catalysis

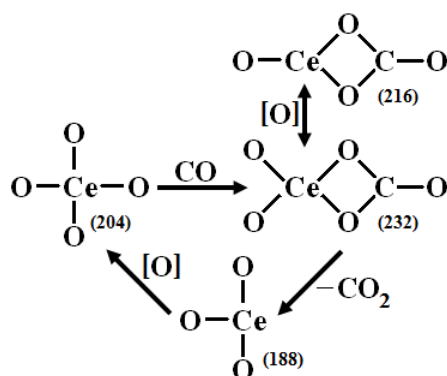


FIG. 4. Representation of possible steps of CO oxidation reaction in according to LDI-TOF spectra (anionic fragments with charge of -1)

References

- [1] Trovarelli A. *Catalysis by Ceria and Related Materials*. World Scientific Publishing Company, Singapore, 2002, 528 p.
- [2] Trovarelli A., Fornasiero P. *Catalysis by Ceria and Related Materials (2nd ed.)*. World Scientific Publishing Company, Singapore, 2013, 908 p.
- [3] Chaudhary S., Sharma P., Kumar R., Mehta S.K. Nanoscale surface designing of cerium oxide nanoparticles for controlling growth, stability, optical and thermal properties. *Ceram. Int.*, 2015, **41**, P. 10995–11003.
- [4] Venkataswamy P., Jampaiah D., Aniz C.U., Reddy B.M. Investigation of physicochemical properties and catalytic activity of nanostructured $\text{Ce}_{0.7}\text{M}_{0.3}\text{O}_{2-\delta}$ (M = Mn, Fe, Co) solid solutions for CO oxidation. *J. Chem. Sci.*, 2015, **127**, P. 1347–1360.
- [5] Vinodkumar T., Durgasri D.N., Maloth S., Reddy B.M. Tuning the structural and catalytic properties of ceria by doping with Zr^{4+} , La^{3+} and Eu^{3+} cations. *J. Chem. Sci.*, 2015, **127**, P. 1145–1153.
- [6] Ingram A.J., Boeser C.L., Zare R.N. Going beyond electrospray: mass spectrometric studies of chemical reactions in and on liquids. *Chem. Sci.*, 2016, **7**, P. 39–55.
- [7] Henderson W., McIndoe J.S. *Mass Spectrometry of Inorganic, Coordination and Organometallic Compounds*. John Wiley & Sons, London, 2005, 292 p.
- [8] Aneggi E., Divins N.J., et al. The formation of nanodomains of Ce_6O_{11} in ceria catalyzed soot combustion. *J. Catal.*, 2014, **312**, P. 191–194.
- [9] Buryak A.K., Serduk T.M. Chromatography–mass spectrometry in aerospace industry. *Russ. Chem. Rev.*, 2013, **82** (4), P. 369–392.
- [10] Zagaynov I.V., Buryak A.K. Mesoporous nanoscale ceria: synthesis from cerium (III) acetylacetonate and mechanism. *J. Sol-Gel Sci. Technol.*, 2015, **74**, P. 103–108.
- [11] Zagaynov I.V. Sonochemical synthesis of mesoporous $\text{Gd}_x\text{Zr}_y\text{Ti}_z\text{Ce}_{1-x-y-z}\text{O}_2$ solid solution. *Ceram. Int.*, 2015, **41**, P. 8730–8734.
- [12] Zagaynov I.V., Liberman, E.Yu., Naumkin A.V. $\text{Gd}_x\text{Zr}_y\text{Ti}_z\text{Ce}_{1-x-y-z}\text{O}_2$ mesoporous catalysts for oxidation reactions. *Surf. Sci.*, 2015, **642**, P. L11–L15.
- [13] Trovarelli A. Catalytic properties of ceria and CeO_2 -containing materials. *Catal. Rev.*, 1996, **38**, P. 439–520.
- [14] Alammari T., Chow Y.-K., Mudring A.-V. Energy efficient microwave synthesis of mesoporous $\text{Ce}_{0.5}\text{M}_{0.5}\text{O}_2$ (Ti, Zr, Hf) nanoparticles for low temperature CO oxidation in an ionic liquid – a comparative study. *New J. Chem.*, 2015, **39**, P. 1339–1347.



NANOSYSTEMS:

PHYSICS, CHEMISTRY, MATHEMATICS

INFORMATION FOR AUTHORS

The journal publishes research articles and reviews, and also short scientific papers (letters) which are unpublished and have not been accepted for publication in other magazines. Articles should be submitted in English. All articles are reviewed, then if necessary come back to the author to completion.

The journal is indexed in Web of Science Core Collection (Emerging Sources Citation Index), Chemical Abstract Service of the American Chemical Society, Zentralblatt MATH and in Russian Scientific Citation Index.

Author should submit the following materials:

1. Article file in English, containing article title, the initials and the surname of the authors, Institute (University), postal address, the electronic address, the summary, keywords, MSC or PACS index, article text, the list of references.
2. Files with illustrations, files with tables.
3. The covering letter in English containing the article information (article name, MSC or PACS index, keywords, the summary, the literature) and about all authors (the surname, names, the full name of places of work, the mailing address with the postal code, contact phone number with a city code, the electronic address).
4. The expert judgement on possibility of publication of the article in open press (for authors from Russia).

Authors can submit a paper and the corresponding files to the following addresses: nanojournal.ifmo@gmail.com, popov1955@gmail.com.

Text requirements

Articles should be prepared with using of text editors MS Word or LaTeX (preferable). It is necessary to submit source file (LaTeX) and a pdf copy. In the name of files the English alphabet is used. The recommended size of short communications (letters) is 4-6 pages, research articles– 6-15 pages, reviews – 30 pages.

Recommendations for text in MS Word:

Formulas should be written using Math Type. Figures and tables with captions should be inserted in the text. Additionally, authors present separate files for all figures and Word files of tables.

Recommendations for text in LaTeX:

Please, use standard LaTeX without macros and additional style files. The list of references should be included in the main LaTeX file. Source LaTeX file of the paper with the corresponding pdf file and files of figures should be submitted.

References in the article text are given in square brackets. The list of references should be prepared in accordance with the following samples:

- [1] Surname N. *Book Title*. Nauka Publishing House, Saint Petersburg, 2000, 281 pp.
- [2] Surname N., Surname N. Paper title. *Journal Name*, 2010, **1** (5), P. 17-23.
- [3] Surname N., Surname N. Lecture title. In: Abstracts/Proceedings of the Conference, Place and Date, 2000, P. 17-23.
- [4] Surname N., Surname N. Paper title, 2000, URL: <http://books.ifmo.ru/ntv>.
- [5] Surname N., Surname N. Patent Name. Patent No. 11111, 2010, Bul. No. 33, 5 pp.
- [6] Surname N., Surname N. Thesis Title. Thesis for full doctor degree in math. and physics, Saint Petersburg, 2000, 105 pp.

Requirements to illustrations

Illustrations should be submitted as separate black-and-white files. Formats of files – jpeg, eps, tiff.



NANOSYSTEMS:

PHYSICS, CHEMISTRY, MATHEMATICS

Журнал зарегистрирован

Федеральной службой по надзору в сфере связи, информационных технологий и массовых коммуникаций

(свидетельство ПИ № ФС 77 - 49048 от 22.03.2012 г.)

ISSN 2220-8054

Учредитель: федеральное государственное автономное образовательное учреждение высшего образования

«Санкт-Петербургский национальный исследовательский университет информационных технологий, механики и оптики»

Издатель: федеральное государственное автономное образовательное учреждение высшего образования

«Санкт-Петербургский национальный исследовательский университет информационных технологий, механики и оптики»

Отпечатано в Учреждении «Университетские телекоммуникации»

Адрес: 197101, Санкт-Петербург, Кронверкский пр., 49

Подписка на журнал НФХМ

На второе полугодие 2017 года подписка осуществляется через

ОАО Агентство «Роспечать»

Подписной индекс 57385 в каталоге «Издания органов научно-технической информации»